Wu, June Young (1985) SWATH vertical motions with emphasis on fixed fins control. PhD thesis

http://theses.gla.ac.uk/6935/

SWATH VERTICAL MOTIONS
WITH EMPHASIS
ON FIXED FINS CONTROL

by

June Young Wu, B.Sc., M.Sc.

PAGE NUMBERS ARE CUT

OFF IN THE ORIGINAL

DEDICATION

TO THE MEMORY OF MY FATHER

SUMMARY

The SWATH ship has been claimed as one of the advanced high performance vessels which can provide good seakeeping characteristics as well as maintaining high speed in rough seas. Despite the considerable amount of research and developmemt carried out in the last fifteen years, there is still a lack of design data in the open literature concerning many of the specialised aspects of SWATH design. Two of these areas are the motion characteristics of hulls which are operating fairly close to the water surface and the design of active control systems to reduce static trim and motions in waves.

This study is an investigation, both theoretically and experimentally using a model, into SWATH motion characteristics in the vertical plane. It aims to have an understanding of the seakeeping behaviour with and without the effect of fins in waves.

The computer program for the motion prediction involves the computation of the hydrodynamic coefficients of the equations of motion on the practical range of frequencies, depth of submergences and column widths. The effects of these factors on the sectional hydrodynamic coefficients are discussed and are curve-fitted into approximate formulae in order to save computer time. The total (three dimensional) hydrodynamic coefficients are integrated stripwise, taking into account the forward speed and viscous effects.

Analytic methods for the wave induced exciting forces were formulated and obtained by two approaches; the modified Morison's formula and the strip theory. The sectional Froude-Krylov force, caused by the undisturbed incident wave pressure and a diffraction

component resulting from the distortion of the wave train by the presence of the hull were integrated over the mean immersed surface of the hull section. Phase differences of the sectional forces are considered during the integration procedure. The forward speed and viscous effects are included together.

In addition, a series of laboratory tests in calm water and waves as well as theoretical studies aimed at the design of vertical-plane control surface(fins), which would keep the SWATH ship on a near level trim at speed in calm water and reducing the inherently low level of motion in wave have been carried out.

The forces generated by fins are composed of inertia effects and viscous induced lift and cross-flow drag. Since the fins are attached to the hull, the lift-curve slope wer corrected by the fin-body effect. Only after fins are considered in the study, the combination of the forward fins are believed could be summed linearly. However, the downwash effect on the after fins by the forward fins are not able to be included.

Since the exciting and restoring forces of a SWATH involved are smaller than those of the comparable monohull, adequate control forces can be generated for a SWATH at speed by reasonably sized fins.

The good agreement of the comparisons of the analytical calculations and the experimental measurements confirms the accuracy of the study.

ACKNOWLEDGEMENT

DECLARATION

Except where reference is made to the work of

others this thesis is believed to be original

SWATH VERTICAL MOTIONS WITH EMPHASIS ON FIXED FINS CONTROL

CONTENTS

LIST OF FIGURES

LIST OF TABLES

NOMENCLATURE

a	: hydrodynamic added mass (or added mass moment of inertia)
a_0	: wave amplitude
Ae	: effect aspect ratio
A_f	: projected area of the fin on a horizontal plane
A_{jk}	: added mass coefficients in the jth mode due to the motion in the kth mode
A_p	: projected area of the hull on a horizontal plane
AR	: geometric aspect ratio
A_{wp}	: the waterplane area of the SWATH ship
$A_{33}^{(f)}$	: heave added mass of the aft fins
b	: hydrodynamic damping per unit velocity
b(x)	: horizontal distance between the centre of the beam of the two hulls and the centre of the beam of one hull
BG	: vertical distance between the centres of buoyancy and gravity
B_{jk}	: damping coefficient in the jth mode due to the motion in the kth mode
$B_m(x)$	: maximum breadth of a cross-section of one hull
C	: restoring force per unit displacement of motion
C_D	: drag coefficient (in Morison's approach)
C_{DF}	: cross-flow drag coefficient of the fin
C_{DH}	: cross flow drag coefficient of the hull
C_h	: chord of the fin
C_{jk}	: restoring coefficient in the jth mode due to the motion in the ith mode
C_L	: lift coefficient of the fin
$C_{L\alpha}$	: lift-curve slope per radian of the fin
C_v	: added mass coefficient (in Morison's approach)
C_w	: wave celerity (= λ/T)
D_f	: cross-flow drag generated by fins

$f_K^{(m)}(x)$: sectional Froude-Krylov force per wave amplitude at station in m mode motion (m = H for heave, m = p for pitch)

F_A : inertial force due to added mass

F_B : velocity force due to wave damping

F_C : hydrostatic force (restoring force)

F_D : diffracted wave force

F_I : incident wave force (Froude-Krylov force)

F_{VE} : vertical force component induced by viscous effect on hull

F_3 : wave-exciting force in heave mode

F_5 : wave-exciting force in pitch mode

g : acceleration due to gravity

$G(y,z;\xi,\eta;k_o)$: Green's function of two-dimensional pulsating source potential of unit intensity at point (ξ,η)

GM_L : metacentric height in the longitudinal direction

GM_T : metacentric height in the transverse direction

h_w : wave surface profile

H : depth of the water surface to the centreline of the hull

HST : half-strut thickness

i : $=\sqrt{-1}$ or subscript designating imaginary part

i_o : mass moment of inertia of the item about its own axis parallel to the structural axis through its centre of gravity

I_f : inertia force generated by fins

I_{wp} : moment of inertia of waterplane about the pitch axis

I_5 : longitudinal mass moment of inertia about the pitch axis

k_o : incident wave number (ω_o^2/g)

K_C : Keulegan-Carpenter number (= UT/D)

ℓ : longitudinal distance from the centre of pressure of the aft fin to th LCG of the ship

L_f : lift force generated by fins

$m^{(f)}$: mass of the fins

M : total body mass

M_p : pitch moment induced by viscous effect on hull

M_{wp} : moment of waterplane area along the longitudinal direction

P_D : dynamic pressure induced by the diffracted wave

P_I : dynamic pressure induced by the incident wave

$Q(\xi, \eta)$: complex source strength (intensities)

R : radius of the circular cross-section

S_p : span of the fin

$S_3, \dot{S}_3, \ddot{S}_3$: displacement, velocity and acceleration of SWATH heave motion from its mean position

$S_5, \dot{S}_5, \ddot{S}_5$: displacement, velocity and acceleration of SWATH pitch motion from its mean position

t : time

T : wave period

u : velocity in the horizontal component

$u^{(o)}, u^{(e)}$: horizontal velocity component for odd and even potential function

U : forward speed of the ship

$v^{(o)}, v^{(e)}$: vertical velocity component for odd and even potential function

v_n : normal velocity of the section

v_w : vertical velocity of the incident wave

X_{Gi} : longitudinal distance of the centre of gravity of the ith item to the LCG of the ship

Z_{Gi} : vertical distance of the centre of gravity of the ith item to the LCG of the ship

α : trim angle or angle of attack

Δ : total mass of the SWATH

∇ : total volume displacement of the SWATH

μ : heading angle of incident wave with respect to the X-axis ($\mu = 0^\circ$ for the following sea case, $\mu = 180^\circ$ for head sea case)

Φ_D : complex velocity potential for diffracted wave

ϕ_I : complex velocity potential for incident wave

ϕ_T : total complex velocity potential

ω : wave encounter frequency $(= \omega_o - k_o U \cos\mu)$

ω_o : incident wave frequency in radians per second

CHAPTER
1

Introduction

and

Overview

CHAPTER 1

INTRODUCTION AND OVERVIEW

1.   TERMINOLOGY

The acronym 'SWATH' (Small-Waterplane-Area-Twin/Triple-Hull),
was selected by the US Navy in 1972 to describe an advanced high
performance marine vehicle, which has been the subject of much
research and development in recent years. Other descriptive names such
as TRISEC, LWP (Low Waterplane Catamaran), MODCAT (Modified Catamaran,
SEMCAT (Semi-Submerged Catamaran) have been seen in the literature.
The most popular names are SSC (Semi-Submerged Catamaran) which is
widely used in Japan, S^3 (Semi-Submerged Ship) and SSP (Semi-Submerged
Platform) which are used in the USA.

2.   BACKGROUND AND HISTORY

For many centuries it has been a dream of Naval
Architects [1] to design a ship which can sail at a higher speed
through rough waves without getting its deck wet, its hull bottom
slammed by waves and without rocking to the tiring cyclic motion.
Seakeeping performance and speed reduction in rough seas are
recognised as very important not only in the field of ocean
development but also in marine transportation and naval activities.

Responding to the strong demand created by various seafaring
needs, the concepts of advanced vessels [2] such as planing boats,
hovercraft, hydrofoils etc, as shown in figure 1.1, have been

developed as high-speed small craft. In other maritime operations, semi-submersibles are being used as stable platforms in severe sea conditions such as the North Sea. Figure 1.2 [3,4] presents comparisons of the hydrodynamic performance of these advanced vessels. As shown in the figure, SWATH is conceived to achieve high performance in terms of both excellent seaworthiness and maintenance of high speed in rough seas.

The history of SWATH [5,6], as shown by a schematic figure 1.3, can be traced back to the multi-hulls which were introduced into Europe by Sir William Petty [7,8] at the time of the Restoration in the 1660's when early catamarans were constructed. The vessels achieved notable fame for their ability to outsail other vessels of the time. Moving the hull(s) beneath the water came later and is usually credited to Lundborg in 1880 [6,9,10] but this was a sigle hull design and not dissimilar to the NAVSHIPS in 1959 [11]. It was not until 1905 that Nelson [12] used two submerged hulls and so designed what was probably the first SWATH. Other early desings were generated by Blair in 1929 and Faust in 1932. In 1965 Frankel [13] proposed the version of the SEMCAT 'MOHOLE' platform for the purpose of open ocean retrieval of large objects.

According to [14], Creed is the one who first brought the modern SWATH concept to the attention of the US Navy in 1943, as a superior platform for aircraft operations. American interest developed in the late sixties with the design and model testing of the TRISEC by Leopold [15] of Litton Industries in 1969. The TRISEC which consists of three major po ʰtions, is shown in fig. 1.4.

Fig.1.1 Concepts of advanced marine vehicles.

Fig.1.2 Concept of advanced ship types

SWATH HISTORY

Nelson (1905)

Blair (1929)

Faust (1932)

Twin Hulls   Petty Polynesia (1660) (c17)

Creed (1946)

SEMCAT   MOHOLE

DUPLUS

Leopold
LWP TRISEC
(1969)

Submerged Hulls   Lundborg (1880)

Lang (1971)

KAIMALINO
(1971)

MARINE ACE
(1977)

SEAGULL
(1979)

OHTORI
(1980)

SUAVE LINO
(1981)

KOTOZAKI
(1981)

KAIYO
(1984)

MARINE WAVE
(1985)

Fig.1.3

UPPER HULL

STRUT

LOWER HULL

Fig. 1.4 TRISEC Geometry

NELSON – 1905

LEOPOLD – 1967

FAUST – 1932

LANG – 1971

CREED – 1946

Tandem Strut SWATH.

Fig.1.5   Patents of SWATH

DUPLUS

Fig.1.6
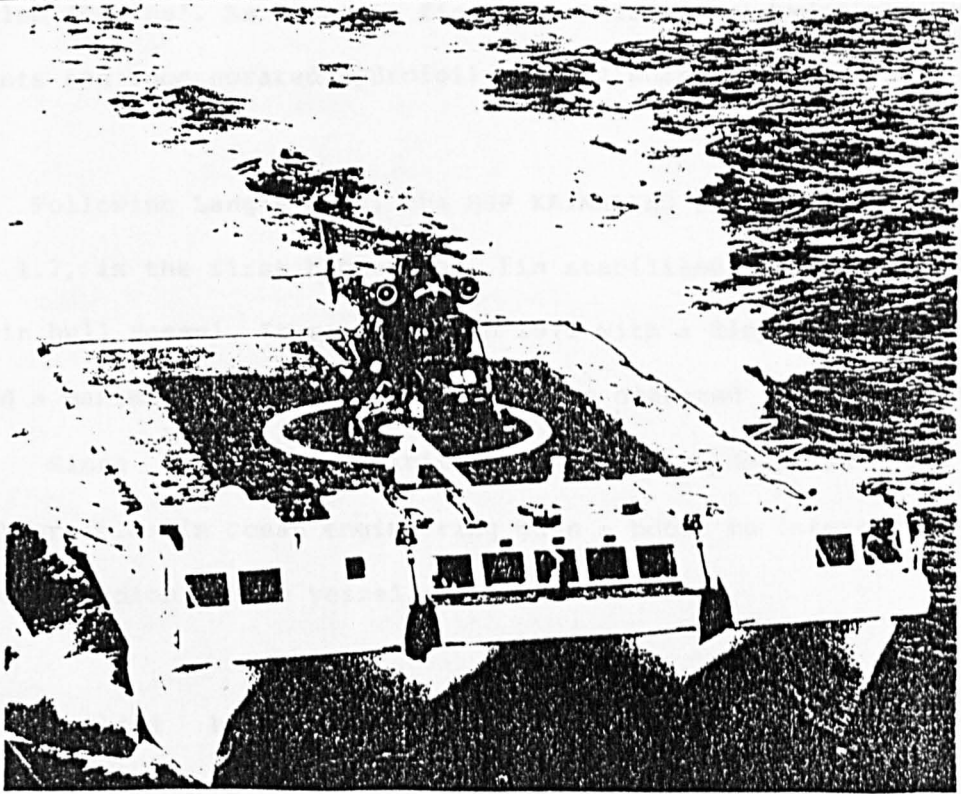
KAIMALINO   U.S. Navy Photo

Fig.1.7

    a. An underwater hull portion (Lower Hull).

    b. An above-water hull portion (Upper hull).

    c. A connection hull portion (Strut).

These earlier designs would provide an acceptable performance at low to moderate Froude numbers but would tend to become dynamically unstable at a high Froude number or design speeds.

Lang (1971) introduced patent claims covering stabilising fins and canard fins in conjunction with control systems [16], twin lower hulls and either single or tandem struts periside. Some of the patents of SWATH are illustrated in fig. 1.5. In 1969, the Netherlands offshore company launched a 1200-ton twin-hulled drilling rig called 'Duplus'. As shown in fig. 1.6, this vessel had a top speed of 8 knots and incorporated hydrofoil control surfaces.

Following Lang's work, the SSP KAIMALINO [17,18,19], as shown in fig. 1.7, is the first high-speed, fin stabilised, small-waterplane Area Twin hull vessel. It was built in 1973 with a displacement of 190 tons and a maximum speed of 25 knots and was operated as a research vessel. Since then the initiative and widespread use of semi-submersibles in ocean engineering gave a boost to interest in a high speed version of the vessel.

Inspired by the KAIMALINO, a succession of Japanese designs [20] demonstrated the capabilities of the SWATH ship. Five vessels have been built by the Mitsui company: the 20 tons experimental craft 'MARINE ACE' in 1977, capable of carrying 20 passengers; the 343 tons passenger ferry 'SEAGULL' (MESA 80), as shown

in fig. 1.8, in 1979, claimed to be capable of carrying 446 passengers for a sea crossing a waveheight of 3-4 metres had no excessive wave impacts on the underside of the cross-structure and provides a service operation with very good passenger comfort and schedule reliability, the 236 tons hydrographic survey vessel 'KOTOZAKI' in 1981, fig. 1.9. Recently the 2849 tons diver support vessel 'KAIYO' in 1984, fig. 1.10, and 'MARINE WAVE' 19 tons leisure cruiser just built (1985), as shown in fig. 1.11. Also Mitsubishi has built a 239 tons survey vessel called 'OHTORI' in 1980 which is about the same size as 'KAIMALINO' and KOTOZAKI'. At about the same time, a private 53 tons 'SUAVE LINO' was constructed in California. All SWATH ships currently operating in the world (as at 1985) are listed in Table 1.1.

In addition to the major achievements continued by Japan and the US Coastguard, research and development is being carried out by the Canadian Navy, the British Royal Navy, Sweden, Italy, Holland and several Universities and other research establishments.

3.   SWATH CONCEPT AND CHARACTERISTICS

From a study of the background and the history of the SWATH ship, it can be seen that the principal concept of this displacement vessel in which the hull forms depart so clearly from conventional designs is not new. The idea is to submerge most of the buoyant volume (that part of the volume which supports its weight) well away from the influence of the waves and minimise the waterplane area (the planform area at the air-sea interface). This is achieved by supporting the deck structure well above the sea surface on streamlined surface-piercing struts. This fundamental concept having been used advantageously by the offshore industry for drilling and exploration

THE MAIN PARTICULARS OF EXISTING SWATH SHIPS

SWATH Name	Completed	Length L_{OA} (m)	Displ (Ton)	Breadth B_{OA} (m)	Max Speed (Kts)	Draft (m)	Start Type	Fin Control	Missions	Made by	Natural Period Heave (sec) Pitch (sec) Roll (sec)	
KAIMALINO	1973	26.8	193/ 224	13.7	18	4.66	Twin	Auto	Navy Work and Demonstration	US Coast Guard	8.6 9.7 15.8	
MARINE ACE	1977	12,35	18.4/ 22.2	6.5	17.3/ 15.4	1.55	Twin/ Single	Auto	Experimental Craft	Japan Mitsui Zosen	5.5 4.8 11.2	3.9 4.5 4.7
MESA 80 (SEAGULL)	1979	35.9	343	17.1	27.1	3.15	Single	Auto	Passenger Ferry (402 Pass)	Japan Mitsui Zosen	6.2 9.5 10.9	
KOTOZAKI	1980	27.0	236	12.5	20.5	3.2	Single	Manual	Hydro- graphic Survey	Japan Mitsui	5.8 8.9 10.7	
OHTORI	1980	27.0	239	12.5	–	3.4	Single	Manual	Hydro- graphic Survey	Japan Mitsubishi		
SUAVE LINO	1981	19.2	53	9.1	18.0	2.13	Single	Auto	Fishing Boat	USA Private Owner		
KAIYO	1984	61.55	2849	28.0	13.25	6.3	Single	Manual	SSC Type Support Ship for U/water work	Japan Mitsui		
MARINE WAVE	1985	15.1	19	6.2	18.0	1.6	Single		Cruiser Toray Industry	Japan Mitsui		
											Without Fins	With Fins
SWATH Model	1982	1.5	0.022	0.944	$2.5ms^{-1}$	0.178	Twin	Fixed Pin	Experimental Model	University of Glasgow	1.7 2.25 –	1.75 2.299 –

TABLE 1.1

6.

General Arrangement

31.500

7.700

5.845

6.750
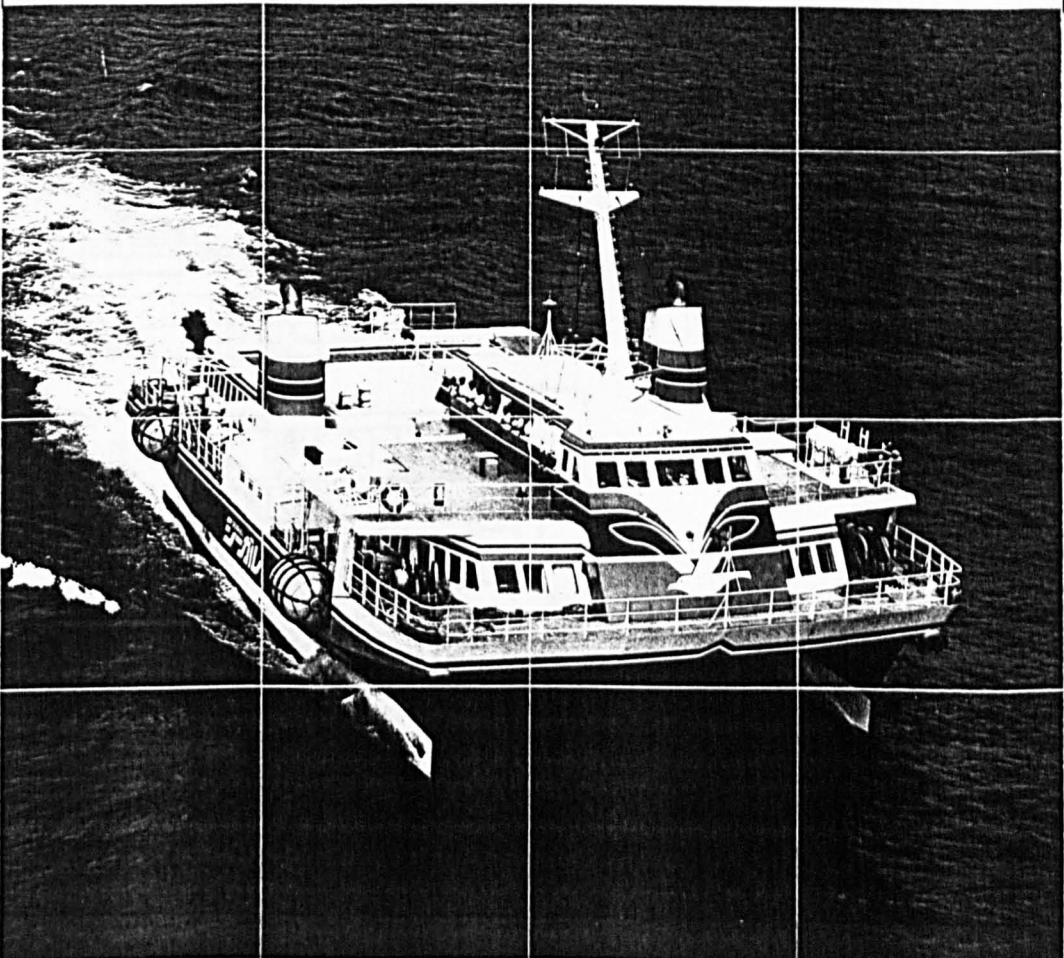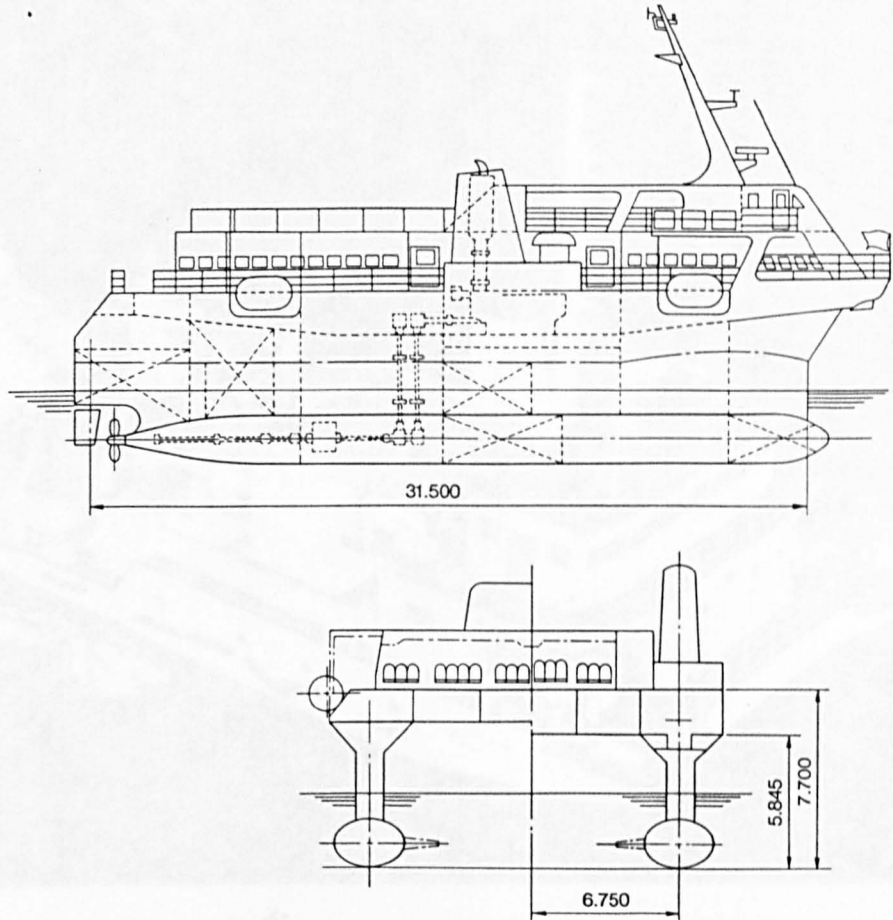
Fig. 1.8 The 'SEAGULL (MESA 80)' and its general arrangement plan
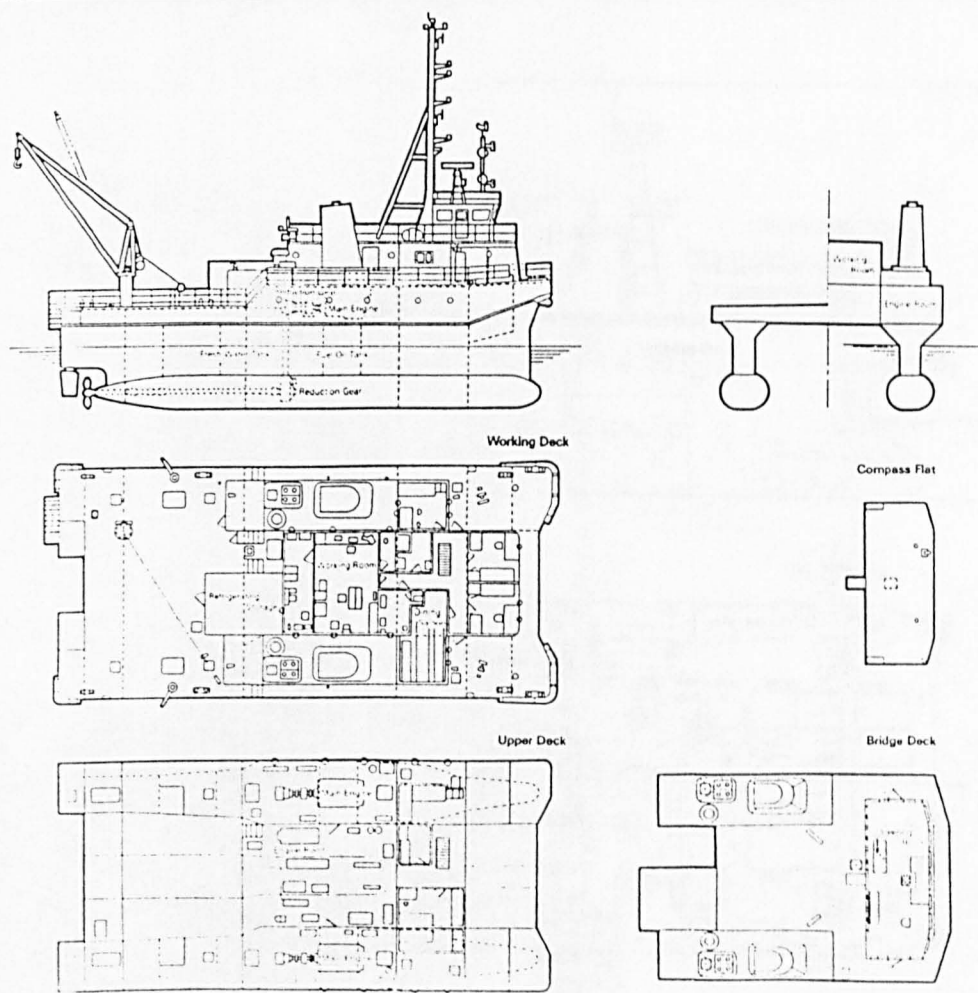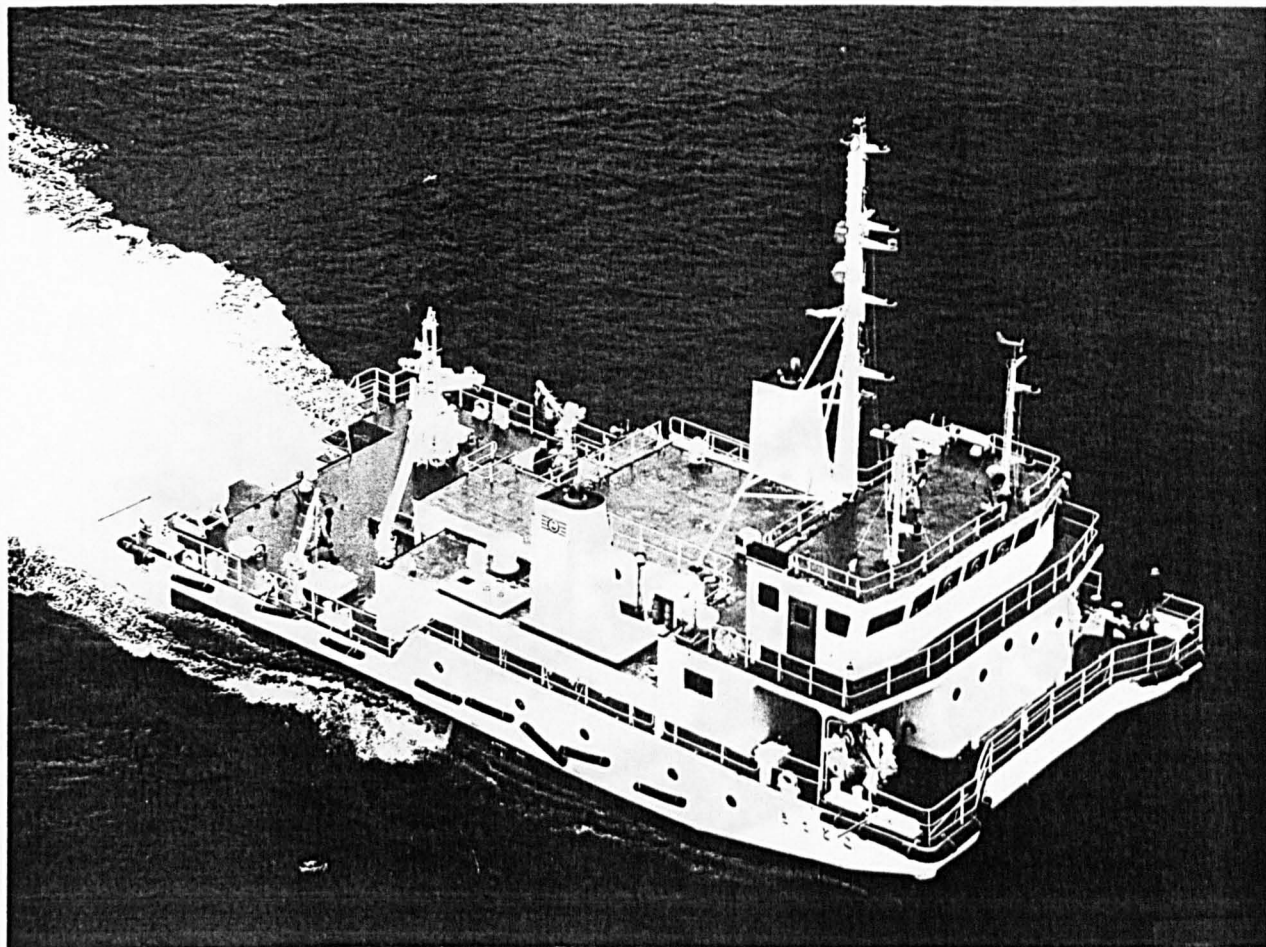
Fig. 1.9 The 'KOTOZAKI' and its general arrangement Plan
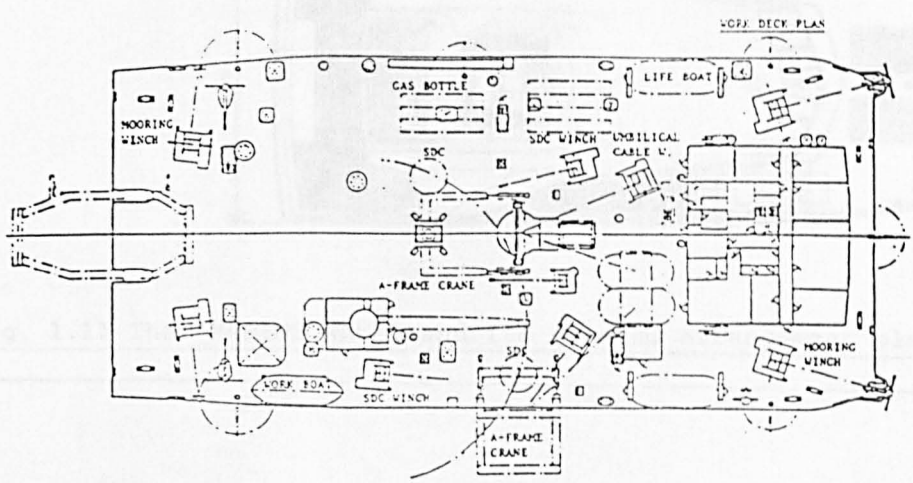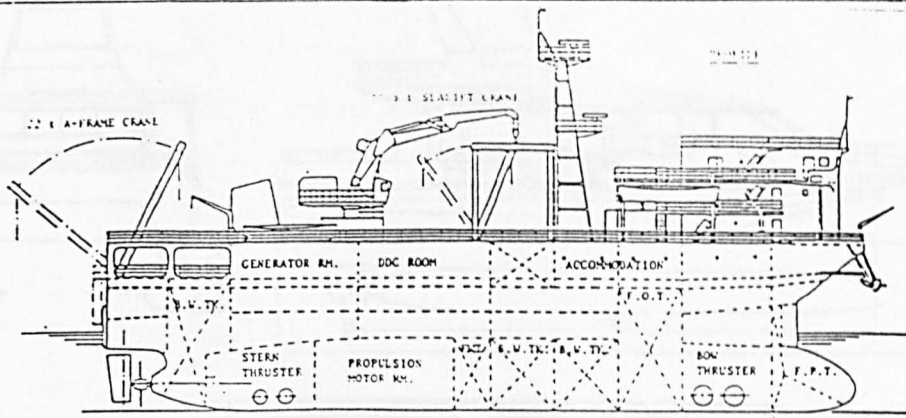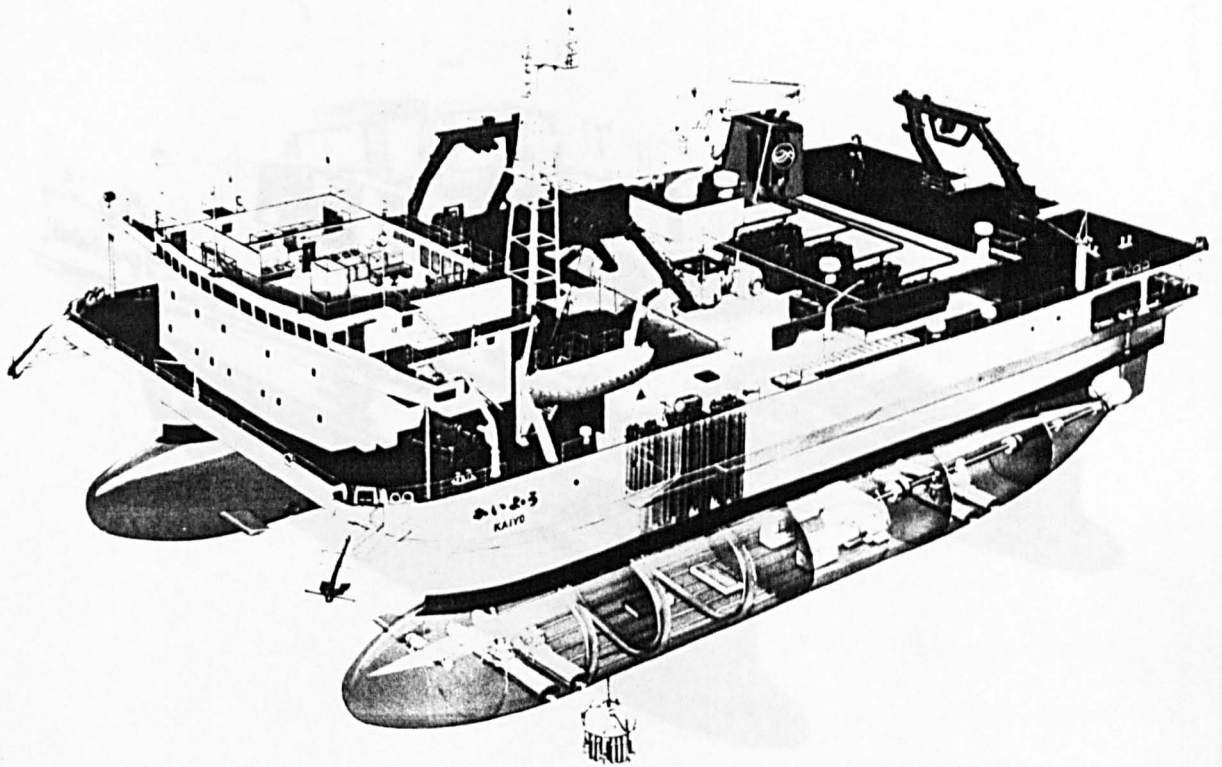
Fig. 1.10 The 'KAIYO' and its general arrangement plan
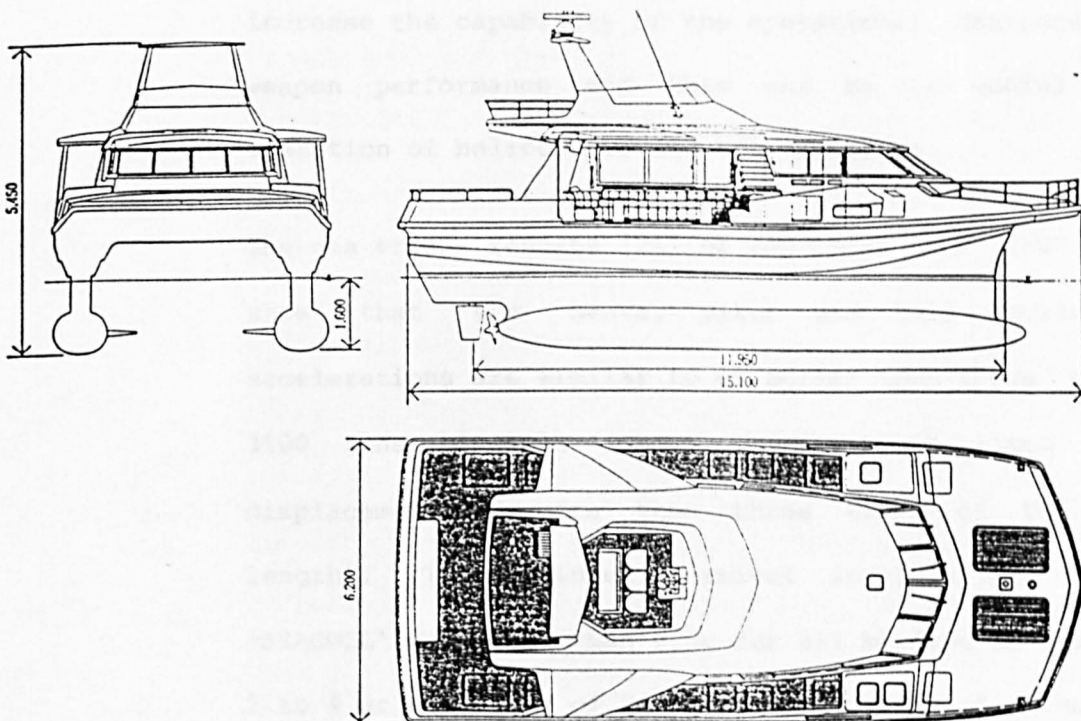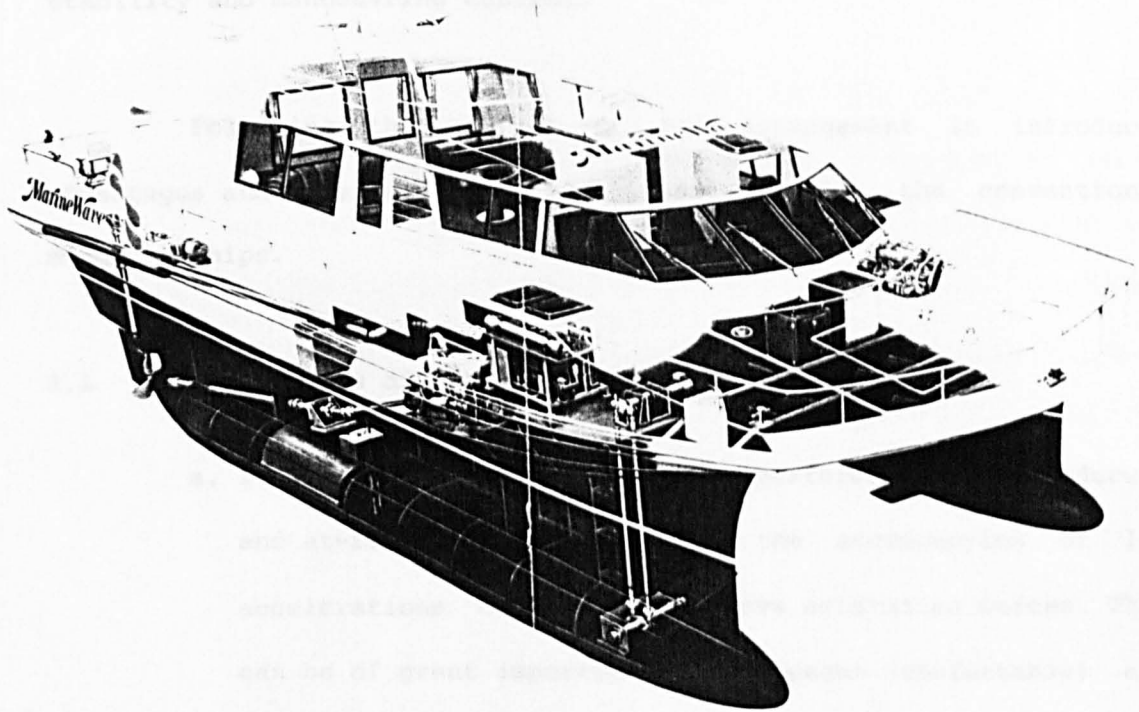
Fig. 1.11 The 'MARINE WAVE' and its general arrangement plan

semi-submersibles. The low waterplane area that results reduces the motions caused by wave-induced forces and the wide spacing of the demi hulls which provide the primary displacement, a high degree of stability and manoeuvring control.

Following the concept of the arrangement it introduces advantages and disadvantages in comparison with the conventional monohull ships.

3.1   The virtues of SWATH can be listed as follows:-

a. It can have very good motion performance, both underway and at-rest in head seas and the accompanying of low accelerations owing to the wave excitation forces. This can be of great importance to passenger (comfortable) and crew (better work on board) and in military terms can increase the capability of the operational equipment and weapon performance and this can be very useful in the operation of helicopters and VTOL aircraft.

The sea trials results [21] of the 'KAIMALINO' (220 tons) show that the heave, pitch and roll motions and accelerations are similar to or better than those of the 3100 tons monohull (which is about 15 times of the displacement and more than three times of the SWATH length). The measured vertical accelerations on the 'SEAGULL' were less than 0.1g for all heading in sea state 3 to 4 at the speed of 24 knots, while that of a monohull of comparable length was 0.6g in head seas [4]. In May 1985 [22], a prediction of motion characteristics was made for the comparison of four monohulls and two SWATHS, by a

range of operability including PTO (percent of time of operation) and LSWH (limiting significant wave height). The results confirmed the superior operability of SWATHS in a seaway.

b. With good design its speed loss in waves can be very low. It can combine the advantages of high speed such as can be achieved by plane boats, hovercraft and hydrofoil with the good seakeeping qualities of semi-submersibles. Therefore in rough seas it can maintain a reliable steady schedule and increase operational economy. As reported during the seakeeping trials of 'SEAGULL' [4], a speed loss of less than 2% in sea state 4 with 27 knots, while maintaining a superior comfortable ride in comparison to monohulls.

c. Its long heave, pitch and roll natural periods (the heave, pitch and roll natural periods are inversely proportional to the square roots of waterplane area, GM_L and GM_T respectively) avoids the occurrence of resonant conditions leading to longer motions and degraded operability for most wave conditions.

d. The spacious unobstructed deck area makes it particularly suitable for the operation of aircraft, helicopters and missiles, which has been proposed as replacements to virtually all types of warship [23]. The SWATH has been suggested as an assault ship [24], with the idea of lowering landing craft vertically into the sheltered water between her twin hulls and therefore it can be expected to play a major role in amphibious operations. The 'KAIMALINO' had been released [25] as the smallest ship in

the US Navy for full daylight air operations using a 5.8 ton helicopter in conditions up to sea state 4. The record showed that pitch, roll and heave during landing/take off at a speed of 13 knots were ±0.5 to ±0.7 degrees and ±0.3m respectively. In addition to take off and landing trials, the manoeuvring tests were performed with helicopters on board. No difficulty was encountered because the SWATH can maintain a level deck during turns.

e. The high degree of directional stability allowed the operator to have much less need to change headings in waves.

f. The deep immersion allows the efficient operation of sonar, sensor and measuring equipment, reduced cavitation and greater flexibility in propeller diameter selection.

Despite the research activity and the advantages of the SWATH concept as demonstrated so far, it is reasonable to ask why all ships today are not of the SWATH type? There is as yet no established commercial demand and although there is a keen naval interest at the research level, there has been no orders for SWATH warships. The virtues can on the other hand also yield certain drawbacks.

3.2   The drawbacks to the vessel compared to monohull are:-

a. It is more costly by virtue of the twin hull and high surface are involved. As shown in Table 1.1, all SWATH ships required a control surface system to attain dynamic pitch stability at higher speeds, which will increase costs. Its wetted surface can be about 60% more than

monohulls of the equivalent size, this can also increase in the powering requirements of the SWATH at low speed due to the greater frictional resistance and the added resistance caused by the control surfaces.

b. The motion characteristics are not very good in certain following sea conditions and, particularly for large single struts designs at at-rest in beam seas.

c. The relatively small waterplane area and short strut length results in a very low TPI (tons per inch immersion) and MTI (moment to change trim one inch) and therefore reduced hydrostatic pitch restoring moment. This also revealed that the SWATH is weight limited, requiring accurate weight and weight distribution control. The reduced TPI of SWATH designs results in a much greater draught change than would occur on an equal displacement monohull for a given change in weight. To substitute for the natural counteractive buoyancy inherent in conventional ships, submarine-type ballast compensation systems are necessary.

d. A number of practical features such as wider beam and deep draught which restrict the harbours, drydocks and channels to which they will have access.

e. Like a semi-submersible which has a larger cross-structure and draught, a SWATH ship built of steel will have a smaller payload to structural weight ratio in comparison with the equivalent monohull. This relatively low dead-weight/displacement ratio limits the SWATH making it unsuited for the carrying of heavy loads, especially if

the payload must be carried in or on the deck box. Although the ratio could be improved by using alluminium, GRP or other advanced composite materials to enhance payload capability, considerable attention must be afforded to efficient structural design, particularly at the hull-strut and strut-deck intersections.

f. The high directional stability, which resists manoeuvring of the SWATH ship. It may be expected to exhibit a higher high-speed turning diameter in relation to its length.

g. The lack of design data, owing to the small number of existing SWATH ships and the limited understanding of the high number of variables such as; shape of hulls, number of struts, shape of struts, above water clearance and the conventional parameters. A greater freedom in the SWATH design gives the designer more choice and consequently more difficulty compared with a conventional ship design.

4. THE SWATH GEOMETRY

The hull form, as well as number, shape and area of the struts and the position and size of the control surfaces dictate the SWATH design in order to yield good motion and minimum resistance characteristics.

The hull can be of a simple or a contoured form with a cross-section which may be circular, rectangular with round corners or ellipsoidal. The hull form with minimum wave force resistance can be obtained using a program based on the thin ship theory by applying Michell's source distribution for the conventional displacement ship.

A similar design method has been applied to semi-submerged catamarans [26]. The results depend on the Froude numbers for mostly contoured hull forms as shown in Reference [4]. In addition, Koop's experimental work [27] also confirmed that contoured hull form has lower resistance characteristics.

There is no doubt that the cross-section shape of the strut (the shape of the waterplane) should be designed as an airfoil shape or some streamlined shape which gives the lowest drag. One design aspect which is of particular importance is that of determining the number of struts per hull, ie the introduction of a gap in each side as opposed to a continuous strut on each side.

Lang [28] showed that the tandem strut has lower side loads at rest and a shorter turning radius, while the single strut may be simpler in construction. The gap between the struts may mitigate motions in beam seas at very low speed but at higher speeds the twin strut configuration tends to increase the wave making drag significantly, though wetted surface is lower than for a single strut per side.

From a manoeuvring standpoint, the choice of strut number and location affects the inherent directional stability of the design [29]. A twin strut design lends itself to the use of extended struts to place the rudder behind the propeller as in the case of the 'KAIMALINO'. A series of sea trials and mdel tests [4] pointed out that the tandem strut has longer natural heave and roll periods and greater resistance with considerable spray drag component at high speeds. It was also found that single strut givces a stiffer roll motion.

Strictly speaking, the comparisons between single and tandem strut strongly depend on the definition of the equivalent conditions. For example, in Reference [4], the waterplane area of the tandem is nearly one half the waterplane area of a single strut. The reduction in the waterplane area changes the restoring force and moment values and, consequently, this will alter the natural period values in heave, roll and pitch mode of oscillations affecting the restoring force. Auxiliary equipment, ballast tanks, etc, could also be placed in the struts. Therefore, for the designer, the selection will depend upon the particular applications.

5. THE SWATH VERTICAL PLANE MOTION

The SWATH ship at sea encounters excitation in six degrees of freedom of motion. Several reports on SWATH ship motion have been written, including that by Salvesen [30], Smith [31] which compare the motion of SWATH and mono-hulls. The nature of SWATH ship motions are focused on two distinct types of motions; one termed 'platforming' in which it is desired that the ship presents the appearance of a stable platform relative to an inertial reference, ie the minimum absolute motion is required. The other, is termed 'contouring', when rough seas are encountered.

Normally submerged parts such as propellers and sonar equaipment may tend to break the surface, or excessive slamming may occur, in which the ship should follow the contours of the waves and direct the ship to rise and fall with the general level of the sea. Because these two types of motions are sensitive in the vertical plane, and a ship with low vertical motions was part of the original

idea behind SWATH designs, the motions in the vertical plane, consisting essentially of pitching and heaving, are the principal concerns.

In the past few years, many theoretical predictions of ship motion have been developed. Most of these use the strip theory to evaluate the hydrodynamic coefficients with the motion of ships. The two-dimensional strip theory was initially put forward by Korvin-Kroukovsky et al [32,33] and typical applications are well described by Salvesen, Tuck and Faltinsen [34] and Kim [35] for the mono-hull ship under potential flow assumption.

The SWATH ship, being a geometric slender body (length/beam = 16.8 in this study) is believed suitable to apply the strip theory for the motion prediction although there are certain assumptions and limitations involved. One fundamental assumption is that when reducing the three-dimensional body to a summation of 2-D section in order to satisfy the free surface condition, the encounter frequency should be larger than the longitudinal gradient of body surface multiplied by the forward speed, $\omega \gg U(\frac{\partial}{\partial x})$, ie the frequency is assumed relatively high so that the wave created by the ship's oscillations should have a wave length of the order of ship beam rather than the ship length [34]. This assumption results in the inaccurate prediction of the hydrodynamic coefficients at the low frequency range, for example the sectional added mass becomes infinite as frequency approaches zero.

The limitation is that the prediction is generally pessimistic in short waves (high frequencies) at high speeds, particularly when the motions are affected by the interaction of

dynamic lift due to the fins and hull. However, generally the motions are very low at these frequencies and this is not a great problem. To overcome the weakness, some new theories are being developed.

Hong [36,37] (1982) utilised the unified slender body theory which was developed by Newman and Sclavounos [38] for the prediction of motions of high-speed SWATH ship in head and following seas. While two-dimensional theory was applied in the outer region of the hydrodynamic domain. At low frequencies, the added mass predicted by the slender-body theory is larger than those from strip theory and the damping is slightly less than for strip theory. These results were found to be in better agreement with the experiments. At high frequencies the results of strip theory and slender-body theory are almost the same. However, the wave exciting forces are found to be larger than those for strip theory and the theory seems only to be good for heave for a limited range of λ/L in following seas and, for pitch, the results are consistently worse than strip theory.

In fact, when we look back the uncoupled equation of motion in pitch mode, when frequency is very low ($\omega \approx 0.0$), the strip theory is not valid, even though A_{55} are very large, $\omega^2 A_{55}$ become very small. Consequently C_{55} becomes very important. Therefore, the vertical plane motions are dominated by hydrostatic restoring forces rather than the inaccurate predictions of hydrodynamic forces by strip theory.

In order to improve the theoretical technique at low frequencies, a careful treatment on the hydrostatic data such as C_{55} which involved the effects by the cross flow drag, body-lift, fin cross flow drag and lift curve slope would be rather important.

Therefore, within the practical frequency range in which we are interested, unless better theories have been developed, the two-dimensional flow strip theory is adequate for the prediction of ship motions of SWATH.

One of the areas where there was a lack of data at the time of commencement of this thesis was the design of control systems to reduce sinkage and trim at the higher speeds and to use the same system to reduce motion in waves. The trim which develops with forward speed is due to the MUNK moment and this must be corrected by a control surface or in wave conditions, the higher waves will continually strike the underside of the deck box at the forward end. Further it is desirable for the SWATH hulls to operate much nearer the water surface than would be normal for a semi-submersible in its operational conditions. This is to reduce draft and minimise wetted area which at the same time not imposing too large a penalty in terms of wave making resistence.

Apart from the need for a control system which will limit the SWATH's motions so that neither does the hull emerge nor the deck become immersed, the low hull immersion poses further problems in the theory of motion. The general principles of calculating the motions of semi-submersibles have been dealt with in a number of papers but it is generally assumed that the hulls are so deeply immersed that the added mass is independent of frequency and the columns are short compared to the hulls. Neither of these assumptions are valid for SWATHS and so there was a need to develop the motion theory to examine these factors in greater detail.

6.   LITERATURE SURVEY

Although the basic concept of having a small waterplane area is to try to reduce the wave exciting forces, the motion responses are not necessarily improve because the wave damping is also reduced. Also not enough pitch restoring moments can be generated to counteract the destabilising Munk moment [39]. However, this allows the SWATH ship to be more responsive to the forces generated by control surfaces than a conventional mono-hull ship in order to ensure the dynamic stability and to reduce the motions.

Research on ship motion reduction with control surface began in 1945 with Allan [40] and continued in 1969 with Conolly [41] and Lloyd [42]. Active stabilisers have been fitted to reduce rolling for conventional warships and many high speed merchant ships.

In 1959, a theoretical analysis backed by model experimental work on the reduction of the pitch motion of conventional mono-hull ships by anti-pitching fins at the bow was presented by Abkowitz [43]. The results showed that pitch motion can be reduced to 50% by using a reasonable area of anti-pitching fins. (Area of 7%, 7.2% and 4.7% of the waterplane area were required for a modern single-screw cargo ship (series 60, C_b = 0.6), a destroyer and an aircraft carrier respectively). The concept of activated anti-heaving, anti-pitching fins in which the controls can be made sensitive or proportional (with or without time lag) to the displacement (angle), (angular) velocity or (angular) acceleration was discussed in detail. Matsui [44] (1966) reported that the active control anti-pitching fin for a small passenger ship can reduce pitching completely at some wave-length, the

added mass effect of fins was neglected in the study.

In 1967, Vugts [45] gave another analytical and model experiment investigation on anti-pitch and heave fins with both fixed and variable control bow fins for a series 60 general cargo ship. The activated fins were controlled by a non-linear feedback signal of the pitch velocity. The results show a pitch reduction of about 30%, while the heaving was not changed significantly. The additional advantage of activated over fixed fins was very slight. Only bow fins have been considered for almost all the studies of pitch reduction of conventional mono-hull vessels. This is because of the greater angles of attack at the bow and a longer distance from LCG and the phase relation between the motions and wave. Moreover aft fins may be influenced by the boundary layer and affect the propeller performance. Also the dynamical response to the slamming which would accompany the large amount of bow emergence. Bow fins are therefore considered to be much more effective than the after fin.

It was not until 1963, that the first study of control for a semi-submarine was reported by Jonckheere [46]. Fins were utilised to control heave and pitch for regular following seas and the position of anti-pitching fins was suggested at the stern, were the lift works in the direction opposite to the pitching angle. The positions of anti-heaving fin was suggested to be near the LCG. This prevents the effect of the anti-pitching fin being anullified by the anti-heaving fins. The fin size was 2.5% of the waterplane area. Several control systems had been tried and it was found difficult to control heave and pitch at low speed in long waves. It was also found that cavitation decreased the lift coefficient at speeds above 25 knots.

Following the initial efforts of Lee, based on the theoretical analysis for Catamarans and SWATHS [47,48,49], a considerable amount of study has been devoted to SWATH motion with fin control during the last ten years [50,56]. Most studies used frequency domain motion equations or state-space optimal control techniques. Some of the model time simulations or full scale tests [4,57,58] claimed that vertical motion can be significantly reduced. An automatic controller such as that discussed by British Marine Technology [56] allows the ship to contour the waves in very high sea states or in following seas and maintaining platforming behaviour in other wave conditions so that the all round seakeeping performance is much improved.

The purpose of this thesis is to try and clarify the design problems associated with the understanding of the sinkage and trim of the vessel when at speed and the control of its motion in waves. A review has been carried out of the hydrodynamic theory of SWATH motions (chapter 2) and particular attention has been devoted to certain aspects.

a. Added mass and damping data have been produced to cover a practical range of frequency, depth of submergence and column width ratio. The effects of these factors has been discussed and approximate formulae are developed by using a curve-fitting technique. These sectional added mass and damping data are expressed as a function of the variable factors. An easy way to interpolate the potential flow added mass and damping coefficients for the circular hull and rectangular strut combination sections is presented.

b. Viscous effects have been examined in detail and their

effects were formulated in various ways. The incompressible aerodynamics of viscous cross-flow about a missile (slender) body are utilised, a lift-curve slope which is significant at low incident angle and a cross-flow coefficient which is significant at higher incidences are discussed.

c. A theory and design procedure has been produced for fin control surfaces, these may be at the aft end only or aft and forward. The required fin size was determined based on the coupled vertical plane equations of motion and the Routh stability criteria for dynamic stability.

d. An analytical technique based on the beamwise strip method for prediction of the vertical wave exciting forces as well as the coupled motion in regular head seas is presented. The sectional diffraction and radiation problems were solved using the Frank Close-fit or source distribution method. The predictions were performed on the bare hull assuming small amplitude motions with zero forward seed. This was further extended to include forward speed, viscous damping and the hydrodynamic effects induced by fins.

e. Another theoretical approach based on the Morison's formula has been utilised to calculate the wave exciting heave force and pitch moment. In this approach, the vertical and horizontal pressure, inertia and velocity forces acting on the hull and struts were summed to yield heave forces and pitch moments in the frequency domain at zero speed.

f. A series of model experiments were undertaken, involving the measurement of dynamic stability, trim and sinkage, heave and pitch motion responses both with and without after fins at zero and forward speeds. Aft fins were set at several fixed fin angles and the model tests repeated in head and following seas.

g. The investigation of the motion responses and the effects of fins and fin angle from the experimental results are discussed and are compared with the analytical calculations as given in chapter 5. Good agreement confirms the accuracy of the studies.

h. The outlined approach is intended primarily for SWATH ships. It is believed that the prediction capability can be extended to cover other conventional slender mono or multi-hulled configurations, catamarans and some semi-submersibles with regular cross-sections.

The computer program development started on a PDP 11/40 minicomputer and later continued on a VAX 11/730 system in the Hydrodynamics Laboratory at the University of Glasgow after the transfer of the developed program from the PDP 11/40. Although only vertical plane motion responses were programmed, the methods can be extended for other modes of motion without diffculty.

Initially, this study was aimed at carrying out both theoretical and experimental investigations on automatic fin control by applying optimal control techniques. However, as a result of the time limitation and lack of technical back-up it was not possible to carry out the task.

CHAPTER
2

Formulation

of

The Problem

CHAPTER 2

GENERAL FORMULATION OF THE PROBLEM

1.   THE CONCEPT OF THE FLUID FORCES ACTING ON A SWATH SHIP IN
      WAVES

The fluid forces acting on a SWATH ship as shown in figure 2.1 can be divided into components and are explained as follows. The external oscillatory forces can be divided into wave-induced and motion-induced reaction forces. The motion-induced reaction forces consist of three components:-

    a. hydrostatic buoyancy force F_C.

    b. velocity induced force F_B.

    c. acceleration force F_A.

The buoyancy force is caused by the changes in the immersed buoyant volume, which always tend to bring the ship back to its equilibrium position. Since the hydrostatic pressure remains unchanged regardless of the state of water motion, these restoring forces and moments are directly proportional to the still water draft and are independently treated.

The velocity induced force which provides the damping in the system has two components:-

    a. A wave making component due to the inertial motion of the struts and the hulls if they are near the surface.

    b. A viscosity induced force which is proportional to the square of the velocity but is commonly treated in a

FLUID OSCILLATORY FORCES

Potential Flow

Real Flow

Force due to Water Pressure
(Hydromechanical Force)

Force due to Viscosity
(Viscous Damping Force)

Hydrostatic Force
(Restoring Force)
F_C

Hydrodynamic
Force

Due to Body-
Motion-Induced
Fluid motion

Due to Wave-
Induced Fluid
Motion

Body Motion-Induced
Force (Radiation
Force)
F_R

Wave-Induced Force
(Wave-Exciting
Force)
F_W

Inertial Force
due to
Added Mass
F_A

Velocity Force
due to
Wavemaking
Damping
F_B

Incident Wave
Force (Froude-
Krylov Force)
F_I

Diffracted Wave
Force
F_D

Fig. 2.1 Concept of Fluid Forces in Waves

linearised manner. This linearisation will be discussed in greater detail later. A SWATH ship, due to its slim wall-side struts, does not generate large surface waves when it oscillates in the vertical plane. The wave making damping is relatively small compared with a conventional displacement ship and the viscous damping tends to dominate and have to be taken into account.

The acceleration induced from which standard textbooks show to be equal to the added virtual mass of the structure times the acceleration.

The wave-induced exciting forces consists of the Froude-Krylov force F_I, which is caused by the hydrodynamic pressure of the incident waves as they pass the hull assuming they are undisturbed by the presence of the hull and a diffraction component F_D, which results from the disturbance of the wave pressure field due to the presence of the hull.

If the motion displacement is S, the above components of force can be expressed as:-

Inertial force	$F_A = - a\ddot{S}$	
Damping force	$F_B = - b\dot{S}$	
Restoring force	$F_C = - CS$	
Wave exciting force	$F_W = (F_I + F_D) e^{-i\omega t}$	

and following Newton's second law, the forces equilibrium equation is:-

$$M\ddot{S} = F_W + F_A + F_B + F_C \qquad (2-1)$$

or

$$(M + a) \ddot{S} + b\dot{S} + CS = F_W \qquad (2-2)$$

2.   THE EQUATION OF MOTION IN REGULAR WAVES

In general the SWATH ship, similar to a conventional ship, experiences six degrees of freedom of motion in an actual seaway, three translatory displacements and three angular displacements. Under the assumptions that the responses are linear and harmonic, the six linear coupled differential equations of motion can be written as:-

$$\sum_{k=1}^{6} (M_{jk} + A_{jk})\ddot{S}_k + B_{jk}\dot{S}_k + C_{jk}S_k = F_j e^{-i\omega t} \quad j=1,\ldots6 \quad (2-3)$$

where M_{jk} is   the   mass   matrix   containing the mass, mass moment and mass moment of inertia of the body.

A_{jk} is the added mass, added mass moment and added mass moment of inertia matrix.

k   is the mode of motion, (1, 2, 3 for surge, sway, heave translatory displacement 4, 5, 6 for roll, pitch, yaw rotational motion).

j   is the mode of excitation and take the same value as   for the corresponding modes.

B_{jk} is the matrix of damping coefficients

C_{jk} is the matrix of hydrostatic restoring coefficients.

F_j is the complex amplitudes of the exciting force and moment.

ω is the frequency of encounter and is the same as the frequency of motion response.

$S_k, \dot{S}_k, \ddot{S}_k$ are the linear or angular complex displacement, velocity and   acceleration of the ship from its mean position in the kth mode.

2.1   Vertical-Plane Equations of Motion

For a SWATH ship, the symmetry of the hulls with respect to the longitudinal centreplane of twin hulls leads to the decoupling of the vertical-plane modes (surge, heave and pitch) from the horizontal-plane modes (sway, roll and yaw). Therefore, the equations of motion can be divided into two groups, as mentioned in the previous section, because of the special missions requirements of SWATH (especially for military purposes). The vertical velocity and acceleration at the flight deck or helicopter pad are important factors governing the aircraft landing and take-off operations. Further, deck wetness, slamming, propeller and rudder emergence phenomena for a high speed craft such as SWATH are also related to the vertical plane motion. In addition, the model test investigation in the vertical plane motion can be easily carried out in a towing tank. Thus, in this study, special attention has been focused on the vertical-plane motions.

For the vertical plane motion of a SWATH using the long slender hull assumption, the hydrodynamic forces of the surge mode are assumed negligibly small and, therefore, the theoretical predictions with strip theory described in section 3.3 of this chapter, which would normally involve three coupled equations of motion for surge, heave and pitch are reduced to two coupled equations for heave and pitch. However, during the model tests carried out in following seas, it was found that considerably large surge motion along with pitching was observed. Also, in section 3.2 the calculation showed that the horizontal surge force components from struts and from the hull influenced the pitching moment because of the vertical centre of gravity of the model being far away from the longitudinal axis of the

main hull. Therefore, in lower encounter frequencies, particularly in following and stern-quartering seas, the coupling between surge and pitch does not appear to be negligible for SWATH-type ships. However, another important point, as Salvesen et al mentioned [34], arises when the strip theory approach is employed to represent three-dimensional SWATH geometry by a series of two-dimensional sections it must be assumed that the encounter frequency is relatively high. This means the waves generated by the ship's oscillations should have a shorter wave length of the order of ship beam rather than the ship length. This is also a critical assumption for a SWATH ship, because it has low natural frequencies in pitch and heave and hence, the peak motions occur in the long wave region. However, this can be proved to be less significant when an analogy is made between the mass-dashpot-spring system and the oscillation of a SWATH ship in vertical plane. That is to say, the inertia force dominates at the higher frequencies, while the spring force (equivalent to hydrostatic force) dominates at the lower frequencies. Consequently, the inaccurate estimation of the hydrodynamic coefficients at the lower frequencies are expected to have a minor effect on the motion prediction.

The coupled equations of vertical plane motion may be written as:-

$$(M + A_{33})\ddot{S}_3 + B_{33}\dot{S}_3 + C_{33}S_3 + A_{35}\ddot{S}_5 + B_{35}\dot{S}_5 + C_{35}S_5 = E_3 e^{-i\omega t} \quad (2-4)$$

$$(I_5 + A_{55})\ddot{S}_5 + B_{55}\dot{S}_5 + C_{55}S_5 + A_{53}\ddot{S}_3 + B_{53}\dot{S}_3 + C_{53}S_3 = E_5 e^{-i\omega t} \quad (2-5)$$

where S_3 is the heave motion

and S_5 is the pitch motion

Since F_3, F_5 are complex, the resulting motion displacement S_3 and S_5 are also assumed to be complex and given by:-

$$S_3 = \bar{S}_3 e^{-i\omega t} \qquad (2\text{-}6)$$

and

$$S_5 = \bar{S}_5 e^{-i\omega t} \qquad (2\text{-}7)$$

where $\bar{S}_3$, $\bar{S}_5$ are complex heave and pitch amplitudes:-

$$\bar{S}_3 = S_{3R} + iS_{3I} \qquad (2\text{-}8)$$

and

$$\bar{S}_5 = S_{5R} + iS_{5I} \qquad (2\text{-}9)$$

The amplitudes (maximum) of the heave and pitch motions are found by:-

$$\left|\bar{S}_3\right| = (S_{3R}^2 + S_{3I}^2)^{\frac{1}{2}} \qquad (2\text{-}10)$$

and

$$\left|\bar{S}_5\right| = (S_{5R}^2 + S_{5I}^2)^{\frac{1}{2}} \qquad (2\text{-}11)$$

The phases of the maximum motion amplitude relative to the maximum of the incident wave at the origin of the co-ordinate system are:-

$$\tan^{-1}\left(\frac{S_{3I}}{S_{3R}}\right) \qquad (2\text{-}12)$$

and

$$\tan^{-1}\left(\frac{S_{5I}}{S_{5R}}\right) \qquad (2\text{-}13)$$

Take the real part of equations (2-6) to (2-9):-

$$S_3 = S_{3R}\cos\omega t + S_{3I}\sin\omega t \qquad (2\text{-}14)$$

and

$$S_5 = S_{5R}\cos\omega t + S_{5I}\sin\omega t \qquad (2\text{-}15)$$

Similarly, the complex F_3 and F_5 may be written as:-

$$F_3 = F_{3R} \cos\omega t + F_{3I} \sin\omega t \qquad (2-16)$$

and

$$F_5 = F_{5R} \cos\omega t + F_{5I} \sin\omega t \qquad (2-17)$$

3.   WAVE-EXCITING FORCES/MOMENTS ON SWATH BARE HULL

3.1.   Introduction

The concept of a SWATH type ship has similar geometry to a semi-submersible but the essential difference between the SWATH and a semi-submersible is that the former is designed to be propelled at speed through waves, whereas the latter tends to operate in a stationary mode or at low speeds. Thus, the geometry of the SWATH is largely dictated by the need to have low resistance to forward motion. To this end, the columns and any bracing are made of airfoil sections and low drag hulls must be used. Because of the change in column geometry, the more variable shape of the hull and the effects of forward speed, the majority of computer programs developed for semi-submersibles cannot be applied directly to SWATHs.

The main objective of this section is to describe the methods developed to calculate the wave exciting heave force and pitching moment in small amplitude regular sinusoidal waves for a SWATH ship composed of a circular bare hull with tapered endings and airfoil struts. The first approach uses the potential flow theory for small bodies with modifications to include viscosity effects (Morison approach).

The heave forces are calculated by integrating the vertical

section force due to pressure, inertia and velocity force components and the effect of the struts (columns) on the hull pressure forces were taken into account. The vertical centre of gravity was located at a position close to the water line level. The horizontal forces acting on the struts and hulls could affect the pitch motion prediction and, therefore, the calculation included the exciting force in the horizontal direction.

The second analytical method was based on strip theory. The technique involves distributing two-dimensional pulsating sources on the boundary of transverse strip sections along the hull and including strut sections where struts intersect the hull by using the Green's function integral equation method, ie the Frank close-fit technique [59].

Linearised potential theory was used to evaluate the wave exciting forces. The SWATH ship was split into 21 non-equally spaced beamwise strips along its length for applying the strip theory approach. The incident wave and diffraction potential are combined to obtain the sectional wave exciting forces and the phase angles.

3.2.   The First Theoretical Approach - 'Morison's Formula'

This section outlines the main aspects of the theoretical approach to heave, surge and pitch motion prediction for a circular hull SWATH with two airfoil type struts per hull.

The total force [60] acting on the body is assumed to be due to the waves and the following effects were considered:-

a. The Froude-Krylov force, which results from the variation in pressure due to the passage of the wave.

b. The inertia force, due to the effect of the acceleration of the particles with the wave on the mass and added virtual mass of the body [62].

c. The velocity force, which is the viscous pressure effect arising from the velocity of the wave particles.

The equation of the wave surface was taken as:-

$$h_w = a_0 \cos k(x - c_w t) \qquad (2\text{-}18)$$

where k is the wave number

c_w is the wave celerity

a_0 is the wave amplitude

and   t is the time

and, using the wave velocity potential expression, the following may be obtained:-

$$\text{horizontal water velocity } U = c_w k a_0 e^{-kz} \cos k(x - c_w t) \qquad (2\text{-}19)$$

$$\text{vertical water velocity } V = c_w k a_0 e^{-kz} \sin k(x - c_w t) \qquad (2\text{-}20)$$

$$\text{horizontal acceleration } A = k g a_0 e^{-kz} \sin k(x - c_w t) \qquad (2\text{-}21)$$

$$\text{vertical acceleration } A = -k g a_0 e^{-kz} \cos k(x - c_w t) \qquad (2\text{-}22)$$

$$\text{dynamic pressure } p = a_0 \rho g e^{-kz} \cos k(x - c_w t) \qquad (2\text{-}23)$$

where ρ is the water density, and g is the acceleration due to gravity. The wave co-ordinate system is shown in fig. 2.2.

3.2.1 The vertical hull pressure force

At depth Z below the still water surface, the dynamic pressure is:-

$$\rho g a_o e^{-kZ} \cos k(x-c_W t) \qquad (2-24)$$

and the vertical pressure force per unit length of circular hull is to a first order approximation.

$$- \rho g a_o k \pi R^2 e^{-kH} \cos k(x-c_W t) \qquad (2-25)$$

where R is the radius of the cross-section of circular hull and H is the depth to the centr,line of the hull.

The approximation only becomes significant when the hull diameter is greater than one fifth of the wave length.

The magnitude and direction of this force is governed by the change of pressure on the upper half of the circular hull since, due to the exponential effect, the pressure change on the lower half is always smaller. In the wave crest $\cos k(x-c_W t) = 1$ and the force is in the downward direction, while in the trough the force is upward.

3.2.2 The vertical hull inertia force

For circular hulls the vertical inertia force per unit length is (to a first order approximation):-

$$\rho C_V \pi R^2 [-kga_o e^{-kH} \cos k(x-c_W t)] \qquad (2-26)$$

which is equal to the pressure force. Hence, the combined vertical

inertia and pressure forces on the hull may be written as:-

$$\int_{-L/2}^{L/2} - \rho g a_o (1 + C_V) . \pi R^2 . k . e^{-kH} \cos k(X - c_W t) dx \qquad (2-27)$$

where C_V is the added mass coefficient for each hull and strut combined cross-section, as calculated from Reference [62].

In Reference [62], the author obtained the variation of C_V with depth of immersion, frequency, hull spacing and strut thickness but for circular sections some further variations with Reynolds Number, Keulegan-Carpenter Number ($K_C = \frac{UT}{D}$) and roughness is possible but has not been taken into account.

3.2.3   The vertical hull velocity force

The vertical velocity force acting on a circular hull was obtained from the expression:-

$$\tfrac{1}{2}\rho . C_D . A . V^2$$

$$= \tfrac{1}{2}\rho C_D (2R) dx \; k^2 \; a_o^2 \; c_W^2 \; e^{-2kH} \left| \sin k(x - c_W t) \right| \sin k(x - c_W t) \quad (2-28)$$

where C_D is the drag coefficient and is independent on Reynolds Number, Keulegan-Carpenter Number and roughness and A is the projected area of the hull in the horizontal plane.

3.2.4.   The effect of the struts (columns) on the hull pressure forces

When calculating the pressure force on the circular hull, as shown in Section 3.2.1, the effect of the areas covered up by the strut bases must be corrected as follows.

The pressure forces acting on the strut base was determined by considering a small element of hull and strut, as shown in fig. 2.3.

The vertical pressure force acting may be obtained using the expression:-

$$-\int_{-0}^{2\pi} \rho g a_0 e^{-k(H-R\sin\theta)} \cos k(x - c_w t)(Rd\theta\sin\theta\,dx)$$

$$-\int_{\frac{\pi}{2}-\alpha}^{\frac{\pi}{2}+\alpha} - \rho g a_0 e^{-k(H-R\sin\theta)} \cos k(x - c_w t)(Rd\theta\sin\theta\,dx) \quad (2-29)$$

$$= - \rho g a_0 R e^{-kH} \cos k(x - c_w t)dx[\underbrace{\pi kR\ (1 + \frac{1}{8}k^2R^2+ \ .....)}_{(I)}$$

$$(2-30)$$

$$\underbrace{- \{2\sin\alpha + kR(\alpha - \sin\alpha\cos\alpha)\}]}_{(II)}$$

where   H is the distance between still water and the hull centre,

   HST is the half-strut thickness

   α is the section angle subtending the strut base, which is equal to:-

$$\sin^{-1}(\frac{HST}{R})$$

Considering equation (2-30), the first term in the square brackets is for a circular section without the strut, while the second term is the effect of the pressure force from the area covered up by the strut base. This force is always opposed to the direction of the pressure force on the hull and can be written as:-
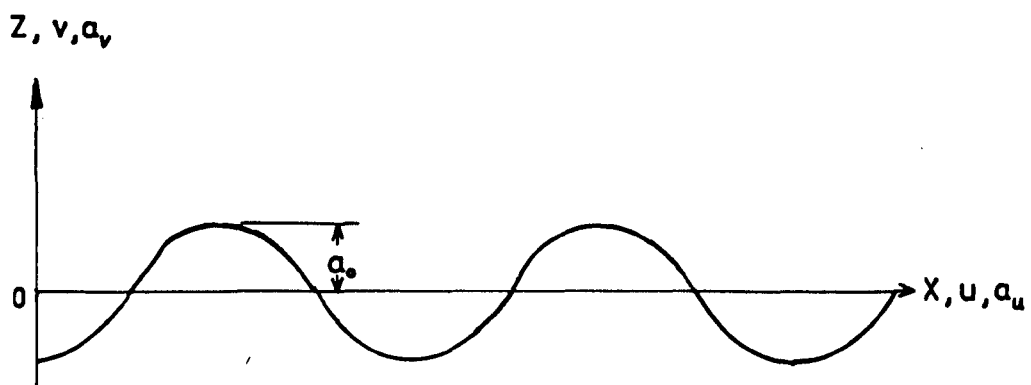
Fig. 2.2
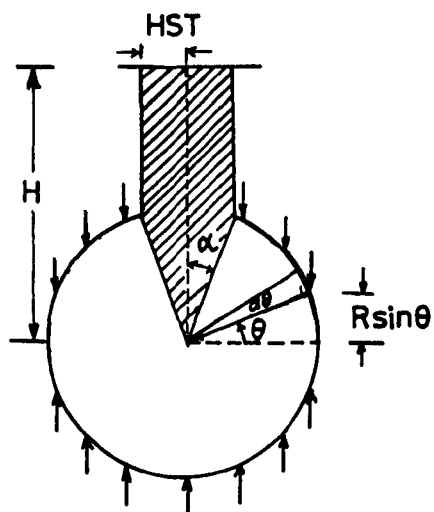
Fig. 2.3

$$\rho g a_o e^{-kH} R \cos k(x - c_w t)(2\sin\alpha + kR(\alpha - \sin\alpha\cos\alpha)) \qquad (2\text{-}31)$$

It may be deduced from the equation that if there is no strut on the hull section, then HST = 0.0 and α = 0.0, ie there is no strut pressure force effect.

The total heave exciting force acting on both hulls was obtained by integrating the various force components acting at the hull stations along their length. Since parts of the structure have tapering circular section members, numerical integration using Simpson's rule was applied.

3.2.5   The horizontal exciting force [60,61]

The total horizontal force was treated by subdividing it into five parts:-

    a. the horizontal pressure force on the struts

    b. the horizontal velocity force on the struts

    c. the horizontal inertial force on the struts

    d. the horizontal pressure force on the hulls

    e. the horizontal inertial force on the hulls

which are detailed in the following sections.

3.2.6   The horizontal pressure force on the struts

The horizontal pressure on the struts was determined by dividing the immersed depth (to the wave surface) of the strut into five stations in the direction of the Z-axis and dividing the airfoil cross-section at each of the five stations into nine stations in the

direction of the Y-axis, fig. 2.4. The net resultant fore and aft pressure forces acting on each strip or section station were integrated over the strut thickness to obtain the total pressure force acting on the cross-section, accounting for the vertical location of each strip or section station relative to the wave profile and axis origin. The horizontal strut pressure force per hull (two struts) is:-

$$\rho g a_o [e^{-kZL1} sink(XL1 - c_w t) - e^{-kZR1} sink(XR1 - c_w t)$$

$$(2-32)$$

$$+ e^{-kZL2} sink(XL2 - c_w t) - e^{-kZR2} sink(XR2 - c_w t)]$$

where XR1, XL1 are the longitudinal distances of the forward and aft section station ends, respectively, from the axis origin for strut 1.

XR2, XL2 are the longitudinal distances of the forward and aft section station ends, respectively, from the axis origin for strut 2 and

ZR1, ZL1, ZR2 and ZL2 are the vertical distances of the forward and aft section stations, respectively, of strut 1 and strut 2, below the wave profile as shown in fig. 2.4.

The total horizontal pressure force acting on the strut was then obtained by integrating in the vertical direction the five sets of forces determined at the horizontal sections.

3.2.7   The horizontal velocity force on the struts

The calculation of the horizontal velocity force on the struts was performed and integrated using the same procedure as used

to determine the pressure force in section 3.2.6. The equation is:-

$$\tfrac{1}{2}\rho ga_o^2 . C_D . k . 2TYY(5) [e^{-2kZL1} |cosk(XL1 - c_w t)| cosk(XL1 - c_w t)$$

$$- e^{-2kZR1} |cosk(XR1 - c_w t)| cosk(XR1 - c_w t) + e^{-2kZL2} |cosk(XL2 - c_w t)|$$

$$cosk(XL2 - c_w t) - e^{-2kZR2} |cosk(XR2 - c_w t)| cosk(XR2 - c_w t)] \qquad (2-33)$$

where TYY (5) is the max half-beam of the Z strut section, as shown in fig. 2.6 and a constant C_D appropriate to the strut section is used.

3.2.8   The horizontal inertia force on the struts

The horizontal inertia force on the struts was calculated by the equation:-

$$\rho ga_o k\pi (TYY(5))^2 C_V [e^{-kH1} sink(- x_c - c_w t) + e^{-kH2} sink(x_c - c_w t)] \qquad (2-34)$$

where H1 and H2 are the depths to the free surface measured from the centres of strut 1 and strut 2, respectively, fig. 2.5. The added mass coefficient of the strut cross-section in surge C_V was calculated by the Frank Close-fit method for the heave case, with the depth of submergence equal to ten times the depth of the strut section, fig. 2.6, and x_c is the distance from origin to the centre of the strut, fig. 2.5. This neglects free surface effects which may be important in this case but which cannot be tested properly by the theory.

3.2.9   The horizontal pressure forces on the hull

The horizontal pressure force acting on the hulls was treated in a similar manner to that of the struts, described in the previous section. The hull (circular section) was cut into nine sections in the
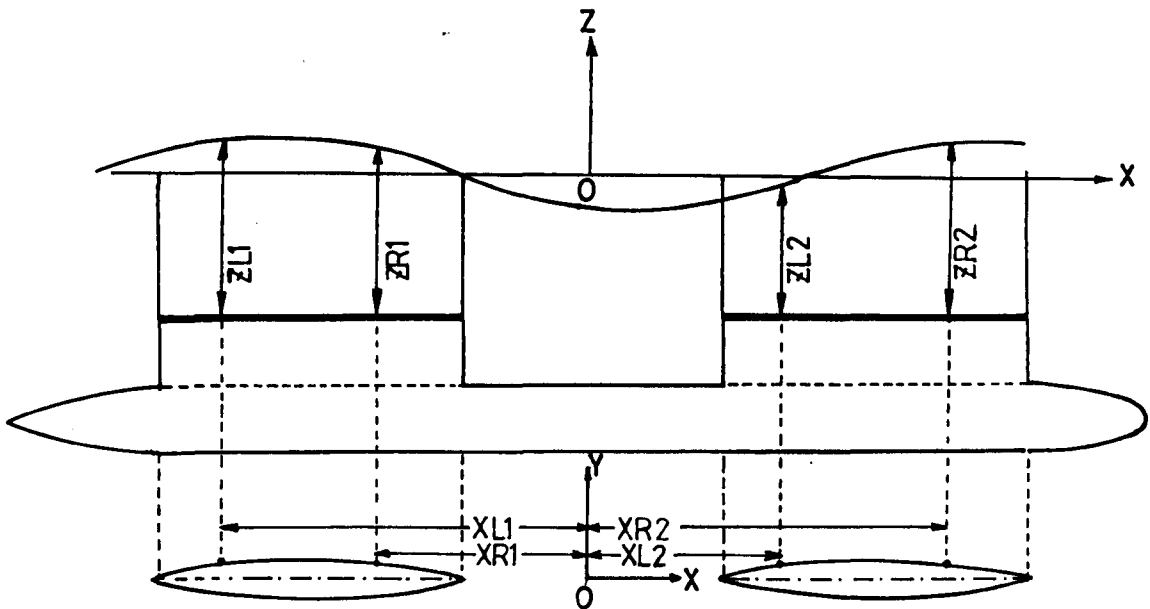
Fig. 2.4
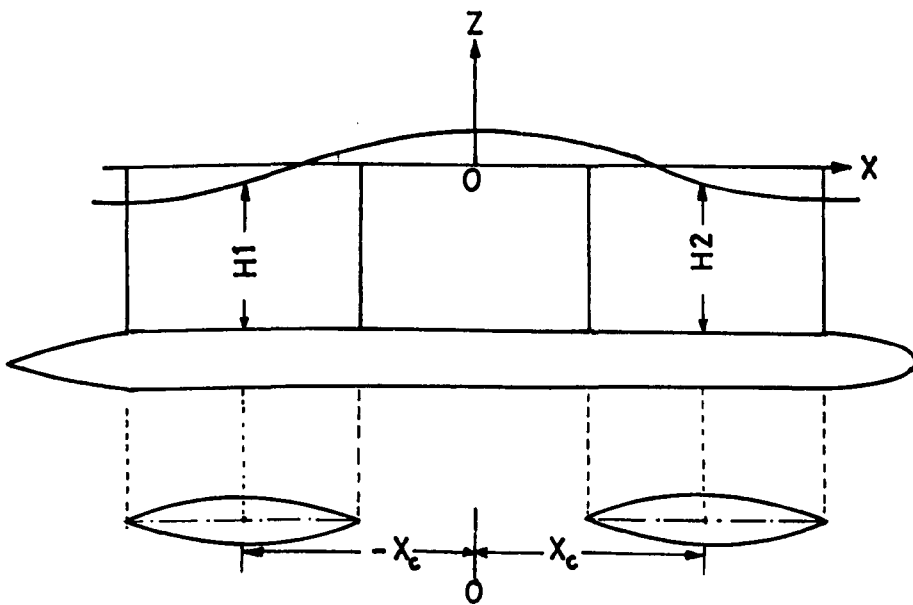
Fig. 2.5
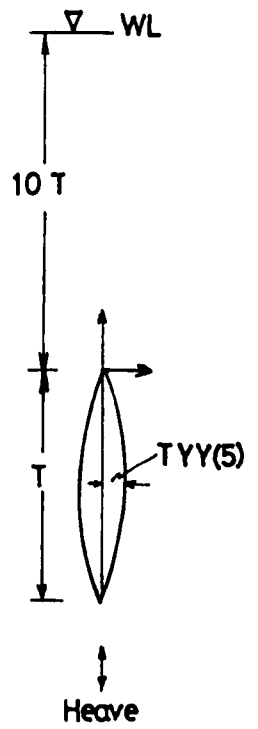
Fig. 2.6

vertical Z-direction and each section into nine stations along the transverse Y-direction.

The net longitudinal pressure force acting on each station was integrated along the Y-direction first and then integrated along the Z-direction (vertically) to obtain the total as shown in fig. 2.4. The equation used to obtain the pressure force was:-

$$ga_o e^{-kZ(I)} (cosk(-x_L - c_W t) - cosk(x_R - c_W t)) \qquad (2-35)$$

where $Z(I)$ is the vertical distance from the considered Z-plane station I to the still water plane and x_L is the distance of each station on the aft position of the plane to the origin, while x_R is the distance of each station on the forward position of the plane to the origin, as shown in fig. 2.7.

3.2.10 The horizontal inertial force acting on the hull

The horizontal inertia force on the hull was calculated by approximating the hull added mass by that of a prolate ellipsoid. The added mass of entrained liquid in the surge mode is:-

$$K_2 \cdot (\frac{4}{3}\rho\pi ab^2) \qquad (2-36)$$

and in heave mode is:-

$$K_1 \cdot (\frac{4}{3}\rho\pi ab^2) \qquad (2-37)$$

where K_1, K_2 are added mass constants and depend on a/b [61], where a, b are the major and the minor axis of the ellipsoid. For the SWATH model, consider $K_{1A} = 0.0706$, $K_{1F} = 0.0984$.

The horizontal inertia force acting on one hull was then
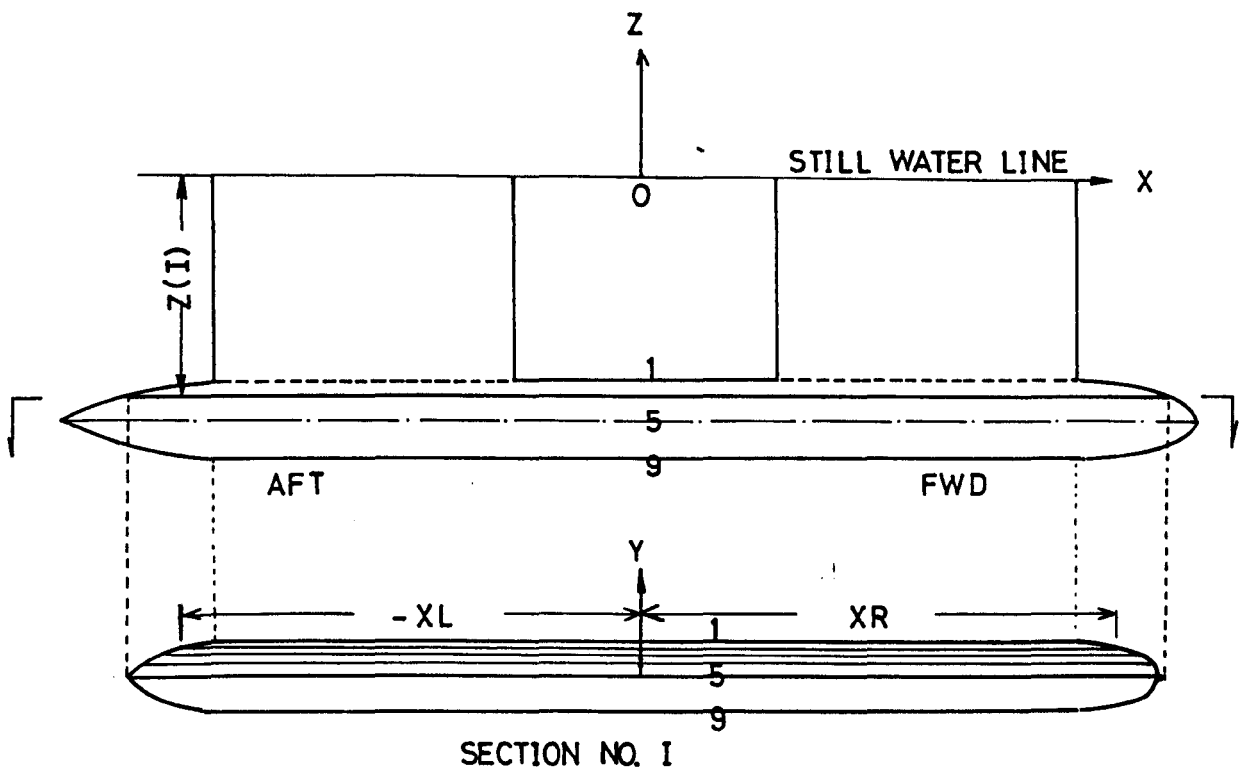
Fig. 2.7
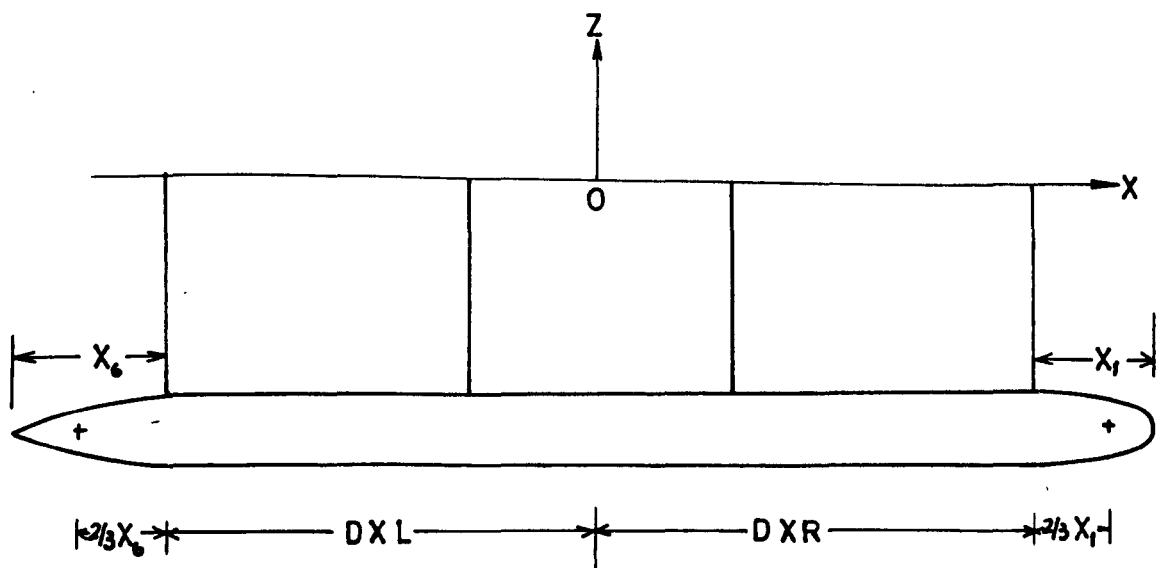
Fig. 2.8

calculated by:-

$$(\tfrac{1}{2} \cdot \tfrac{4}{3}\rho\pi R^2 \cdot K_{1A} \cdot X_6) \cos k(- DXL - \tfrac{2}{3}X_6 - c_w t)$$

$$+ (\tfrac{1}{2} \cdot \tfrac{4}{3}\rho\pi R^2 \cdot K_{1F} \cdot X_1) \cos k(DXR + \tfrac{2}{3}X_1 - c_w t) \qquad (2-38)$$

where R is the max radius of the circular cross-section and X_6, X_1,

DXL, DXR are distances in the longitudinal x-direction as shown in

fig. 2.8.

3.2.11   The exciting pitch moment

The pitching moment is considered to be composed of moments

resulting from the heave and surge forces. Since the LCG is nearly at

mid-length, the integration of the moment of the vertical forces is

comparatively straightforward. However, for the horizontal forces the

lever arms from the elementary strip on the struts and hulls depends

on the height of the CG above the base (KG) and clearly this must be

accurately determined. An error in the CG position can easily change

the sign of the pitching moment due to the horizontal forces.

3.3.   The Second Theoretical Approach - 'Strip Theory'

The wave exciting forces derived from the velocity potential

generated by the sinusoidal wave and resulting from the presence of

the SWATH hull body, may be expressed as:-

$$\Phi_T = \Phi_I + \Phi_D \qquad (2-39)$$

where Φ_I is the incident wave velocity potential

and Φ_D is the diffraction velocity potential.

3.3.1 The incident wave velocity potential at zero speed

The incident wave profile h_W, with heading angle μ in the body co-ordinate system, as shown in fig. 2.9 can be expressed as [35]:-

$$h_W = a_o e^{i(k_o x \cos\mu + k_o y \sin\mu - \omega_o t)} \qquad (2-40)$$

Since the profile will vary with the depth, we need to take into account this effect represented by the term $e^{k_o z}$ in equation (2-40), ie:-

$$h_W = a_o e^{k_o z} . e^{i(k_o x \cos\mu)} . e^{i(k_o y \sin\mu)} . e^{-i\omega_o t} \qquad (2-40a)$$

which generates the above wave profile (h_W). We use the linearised dynamic free surface equation:-

$$h_W = -\frac{1}{g}\frac{\partial \Phi_I}{\partial t}\bigg|_{z=0} \qquad (2-41)$$

Therefore, by substituting equation (2-40a) into equation (2-41):-

$$\frac{\partial \Phi_I}{\partial t} = - g a_o e^{k_o z} e^{i(k_o y \sin\mu + k_o x \cos\mu)} . e^{-i\omega_o t} \qquad (2-42)$$

$$\Phi_I = -\frac{ig}{\omega_o} a_o e^{k_o z} e^{i(k_o y \sin\mu)} . e^{i(k_o x \cos\mu - \omega_o t)} \qquad (2-43)$$

Since strip theory is used, the three-dimensional velocity potential $\Phi_I(x,y,z;t)$ can be re-arranged in terms of a two-dimensional form by separating the third term in the above expression as follows:-

$$\Phi_I(x,y,z;\mu,t) = \phi_I(y,z) e^{i(k_o x \cos\mu - \omega_o t)} \qquad (2-44)$$

$$\text{with } \phi_I(y,z) = -\frac{iga_o}{\omega_o} e^{k_o z} e^{ik_o y \sin\mu} \qquad (2-45)$$

The real (Re) and imaginary (Im) parts of the $\phi_I(y,z)$ in terms of $\sin(k_o y \sin\mu)$ and $\cos(k_o y \sin\mu)$ corresponding to its odd (o) and even (e) function forms, respectively, are:-

$$\phi_I(y,z) = Re\phi_I(y,z) + iIm\phi_I(y,z) \qquad (2-46)$$

$$\phi_I^{(o)}(y,z) = Re\phi_I(y,z) = \frac{ga_o}{\omega_o}e^{k_o z}\sin(k_o y \sin\mu) \qquad (2-47)$$

$$\phi_I^{(e)}(y,z) = Im\phi_I(y,z) = -\frac{ga_o}{\omega_o}e^{k_o z}\cos(k_o y \sin\mu) \qquad (2-48)$$

By examining the vertical and horizontal velocities, the appropriate components of the heave and sway modes will be obtained. For the odd velocity potential, the velocity components are:-

$$U^{(o)} = \frac{\partial}{\partial y}[Re\phi_I] = \frac{ga_o}{\omega_o}e^{k_o z}(k_o \sin\mu)\cos(k_o y \sin\mu) \qquad (2-49)$$

$$V^{(o)} = \frac{\partial}{\partial z}[Re\phi_I] = \frac{ga_o}{\omega_o}e^{k_o z}.k_o.\sin(k_o y \sin\mu) \qquad (2-50)$$

For the even velocity potential, the velocity components are:-

$$U^{(e)} = \frac{\partial}{\partial y}[Im\phi_I] = \frac{ga_o}{\omega_o}e^{k_o z}(k_o \sin\mu)\sin(k_o y \sin\mu) \qquad (2-51)$$

and

$$V^{(e)} = \frac{\partial}{\partial z}[Im\phi_I] = \frac{ga_o}{\omega_o}e^{k_o z}.k_o.\cos(k_o y \sin\mu) \qquad (2-52)$$

For a sectional point $(y,-z)$ and its symmetry point $(-y,-z)$, the vertical component owing to the odd potential will cancel each other, as shown in fig. 2.10 and the horizontal components generate the asymmetric sway forces.

On the other hand, for the even potential, as shown in fig. 2.11, the horizontal component will cancel out and the vertical component generates the symmetric heave force.
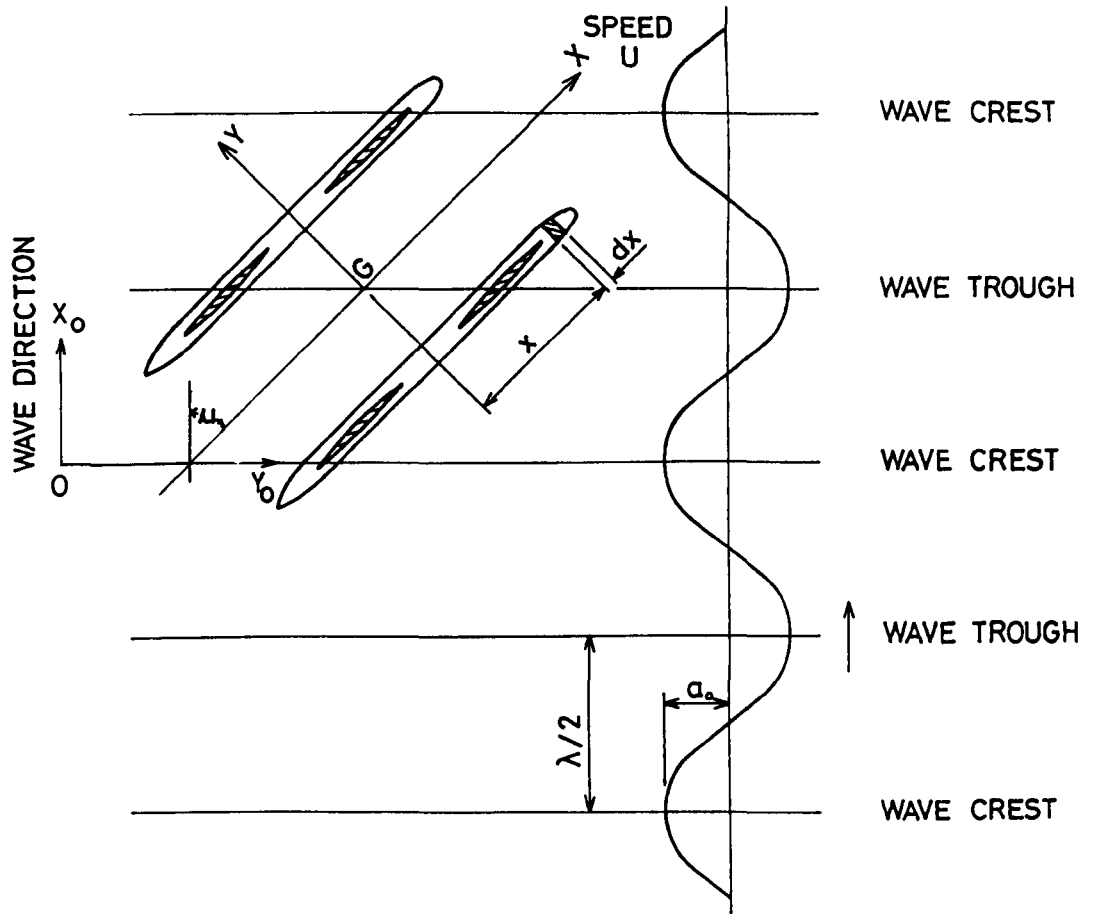
SWATH IN A REGULAR SINUSOIDAL WAVE

Fig. 2.9

$$\cos(-\theta) = \cos\theta$$
$$\sin(-\theta) = -\sin\theta$$
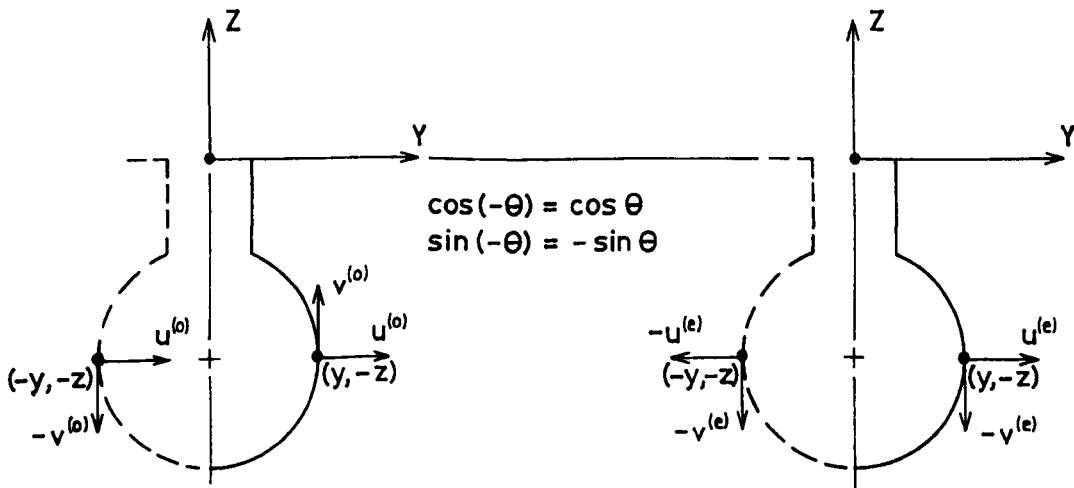
Odd Function Case

Fig. 2.10

Even Function Case

Fig. 2.11

3.3.2   The diffraction wave velocity potential

As presented in equation (2-39), the term ϕ_D represents the diffracted velocity potential of the free incident wave due to the existence of the body surface and can be written in the following form:-

$$\Phi_D(x,y,z;\mu,t) = \phi_D(y,z)e^{i(k_O x \cos\mu - \omega_O t)} \qquad (2-53)$$

In 1967, Frank [59] represented this disturbance by distributing a number of source singularities along the sectional contour. The contour is approximated by a series of straight line elements with a single pulsating source located at the centre of each element. Following the method, the two-dimensional diffraction potential can be written in the form:-

$$\phi_D(y,z) = \int_S Q(\xi,\eta)G(y,z;\xi,\eta,k_O)ds \qquad (2-54)$$

where the Green function G, is the two-dimensional source potential of unit strength at the point (ξ,η) in the lower half of the (y,z) plane [59,63]. The 's' indicates that the integral is to be taken along the section contour which is below the water surface. The unknown source strengths Q are determined by satisfying the kinematic boundary condition:-

$$V_n = \frac{\partial\phi}{\partial n} = 0 \qquad (2-55)$$

where V_n is the normal velocity of the section. The value $V_n = 0$ indicates that the body is assumed rigidly fixed, ie, the normal velocity of the fluid at the body surface equals the normal components

of the forced velocity of the body, (no flow across the body sectional contour).

Inserting equation (2-39) into equation (2-55) gives:-

$$\frac{\partial \Phi_D}{\partial n} = - \frac{\partial \Phi_I}{\partial n} \tag{2-56}$$

where $\frac{\partial}{\partial n} = \vec{n} \cdot \vec{\nabla}$

$$= (\sin\alpha\vec{i} - \cos\alpha\vec{j}) \cdot (\frac{\partial}{\partial y}\vec{i} + \frac{\partial}{\partial z}\vec{j})$$

$$= (\sin\alpha\frac{\partial}{\partial y} - \cos\alpha\frac{\partial}{\partial z}) \tag{2-57}$$

where $\vec{n}$ is the outward normal vector [59],

The normal derivative of the odd potential $\phi_I^{(o)}$ is:-

$$\frac{\partial \Phi_I^{(o)}}{\partial n} = (\vec{n} \cdot \vec{\nabla})\phi_I^{(o)}$$

$$= (\sin\alpha\frac{\partial}{\partial y} - \cos\alpha\frac{\partial}{\partial z}) (\frac{ga_o}{\omega_o}e^{k_o z}\sin(k_o y \sin\mu))$$

$$= \frac{ga_o}{\omega_o}e^{k_o z}\sin\alpha \cdot k_o \cdot \sin\mu\cos(k_o y \sin\mu)$$

$$- \frac{ga_o}{\omega_o}k_o \cdot e^{k_o z}\cos\alpha\sin(k_o y \sin\mu)$$

which can be re-written as:-

$$\therefore \frac{1}{a_o} \frac{\partial \phi_I^{(o)}}{\partial n} = \omega_o e^{k_o z}[\sin\alpha\sin\mu\cos(k_o y \sin\mu) - \cos\alpha\sin(k_o y \sin\mu)] \tag{2-58}$$

and the normal derivative of the even potential $\phi_I^{(e)}$ is:-

$$\frac{\partial \phi_I^{(e)}}{\partial n} = (\vec{n} \cdot \vec{\nabla}) \phi_I^{(e)}$$

$$= (\sin\alpha \frac{\partial}{\partial y} - \cos\alpha \frac{\partial}{\partial z})(- \frac{ga_o}{\omega_o} e^{k_o z} \cos(k_o y \sin\mu))$$

$$= - \frac{ga_o}{\omega_o} e^{k_o z} (- k_o \sin\mu) \sin(k_o y \sin\mu) . \sin\alpha$$

$$+ \cos\alpha \frac{ga_o}{\omega_o} k_o e^{k_o z} \cos(k_o y \sin\mu)$$

$$\frac{1}{a_o} \frac{\partial \phi_I^{(e)}}{\partial n} = \omega_o e^{k_o z} [\sin\alpha \sin\mu \sin(k_o y \sin\mu) + \cos\alpha \cos(k_o y \sin\mu)] \qquad (2-59)$$

Re-writing (2-54) into real and imaginary form:-

$$\phi_D = \int_S (Q_R + iQ_I)(G_R + i(- G_I)) ds \qquad (2-60)$$

$$= \int_S [(Q_R G_R + Q_I G_I) + i(G_R Q_I - G_I Q_R)] ds \qquad (2-61)$$

If equation (2-61) is applied at the centre of each of the N segments to approximate the contour, each of which is denoted j=1,2,....N, the normal derivative of ϕ_D can be written as:-

$$\frac{\partial \phi_D}{\partial n} = [\sum_{j=1}^{N} Q_j I_{ij} + \sum_{j=1}^{N} Q_{N+j} J_{ij}] + i[\sum_{j=1}^{N} - Q_j J_{ij} + \sum_{j=1}^{N} Q_{N+j} I_{ij}] \qquad (2-62)$$

where $I_{ij} = (\vec{n}.\vec{\nabla}) \int G_R ds$) influence coefficients for

$J_{ij} = (\vec{n}.\vec{\nabla}) \int G_I ds$) real and imaginary parts $\qquad (2-63)$

$Q_j = Q_R$) real and imaginary parts of

$Q_{N+j} = Q_I$) the unknown source densities $\qquad (2-64)$

Substituting the above normal derivatives (2-58), (2-59) and

(2-62) to satisfy:-

$$\frac{\partial \phi_D}{\partial n} = - \frac{\partial \phi_I}{\partial n}$$

and, for the heave mode:-

$$\frac{\partial \phi_I^{(o)}}{\partial n} = 0$$

ie, only the even potential function for the reasons explained earlier
are obtained.

Real part: $\quad \sum\limits_{j=1}^{N} Q_j I_{ij} + \sum\limits_{j=1}^{N} Q_{N+j} J_{ij} = 0 \qquad\qquad\qquad$ (2-65)

Imaginary
Part: $\quad - \sum\limits_{j=1}^{N} Q_j J_{ij} + \sum\limits_{j=1}^{N} Q_{N+j} I_{ij} = - \omega_o e^{k_o z}[\sin\mu \sin(k_o y \sin\mu)\sin\alpha$

$\qquad\qquad\qquad\qquad\qquad\qquad\qquad\qquad\qquad\qquad\qquad\qquad$ (2-66)

$$+ \cos(k_o y \sin\mu)\cos\alpha]$$

For the sway mode (horizontal plane force) $\dfrac{\partial \phi_I^{(e)}}{\partial n} = 0$ and only the odd
potential function causes the force.

By solving the above algebratic equations, the complex source
strengths of the diffraction potential $\phi_D^{(e)}$ and $\phi_D^{(o)}$ corresponding to
the incident wave potential can be obtained.

3.3.3   Froude-Krylov force

From the linear Bernoulli equation, the dynamic pressure
induced by the incident wave can be expressed as:-

$$P_I = -\rho \frac{\partial \phi_I}{\partial t} \qquad\qquad\qquad (2-67)$$

Since only the real part will be of interest, it is convenient to re-define the incident potential into the detailed components as:-

$$\Phi_I = [(\Phi_I)_{Re} + i(\Phi_I)_{Im}]e^{-i\omega_o t} \qquad (2\text{-}68)$$

$$\frac{g}{\omega_o}a_o e^{k_o z}\sin(k_o y\sin\mu + k_o x\cos\mu) \qquad -\frac{g}{\omega_o}a_o e^{k_o z}\cos(k_o y\sin\mu + k_o x\cos\mu)$$

$$(2\text{-}69)$$

$$\frac{g}{\omega_o}a_o e^{k_o z}[\sin(k_o y\sin\mu)\cos(k_o x\cos\mu) + \cos(k_o y\sin\mu)\sin(k_o x\cos\mu)]$$

$$(\Phi_I)_{Re}^{(o)} + (\Phi_I)_{Re}^{(e)} \qquad (\Phi_I)_{Im}^{(o)} + (\Phi_I)_{Im}^{(e)}$$

According to the new formulation, the components are listed as:-

$$(\Phi_I)_{Re}^{(o)} = \frac{ga_o}{\omega_o}e^{k_o z}\sin(k_o y\sin\mu)\cos(k_o x\cos\mu)$$

$$(\Phi_I)_{Re}^{(e)} = \frac{ga_o}{\omega_o}e^{k_o z}\cos(k_o y\sin\mu)\sin(k_o x\cos\mu)$$

$$(\Phi_I)_{Im}^{(o)} = \frac{ga_o}{\omega_o}e^{k_o z}\sin(k_o y\sin\mu)\sin(k_o x\cos\mu)$$

$$(\Phi_I)_{Im}^{(e)} = \frac{-ga_o}{\omega_o}e^{k_o z}\cos(k_o y\sin\mu)\cos(k_o x\cos\mu)$$

Table 2.1

From equations (2-67) and (2-68)

$$P_I = -\rho\frac{\partial}{\partial t}\{[(\Phi_I)_{Re} + i(\Phi_I)_{Im}]e^{-i\omega_o t}\} \qquad (2\text{-}70)$$

Taking the real part,

$$P_I = -\rho\omega_o(\Phi_I)_{Im}\cos\omega_o t + \rho\omega_o(\Phi_I)_{Re}\sin\omega_o t \qquad (2\text{-}71)$$

To obtain the heave pressure per wave amplitude, the 'even' part of equation (2-71) will be taken:-

$$P_I^{(H)} = - \rho\omega_o(\Phi_I)_{Im}^{(e)}\cos\omega_o t + \rho\omega_o(\Phi_I)_{Re}^{(e)}\sin\omega_o t \qquad (2-72)$$

$$= \rho g e^{k_o z}[\cos(k_o y\sin\mu)\cos(k_o x\cos\mu)]\cos\omega_o t$$

$$+ \rho g e^{k_o z}[\cos(k_o y\sin\mu)\sin(k_o x\cos\mu]\sin\omega_o t$$

and to obtain the sway mode we take the 'odd' part in equation (2-71) as:-

$$P_I^{(S)} = - \rho\omega_o(\Phi_I)_{Im}^{(o)}\cos\omega_o t + \rho\omega_o(\Phi_I)_{Re}^{(o)}\sin\omega_o t \qquad (2-73)$$

In order to calculate the Froude-Krylov force, assuming that the pressure at the ith midpoint is the mean pressure for the ith segment, and summing up the pressure for all the elements, then the forces and moments per wave amplitude on the strip section are:-

$$f_K^{(m)}(x) = \int_{s(x)} P_I^{(m)} . \vec{n}_i^{(m)} \, ds \qquad (2-74)$$

where $f_K^{(m)}(x)$ is the sectional Froude-Krylov force per unit wave amplitude at the x position.

ds is the segment length

$\vec{n}_i$ is the outward unit normal vector at the ith segment midpoint.

m is the mode of motion (H for heave, S for sway, etc)

$\vec{n}_i^{(H)} = \cos\alpha_i$ and $\vec{n}_i^{(S)} = -\sin\alpha_i$, as explained in Ref[59].

For the heave mode:-

$$f_K^{(H)} = \int_S \rho g e^{k_0 z} (\cos(k_0 y \sin\mu) \cos(k_0 x \cos\mu) \cos\omega_0 t$$

(2-75)

$$+ \cos(k_0 y \sin\mu) \sin(k_0 x \cos\mu) \sin\omega_0 t) \cos\alpha_i ds$$

Integrating the $\cos\omega_0 t$ and $\sin\omega_0 t$ terms separately:-

$$FRA(I) = \sum_{i=1}^{Nos} \rho g e^{k_0 z} [\cos(k_0 y \sin\mu) \cos(k_0 x \cos\mu)] \cos\alpha_i \cdot |s_i| \qquad (2-76)$$

$$FRV(I) = \sum_{i=1}^{Nos} \rho g e^{k_0 z} [\cos(k_0 y \sin\mu) \sin(k_0 x \cos\mu)] \cos\alpha_i \cdot |s_i| \qquad (2-77)$$

The magnitude of the sectional heave force is:-

$$f_K^{(H)} = (FRA^2(I) + FRV^2(I))^{\frac{1}{2}}$$

$$= \sum_{i=1}^{N} \rho g e^{k_0 z} \cos(k_0 y \sin\mu) \cos\alpha_i |s_i| \qquad (2-78)$$

In equation (2-78), the phase effect terms $\cos(k_0 x \cos\mu)$ and $\sin(k_0 x \cos\mu)$ disappear, thus indicating that when integrating the sectional Froude-Krylov force, it is not necessary to consider the phase effects.

Integrating these sectional forces along the ship length and taking into account the phase difference relating to the original wave position (origin at the L.C.G) the resultant Froude-Krylov heave force and pitch moment per unit wave amplitude at zero forward speed are:-

$$F_K^{(H)} = \int_L e^{ik_0 x \cos\mu} \cdot f_K^{(H)}(x) dx \qquad (2-79)$$

$$F_K^{(P)} = \int_L e^{ik_0 x \cos\mu} \cdot f_K^{(H)}(x)(-x) dx \qquad (2-80)$$

3.3.4 Diffraction pressure force

Combining equations (2-53) and (2-61):-

$$\Phi_D = [(\Phi_D)_{Re} + i(\Phi_D)_{Im}]e^{-i\omega_o t} \tag{2-81}$$

where

$$(\Phi_D)_{Re} = \int_s (Q_R G_R + Q_I G_I)\cos(k_o x\cos\mu)ds + \int_s (Q_R G_I - Q_I G_R)\sin(k_o x\cos\mu)ds \tag{2-82}$$

$$(\Phi_D)_{Im} = \int_s (Q_R G_R + Q_I G_I)\sin(k_o x\cos\mu)ds - \int_s (Q_R G_I - Q_I G_R)\cos(k_o x\cos\mu)ds \tag{2-83}$$

Using the definition given in equations (2-63) and (2-64) this may be re-written at:-

$$(\Phi_D)_{Re} = (\sum_{j=1}^{N} Q_j I_{ij} + \sum_{j=1}^{N} Q_{N+j} J_{ij})\cos(k_o x\cos\mu)$$

$$+ (\sum_{j=1}^{N} Q_j J_{ij} - \sum_{j=1}^{N} Q_{N+j} I_{ij})\sin(k_o x\cos\mu) \tag{2-84}$$

$$(\Phi_D)_{Im} = (\sum_{j=1}^{N} Q_j I_{ij} + \sum_{j=1}^{N} Q_{N+j} J_{ij})\sin(k_o x\cos\mu)$$

$$- (\sum_{j+1}^{N} Q_j J_{ij} - \sum_{j=1}^{N} Q_{N+j} I_{ij})\cos(k_o x\cos\mu) \tag{2-85}$$

The hydrodynamic diffraction pressure:-

$$P_D = -\rho\frac{\partial\Phi_D}{\partial t}$$

$$= i\rho\omega_o [(\Phi_D)_{Re} + i(\Phi_D)_{Im}]e^{-i\omega_o t} \tag{2-86}$$

Taking the real part:-

$$P_D = - \rho\omega_o(\Phi_D)_{Im}\cos\omega_o t + \rho\omega_o(\Phi_D)_{Re}\sin\omega_o t \qquad (2\text{-}87)$$

$$= - \rho\omega_o\{(\sum_{j=1}^{N} Q_j I_{ij} + \sum_{j=1}^{N} Q_{N+j} J_{ij})\sin(k_o x\cos\mu)$$

$$- (\sum_{j=1}^{N} Q_j J_{ij} - \sum_{j=1}^{N} Q_{N+j} I_{ij})\cos(k_o x\cos\mu)\}$$

$$\qquad (2\text{-}88)$$

$$+ \rho\omega_o\{(\sum_{j=1}^{N} Q_j I_{ij} - \sum_{j=1}^{N} Q_{N+j} J_{ij})\cos(k_o x\cos\mu)$$

$$+ (\sum_{j=1}^{N} Q_j J_{ij} - \sum_{j=1}^{N} Q_{N+j} I_{ij})\sin(k_o x\cos\mu)\}$$

3.3.5   Forward speed effect

When the co-ordinate on the body (x,y,z) moves at a steady forward speed U along the X-axis. The relationship between the space-fixed co-ordinate (X_o,Y_o,Z_o) and the body co-ordinate system, as shown in fig. 2.9 is:-

$$X_o = x + Ut, \quad Y_o = y, \quad Z_o = z \qquad (2\text{-}89)$$

and the encounter frequency:-

$$\omega = \omega_o - Uk_o\cos\mu \qquad (2\text{-}90)$$

where ω_o is the incident wave frequency and

k_o is the wave number $= \omega_o^2/g$

μ is the heading angle (180 degrees for head sea).

3.3.6   The speed effect on the incident wave potential (Φ_I)

According to the above definitions, when the model moves with the speed U, the incident wave potential is identical to that at zero speed which is given by equations (2-44) and (2-45) except for a change in the encounter frequency [35,64]:-

$$\Phi_I = \phi_I e^{i(k_o x \cos\mu - \omega t)} \qquad (2-91)$$

with

$$\phi_I = -\frac{iga_o}{\omega_o} e^{k_o z} e^{ik_o y \sin\mu} \qquad (2-92)$$

The wave number, $k_o = \dfrac{\omega_o^2}{g}$, remains unchanged. Therefore, the Froude-Krylov excitng force with respect to the moving frame is equal to equation (2-74), which is the same as for zero speed.

3.3.7   The speed effect on the diffracted wave potential (Φ_D)

Since the body is moving forward with respect to the fixed co-ordinate system, the time derivative $(\frac{\partial}{\partial t})$ of the diffracted velocity potential has to be replaced by $(\frac{\partial}{\partial t} - U\frac{\partial}{\partial x})$. The diffraction pressure is given by:-

$$P_D = e^{ik_o x \cos\mu} \cdot (i\omega + U\frac{\partial}{\partial x})\phi_D \qquad (2-93)$$

where

$$\phi_D = \phi_D^{(o)} + i\phi_D^{(e)} \qquad (2-94)$$

Integrating the pressure over the wetted surface contour and along the length yields the diffraction force and the following expression for

heave force is obtained:-

$$F_D^{(H)} = \int_L e^{ik_0 x \cos\mu} dx \int_s i\rho\omega\phi_D^{(e)} dy + \frac{U}{i\omega} \int_L e^{ik_0 x \cos\mu} dx \cdot \frac{\partial}{\partial x} \int_s i\rho\omega\phi_D^{(e)} dy$$

(2-95)

$$= \int_L e^{ik_0 x \cos\mu} f_D^{(H)}(x) dx + \frac{U}{i\omega} f_D^{(H)}(x) \cdot e^{ik_0 x \cos\mu} \Big|_L$$

where

$$f_D^{(H)}(x) = \int_s i\rho\omega\phi_D^{(e)} dy$$

(2-96)

Similar procedure for the pitch moment is:-

$$F_D^{(P)} = -x F_D^{(H)} = -\int_L x e^{ik_0 x \cos\mu} f_D^{(H)}(x) dx$$

(2-97)

$$+ \frac{U}{i\omega} \int_L e^{ik_0 x \cos\mu} f_D^{(H)}(x) dx - \frac{Ux}{i\omega} f_D^{(H)} e^{ik_0 x \cos\mu} \Big|_L$$

and $\Big|_L$ indicates the summation of the values which exist at the extreme ends (foremost and aftermost sections) of the body. The second term in equation (2-95) is the so-called ends term, which exists only if the foremost and/or aftermost sections have a sectional area. For the SWATH model in this study, both end sections are zero and, consequently, the end term effect does not exist. The second term in (2-97) is the speed-dependent term (for pitch moment).

3.3.8 Viscous damping effect

The SWATH configuration submerges most of its volume below the water surface so that when oscillating in the vertical plane its very small waterplane area does not generate large surface waves. Thus, wave damping is relatively small compared with a conventional ship and viscous damping tends to dominate having the same order of

magnitude as wave damping. When the viscous contribution to the damping is neglected, the computed motion amplitude has a high spiked value at the resonant frequency. Therefore, viscous damping efects must be taken into account in the motion prediction.

The analytical study of SWATH viscous effects originally followed from Thwaite's [65] experimental results and the work of Lee [49,66]. In the application of the viscous cross-flow about a slender body as in figure 2-12, the important parameter of the expression $F_{VE}/\frac{1}{2}\rho U^2 A_p \sin^2\alpha$ was found by experimental correlation to vary with the values of α, as:-

$$F_{VE}/\frac{1}{2}\rho U^2 A_p \sin^2\alpha = A_o \cot\alpha + C_{DH}$$

The first term on the right hand side, A_o being the lift-curve slope for a very low incidence, which generates the viscous lift on an inclined hull with forward speed, and the second term C_{DH}, being the cross-flow drag coefficient which becomes significant at higher incidences and generated viscous damping.

Applying these two effects for a slender body, such as a SWATH with moderate angle of attack, the vertical force can be expressed as:-

$$F_{VE} = \frac{1}{2}\rho A_p U^2 \sin\alpha |\sin\alpha| (A_o |\cot\alpha| + C_{DH}) \qquad (2-98)$$

where A_p is the projected area of the hull on a horizontal X-Y plane.

α is the angle of attack.

ρ is th density of water.

U is the forward speed.

A_o is the viscous lift coefficient.

C_{DH} is the hull cross-flow drag coefficient,
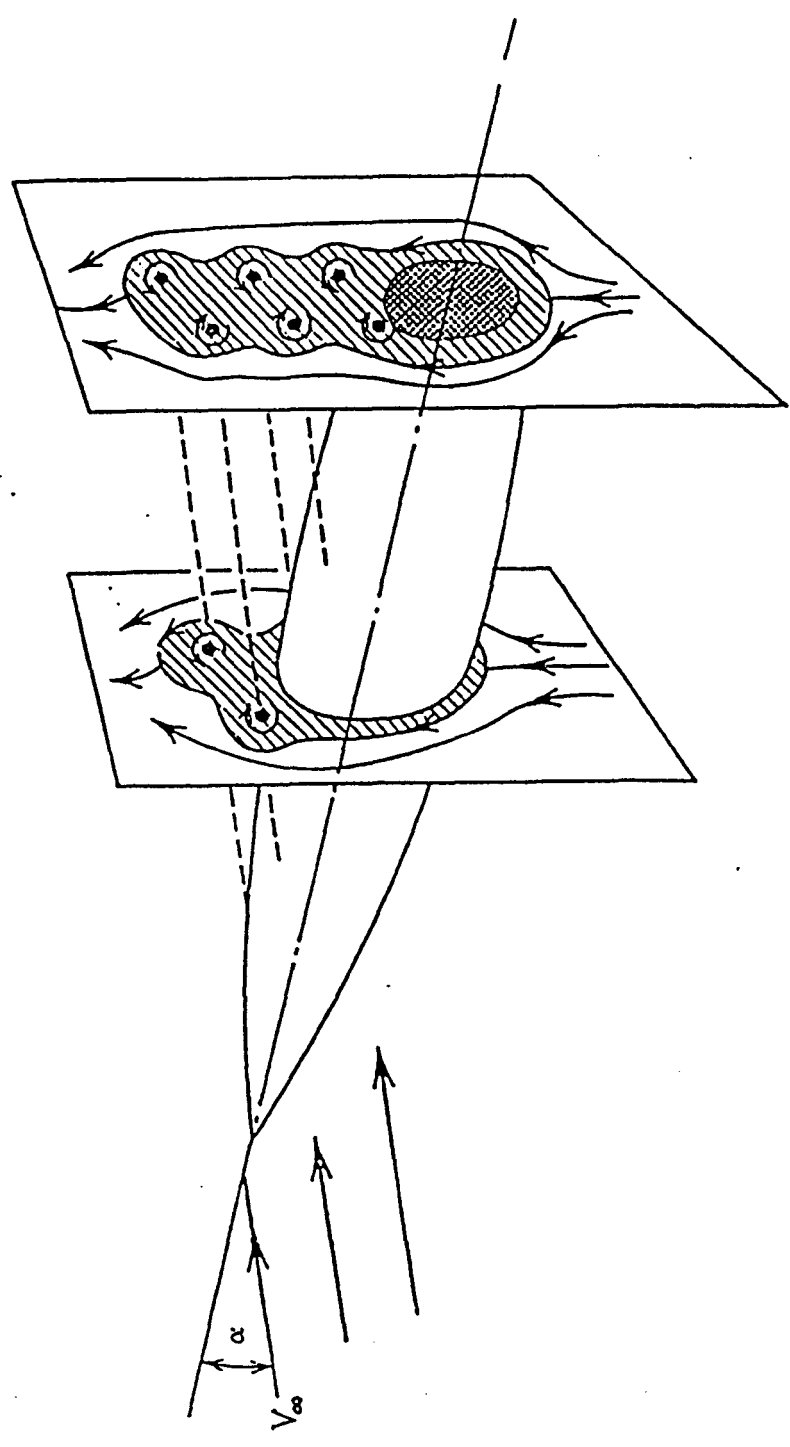
Fig 2.12 A sketch illustrating the cross-flow in planes perpendicular to the axis of a body of revolution at incidence.

Assuming that there is a harmonically oscillating body in the vertical-plane with forward speed U in regular waves, the force arising from equation (2-98) will be assumed to take the form:-

$$F_{VE} = \tfrac{1}{2}\rho A_p (U^2 A_o \alpha + C_{DH} \dot{z} |\dot{z}|)$$ (2-99)

where $\dot{z}$ is the relative fluid velocity with respect to the body and given by:-

$$\dot{z}(x) = \dot{S}_3 - x\dot{S}_5 - V_w(x, \pm b(x), - d(x))$$ (2-100)

$$= U(\alpha - S_5)$$

and

$$\alpha = S_5 + \frac{\dot{S}_3 - x\dot{S}_5 - V_w}{U}$$ (2-101)

where $\dot{S}_3$, $\dot{S}_5$ are heave and pitch velocity (ms^{-1}, $rad\ s^{-1}$)

V_w is the vertical velocity of the incident wave

b(x) is the transverse distance from X-axis to the

centre of the hull, as shown in fig. 2.13.

d(x) is the depth from the waterline to the maximum

breadth of the hull.

The angle of attack α as shown in fig. 2.14. There is another component '$y\dot{S}_4$', due to rolling velocity which was neglected because the SWATH was assumed to have a symmetric vertical motion with respect to the centreplane.

The vertical incident wave velocity:-

$$V_w(x,y,z,t) = \frac{\partial \Phi_I}{\partial z}$$ (2-102)
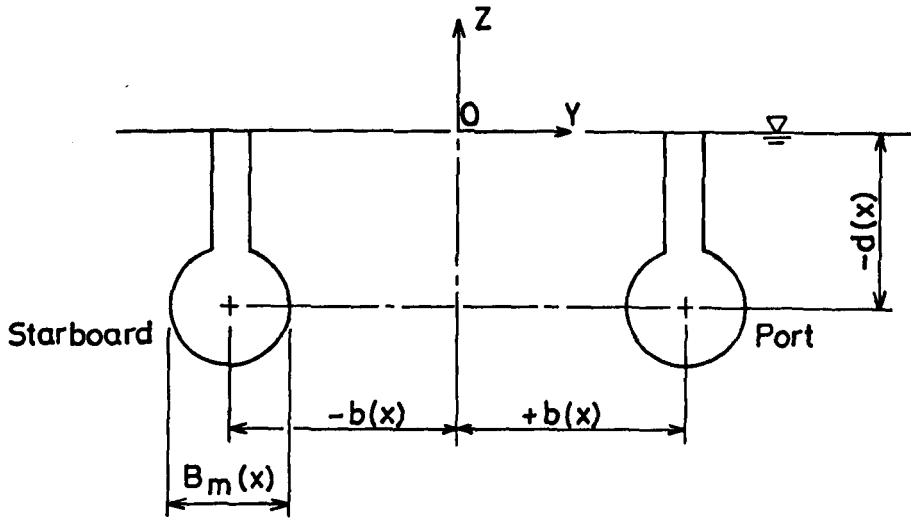
Fig. 2.13
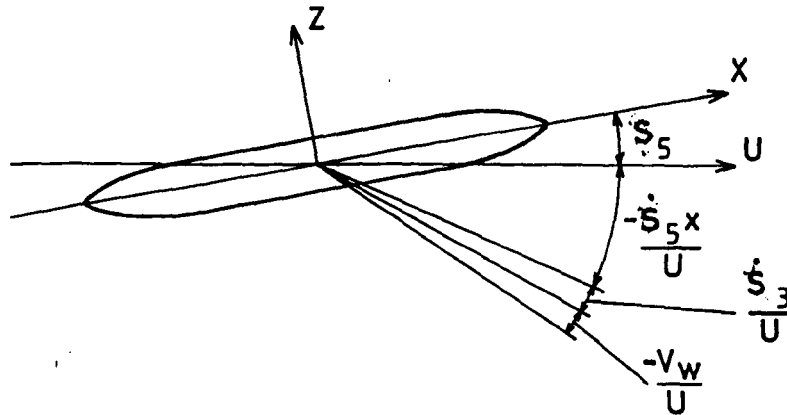
Angle of Attack (radians)
- by heaving velocity $\dfrac{\dot{S}_3}{U}$
- by pitch angle $\dot{S}_5$
- by pitching velocity $\dfrac{-\dot{S}_5 x}{U}$
- by orbital motion of incident wave $\dfrac{-V_w}{U}$

$$\alpha = S_5 + \frac{\dot{S}_3 - x\,\dot{S}_5 - V_w}{U}$$

Fig. 2.14

$$\Phi_I = -\frac{iga_o}{\omega_o}e^{k_o z}\cos(k_o y \sin\mu)e^{i(k_o x\cos\mu-\omega t)} \qquad (2-103)$$

$$V_w = -i\omega_o a_o e^{k_o z}e^{i(k_o x\cos\mu-\omega t)}\cos(k_o y\sin\mu) \qquad (2-104)$$

for head seas:-

$$\cos\mu = -1, \quad \sin\mu = 0, \quad V_w = i\omega_o a_o e^{k_o z}e^{-i(k_o x+\omega t)} \qquad (2-105)$$

The wave vertical velocity on the starboard hull $(\dot{Z}_s)$ will, thus, be the same as on the port hull $(\dot{Z}_p)$:-

where

$$\dot{Z}_s = \dot{S}_3 - x\dot{S}_5 - V_w(x, - b(x), - d(x)) \qquad (2-106)$$

and

$$\dot{Z}_p = \dot{S}_3 - x\dot{S}_5 - V_w(x, + b(x), - d(x)) \qquad (2-107)$$

and, thus, $\dot{Z}_s = \dot{Z}_p$ for the case under consideration.

In equation (2-99) the projected area A_p was calculated by integrating the maximum beam of one hull cross-section $B_m(x)$, as shown in fig. 2.13, along the X-axis. Thus, the viscous force may be written as:-

$$F_{VE} = \frac{\rho}{2}\int_L B_m(x)[2A_o U^2 S_5 + 2A_o U\dot{Z}_p + 2C_{DH}\dot{Z}_p|\dot{Z}_p|]dx \qquad (2-108)$$

For the pitch moment:-

$$M_p = -\int F_{VE}(x).x.dx$$

$$= -\rho\int_L xB_m(x)[A_o U^2 S_5 + A_o U\dot{Z}_p + C_{DH}\dot{Z}_p|\dot{Z}_p|]dx \qquad (2-109)$$

In equation (2-108) the cross-flow drag terms are non-linear. In order to include these in a linearised computational procedure, the non-linear term needs to be replaced by an equivalent linear one.

Since the vertical velocity given by $(\dot{S}_3 - x\dot{S}_5 - V_w)$ is a sinusoidal function [67] of ωt, it can be defined as:-

$$\dot{S}_3 - x\dot{S}_5 - V_w = V_o \cos(\omega t + \theta) \tag{2-110}$$

$$(\dot{S}_3 - x\dot{S}_5 - V_w)\left|\dot{S}_3 - x\dot{S}_5 - V_w\right| = V_o^2 \cos(\omega t + \theta)\left|\cos(\omega t + \theta)\right| \tag{2-111}$$

By using Fourier series theory:-

$$\cos x \left|\cos x\right| = \sum_{n=1}^{\infty} a_{2n-1}\cos(2n-1)x \tag{2-112}$$

where $a_n = 0$ for n even

$$a_n = (-1)^{\frac{n+1}{2}}\frac{8}{n(n^2-4)\pi} \qquad \text{for n odd}$$

$$a_1 = \frac{8}{3\pi}, \qquad a_3 = \frac{8}{15\pi}, \qquad a_5 = -\frac{8}{105\pi}, \ldots\ldots\ldots$$

Taking the first term yields an approximation of:-

$$\cos x \left|\cos x\right| \simeq \frac{8}{3\pi}\cos x \tag{2-113}$$

Applying equation (2-113) into equation (2-111):-

$$V_o^2\cos(\omega t + \theta)\left|\cos(\omega t + \theta)\right| \simeq \frac{8}{3\pi}V_o(\dot{S}_3 - x\dot{S}_5 - V_w) \tag{2-114}$$

Thus, the viscous damping takes a linear form:-

$$\rho \cdot \frac{8}{3\pi}V_o \cdot C_{DH}\int(\dot{S}_3 - x\dot{S}_5 - V_w)\cdot B_m(x)\,dx \tag{2-115}$$

In order to substitute these linearised cross-flow drag terms it is necessary to have a prior knowledge of the amplitude of the motion. An iterative solution is used in which the first amplitude of motion is obtained by solving the equation without the cross-flow damping terms and then recalculated with the equivalent linearised damping terms. This process is repeated until a reasonable convergence on the motion amplitude is obtained.

3.3.9 Computation

The viscous effects on the reaction terms and wave exciting terms of the coupled heave and pitch equations can be analysed from the following expressions:-

$$F_{VE}=\int_{L}\{\rho B_{m}(x)A_{o}U^{2}S_{5}+\rho A_{o}UB_{m}(x)(\dot{S}_{3}-x\dot{S}_{5}-V_{w})+\rho\frac{8V_{o}}{3\pi}C_{DH}B_{m}(x)(\dot{S}_{3}-x\dot{S}_{5}-V_{w})\}dx$$

$$(2-116)$$

$$M_{p}=(-x)F_{VE} \qquad (2-117)$$

The corresponding terms, as shown at the right hand column in Table 2-2, combine all these correction terms into the calculation to yield the viscous effect.

4.   FIN GENERATED FORCES

The contribution of fins to the vertical plane forces and moments can be described in three main parts. If there are several fins fitted along the hulls their separate effects can be added linearly. In the following discussion, for simplicity, only aft fins are considered [68].

The three main forces generated by fins are, a vertical inertia force I_f, lift force L_f, and cross-flow drag D_f.

4.1.   Vertical inertia force I_f

When fins oscillate vertically the inertia force $I_f(t)$,

Body-motion	S_5 Pitch Displacement	$\rho A_o U^2 \int B_m(x)dx$	C_{35}
		$\rho A_o U^2 \int -x B_m(x)dx$	C_{55}
Reaction	S_3	$\rho A_o U \int B_m(x)dx$	B_{33}
		$\rho A_o U \int -x B_m(x)dx$	B_{35}
	Heave	$\rho \dfrac{8V_o}{3\pi} C_{DH} \int B_m(x)dx$	B_{33}
Force	Velocity	$\rho \dfrac{8V_o}{3\pi} C_{DH} \int -x B_m(x)dx$	B_{35}
	S_5	$\rho A_o U \int -x B_m(x)dx$	B_{53}
		$\rho A_o U \int x^2 B_m(x)dx$	B_{55}
Terms	Pitch	$\rho \dfrac{8V_o}{3\pi} C_{DH} \int -x B_m(x)dx$	B_{53}
	Velocity	$\rho \dfrac{8V_o}{3\pi} C_{DH} \int x^2 B_m(x)dx$	B_{55}
Wave- **Exciting**	F_3 Heave Force	$\rho A_o U \int B_m(x) V_w(x)dx$	F_3
		$\rho \dfrac{8V_o}{3\pi} C_{DH} \int B_m(x) V_w(x)dx$	F_3
Force **Terms**	F_5 Pitch Moment	$\rho A_o U \int -x B_m(x) V_w(x)dx$	F_5
		$\rho \dfrac{8V_o}{3\pi} C_{DH} \int -x B_m(x) V_w(x)dx$	F_5

TABLE 2.2

The Corrections due to the viscous effect

associated with the accelerations of heave and pitch motion, can be expressed as:-

$$I_{\dot{f}} = (m^{(f)} + A_{33}^{(f)})(\ddot{S}_3 - \ell\ddot{S}_5) \qquad (2\text{-}118)$$

where $m^{(f)}$ is the mass of the fins and $A_{33}^{(f)}$ is the added mass of fins which are approximated [49] by $\rho.\frac{\pi}{4}.S_p.C_h^2$ or by a flat plate [43] approximation by:-

$$\rho\frac{\pi}{4}.\frac{S_p^2 \cdot C_h^2}{(S_p^2 + C_h^2)^{\frac{1}{2}}}$$

where S_p is the span of the fin

$\quad$ C_h is the chord of the fin

$\quad$ $\ddot{S}_3$, $\ddot{S}_5$ are the accelerations in the heave and pitch mode

$\quad$ ℓ is the longitudinal distance from the centre of pressure of the fin to the LCG of the SWATH body.

4.2.   Lift Force, L_f

Assuming that there are no surface effects, ventilation or cavitation, the lift on the fin with a small angle of attack can be expressed by:-

$$L_f = \tfrac{1}{2}\rho U^2 (\text{area}).C_L \qquad (2\text{-}119)$$

$$C_L = C_{L\alpha}.\alpha \qquad (2\text{-}120)$$

where (area) is the area of fins projected in the XY-plane (at zero angle of attack)

$\quad$ $C_{L\alpha}$ is the lift-curve slope

$\quad$ α is the angle of attack of the fin. For small angles the

angle of attack is assumed to be the same as that defined in fig. 2.14.

$$\alpha = S_5 + \frac{\dot{S}_3 - \ell\dot{S}_5 - V_{wf}}{U} \qquad (2\text{-}121)$$

where S_5 is the pitch angle in radian

$\dot{S}_3$, $\dot{S}_5$ are the heave velocity and pitch angular velocity, respectively.

V_{wf} is the vertical wave-induced velocity at the fin position.

4.3. Cross-flow drag D_f

The cross-flow drag term for fins is of the same form as that for the hull, ie:-

$$D_f = \tfrac{1}{2}\rho A_f \cdot C_{DF}(\dot{S}_3 - \ell\dot{S}_5 - V_{wf})|\dot{S}_3 - \ell\dot{S}_5 - V_{wf}| \qquad (2\text{-}122)$$

where C_{DF} is the cross-flow drag coefficient of the fins.

Applying the same linearising procedure as for the hull, let V_{of} be the magnitude of the relative fluid velocity, then:-

$$\dot{S}_3 - \ell\dot{S}_5 - V_{wf} = V_{of}\cos(\omega t + \theta) \qquad (2\text{-}123)$$

$$(\dot{S}_3 - \ell\dot{S}_5 - V_{wf})|\dot{S}_3 - \ell\dot{S}_5 - V_{wf}| = V^2_{of}\cos(\omega t + \theta)|\cos(\omega t + \theta)|$$
$$\qquad (2\text{-}124)$$

therefore,
$$\simeq \frac{8}{3\pi}V_{of}(\dot{S}_3 - \ell\dot{S}_5 - V_{wf})$$

$$D_f = \tfrac{1}{2}\cdot\rho\cdot\frac{8}{3\pi}V_{of}\cdot C_{DF}\cdot A_f(\dot{S}_3 - \ell\dot{S}_5 - V_{wf}) \qquad (2\text{-}125)$$

The total vertical force generated by a pair of aft fins is:-

$$F_f = I_f + L_f + D_f$$

$$= 2(m^{(f)} + A_{33}^{(f)})(\ddot{S}_3 - \ell\ddot{S}_5) + \rho U^2 A_f C_{L\alpha}\{S_5 + \frac{\dot{S}_3 - \ell\dot{S}_5 - V_{wf}}{U}\}$$

$$+ \rho\frac{8}{3\pi}V_{of}C_{DF}A_f(\dot{S}_3 - \ell\dot{S}_5 - V_{wf}) \qquad (2\text{-}126)$$

and the pitch moment

$$M = -\ell F_f$$

$$= -2\ell(m^{(f)} + A_{33}^{(f)})(\ddot{s}_3 - \ell\ddot{s}_5) - \ell\rho U^2 A_f C_{L\alpha}\{s_5$$

$$(2-127)$$

$$+ \frac{\dot{s}_3 - \ell\dot{s}_5 - V_{wf}}{U}\} - \rho\ell\frac{8}{3\pi}V_{of}\cdot C_{DF}\cdot A_f\cdot(\dot{s}_3 - \ell\dot{s}_5 - V_{wf})$$

The corresponding terms in the coupled heave and pitch equations for the complete SWATH are identified in Table 2.3.

4.4.   Determination of lift-curve slope $C_{L\alpha}$

For fins attached to the hull, the lift-curve slope should be determined by considering the effects of aspect ratio, the free surface and the boundary layer. Since these are beyond the scope of the present study use was made of the work of Lee [49], which assumed $C_{L\alpha}$ to be composed as follows:-

$$C_{L\alpha} = (K_{F(H)} + K_{H(F)})C_{L\alpha_o} \qquad (2-128)$$

where $K_{F(H)} = (C_{L\alpha})_{F(H)}/C_{L\alpha_o} \qquad (2-129)$

$$K_{H(F)} = (C_{L\alpha})_{H(F)}/C_{L\alpha_o} \qquad (2-130)$$

subscript 'o' represents the fins alone, (no hull-body exists)

H(F) is the lift on hull induced by the fins

and   F(H) is the lift on fins induced by hull.

For a low aspect ratio fin, the empirical formula [69] for $C_{L\alpha_o}$ is:-

Body-	$\ddot{S}_3$	$2(m^{(f)} + a_{33}^{(f)})$	A_{33}
		$-\ell\{2(m^{(f)} + a_{33}^{(f)})\}$	A_{35}
	$\ddot{S}_5$	$-\ell\{2(m^{(f)} + a_{33}^{(f)})\}$	A_{53}
		$\ell^2\{2(m^{(f)} + a_{33}^{(f)})\}$	A_{55}
Motion	$\dot{S}_3$	$\rho A_f U C_{L\alpha}$	B_{33}
		$-\ell\rho A_f U C_{L\alpha}$	B_{35}
Reaction		$\dfrac{8V_{of}}{3\pi}\rho.A_f C_{DF}$	B_{33}
		$-\dfrac{8V_{of}}{3\pi}\rho\ell A_f C_{DF}$	B_{35}
Force	$\dot{S}_5$	$-\ell\rho A_f U C_{L\alpha}$	B_{53}
		$\ell^2\rho A_f U C_{L\alpha}$	B_{55}
		$-\ell\dfrac{8V_{of}}{3\pi}\rho A_f C_{DF}$	B_{53}
Terms		$\ell^2\dfrac{8V_{of}}{3\pi}\rho A_f C_{DF}$	B_{55}
	S_5	$\rho U^2 A_f C_{L\alpha}$	C_{35}
		$-\rho U^2\ell A_f C_{L\alpha}$	C_{55}
Wave-	V_w	$-\rho A_f\ell U^2 C_{L\alpha}V_{wf}$	F_5
Exciting		$-\ell\dfrac{8V_{of}}{3\pi}\rho A_f C_{DF}.V_{wf}$	F_5
Force		$\rho A_f U^2 C_{L\alpha}.V_{wf}$	F_3
Terms		$\dfrac{8V_{of}}{3\pi}\rho A_f C_{DF}.V_{wf}$	F_3

TABLE 2-3

The Corrections due to the effect of fins

$$C_{L\alpha_O} \cdot = \frac{1.8\pi \, Ae}{1.8 + \sqrt{Ae^2 + 4}} \quad \text{per radian} \qquad (2\text{-}131)$$

$$(2\text{-}132)$$

$$\text{where } Ae = \{(R + S_p) - \frac{R^2}{(R + S_p)}\}/C_h \text{ is the effective} \qquad (2\text{-}132)$$

$$\text{aspect ratio}$$

R is the radius of the hull body to which the fin is attached.

S_p is the span of the fin.

C_h is the chord of the fin.

4.4.1   The effect of aspect ratio

For fins with finite aspect ratio (ie a three-dimensional section) the cross flow occurs over the tip of the fin when flows go from the higher pressure side to the lower pressure side. This cross flow will increase as the span decreases, and consequently, decreases the lift. When fins are attached to the hull body the flow is forced to go outwards towards the edge of the fin area and is prevented passing through the hull surface, according to mirror image principle of the vortex singularity, and the lift coefficient generated will be identical to the fin of twice its geometric aspect ratio (span/chord). Therefore, in general, the effective aspect ratio which equals $2(\frac{S_p}{C_h})$ should be used when the fin is mounted on a rigid surface.

Relatively, a SWATH ship has a small hull section. For example in this study the ratio of fin span to hull radius is equal to 2.52. The rigid surface can be considered as a curved surface instead of a plane wall. The image singularity moves closer to the surface and is located at the inverse point at a distance of $R^2/(R + S_p)$ if a vortex is put at the tip of the fin and the reflected image inside the centre of the circular hull. When S_p is the span and R is the radius of hull, the image-image vortex singularity has a distance equal to

$[(R + S_p) - R^2/(R + S_p)]$. Thus, taking this distance as an 'effective span' of the fin, the effective aspect ratio can be obtained as in equation (2-132) rather than taking twice the value of geometric aspect ratio and, according to the slender body theory [70] and [71]:-

$$K_{F(H)} = \frac{2}{\pi(1-r)^2}\left[(1+r^4)\{\tfrac{1}{2}\tan^{-1}\}(\tfrac{1}{r} - r) + \tfrac{\pi}{4}\} - r^2\{(\tfrac{1}{r} - r) + 2\tan^{-1}r\}\right] \qquad (2\text{-}133)$$

$$K_{H(F)} = \frac{1}{(1-r^2)}\left[(1-r^2)^2 - \tfrac{2}{\pi}\left[(1+r^4)\{\tfrac{1}{2}\tan^{-1}\}(\tfrac{1}{r} - r) + \tfrac{\pi}{4}\}\right.\right.$$
$$\left.\left. - r^2\{(\tfrac{1}{r} - r) + 2\tan^{-1}r\}\right]\right] \qquad (2\text{-}134)$$

where $r = \dfrac{R}{R + S_p}$

Another method of predicting $C_{L\alpha}$ is given by Abkowitz [43] which represented a thin hydrofoil by an elliptical distribution. $C_{L\alpha}$ is calculated to be:-

$$\frac{2\pi}{1 + \dfrac{2}{Ae}} \quad \text{for potential flow} \qquad (2\text{-}135)$$

and

$$\frac{5.7}{1 + \dfrac{2}{Ae}} \quad \text{for real (viscous) flow} \qquad (2\text{-}136)$$

Since the fins are attached to the hull the effective aspect ratio of the hydrofoil, Ae in the above expression is defined as twice the geometric aspect ratio.

Lee [72] also carried out an experimental investigation by measuring C_{35} and C_{55} of the bare-hull and subtracted these values from those of the hull with fin, at the corresponding speeds. From the experimental results the difference:-

$$\Delta C_{35} = \rho U^2 \Sigma A_f \cdot C_{L\alpha} \qquad (2\text{-}137)$$

$$\Delta C_{55} = - \rho U^2 \Sigma A_f \cdot \ell \cdot C_{L\alpha} \qquad (2\text{-}138)$$

indicated that $C_{L\alpha}$ changed with speed. The comparison of the numerial values according to these various methods for the aft fins in this study are listed in Table 2.4 and the comparison of the heave and pitch motion due to the variation of $C_{L\alpha}$ is plotted in Chapter 5.

Method	$C_{L\alpha}$
Body-fin Effect	3.3268
M A Abkowitz	3.43 for non-viscous flow 3.11 for real flow
Two-dimensional fin theory	2π
Lee's Experimental	4.3 for $F_n = 0.26$ 3.7 for $F_n = 0.52$

Table 2.4

5. THE HYDRODYNAMIC COEFFICIENTS

5.1. Introduction

A knowledge of the hydrodynamic derivatives, added mass and damping coefficients in the equations of motion, is a primary requirement for the study of SWATH body motion responses due to wave exciting forces. As mentioned in the previous chapter, the three-dimensional added mass and damping coeffiients of geometrically slender bodies as in SWATH ship geometry can be approximated by a strip-theory synthesis, in which the flow at each cross-section is assumed to be locally two-dimensional.

Three methods have been widely used within the framework of potential flow assumptions for computing the frequency dependent two-dimensional sectional hydrodynamic coefficients. These are the Lewis-form technique, the Tasai-Porter Close-fit mapping method, and the Frank Close-fit source distributing method. Perhaps the Frank Close-fit source distribution method is the most widely used of these three methods. The comparison of these methods is discussed in detail in References [34,73]. The reason for selecting the Frank Close-fit method are its suitability for the small sectional area such as SWATH hull and strut combination shapes and the extensive expertise developed in the Department of Naval Architecture and Ocean Engineering at the University of Glasgow, where the author carried out his research [73]. In addition, the method has proved to compare quite well with the experimental results [34,72].

Since the accuracy of motion and wave-force predictions depends largely on the accuracy of these coefficients, the Frank Close-fit method was used in this study only under the potential flow assumption at zero speed. The viscous fluid effect associated with forward speed and the effects of stationary fins were also considered in Sections 3.3 and 5.6 of this Chapter.

5.2.   Theoretical review of the Frank Close-fit method

Consider a semi-submerged horizontal cylinder whose cross-section is simply connected, as shown in fig. 2.15 and assume that it oscillates vertically in calm water with an amplitude which is assumed small compared to the beam of the cylinder. The oscillatory velocity potential can be expressed in the following form within

potential theory assumptions, ie inviscid, incompressible and irrotational fluid:-

$$\Phi(y,z,t) = Re[\phi(y,z)e^{-i\omega t}]$$

$$= \phi_c\cos\omega t + \phi_s\sin\omega t \qquad (2-139)$$

where $\phi(y,z) = \phi_c + i\phi_s$, ϕ_c is the real part of the velocity

potential associated with the cos term

ϕ_s is the imaginary part of the velocity

potential associated with the sin term.

The simple harmonic motion of a point on the surface of the section can be expressed as:-

$$S(t) = h_o\sin\omega t \qquad (2-140)$$

where h_o is the maximum amplitude of the oscillation motion.

The required velocity potential ϕ, which is represented by:-

$$\phi = Re \int_{c_o} Q(\xi,\eta)G(y,z;\xi,\eta)ds \qquad (2-141)$$

must satisfy the boundary conditions as presented in fig. 2.15 and the solution of $\phi(y,z)$, as suggested by Frank [59], is found by determining the strengths over the immersed contour of the cylinder.

The complex potential at the field point (y,z) of a pulsating source of unit strength located at (ξ,η), see fig. 2.16, is given as:-

$$S(t) = h_o \sin \omega t$$

$$\phi_{tt} + g\phi_{\bar{\jmath}} = 0$$

$$\nabla^2 \phi = 0$$

$$\phi_n = h_o \omega \cos(n.\bar{\jmath}) = V_n$$

$$\phi_{\bar{\jmath}}(0,\bar{\jmath}) = 0$$

$$\nabla\phi(y,-\infty) = 0$$
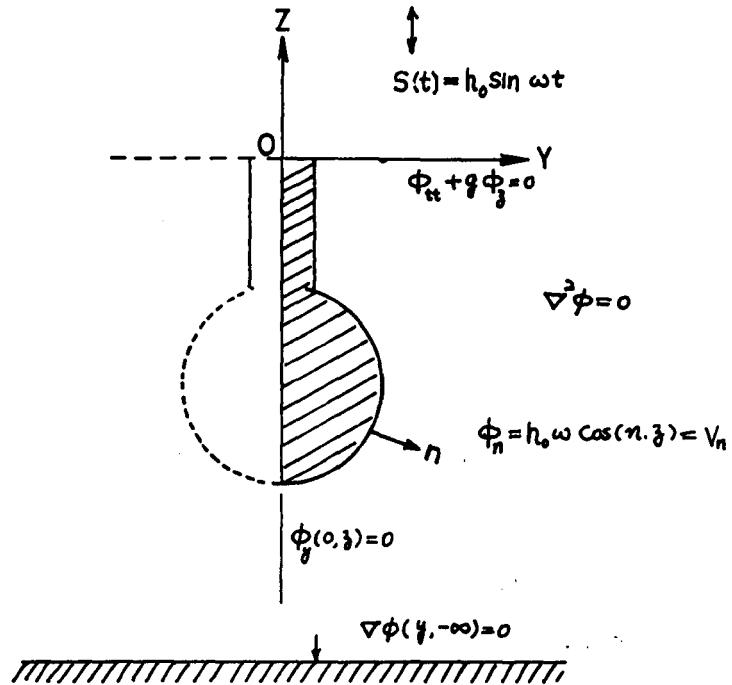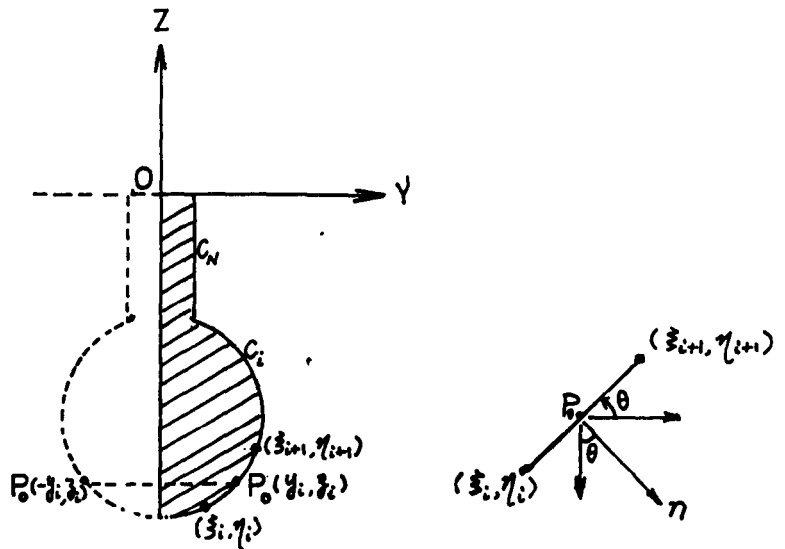
Fig. 2.15

Fig. 2.16

$$G(y,z;\xi,\eta) = \text{Re}\{\frac{1}{2\pi}\left[\log(x-\zeta) - \log(x-\bar{\zeta}) + 2p.V\int_{0}^{\infty}\frac{e^{-ik(x-\bar{\zeta})}}{K-k}\,dk\right]\} \quad (2\text{-}142)$$

$$-i\text{Re}\left[e^{-iK(x-\bar{\zeta})}\right]$$

$$= G_R + iG_I$$

with $\quad x = y + iz$

$\zeta = \xi + i\eta$

$\bar{\zeta} = \xi - i\eta$

$K = \omega^2/g$, wave number.

$p.V\int$ is the principle value integral

$Q(\xi,\eta)$ is the unknown source density as a function

of position along the contour c_0.

k is the spring constant.

Assuming that the contour of the cylinder can be approximated by N number of straight line segments and the source strength on each segment is treated as constant but varies from segment to segment, then equation (2-141) can be rewritten as:-

$$\phi(y,z) = \sum_{j=1}^{N} Q_j(\xi,\eta)\text{Re}\int_{c_j} G(y,z;\xi,\eta)\,ds \quad (2\text{-}143)$$

In order to determine the unknown source strength the application of the kinematic boundary condition on the section contour yeilds:-

$$V_n = \phi_n = \nabla\phi.\vec{n}$$

It follows:-

$$\phi_n(y_0,z_0) = \sum_{i=1}^{N} Q_j (n.\nabla)\text{Re} \int_{cj} G(y,z;\xi,\eta)ds \Big|_{p=p_0} \tag{2-144}$$

$$= h_0\omega\cos\theta$$

From the linearised Bernoulli equation, the hydrodynamic pressure at point (y_0,z_0) is:-

$$p(y_0,z_0,t) = - \rho\Phi_t(y_0,z_0,t) \tag{2-145}$$

$$= - \rho\text{Re}[- i\omega\phi(y_0,z_0)e^{-i\omega t}] \tag{2-146}$$

$$= - \rho\omega(\phi_s\cos\omega t - \phi_c\sin\omega t) \tag{2-147}$$

The vertical hydrodynamic force acting on the section is:-

$$F = - \int_{c_0} p\cos\theta ds \tag{2-148}$$

$$= \rho\omega[\cos\omega t \int_{c_0} \phi_s\cos\theta ds - \sin\omega t \int_{c_0} \phi_c\cos\theta ds] \tag{2-149}$$

This total hydrodynamic force induced by the motions of the cylinder has two components which are linearly proportional to acceleration and velocity of motion and are given by the form:-

$$F = - a\ddot{S} - b\dot{S} \tag{2-150}$$

If $S(t) = h_0\sin\omega t$ is substituted, then:-

$$F = h_0\omega^2 a\sin\omega t - h_0\omega b\cos\omega t \tag{2-151}$$

and the corresponding terms from equations (2-149) and (2-151) are:-

$$\text{Added Mass } a = - \frac{\rho}{h_0\omega} \int_{c_0} \phi_c\cos\theta ds \tag{2-152}$$

$$\text{Damping} \quad b = \frac{\rho}{h_0 \omega} \int_{C_0} \phi_s \cos\theta ds \tag{2-153}$$

5.3   The calculation procedure

A computer program, utilising the above Frank Close-fit technique, which was developed by Atlar [73], was used to calculate the hydrodynamic coefficients. The program calculates the non-dimensional pressures, added mass and damping coefficients of a horizontal cylinder oscillating in heave, sway or roll while the cylinder is located in the free surface for a range of encounter frequencies f, of 0.05, 0.075, 0.1, 0.15, 0.3, 0.5, 0.7 and 0.9 Hz (the corresponding wave lengths being 624m, 277m, 156m, 69m, 17m, 6m, 3m and 1.9m) and for half strut-thickness ratios (HST/R) of 0.0, 0.1, 0.3, 0.5, 0.7 and 1.0 and section submergence depths of 3R, 4R, 5R, 6R, where R is the circular cross-section radius and the submergence depth is measured to the bottom of the cylinder.

In the program, the definition of the non-dimensional added mass coefficients is different in submerged and floating cases. For the submerged case, C_V = Added mass/$\rho\pi R^2$, while for the floating case, C_{V1} = Added mass/$\frac{1}{2}\rho\pi(HST)^2$.

In order to use the same definition, C_{V1} is redefined as the added mass coefficient C_V for the submerged case, ie non-dimensionalised by $\rho\pi R^2$. Consequently, C_{V1} is rewritten as $C_V = (HST)^2/2R^2.C_{V1}$ for the floating case.

The heave added mass per unit length of the cylinder and strut combination is:-

$$C_V . \rho . \pi R^2$$

The heave damping per unit length of the cylinder and strut combination is:-

$$B_{33} . \rho . \omega . \pi R^2$$

The definitions and co-ordinate system used in the program are as shown in figs. 2.17a and 2.17b and the symbols used are:-

R is the Radius of Circular Hull (m) (= 1.0m)

HST is the half strut thickness (m) (HST/R = 0.0, 0.1, 0.3, 0.5, 0.7, 1.0)

H is the depth of the section (m) (H/R = 3.0, 4.0, 5.0, 6.0)

f is the frequency (Hz) (f = 0.05, 0.075, 0.1, 0.15, 0.3, 0.5, 0.7, 0.9)

$\omega^2 R/g$ is non-dimensional frequency ($\omega = 2\pi f$, g, the acceleration due to gravity is $9.81 ms^{-2}$)

C_V is non-dimensional Added Mass Coefficient in heave

B_{33} is non-dimensional Damping Coefficient in heave

The segment ordinates, both in the submerged case and the floating case (for H/R = 6.0, HST/R = 0.3), are shown in fig. 2.17 and tabulated as follows.

For the submerged case (HST = 0.0), the origin of the axis is located on the top side of the submerged cylinder in the y = 0 plane of symmetry, as shown in fig. 2.17b. The ordinates are spaced at ten

(a)

Floating case
HST≠0.0

(b)

Submerged case
HST= 0.0

Fig. 2.17

intervals along the cylinder circumference.

Ordinate No.	X	Y	Ordinate No.	X	Y
1	0.0000	-2.0000	6	1.0000	-1.0000
2	0.3090	-1.9510	7	0.9510	-0.6910
3	0.5877	-1.8090	8	0.8090	-0.4123
4	0.8090	-1.5878	9	0.5877	-0.1910
			10	0.3090	-0.0490
5	0.9510	-1.3090	11	0.0000	-0.0

For the floating case (HST = 0.0), the origin of the X-Y axes is on the waterline at half of strut thickness. The spacing of the ordinates along the strut is 1.0m and then divided by ten intervals. Circumference of the cylinder, see fig. 2.17a. For example, if H/R = 6.0, HST/R = 0.3, the ordinates are:-

Ordinate No.	X	Y	Ordinate No.	X	Y	Ordinate No.	X	Y
1	0.0000	-6.000	6	0.9884	-5.1518	11	0.3000	-4.0000
2	0.2799	-5.9600	7	0.9914	-4.8690	12	0.3000	-3.0000
3	0.5374	-5.8433	8	0.9151	-4.5968	13	0.3000	-2.0000
4	0.7519	-5.6592	9	0.7656	-4.3567	14	0.3000	-1.0000
5	0.9064	-5.4223	10	0.5550	-4.1682	15	0.3000	0.0000

5.4   Results and discussion

The non-dimensional heave added mass and wave damping coefficients for various depths of submergence for a single hull section are shown in figs. 2.18 to 2.23. Figure 2.18 is a submerged case where HST/R = 0.0. At very low frequencies the added mass values

are decreased as the submergence of the section increases. After a certain frequency the added mass values increase as the submergence of the section increases, which is the opposite phenomenon to the low frequency range. Figures 2.19 to 2.23 are the floating case where HST/R varied from 0.1 to 1.0, a similar characteristic to that of the submerged case. The added mass coefficient approaches a constant value for higher frequencies. It should be observed that the turn over point shifts to higher frequency as the strut thickness increases. The results are curve-fitted in figs. 2.24 and 2.25 for two values of H/R, namely H/R = 3.0 and 6.0. The added mass values decreases as the strut thickness increases in these cases with the exception of HST/R = 1.0.

In contrast to the added mass, for the damping coefficients, both in the submerged and in the floating cases, as the hull moves closer to the free surface, more waves are generated and this yields more wave damping (see figs. 2.26 to 2.28). Figure 2.26 is a submerged case of single circular hull section with HST/R = 0.0, whereas figs. 2.27 and 2.28 show floating cases with the strut thickness equal to half and the full radius of the hull.

The same results are plotted in figs. 2.29 and 2.30 for the depth H/R = 3.0 and 6.0 with different strut thicknesses. Increasing the strut thickness yields larger damping in the lower frequency ranges. The turn over point shifts to higher frequencies as the strut thickness increases. In fig. 2.30 at higher depth of submergence, damping only exists at very low frequencies and dies out as the frequency values increase.

According to the above analysis, the variation of the hydrodynamic coefficients are functions of the geometric section of

the immersed body and, in the presence of a free water surface, strongly depend on the frequency of the body motion.

To obtain reasonably accurate added mass and damping coefficients of a SWATH cross section, at least 15 to 20 points of source distribution on the submerged contour of one hull should be taken for each frequency of oscillation. To obtain all the hydrodynamic coefficients in the linear equation of motion covering all degrees of freedom, the sectional added mass and damping coefficients should be computed for the sway, heave and roll mode for about 20 cross sections along the length of a ship. If the motion of a SWATH ship in irregular waves for different wave headings and ship speeds is to be computed, the foregoing number of calculations should be repeated for each wave heading, ship speed and frequency of oscillation. Thus, it can easily be expected that a significant amount of computer time will be required to evaluate the seakeeping qualities of a SWATH ship.

It seems reasonable to seek a simplified method of obtaining the sectional hydrodynamic coefficients. In order to reduce the computing time for the solutions of hydrodynamic data required in the development of a motion and wave load prediction, routines for SWATH circular hull goemetry have been carried out to derive approximate formulae for expressing the heave, added mass and damping coefficients as a function of the encounter frequency, depth of submergence and strut thickness, References [62,74]. Using a least-square method [75], the values of non-dimensional added mass and damping coefficients have been curve fitted. The work has been extended to the sections of rectangular and rectangular with circular corners by other researchers [76,77].

NON-DIM ADDED MASS
HST/R=0.1

Fig. 2.19

NON-DIM ADDED MASS
HST/R=0.0

Fig. 2.18

NON-DIM ADDED MASS
HST/R=0.5

Fig. 2.21

NON-DIM ADDED MASS
HST/R=0.3

Fig. 2.20

NON-DIM ADDED MASS
HST/R=0.7

Fig. 2.22

NON-DIM ADDED MASS
HST/R=1.0
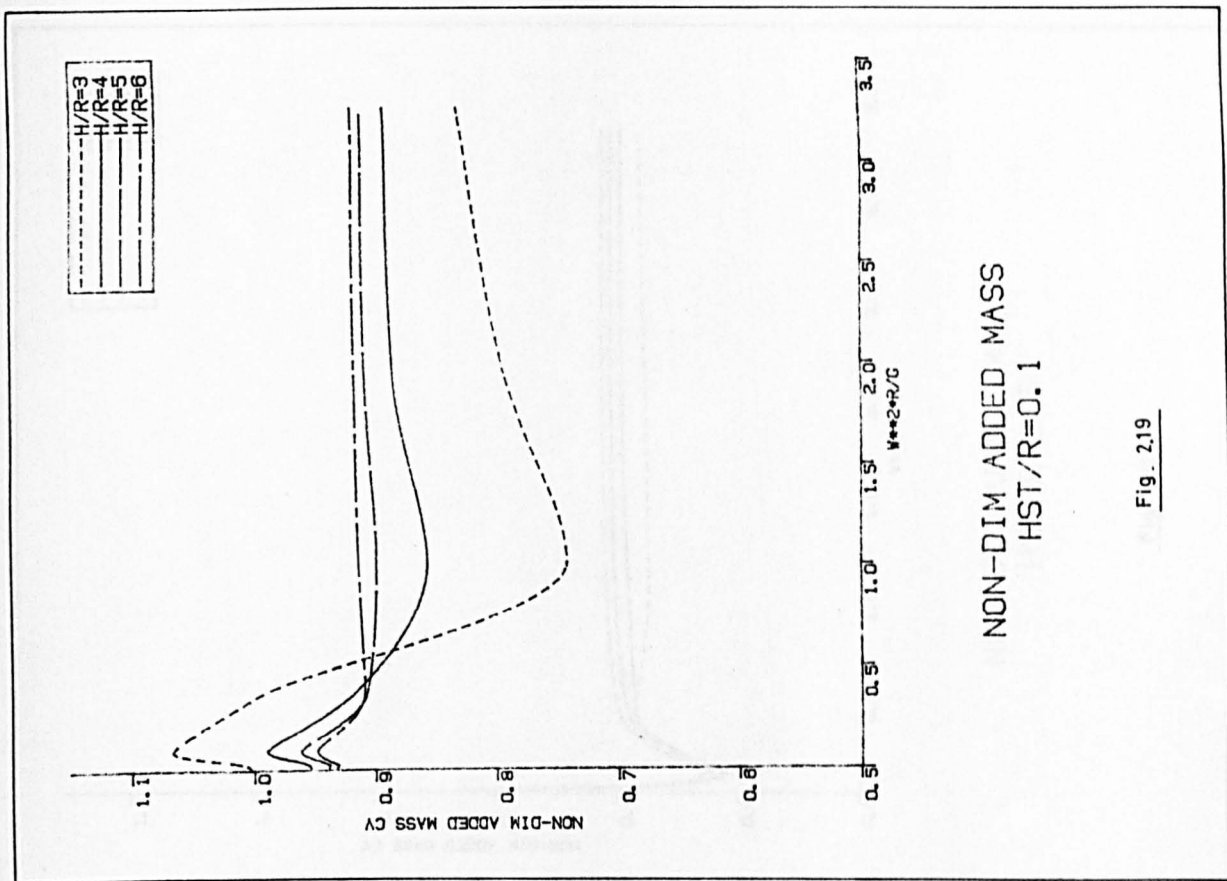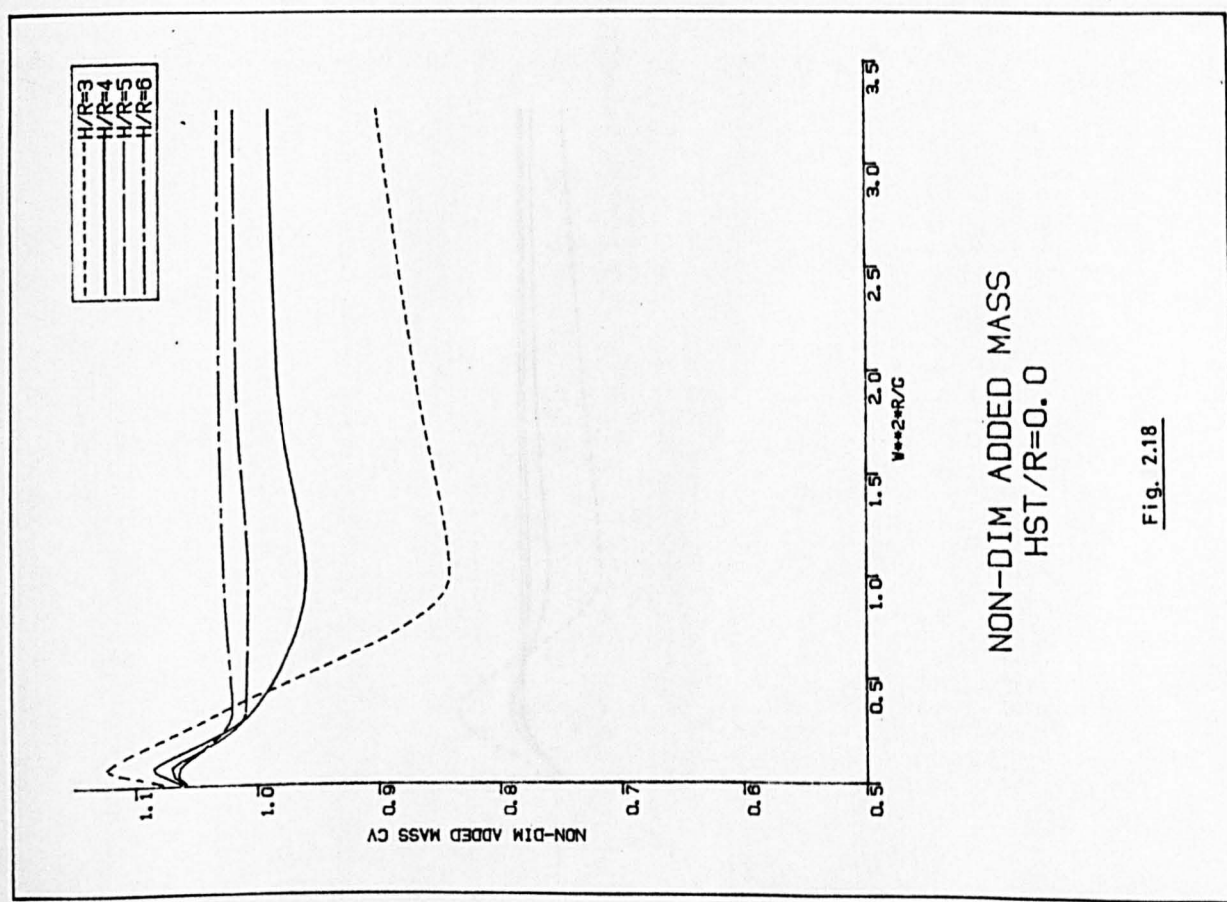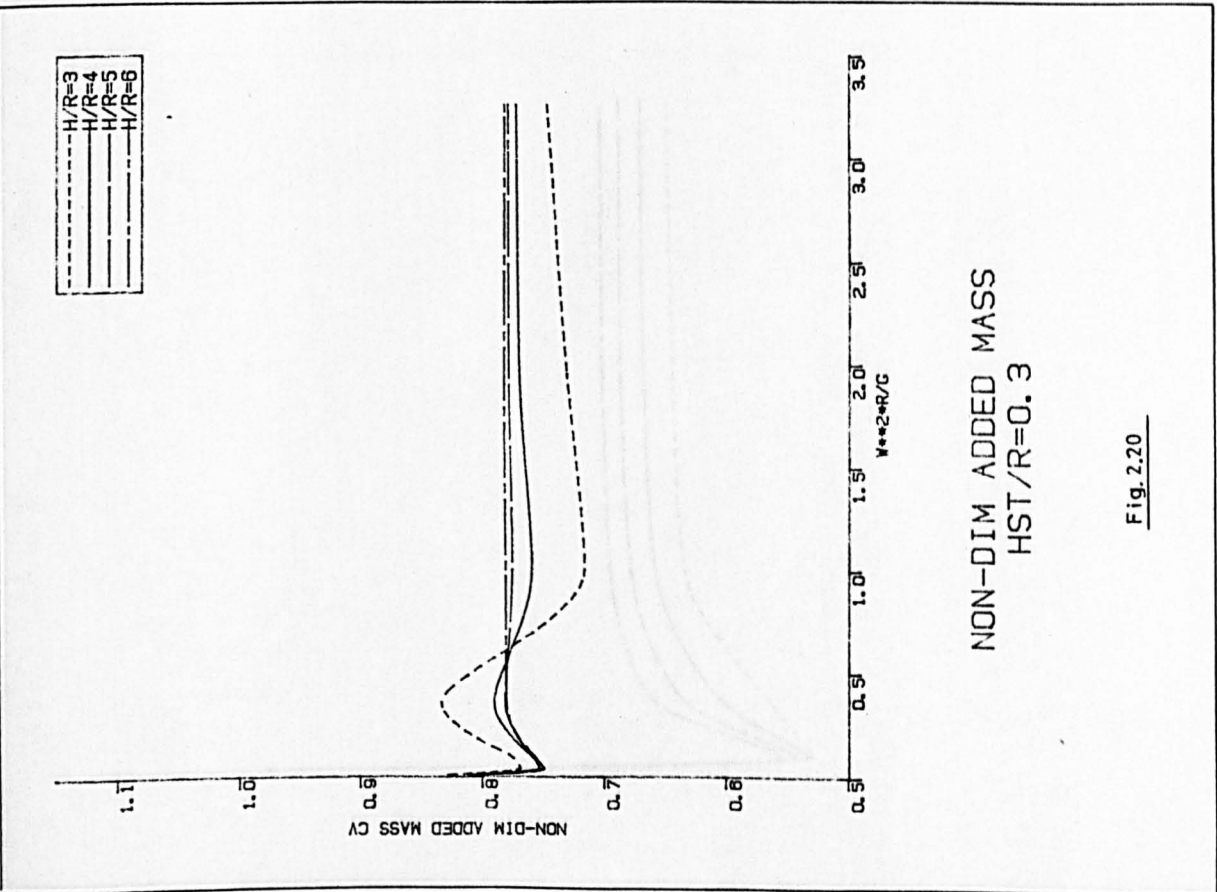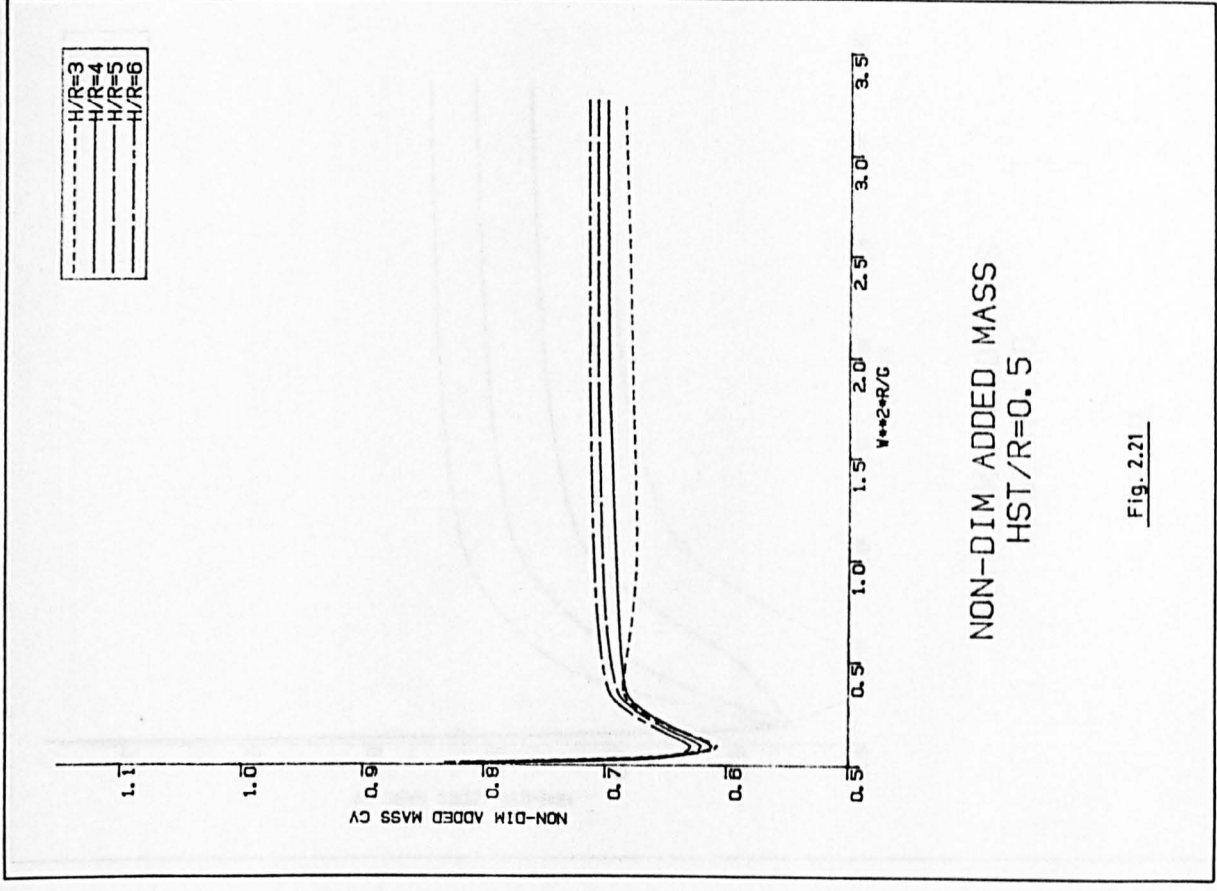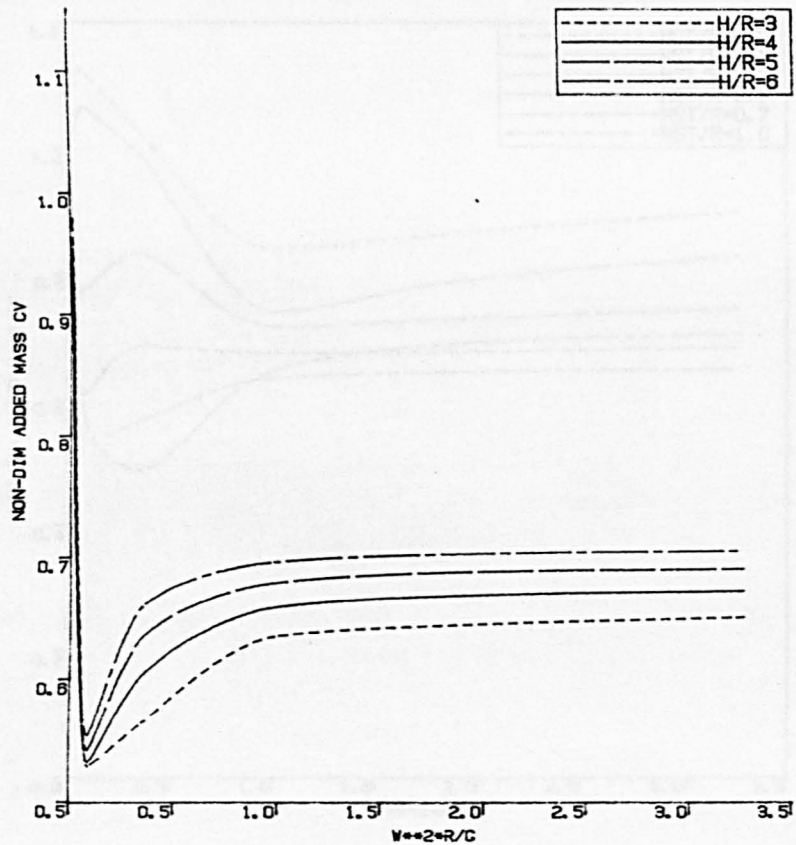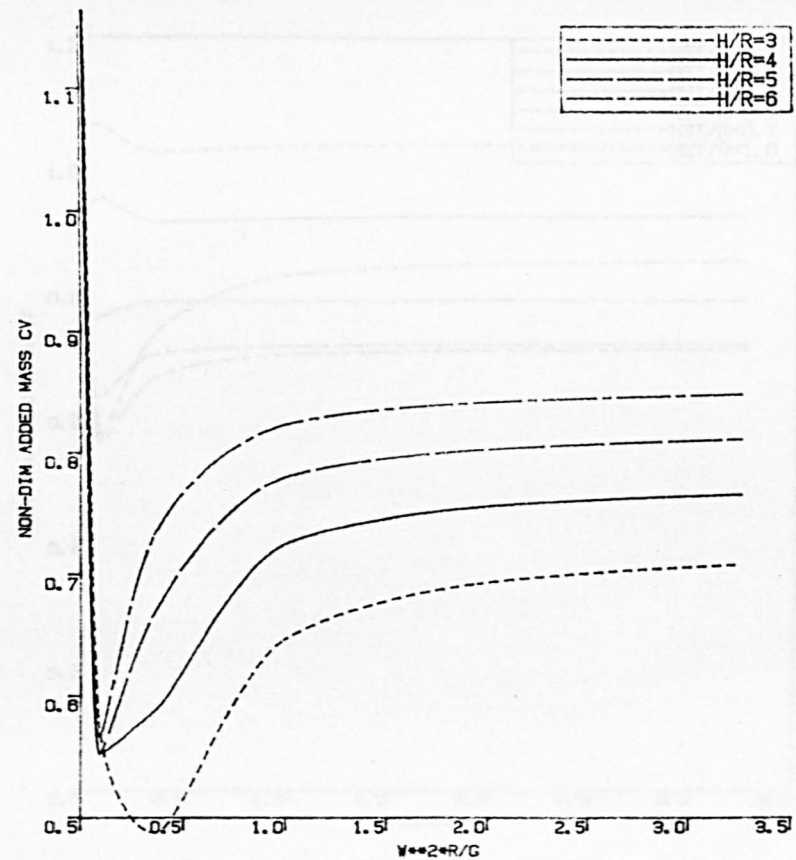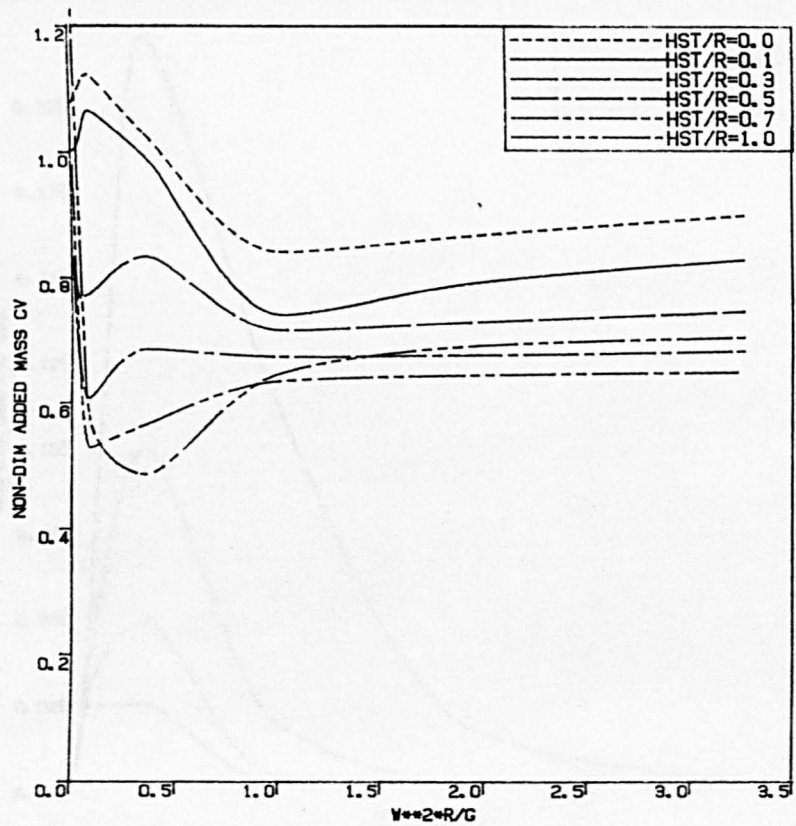
Fig. 2.23

HST/R EFFECT ON ADDED MASS
FOR H/R=3. 0

Fig. 2.24
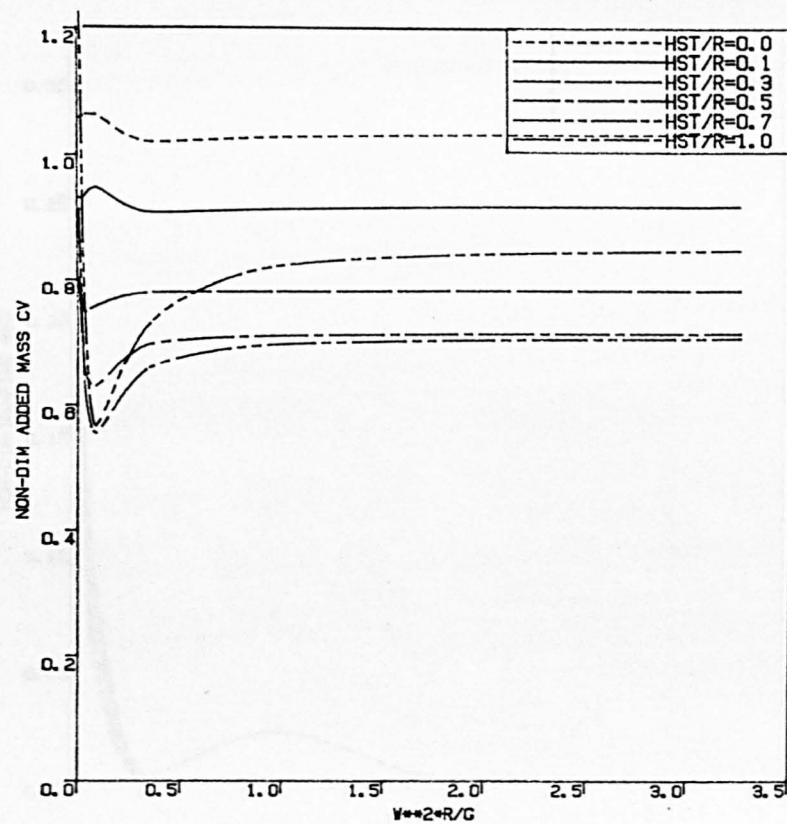
HST/R EFFECT ON ADDED MASS
FOR H/R=6. 0

Fig. 2.25
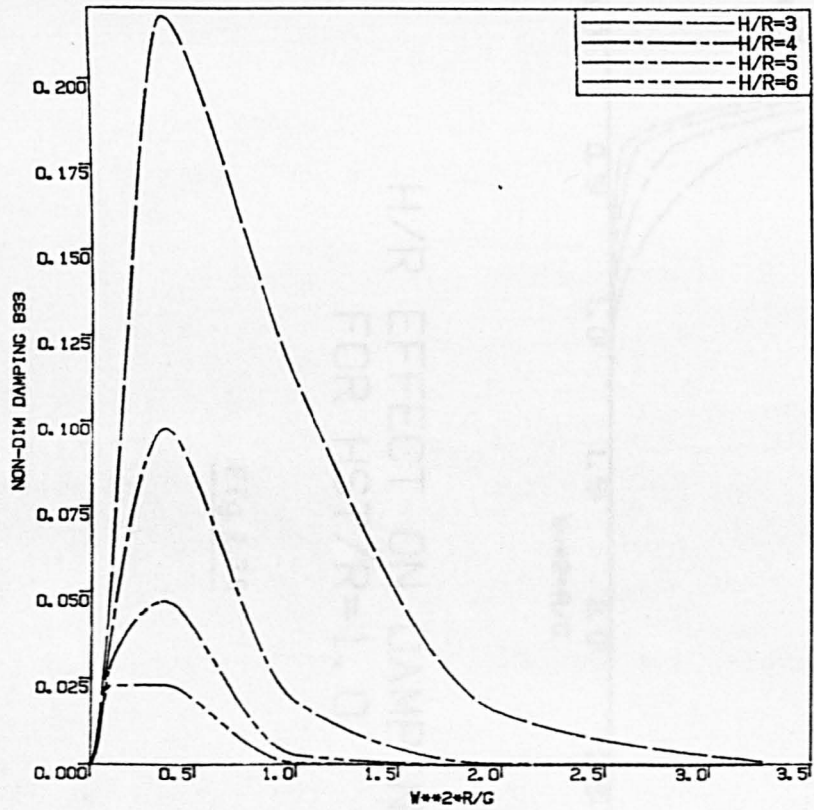
H/R EFFECT ON DAMPING
FOR HST/R=0.0

Fig. 2.26
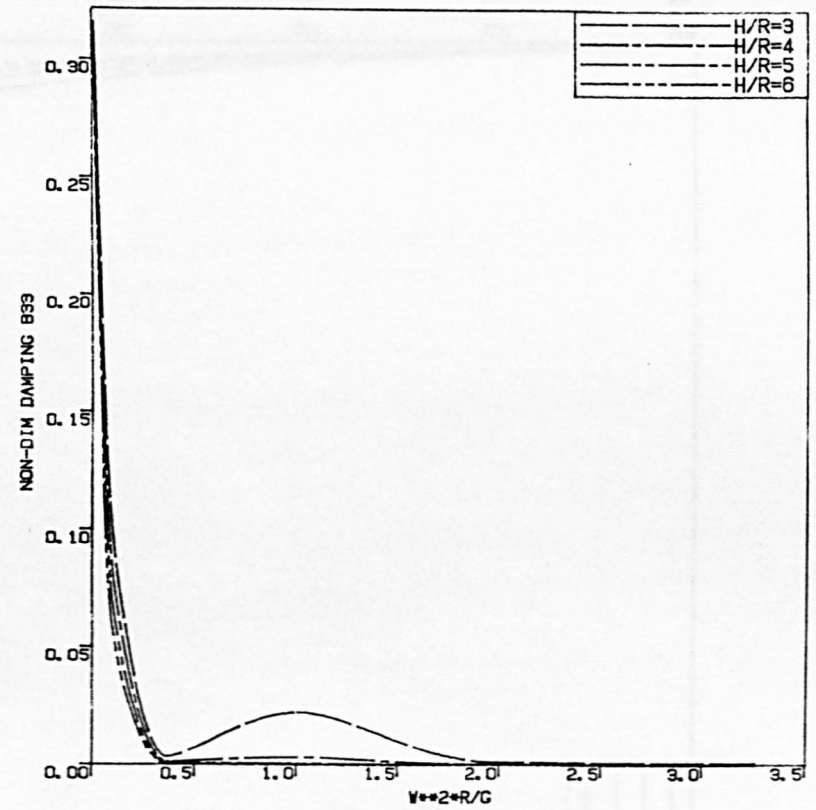
H/R EFFECT ON DAMPING
FOR HST/R=0.5

Fig. 2.27
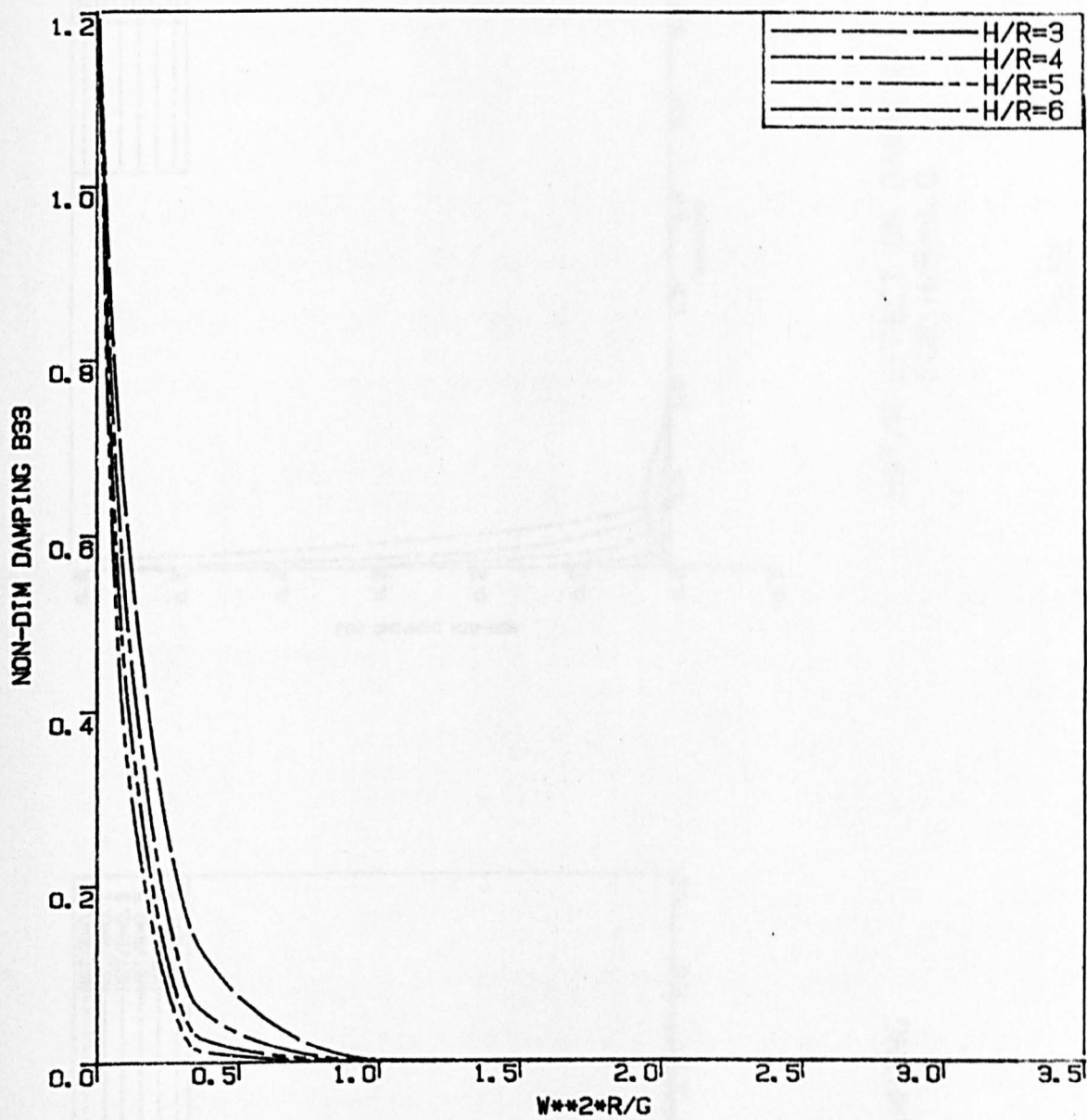
H/R EFFECT ON DAMPING
FOR HST/R=1. 0

Fig.2.28
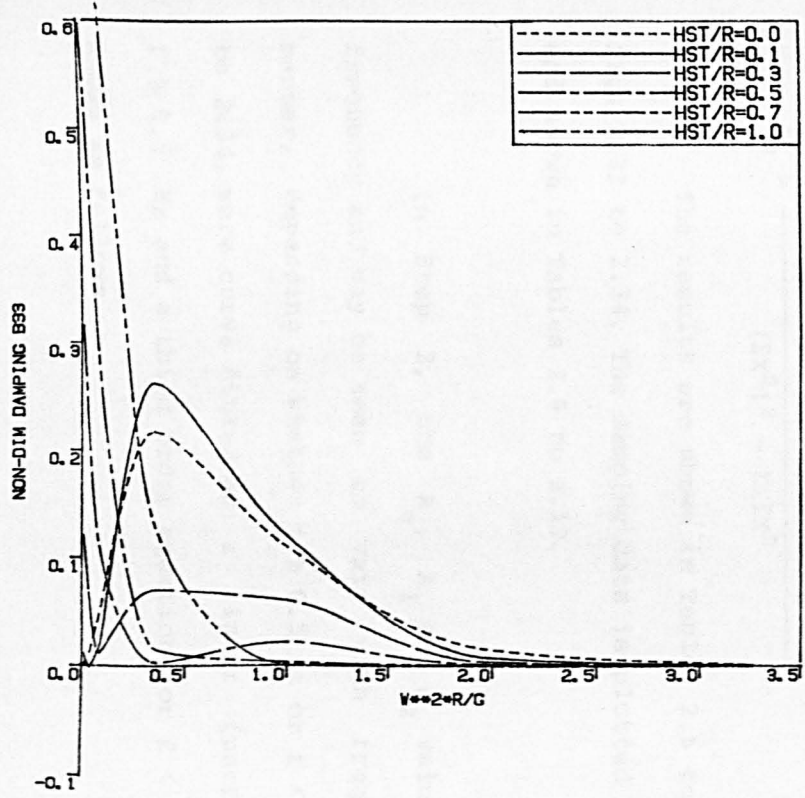
HST/R EFFECT ON DAMPING
FOR H/R=3.0

Fig. 2.29
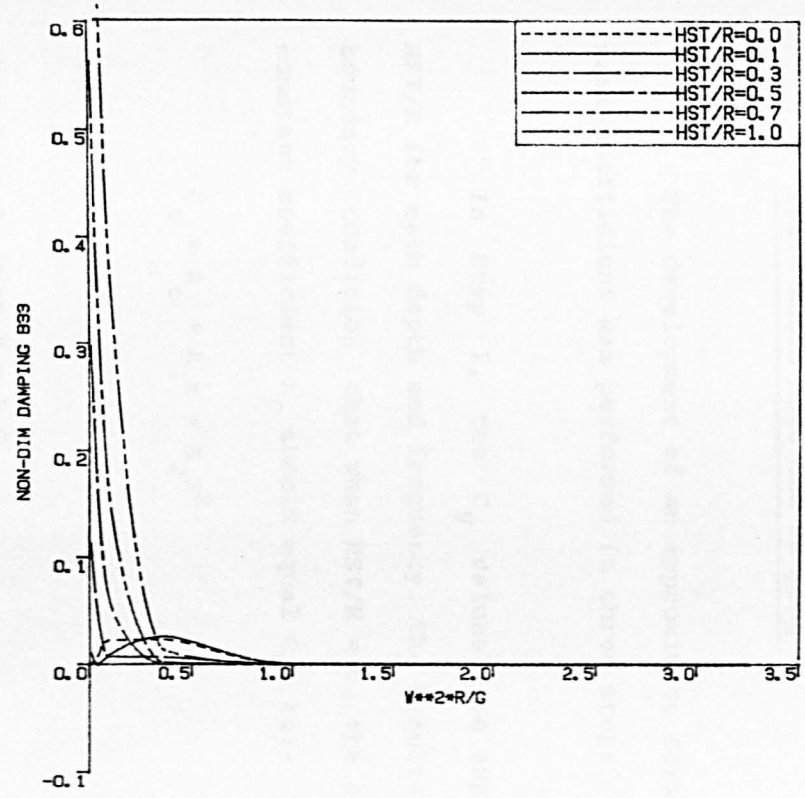
HST/R EFFECT ON DAMPING
FOR H/R=6.0

Fig. 2.30

5.5 The Development of an Approximate Formulae for Heave Added Mass and Damping

The development of an approximate formula for the heave added mass coefficient was performed in three steps.

In Step 1, the C_V values were expressed as a function of HST/R for each depth and frequency. The results are limited to the boundary condition that when HST/R = 0, the submerged condition, the constant coefficient A_o should equal C_V, ie:-

$$C_V = A_o + A_1 x + A_2 x^2$$

where x = HST/R

then $A_o = C_V$ when x = 0.0

and

$$A_1 = \frac{\Sigma (C_V - A_o) \Sigma x^3 - \Sigma (C_V - A_o) x \Sigma x^2}{\Sigma x \Sigma x^3 - (\Sigma x^2)^2}$$

$$A_2 = \frac{\Sigma (C_V - A_o) \Sigma x^2 - \Sigma (C_V - A_o) x \Sigma x}{(\Sigma x^2)^2 - \Sigma x \Sigma x^3}$$

The results are shown in Tables 2.5 to 2.8 and are plotted in figs 2.31 to 2.34. The damping data is plotted in figs. 2.35 to 2.38 and shown in Tables 2.9 to 2.12.

In Step 2, the A_o, A_1 and A_2 values, which depend on the frequency and may be seen to vary with frequency in a different manner, depending on whether $f \geqslant 0.5$ Hz or $f < 0.5$ Hz, see figs. 2.31 to 2.34, were curve fitted as a linear function of frequency for $f \geqslant 0.5$ Hz and a third order equation for $f < 0.5$ Hz. The results are shown as follows.

HEAVE ADDED MASS COEFFICINTS AGAINST HST/R, H, F

H/R=3.0

FREQ. (hz)	HST/R						A0	A1	A2
	0.0	0.1	0.3	0.5	0.7	1.0			
0.050	1.07880	1.00264	0.82919	0.83216	0.97887	1.47570	1.07880	-1.25979	1.63045
0.075	1.08750	1.00640	0.78856	0.72789	0.78843	1.10690	1.08750	-1.31869	1.30939
0.100	1.09930	1.02008	0.76864	0.66219	0.66249	0.85975	1.09930	-1.34188	1.06823
0.150	1.12430	1.06720	0.77428	0.60786	0.52989	0.57460	1.12430	-1.26457	0.66316
0.300	1.02940	0.99376	0.83417	0.68595	0.56651	0.48780	1.02940	-0.67234	0.09199
0.500	0.84230	0.74209	0.71711	0.67532	0.63631	0.64800	0.84230	-0.63856	0.47152
0.700	0.87020	0.79499	0.73158	0.67869	0.64643	0.69345	0.87020	-0.64599	0.47485
0.900	0.90220	0.83156	0.74898	0.68609	0.65217	0.70765	0.90220	-0.68827	0.49181

Table (2- 5)

HEAVE ADDED MASS COEFFICINTS AGAINST HST/R, H, F

H/R=4.0

FREQ. (hz)	HST/R						A0	A1	A2
	0.0	0.1	0.3	0.5	0.7	1.0			
0.050	1.06310	0.95395	0.81152	0.81883	0.95374	1.41365	1.06310	-1.31892	1.66597
0.075	1.06860	0.95484	0.77157	0.71599	0.76413	1.04350	1.06860	-1.36400	1.33339
0.100	1.07540	0.96333	0.75280	0.65435	0.64366	0.80270	1.07540	-1.36922	1.08686
0.150	1.08530	0.98994	0.75792	0.61249	0.53339	0.55285	1.08530	-1.26613	0.71306
0.300	1.00360	0.91820	0.79079	0.68429	0.60640	0.58910	1.00360	-0.86685	0.44814
0.500	0.96000	0.85733	0.75990	0.69205	0.65993	0.72645	0.96000	-0.91272	0.68953
0.700	0.98360	0.88568	0.77059	0.69792	0.67010	0.75590	0.98360	-0.95432	0.73012
0.900	0.99090	0.89340	0.77356	0.70005	0.67417	0.76640	0.99090	-0.97077	0.74841

Table (2- 6)

HEAVE ADDED MASS COEFFICINTS AGAINST HST/R, H, F

H/R=5.0

FREQ. (hz)	HST/R						A0	A1	A2
	0.0	0.1	0.3	0.5	0.7	1.0			
0.050	1.06000	0.93871	0.80543	0.80939	0.93249	1.36315	1.06000	-1.33848	1.64633
0.075	1.06390	0.93856	0.76653	0.70831	0.74465	0.99415	1.06390	-1.37380	1.30683
0.100	1.06830	0.94494	0.74956	0.65108	0.63070	0.76300	1.06830	-1.36719	1.06112
0.150	1.07130	0.96247	0.75641	0.62106	0.54275	0.55320	1.07130	-1.25217	0.72556
0.300	1.00980	0.90674	0.78169	0.69075	0.63744	0.67125	1.00980	-0.98275	0.64893
0.500	1.00790	0.89878	0.77566	0.70265	0.68002	0.78115	1.00790	-1.04845	0.82866
0.700	1.01770	0.90939	0.77977	0.70673	0.68867	0.80325	1.01770	-1.07243	0.86284
0.900	1.02010	0.91195	0.78080	0.70820	0.69205	0.81155	1.02010	-1.07924	0.87505

Table (2- 7)

HEAVE ADDED MASS COEFFICINTS AGAINST HST/R, H, F

H/R=6.0

FREQ. (hz)	HST/R						A0	A1	A2
	0.0	0.1	0.3	0.5	0.7	1.0			
0.050	1.05890	0.93226	0.80210	0.80135	0.91402	1.32055	1.05890	-1.34338	1.61335
0.075	1.06180	0.93165	0.76442	0.70236	0.72880	0.95490	1.06180	-1.37107	1.27060
0.100	1.06480	0.93691	0.74935	0.64966	0.62210	0.73575	1.06480	-1.35632	1.03055
0.150	1.06390	0.94931	0.75822	0.63046	0.55554	0.56735	1.06390	-1.23707	0.73792
0.300	1.02050	0.90931	0.78082	0.69823	0.66214	0.73605	1.02050	-1.06044	0.78325
0.500	1.02810	0.91417	0.78181	0.71030	0.69703	0.82380	1.02810	-1.11829	0.92074
0.700	1.03220	0.91837	0.78369	0.71356	0.70445	0.84170	1.03220	-1.13117	0.94664
0.900	1.03330	0.91950	0.78426	0.71482	0.70734	0.84855	1.03330	-1.13511	0.95612

Table (2- 8)

ADDED MASS FORMULA-A0, A1, A2
H/R=4.0

Fig. 2.32

ADDED MASS FORMULA-A0, A1, A2
H/R=3.0

Fig. 2.31

ADDED MASS FORMULA—A0, A1, A2
H/R=6.0

Fig. 2·34

ADDED MASS FORMULA—A0, A1, A2
H/R=5.0
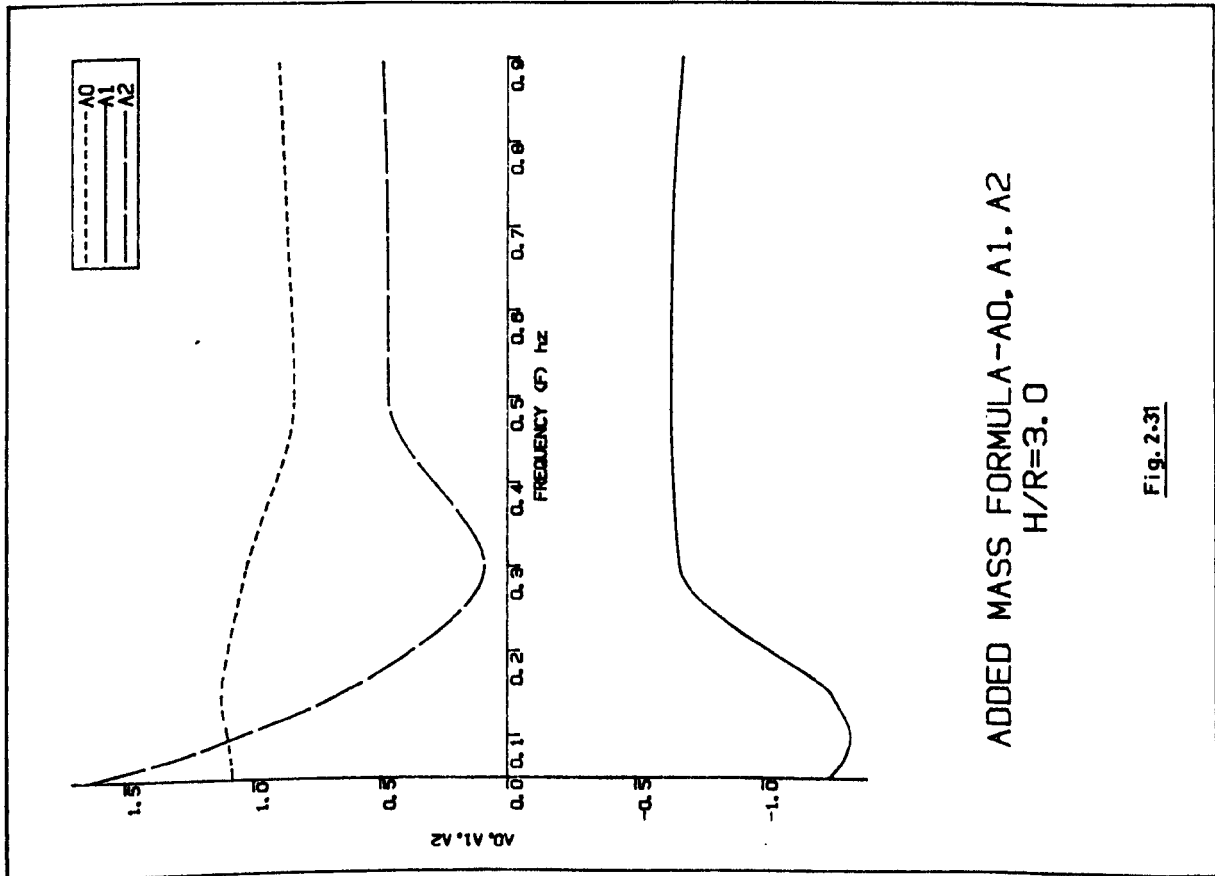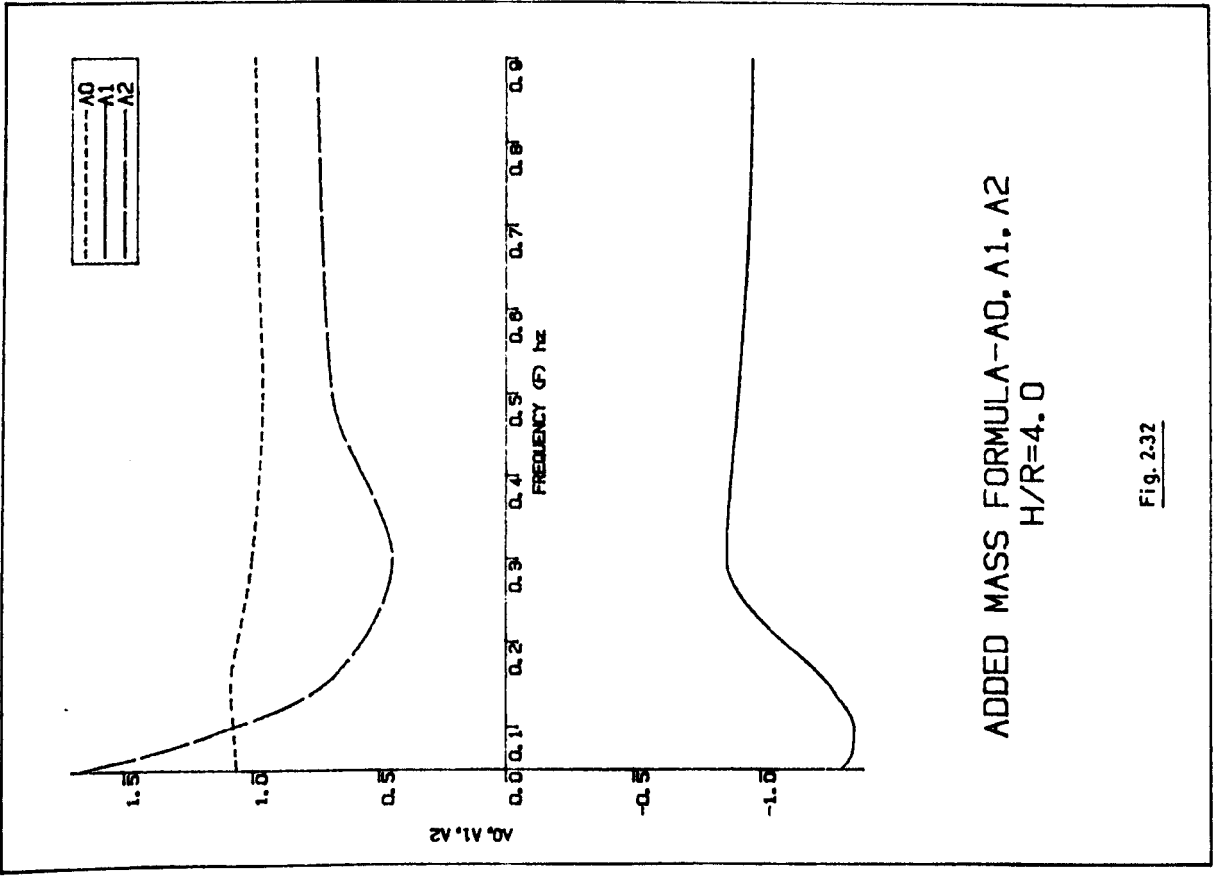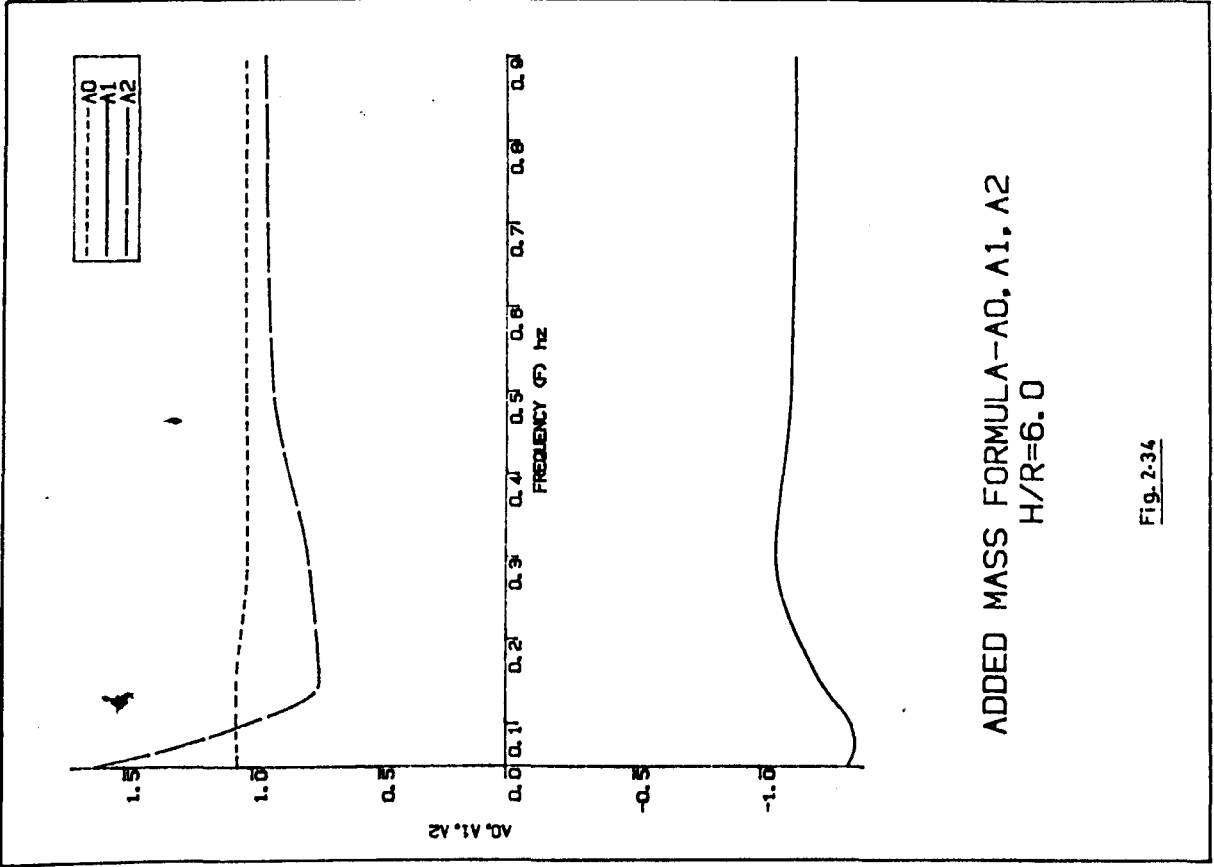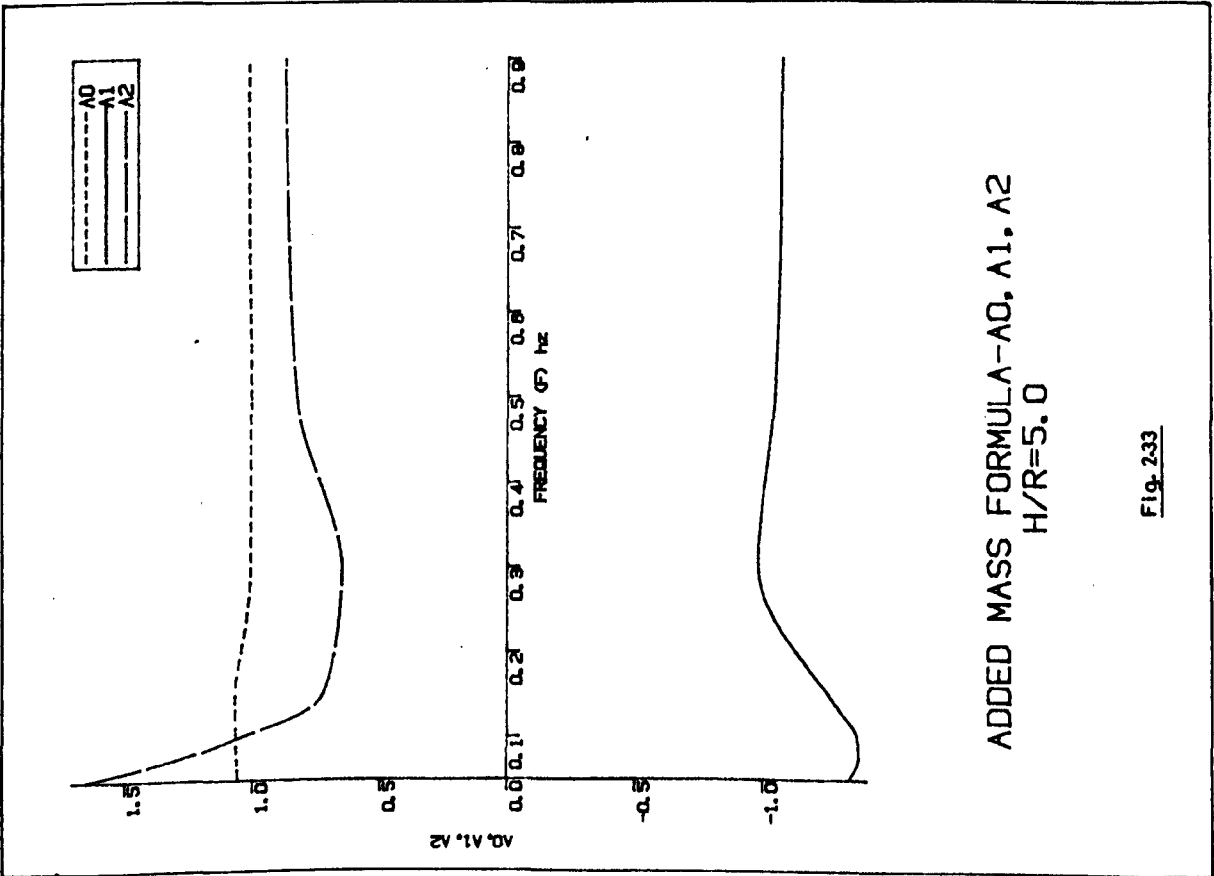
Fig. 2·33

HEAVE DAMPING COEFFICINTS AGAINST HST/R, H, F

H/R=3.0

FREQ. (hz)	HST/R 0.0	0.1	0.3	0.5	0.7	1.0	A0	A1	A2
0.050	0.00140	0.01158	0.12060	0.31538	0.59657	1.19300	0.00140	0.04092	1.15421
0.075	0.00480	0.00361	0.09333	0.26963	0.52822	1.07550	0.00480	-0.04941	1.12758
0.100	0.01250	-0.00107	0.06296	0.21675	0.44982	0.94450	0.01250	-0.16305	1.10564
0.150	0.04720	0.01797	0.01242	0.11139	0.28812	0.67650	0.04720	-0.39799	1.03511
0.300	0.21800	0.26355	0.07092	0.00329	0.01524	0.12930	0.21800	-0.42543	0.27088
0.500	0.11040	0.12045	0.06017	0.02200	0.00343	0.00151	0.11040	-0.13879	0.00891
0.700	0.01560	0.00786	0.00353	0.00105	0.00020	-0.00030	0.01560	-0.05489	0.04188
0.900	0.00080	-0.00007	0.00004	0.00066	0.00006	0.00002	0.00080	-0.00361	0.00332

Table (2- 9)

HEAVE DAMPING COEFFICINTS AGAINST HST/R, H, F

H/R=4.0

FREQ. (hz)	HST/R 0.0	0.1	0.3	0.5	0.7	1.0	A0	A1	A2
0.050	0.00080	0.01129	0.11790	0.30925	0.58555	1.17200	0.00080	0.04109	1.13324
0.075	0.00340	0.00361	0.08915	0.25800	0.50617	1.03250	0.00340	-0.04280	1.07810
0.100	0.00940	-0.00084	0.05832	0.20038	0.41674	0.87800	0.00940	-0.14150	1.01821
0.150	0.03450	0.01315	0.01080	0.09311	0.24128	0.57050	0.03450	-0.31349	0.85403
0.300	0.09780	0.11305	0.03069	0.00129	0.00731	0.06065	0.09780	-0.20828	0.14431
0.500	0.01780	0.01870	0.00846	0.00293	0.00047	0.00002	0.01780	-0.02717	0.00664
0.700	0.00040	0.00011	0.00000	0.00000	0.00002	0.00004	0.00040	-0.00187	0.00165
0.900	0.00000	0.00001	0.00004	0.00000	0.00000	0.00001	0.00000	0.00011	-0.00012

Table (2-10)

HEAVE DAMPING COEFFICINTS AGAINST HST/R, H, F

H/R=5.0

FREQ. (hz)	HST/R 0.0	0.1	0.3	0.5	0.7	1.0	A0	A1	A2
0.050	0.00070	0.01108	0.11552	0.30325	0.57452	1.15100	0.00070	0.03952	1.11365
0.075	0.00310	0.00349	0.08523	0.24688	0.48485	0.99050	0.00310	-0.04167	1.03467
0.100	0.00830	-0.00072	0.05387	0.18525	0.38563	0.81400	0.00830	-0.13011	0.94284
0.150	0.02770	0.01043	0.00910	0.07765	0.20161	0.47850	0.02770	-0.25863	0.71762
0.300	0.04740	0.05375	0.01448	0.00058	0.00351	0.02859	0.04740	-0.10392	0.07288
0.500	0.00260	0.00262	0.00114	0.00039	0.00007	-0.00004	0.00260	-0.00446	0.00151
0.700	0.00000	0.00000	0.00000	0.00000	0.00002	0.00000	0.00000	0.00000	0.00001
0.900	0.00000	0.00000	0.00000	0.00000	0.00000	0.00000	0.00000	0.00002	-0.00002

Table (2-11)

HEAVE DAMPING COEFFICINTS AGAINST HST/R, H, F

H/R=6.0

FREQ. (hz)	HST/R 0.0	0.1	0.3	0.5	0.7	1.0	A0	A1	A2
0.050	0.00060	0.01086	0.11322	0.29737	0.56350	1.12900	0.00060	0.03894	1.09224
0.075	0.00280	0.00336	0.08150	0.23625	0.46427	0.94900	0.00280	-0.03972	0.99111
0.100	0.00750	-0.00065	0.04973	0.17112	0.35672	0.75400	0.00750	-0.12052	0.87324
0.150	0.02270	0.00849	0.00761	0.06470	0.16824	0.40020	0.02270	-0.21487	0.59478
0.300	0.02320	0.02611	0.00697	0.00027	0.00168	0.01354	0.02320	-0.05131	0.03586
0.500	0.00040	0.00035	0.00015	0.00005	0.00001	-0.00001	0.00040	-0.00088	0.00045
0.700	0.00000	0.00000	0.00000	0.00000	0.00000	0.00000	0.00000	0.00000	0.00000
0.900	0.00000	0.00000	0.00000	0.00000	0.00000	0.00000	0.00000	0.00000	0.00000

Table (2-1.2)

DAMPING FORMULA-A0, A1, A2
H/R=4.0

Fig.236

DAMPING FORMULA-A0, A1, A2
H/R=3.0

Fig.235

DAMPING FORMULA-A0, A1, A2
H/R=6.0

Fig. 2-38

DAMPING FORMULA-A0, A1, A2
H/R=5.0
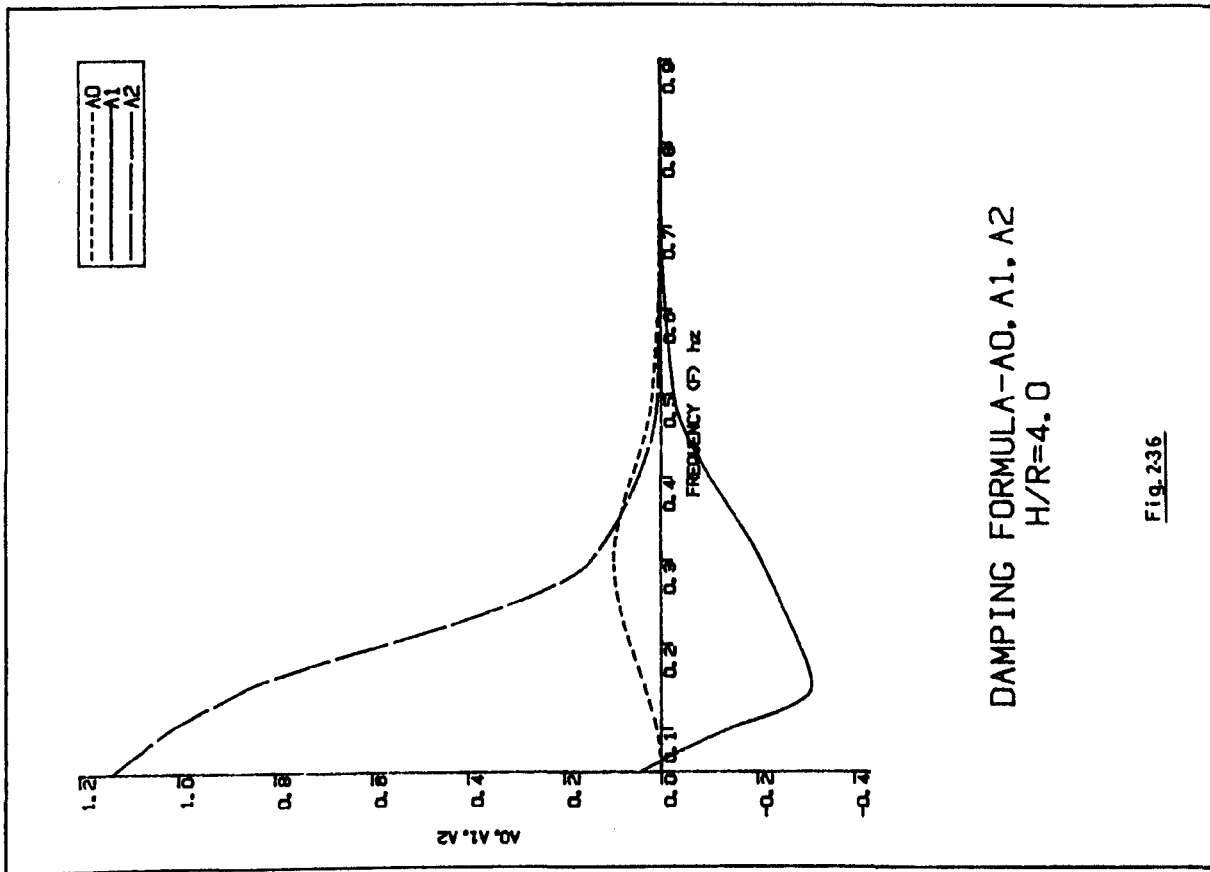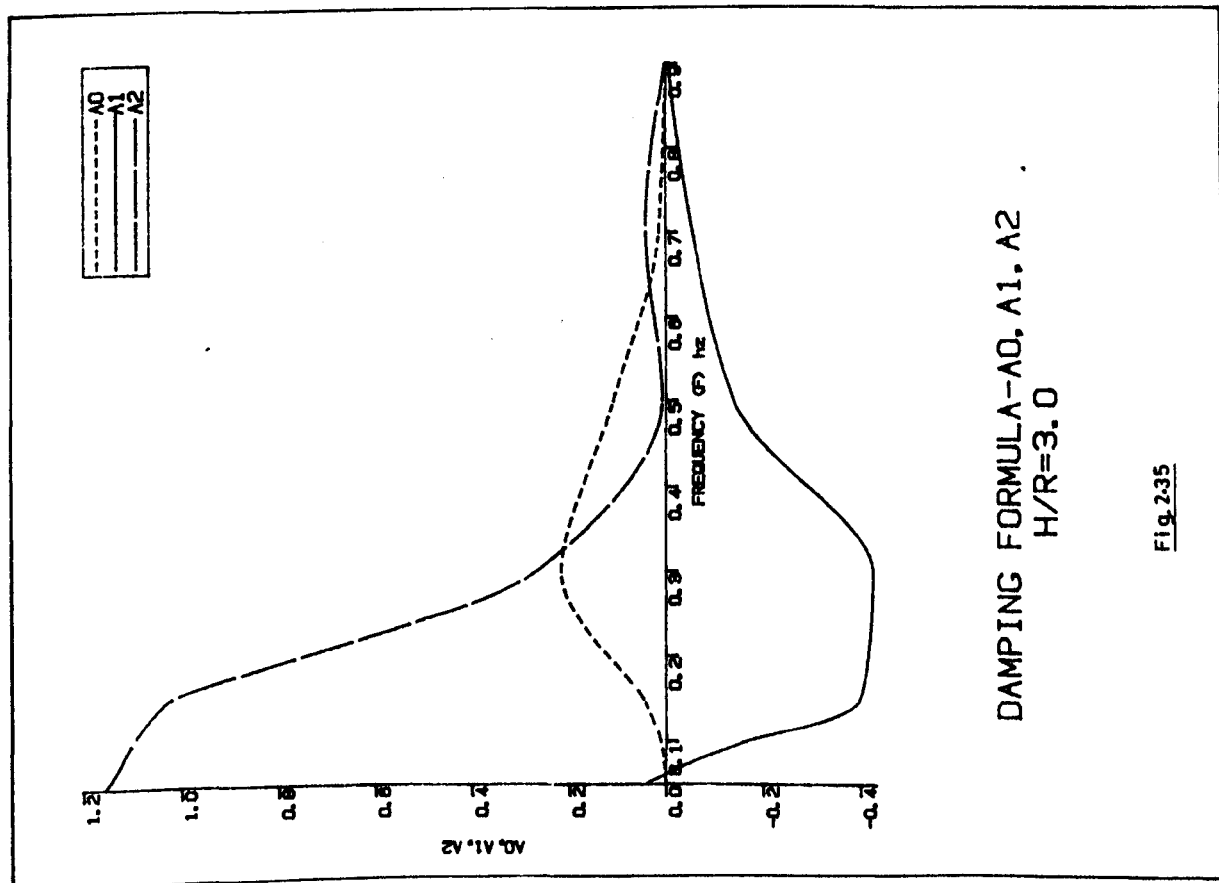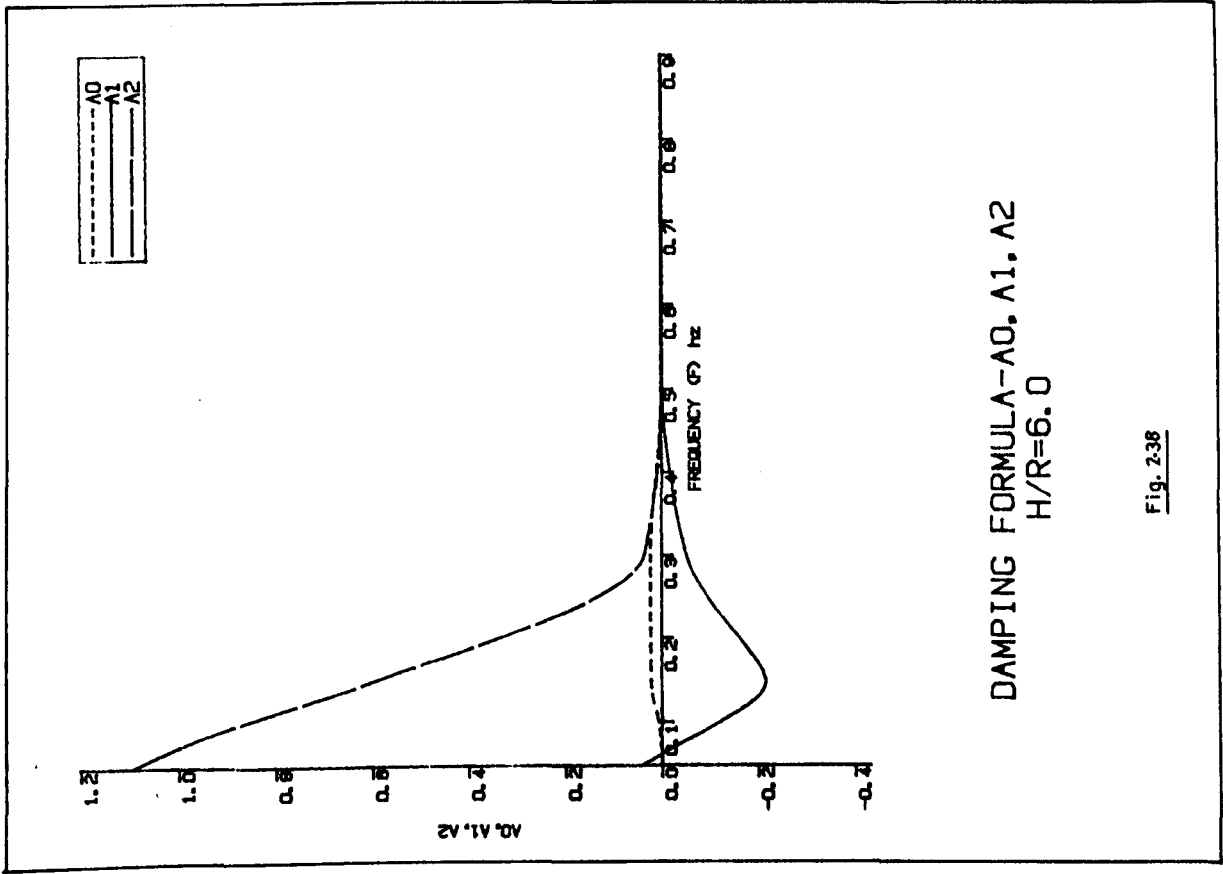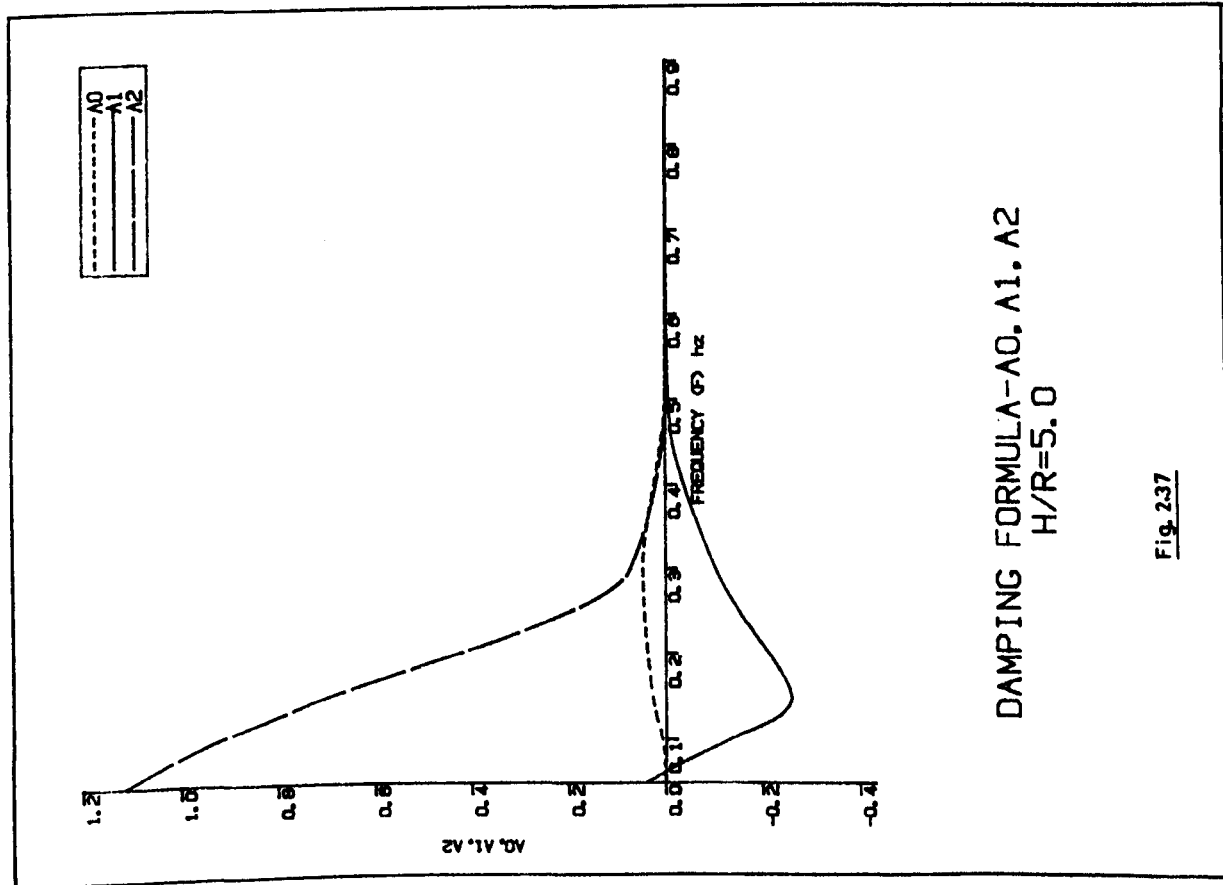
Fig. 2-37

The added mass coefficients for $f < 0.5$:-

$H = 3R$ $A_O = 1.00617 + 1.6669\,f - 7.214f^2 + 6.448f^3$

$A_1 = -1.0 - 7.3899f + 46.38f^2 - 60.33f^3$

$A_2 = 2.3167 - 15.512f + 32.0618f^2 - 16.839f^3$

$H = 4R$ $A_O = 1.00886 + 1.3206857f - 6.86548f^2 + 8.05627f^3$

$A_1 = -1.194938 - 4.101687f + 29.395118f^2 - 40.1289f^3$

$A_2 = 2.480279 - 19.0721378f + 56.0314178f^2 - 50.101188f^3$

$H = 5R$ $A_O = 1.022158 + 0.9534f - 5.3245f^2 + 6.72058f^3$

$A_1 = -1.303037 - 1.90995f + 17.6959f^2 - 25.71974f^3$

$A_2 = 2.515147 - 20.77832f + 69.121483f^2 - 68.6221f^3$

$H = 6R$ $A_O = 1.034308 + 0.6412f - 3.7578f^2 + 4.9009f^3$

$A_1 = -1.3689 - 0.36455f + 9.1780f^2 - 14.8982f^3$

$A_2 = 2.49346 - 21.4036f + 76.14036f^3 - 79.2504f^3$

For $f \geqslant 0.5$

$H = 3R$ $A_O = 0.767425 + 0.14975f$

$A_1 = -0.5764225 - 0.124275f$

$A_2 = 0.446157 + 0.050725f$

$H = 4R$ $A_O = 0.921375 + 0.07725f$

$A_1 = -0.8401575 - 0.145125f$

$A_2 = 0.61593 + 0.1472f$

$H = 5R$ $A_O = 0.99265 + 0.0305f$

$A_1 = -1.0099625 - 0.076975f$

$A_2 = 0.7706725 + 0.115975f$

$H = 6R$ $A_O = 1.0216 + 0.013f$

$A_1 = -1.097265 - 0.04205f$

$A_2 = 0.876515 + 0.08845f$

and the damping coefficients for $f < 0.3$:-

$H = 3R$ $A_0 = 0.01937 - 0.6910f + 7.1654f^2 - 8.8498f^3$

$A_1 = 0.1237 + 0.1477f - 41.77f^2 + 117.257f^3$

$A_2 = 1.2273 - 2.0077f + 13.666f^2 - 58.67f^3$

$H = 4R$ $A_0 = 0.01812 - 0.672f + 7.281f^2 - 13.85f^3$

$A_1 = 0.17 - 1.64f - 22.44f^2 + 78.99f^3$

$A_2 = 1.198 - 0.775f - 11.092f^2 + 6.549f^3$

$H = 5R$ $A_0 = 0.0146 - 0.5611f + 6.403f^2 - 13.89f^3$

$A_1 = 0.2099 - 3.169f - 6.531f^2 + 45.36f^3$

$A_2 = 1.1899 - 0.335f - 26.637f^2 + 51.137f^3$

$H = 6R$ $A_0 = 0.01088 - 0.4381f + 5.2907f^2 - 12.31f^3$

$A_1 = 0.2437 - 4.4475f + 6.9142f^2 + 15.445f^3$

$A_2 = 1.19325 - 0.4401f - 35.91f^2 + 81.722f^3$

For $f \geqslant 0.3$

$H = 3R$ $A_0 = 0.2564 + 0.328f - 1.94f^2 + 1.4f^3$

$A_1 = -1.6075 + 5.976f - 7.8492f^2 + 3.5435f^3$

$A_2 = 2.0185 - 9.6799f + 15.139f^2 - 7.635f^3$

$H = 4R$ $A_0 = 0.435 - 1.7f + 2.207f^2 - 0.95f^3$

$A_1 = -1.062 + 4.423f - 6.088f^2 + 2.76f^3$

$A_2 = 0.8828 - 3.93f + 5.704f^2 - 2.697f^3$

$H = 5R$ $A_0 = 0.2803 - 1.232f + 1.765f^2 - 0.825f^3$

$A_1 = -0.629 + 2.787f - 4.017f^2 + 1.887f^3$

$A_2 = 0.4606 - 2.067f + 3.011f^2 - 1.425f^3$

$$H = 6R \quad A_0 = 0.1475 - 0.6634f + 0.9675f^2 - 0.458f^3$$

$$A_1 = -0.3263 + 1.4675f - 2.14f^2 + 1.0139f^3$$

$$A_2 = 0.23 - 1.037f + 1.515f^2 - 0.719f^3$$

The linear function of added mass for $f \geqslant 0.5Hz$ is of the form:-

$$A_0 = C_0 + D_0 f$$

$$A_1 = C_1 + D_1 f$$

$$A_2 = C_2 + D_2 f$$

while the third order equation of added mass for $f < 0.5Hz$ is of the form:-

$$A_0 = C_0 + D_0 f + E_0 f^2 + F_0 f^3$$

$$A_1 = C_1 + D_1 f + E_1 f^2 + F_1 f^3$$

$$A_2 = C_2 + D_2 f + E_2 f^2 + F_2 f^3$$

where C_0, D_0, F_0, C_1, D_1, E_1, F_1, C_2, D_2, E_2, F_2, are the coefficients of the above equations. These functions are also seen to vary with the depth of submergence.

Consequently, in Step 3, the C_0, D_0, E_0, F_0, C_1, D_1, E_1, F_1, C_2, D_2, E_2, F_2 coefficients were expressed as a function of depth parameter H/R.

The development of an approximate formula for the heave damping coefficients followed a similar procedure. As seen in figs. 2.35 to 2.38, the dependence of heave damping on frequency may be expressed by a third order equation whose coefficients vary, depending on whether $f \geqslant 0.3$ or $< 0.3Hz$. Consequently, the subsequent treatment was divided into two parts as for the added mass coefficients.

The resulting final expressions for the heave added mass coefficient are:-

$$C_V = A_o + A_1(HST/R) + A_2(HST/R)^2$$
$$A_o = C_o + D_o f + E_o f^2 + F_o f^3$$
$$A_1 = C_1 + D_1 f + E_1 f^2 + F_1 f^3$$
$$A_2 = C_2 + D_2 f + E_2 f^2 + F_2 f^3$$

where, for f < 0.5Hz:-

$$C_o = 1.01884 - 0.011514(H/R) + 0.002365(H/R)^2$$

$$D_o = 2.8571 - 0.42097(H/R) + 0.0085(H/R)^2$$

$$E_o = -5.3634 - 1.5499(H/R) + 0.3045(H/R)^2$$

$$F_o = --7.0617 + 7.1152(H/R) - 0.8569(H/R)^2$$

$$C_1 = -0.05695 - 0.41189(H/R) + 0.03227(H/R)^2$$

$$D_1 = -22.1904 + 6.2481(H/R) - 0.4357(H/R)^2$$

$$E_1 = 121.3678 - 31.3812(H/R) + 2.1167(H/R)^2$$

$$F_1 = -147.6932 + 36.17447(H/R) - 2.3449(H/R)^2$$

$$C_2 = 1.3171 + 0.47336(H/R) - 0.04632(H/R)^2$$

$$D_2 = 3.4705 - 8.5415(H/R) + 0.7337(H/R)^2$$

$$E_2 = -87.5739 + 52.6718(H/R) - 4.2377(H/R)^2$$

$$F_2 = 146.3976 - 71.5017(H/R) + 5.65847(H/R)^2$$

and, for f ≥ 0.5Hz:-

$$C_o = -0.04319 + 0.36463(H/R) - 0.03125(H/R)^2$$

$$D_o = 0.5345 - 0.16945(H/R) + 0.01375(H/R)^2$$

$$E_o = 0.0$$

$$F_o = 0.0$$

$$C_1 = 0.73665 - 0.5702(H/R) + 0.044108(H/R)^2$$

$$D_1 = 0.02615 - 0.0940(H/R) + 0.01394(H/R)^2$$

$$E_1 = 0.0$$

$$F_1 = 0.0$$

$$C_2 = -0.27697 + 0.2884(H/R) - 0.01598(H/R)^2$$

$$D_2 = -0.52529 + 0.2872(H/R) - 0.031(H/R)^2$$

$$E_2 = 0.0$$

$$F_2 = 0.0$$

and, similarly, the damping coefficient may be expressed by:-

$$B_{33} = A_o + A_1(HST/R) + A_2(HST/R)^2$$

$$A_o = C_o + D_o f + E_o f + F_o f^2$$

$$A_1 = C_1 + D_1 f + E_1 f + F_1 f^2$$

$$A_2 = C_2 + D_2 f + E_2 f + F_2 f^2$$

for f < 0.3Hz:-

$$C_o = 0.01705 + 0.002658(H/R) - 0.0006175(H/R)^2$$

$$D_o = -0.4879 - 0.147(H/R) + 0.026(H/R)^2$$

$$E_o = 3.628 + 2.1126(H/R) - 0.307(H/R)^2$$

$$F_o = 23.72 - 15.847(H/R) + 1.645(H/R)^2$$

$$C_1 = -0.0525 + 0.068115(H/R) - 0.003125(H/R)^2$$

$$D_1 = 7.0336 - 2.67716(H/R) + 0.1273(H/R)^2$$

$$E_1 = -116.7972 + 29.4393(H/R) - 1.47145(H/R)^2$$

$$F_1 = 256.5148 - 52.6986(H/R) + 2.088(H/R)^2$$

$$C_2 = 1.4068 - 0.08449(H/R) + 0.0081625(H/R)^2$$

$$D_2 = -9.55199 + 3.52176(H/R) - 0.33419(H/R)^2$$

$$E_2 = 132.4834 - 51.2685(H/R) + 3.87125(H/R)^2$$

$$F_2 = -353.9209 + 124.5029(H/R) - 8.6585(H/R)^2$$

for f ⩾ 0.3Hz:-

$$C_o = -0.9827 + 0.6525(H/R) - 0.07785(H/R)^2$$

$$D_o = 12.6448 - 6.0929(H/R) + 0.64915(H/R)^2$$

$$E_o = -26.4627 + 11.9532(H/R) - 1.2361(H/R)^2$$

$$F_o = 15.1495 - 6.6581(H/R) + 0.67925(H/R)^2$$

$$C_1 = -3.9839 + 0.9739(H/R) - 0.0607(H/R)^2$$

$$D_1 = 11.5952 - 2.0415(H/R) + 0.05837(H/R)^2$$

$$E_1 = -13.11136 + 1.6588(H/R) + 0.028999(H/R)^2$$

$$F_1 = 5.6833 - 0.64458(H/R) - 0.0224(H/R)^2$$

$$C_2 = 7.80166 - 2.6152(H/R) + 0.2263(H/R)^2$$

$$D_2 = -39.1043 + 13.3989(H/R) - 1.1799(H/R)^2$$

$$E_2 = 63.6567 - 22.2192(H/R) + 1.9847(H/R)^2$$

$$F_2 = -33.13 + 11.724(H/R) - 1.058(H/R)^2$$

5.6. Comparison of Curve-Fitted Values with Theoretical Values and Conclusions

The comparisons between the Frank Close-fit Method and the approximate formula for the heave added mass coefficient are presented in figs. 2.39 to 2.44. Similar comparisons for the damping coefficient are presented in figs. 2.45 to 2-50.

The comparisons show good agreement with theory and it is concluded that the developed approximate heave added mass and damping formulae presented in the previous section may be used with confidence in the development of the SWATH motion and wave load computer programs or other design purposes.

The use of the formulae is limited to a range of frequencies $0.05 > f > 0.9$ Hz, depth of submergence $3.0 < H/R < 6.0$ and column width $0.1 < HST/R < 1.0$.

5.7 The Speed Effects on the Hydrodynamic Coefficients

When the assumption of potential flow is applied, the speed
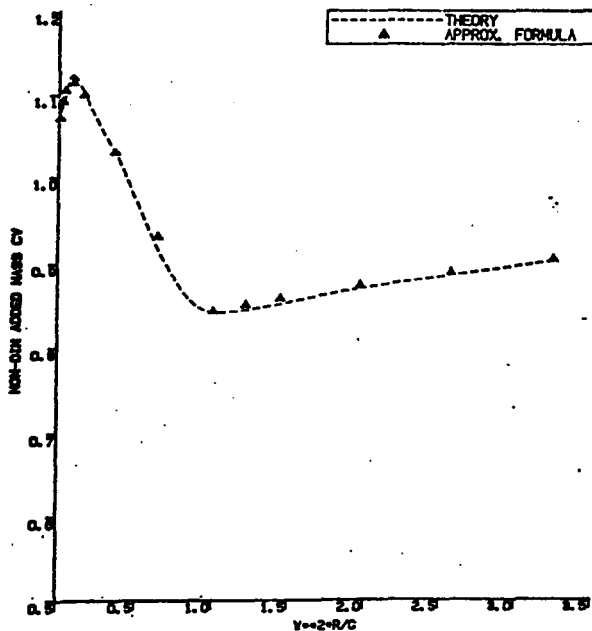
COMPARISON OF ADDED MASS
HST/R=0.0 H/R=3.0
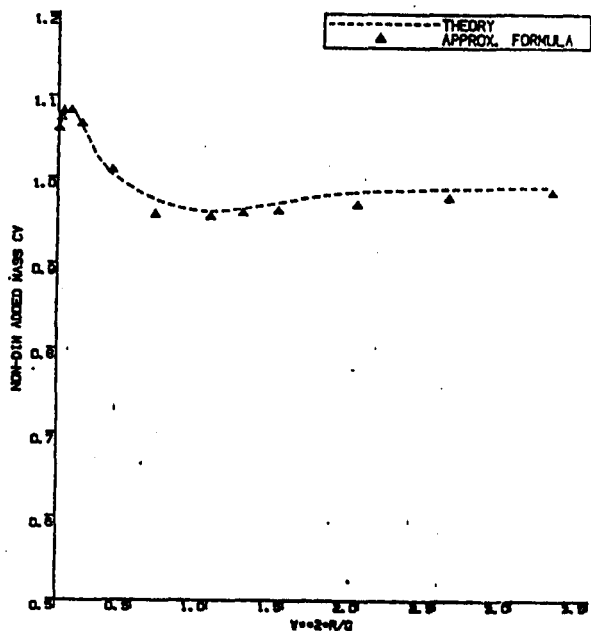
COMPARISON OF ADDED MASS
HST/R=0.0 H/R=4.0
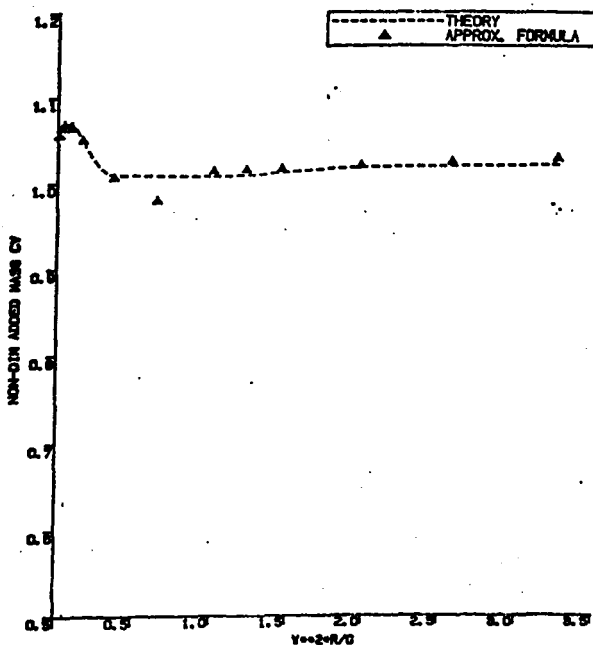
COMPARISON OF ADDED MASS
HST/R=0.0 H/R=5.0
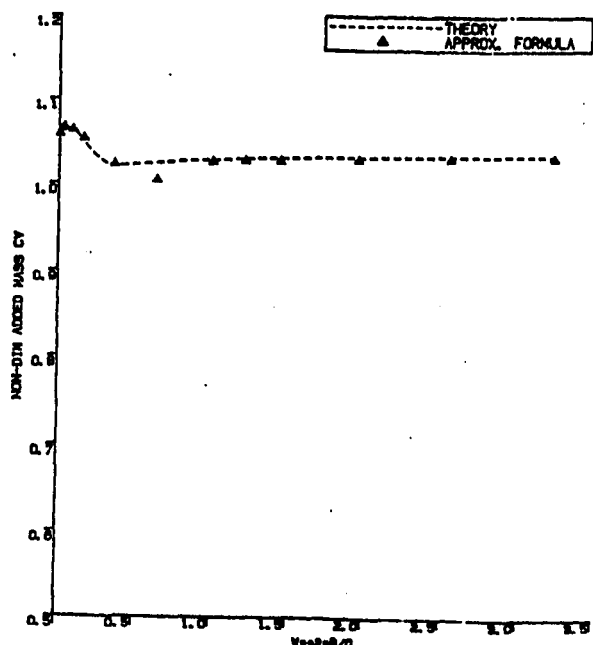
COMPARISON OF ADDED MASS
HST/R=0.0 H/R=6.0

Fig. 2.39
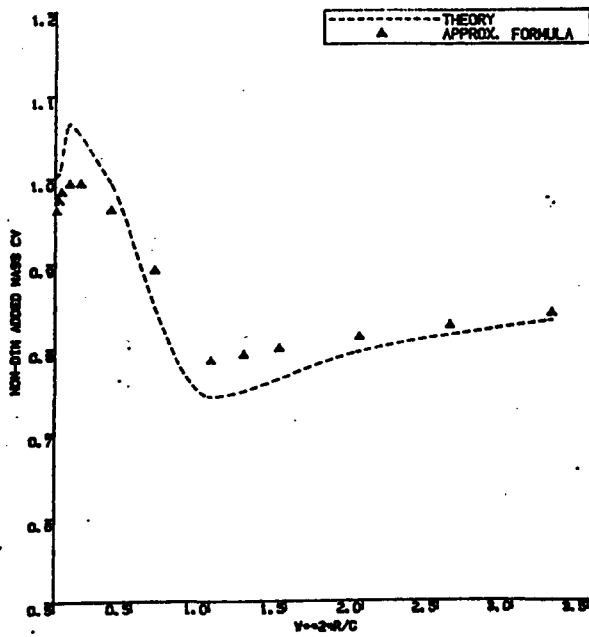
COMPARISON OF ADDED MASS
HST/R=0.1 H/R=3.0
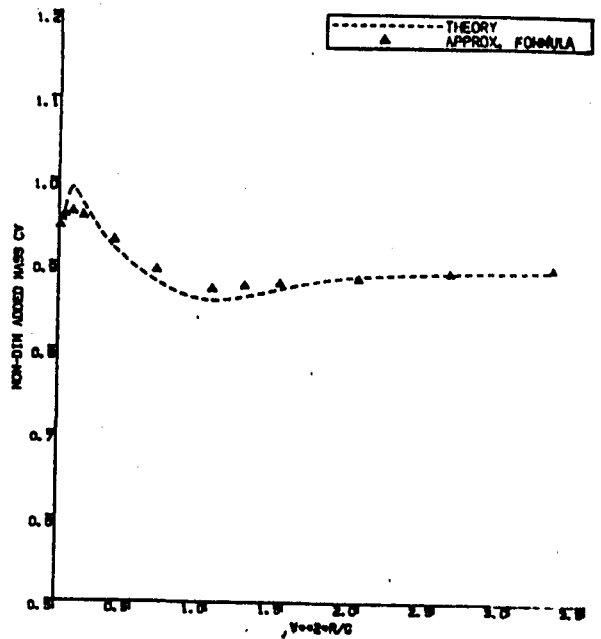
COMPARISON OF ADDED MASS
HST/R=0.1 H/R=4.0
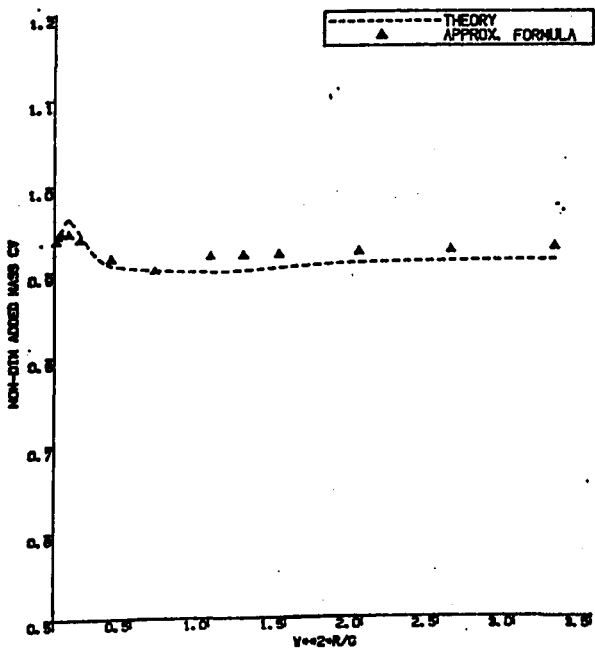
COMPARISON OF ADDED MASS
HST/R=0.1 H/R=5.0
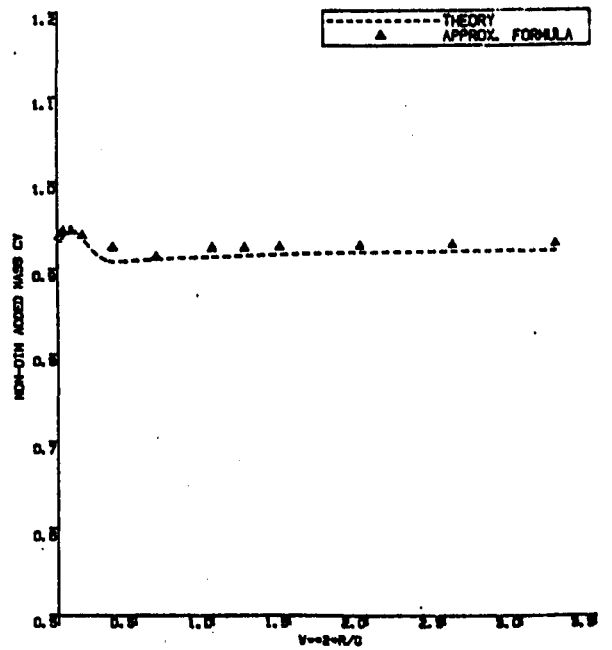
COMPARISON OF ADDED MASS
HST/R=0.1 H/R=6.0

Fig. 2.40
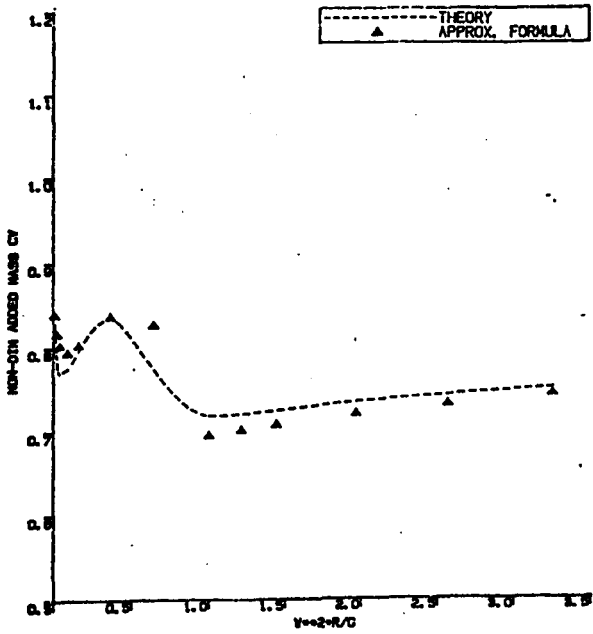
COMPARISON OF ADDED MASS
HST/R=0.3 H/R=3.0
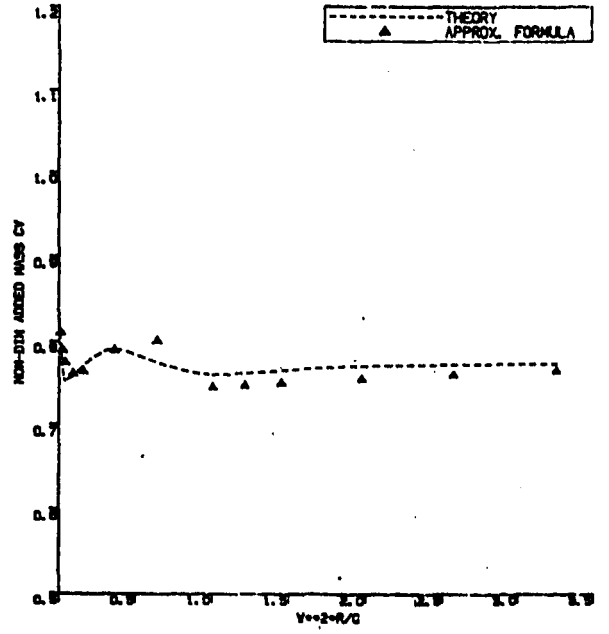
COMPARISON OF ADDED MASS
HST/R=0.3 H/R=4.0
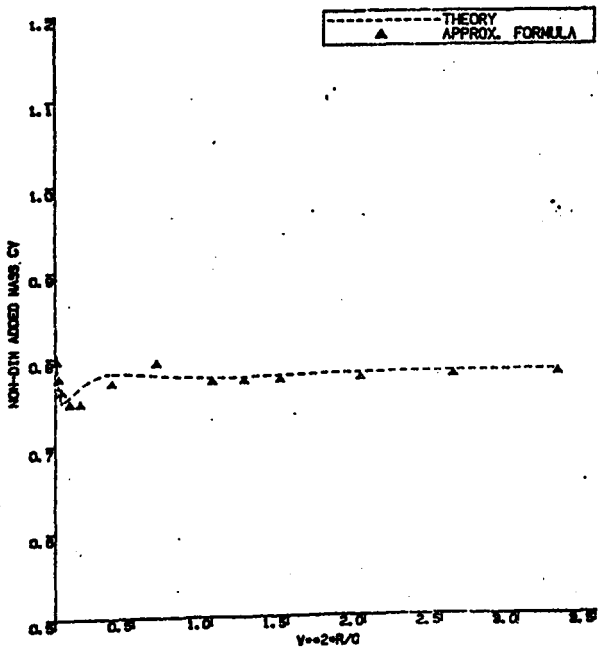
COMPARISON OF ADDED MASS
HST/R=0.3 H/R=5.0
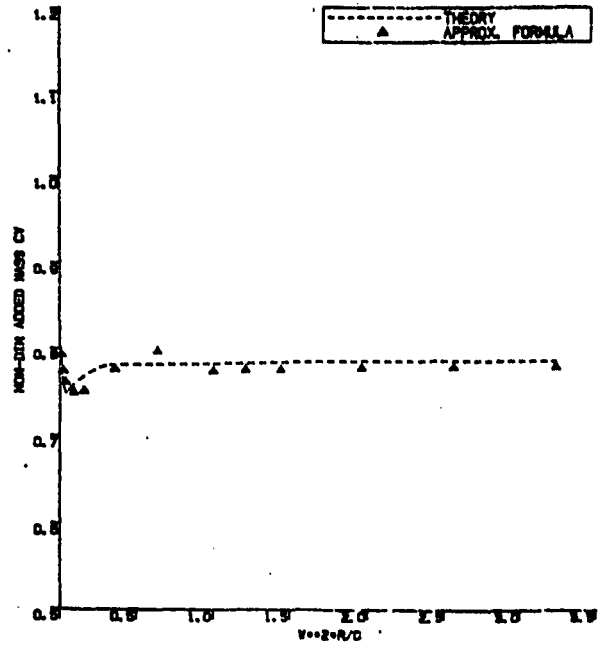
COMPARISON OF ADDED MASS
HST/R=0.3 H/R=6.0

Fig. 2.41
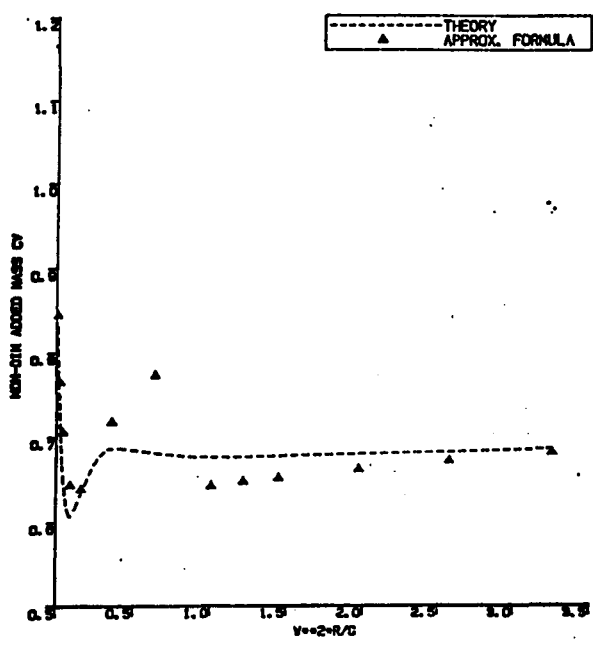
COMPARISON OF ADDED MASS
HST/R=0.5 H/R=3.0
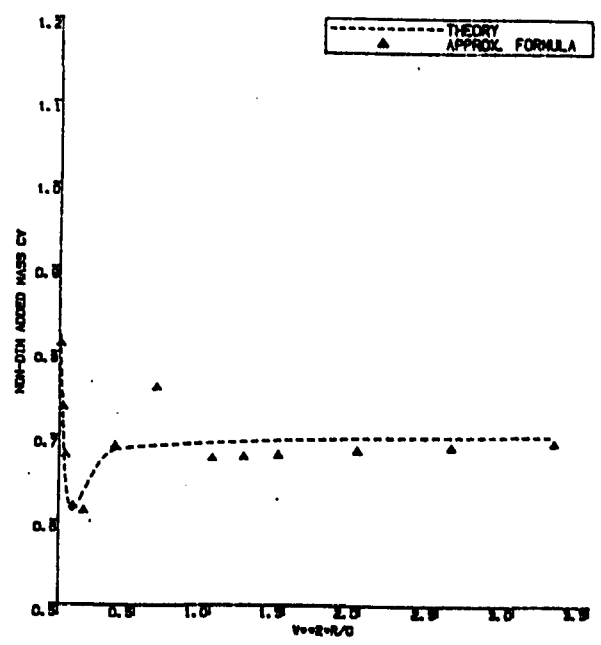
COMPARISON OF ADDED MASS
HST/R=0.5 H/R=4.0
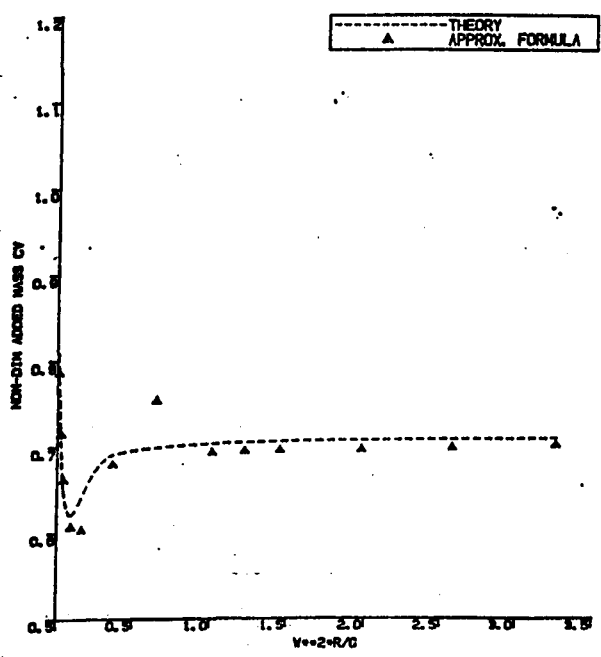
COMPARISON OF ADDED MASS
HST/R=0.5 H/R=5.0
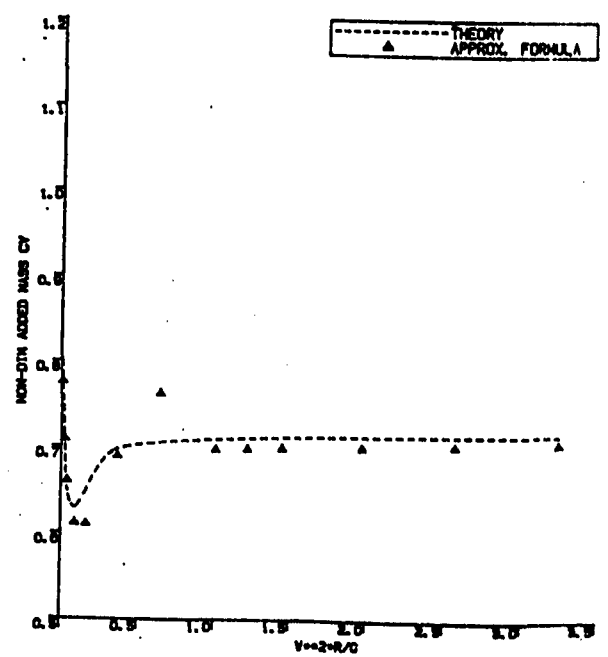
COMPARISON OF ADDED MASS
HST/R=0.5 H/R=6.0

Fig. 2.42
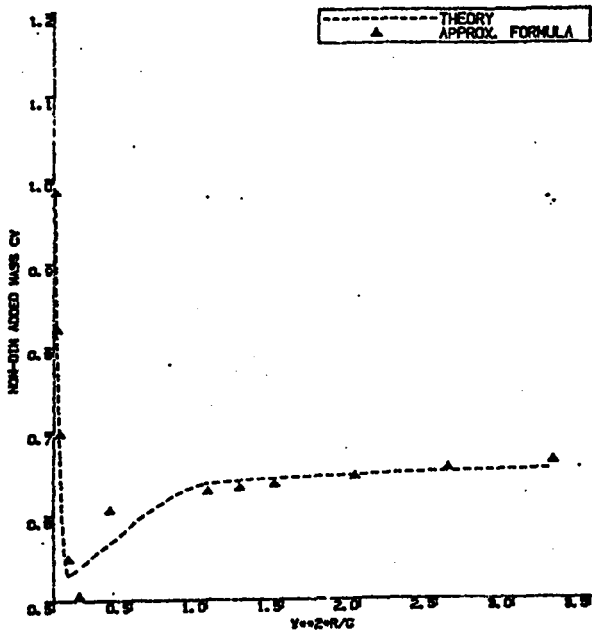
COMPARISON OF ADDED MASS
HST/R=0. 7 H/R=3. 0
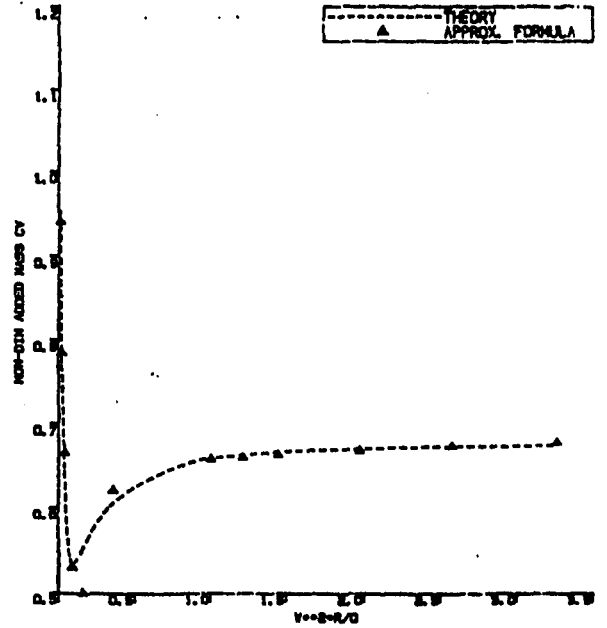
COMPARISON OF ADDED MASS
HST/R=0. 7 H/R=4. 0
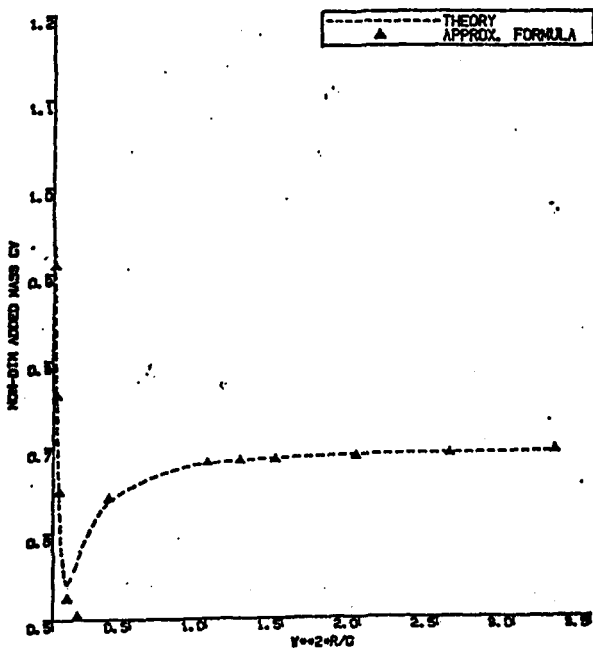
COMPARISON OF ADDED MASS
HST/R=0. 7 H/R=5. 0
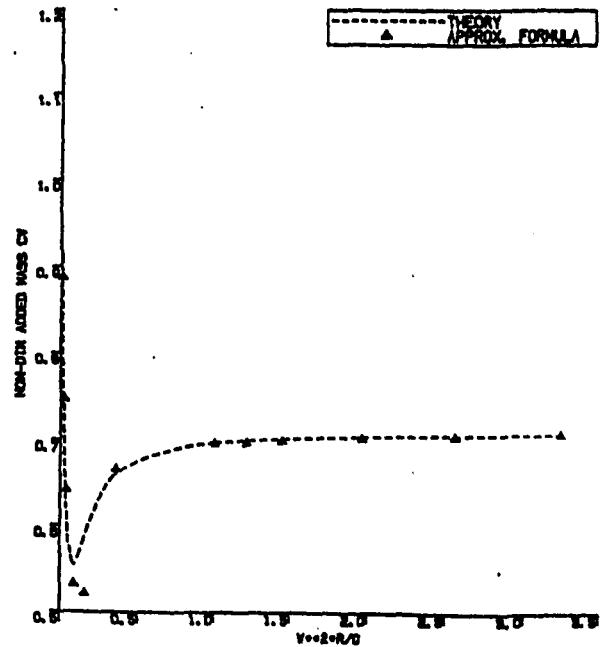
COMPARISON OF ADDED MASS
HST/R=0. 7 H/R=6. 0

Fig. 2.43

117.
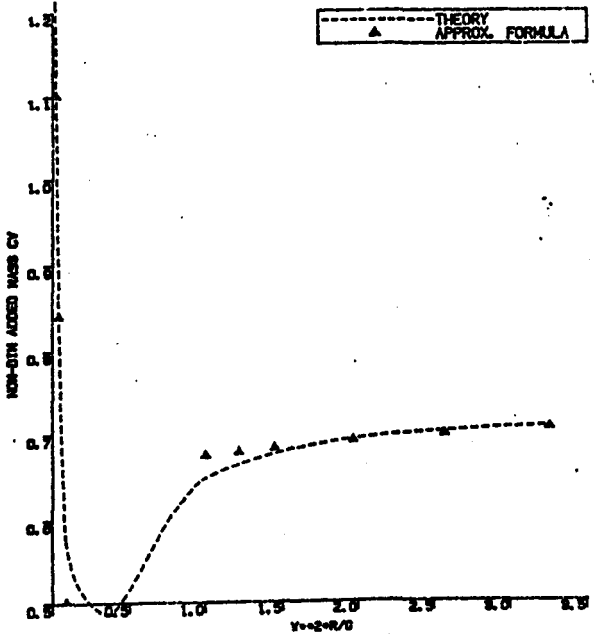
COMPARISON OF ADDED MASS
HST/R=1. 0 H/R=3. 0
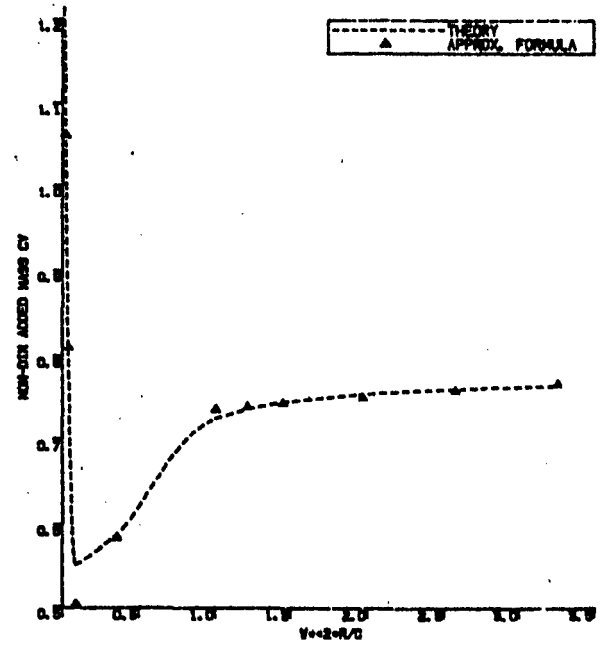
COMPARISON OF ADDED MASS
HST/R=1. 0 H/R=4. 0
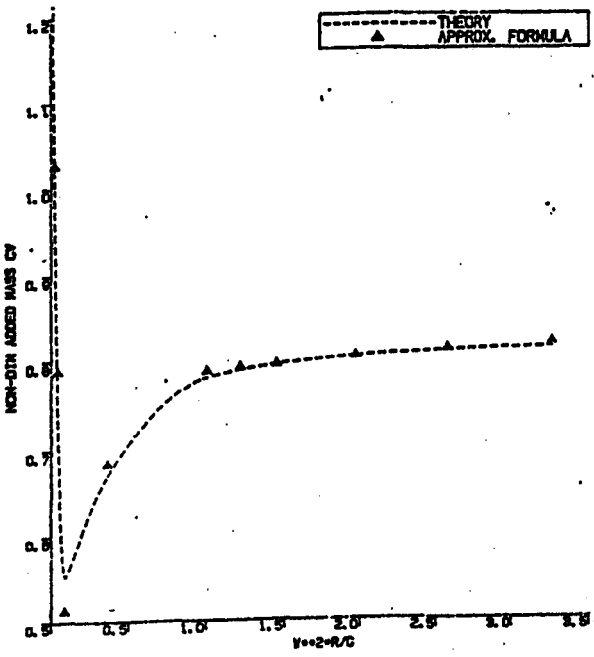
COMPARISON OF ADDED MASS
HST/R=1. 0 H/R=5. 0
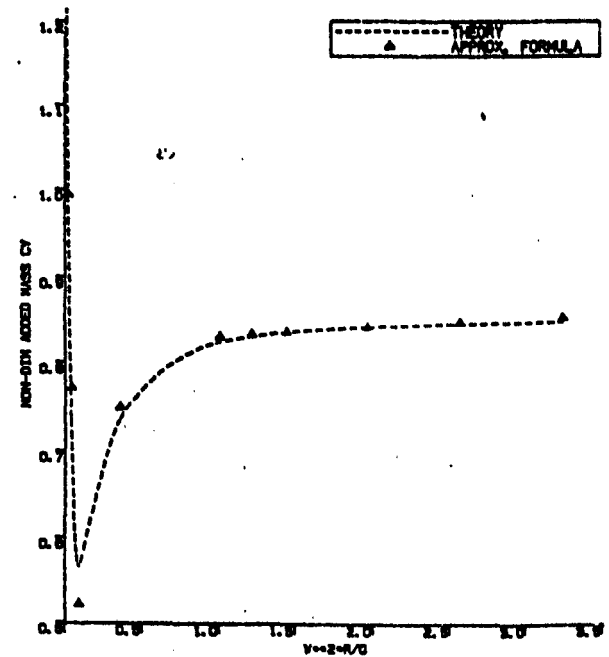
COMPARISON OF ADDED MASS
HST/R=1. 0 H/R=6. 0

Fig. 2.44
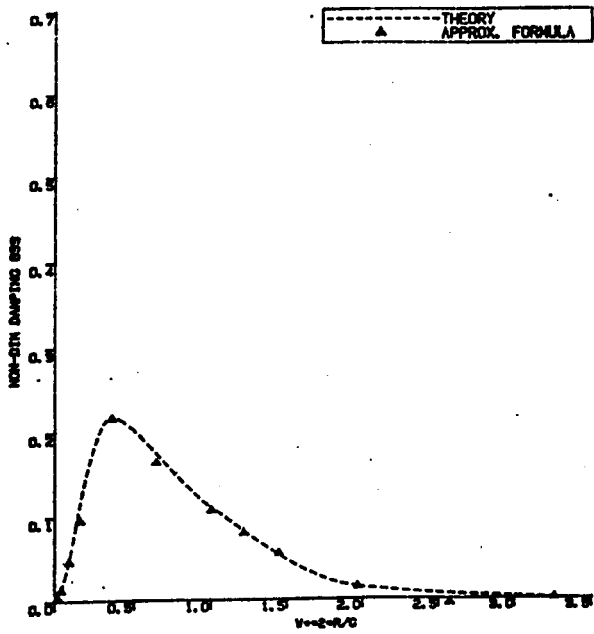
COMPARISON OF DAMPING
HST/R=0.0 H/R=3.0
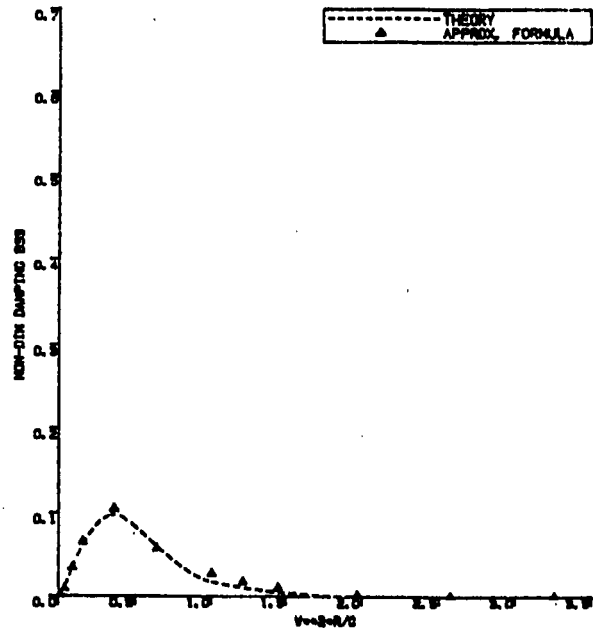
COMPARISON OF DAMPING
HST/R=0.0 H/R=4.0
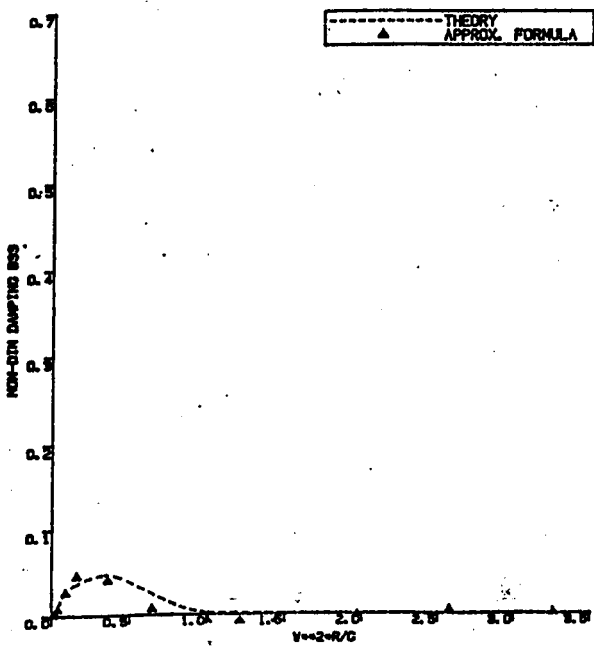
COMPARISON OF DAMPING
HST/R=0.0 H/R=5.0
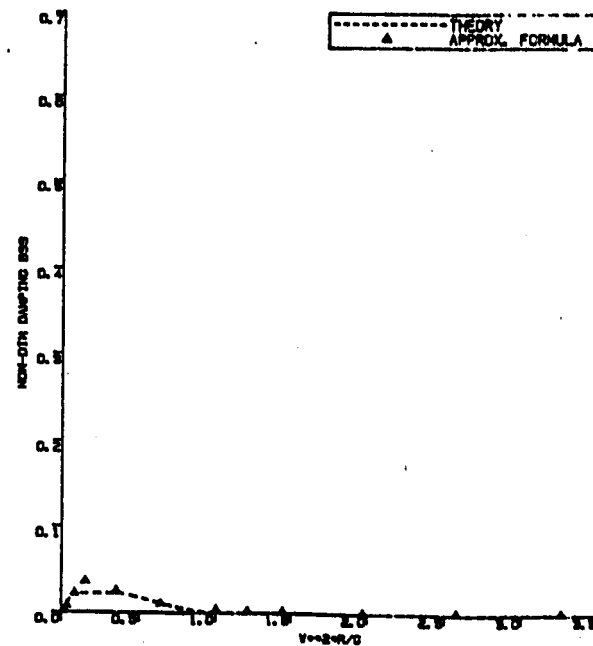
COMPARISON OF DAMPING
HST/R=0.0 H/R=6.0

Fig. 2.45
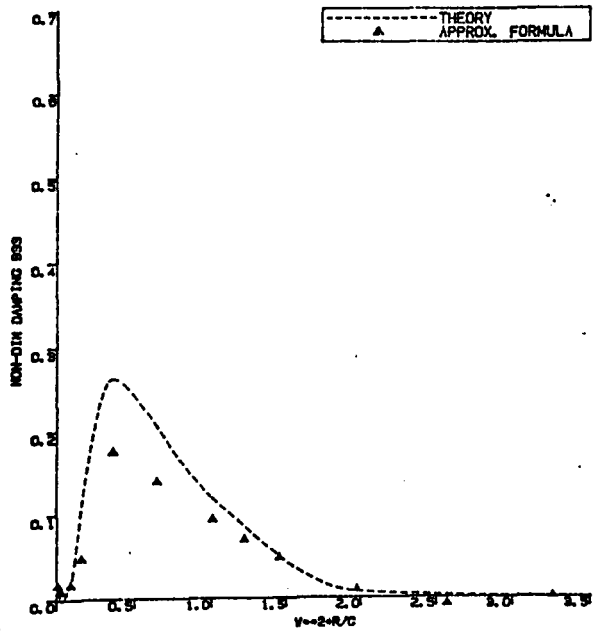
COMPARISON OF DAMPING
HST/R=0.1 H/R=3.0
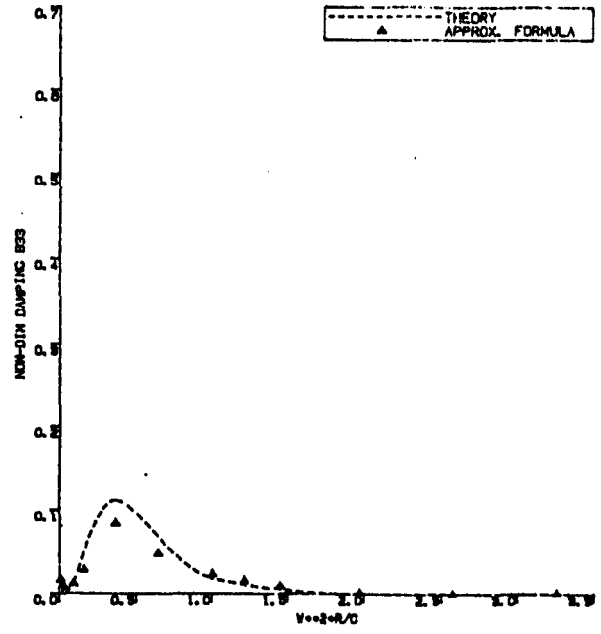
COMPARISON OF DAMPING
HST/R=0.1 H/R=4.0
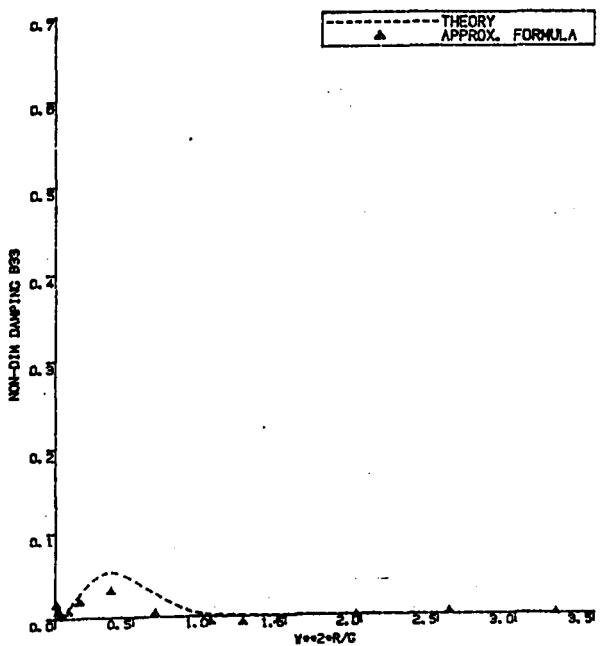
COMPARISON OF DAMPING
HST/R=0.1 H/R=5.0
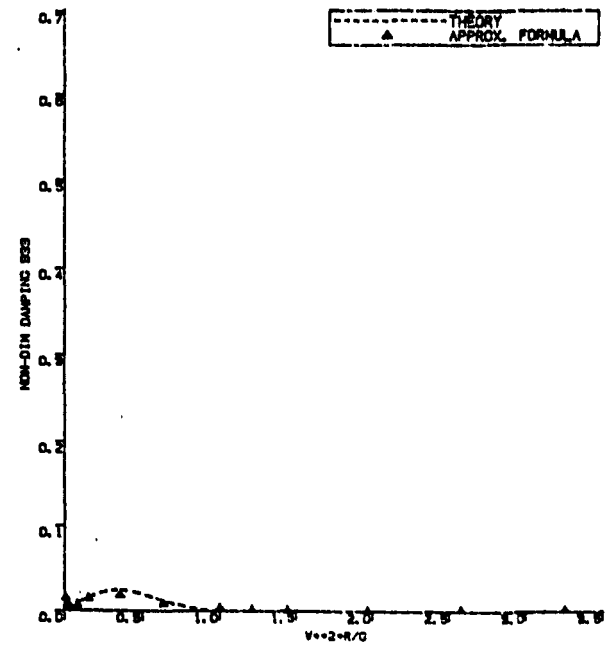
COMPARISON OF DAMPING
HST/R=0.1 H/R=6.0

Fig. 2.46
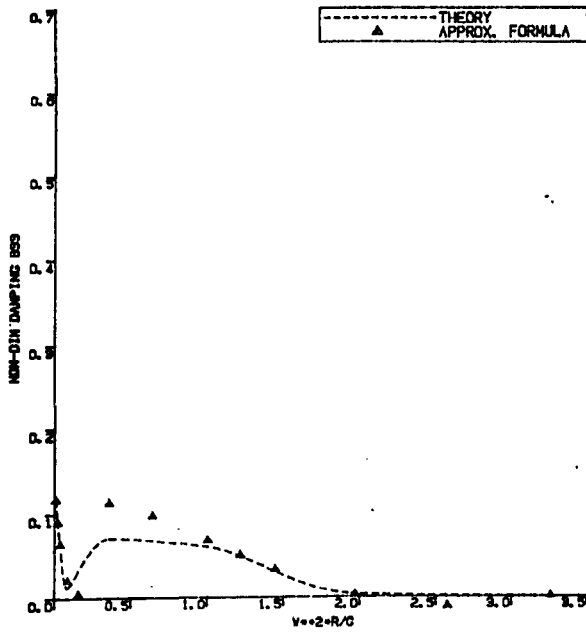
COMPARISON OF DAMPING
HST/R=0.3 H/R=3.0
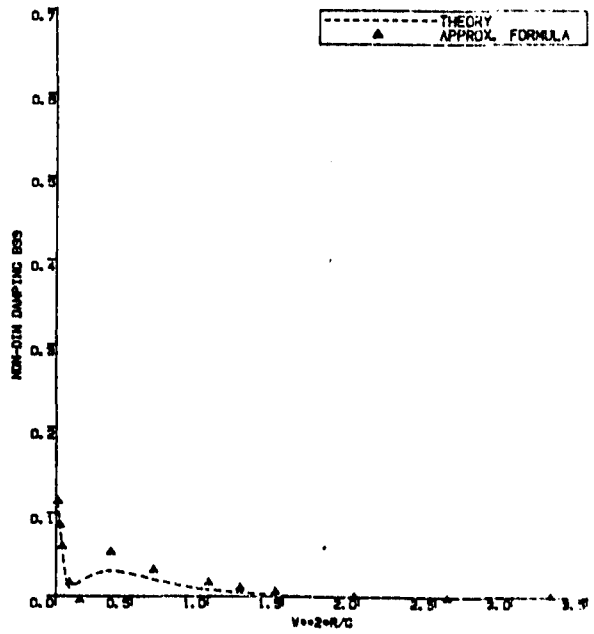
COMPARISON OF DAMPING
HST/R=0.3 H/R=4.0
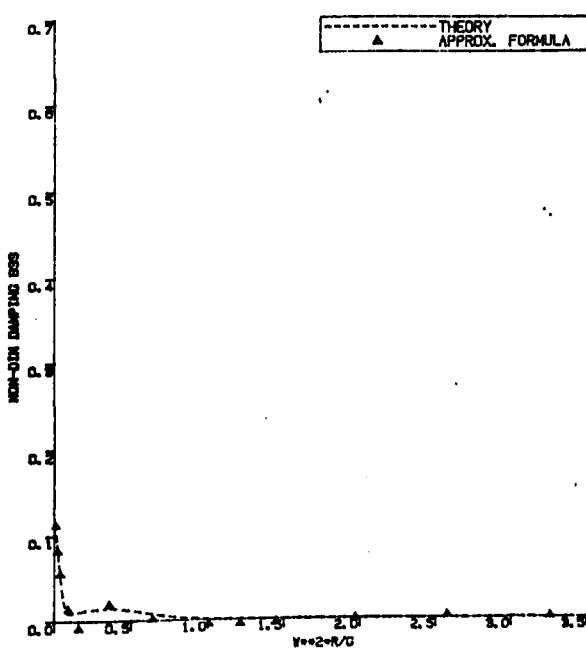
COMPARISON OF DAMPING
HST/R=0.3 H/R=5.0
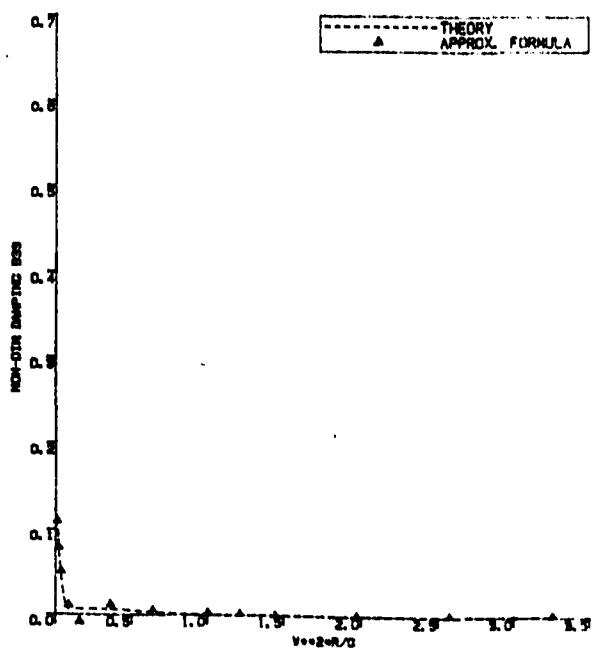
COMPARISON OF DAMPING
HST/R=0.3 H/R=6.0

Fig. 2.47
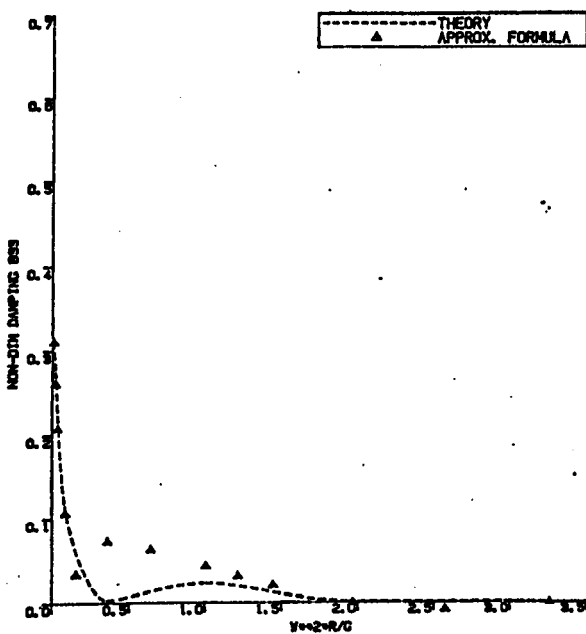
COMPARISON OF DAMPING
HST/R=0. 5 H/R=3. 0
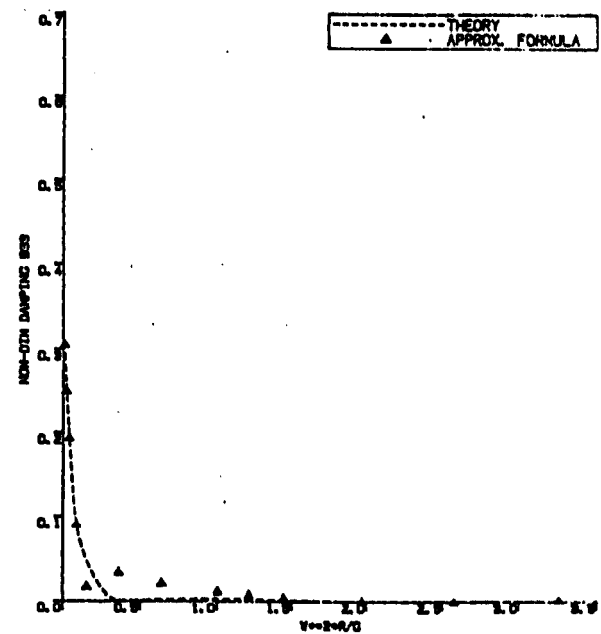
COMPARISON OF DAMPING
HST/R=0. 5 H/R=4. 0
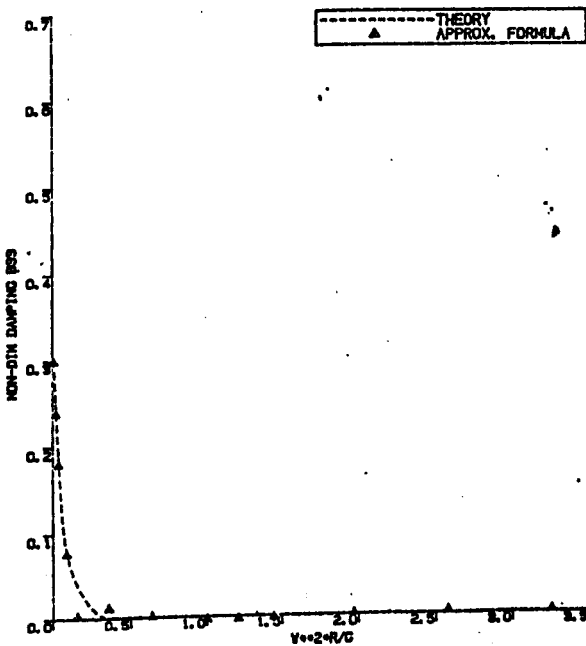
COMPARISON OF DAMPING
HST/R=0. 5 H/R=5. 0
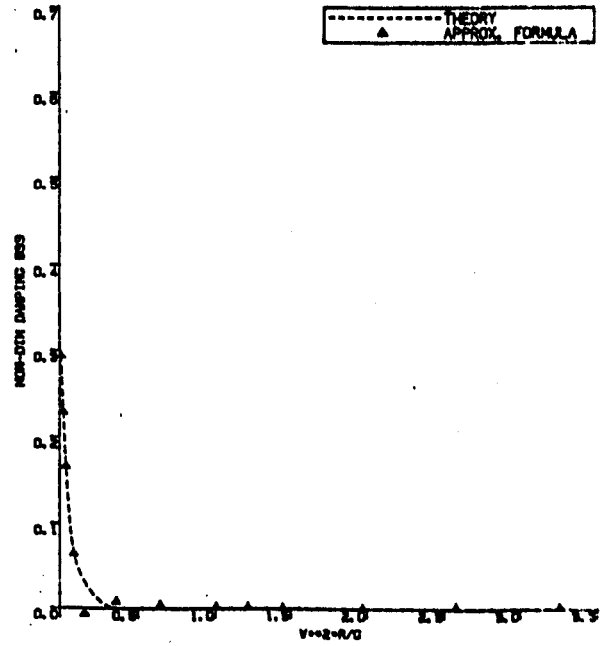
COMPARISON OF DAMPING
HST/R=0. 5 H/R=6. 0

Fig. 2.48
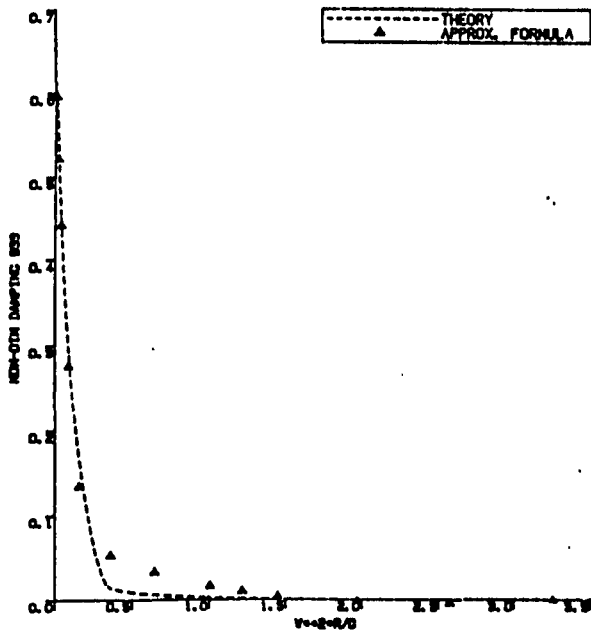
COMPARISON OF DAMPING
HST/R=0.7 H/R=3.0
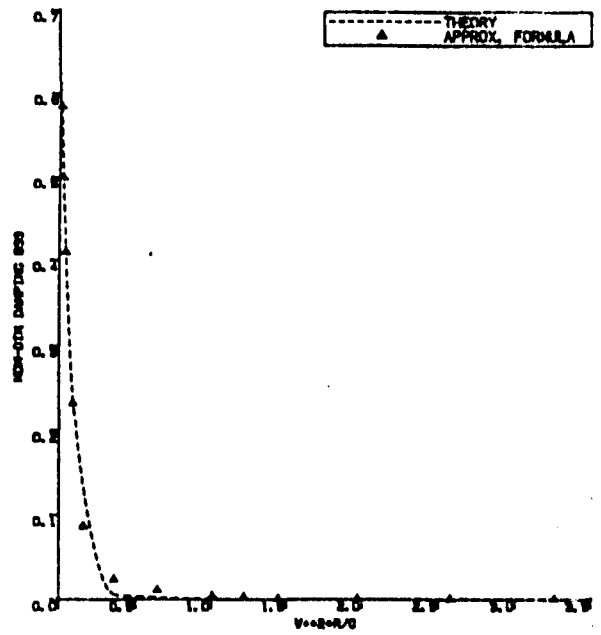
COMPARISON OF DAMPING
HST/R=0.7 H/R=4.0
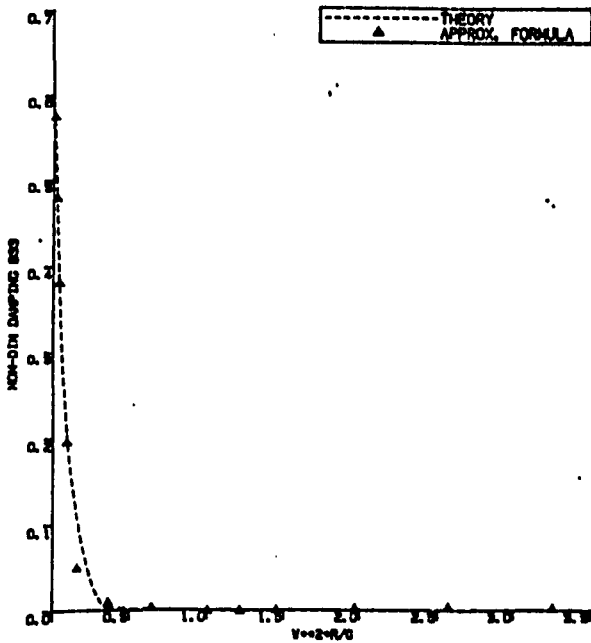
COMPARISON OF DAMPING
HST/R=0.7 H/R=5.0
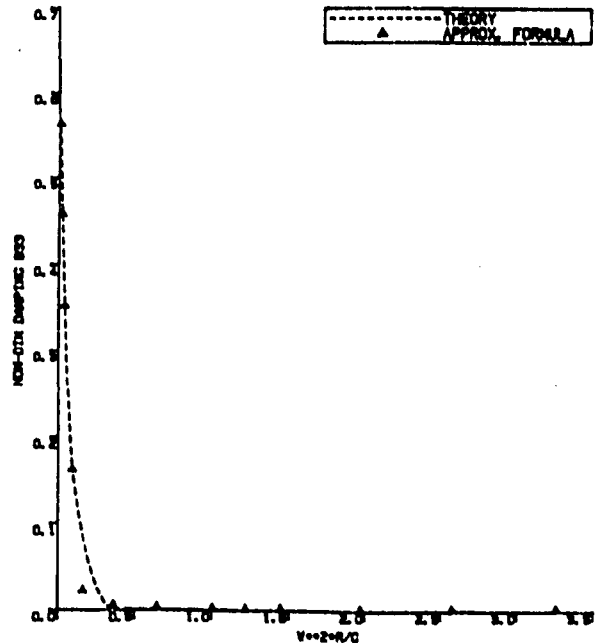
COMPARISON OF DAMPING
HST/R=0.7 H/R=6.0

Fig. 2.49
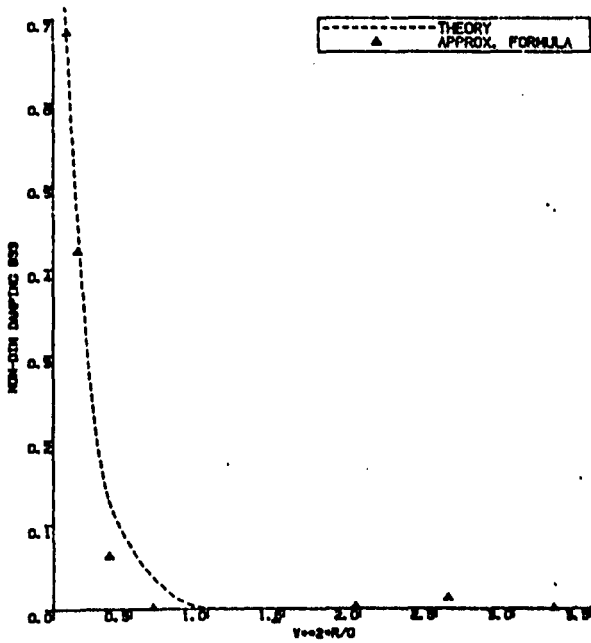
COMPARISON OF DAMPING
HST/R=1.0 H/R=3.0
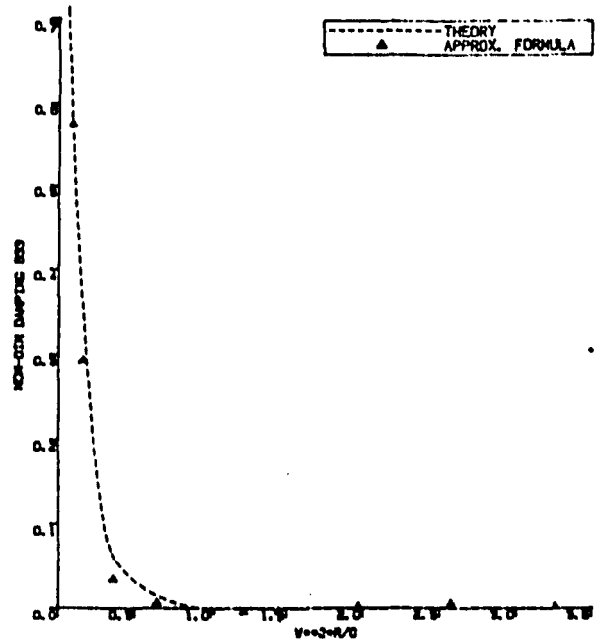
COMPARISON OF DAMPING
HST/R=1.0 H/R=4.0
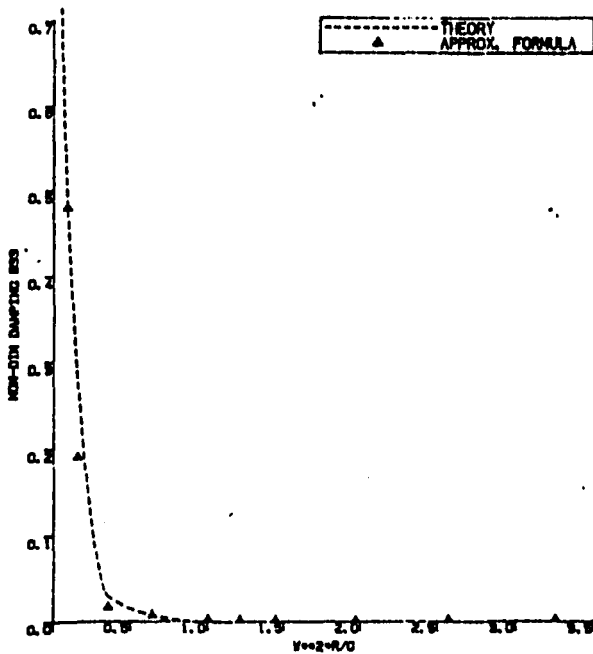
COMPARISON OF DAMPING
HST/R=1.0 H/R=5.0
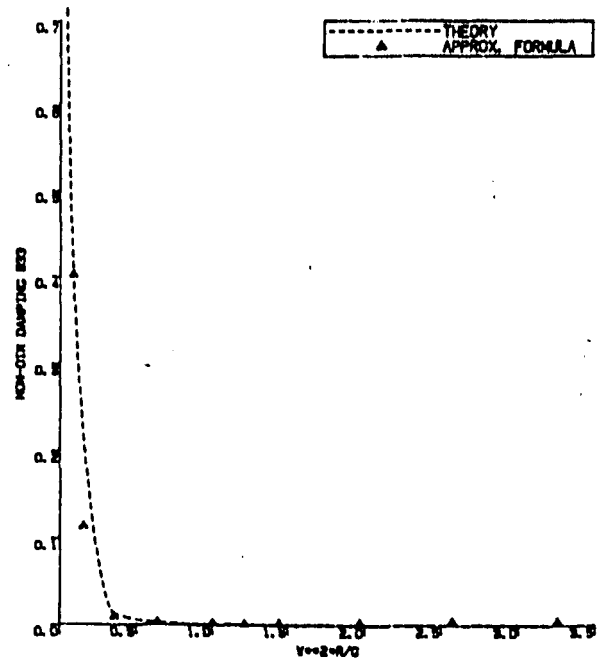
COMPARISON OF DAMPING
HST/R=1.0 H/R=6.0

Fig. 2.50

effect on the hydrodynamic coefficients has been derived by Faltinsen [34] and Lee [49] using the Haskind-Newman relation. The theory used in Reference [34] is similar to that given in Section 3.3.5 of this Chapter where the wave exciting forces are discussed. If the wave potential is represented by:-

$$\Phi = \Phi_I + \Phi_D + \Phi_R \qquad (2\text{-}154)$$

where Φ_R is the fluid disturbance caused by the motion of the body in initially calm water. Let:-

$$\Phi_R = \sum_{k=2}^{6} S_{k_o} \Phi_k \qquad (2\text{-}155)$$

which is the only term relating to the motion-induced force. The symbol S_{k_o} represents the complex amplitudes of the displacement of the body from its mean position. Then the resulting motion-induced pressure is:-

$$p = \rho(i\omega + U\frac{\partial}{\partial x})\Phi_R \qquad (2\text{-}156)$$

$$= \rho(i\omega + U\frac{\partial}{\partial x})(\sum_{k=2}^{6} S_{k_o}\Phi_k) \qquad (2\text{-}157)$$

and the motion-induced force is:-

$$F_j^{(m)} = \iint_S pn_j ds \qquad (2\text{-}158)$$

$$= \rho \sum_{k=2}^{6} S_{k_o}\iint n_j (i\omega + U\frac{\partial}{\partial x})\Phi_k ds \qquad (2\text{-}159)$$

Applying the Kronecker delta function δ_{jk} and from Ogilvie and Tuck [78]:-

$$\iint_S n_j \Phi_x dx = \iint_S (n_3\delta_{j5} - n_2\delta_{j6})\Phi ds - \int_{C(x)} n_j\Phi d\ell \qquad (2\text{-}160)$$

where S is the immersed hull surface of the cross section at x and C(x) is the line integral along the contour of the cross section:-

$$\frac{\partial \Phi_R}{\partial n} = - i\omega(\bar{S}_0 + \bar{\alpha}_0 \times \bar{r}).\bar{n} - U(\bar{\alpha}_0 \times \bar{e}_1).\bar{n} \qquad (2\text{-}161)$$

where $\bar{S}_0 = (S_{20}, S_{30})$

$\bar{\alpha}_0 = (S_{40}, S_{50}, S_{60})$

$\bar{r} = (x, y, z)$

and $\bar{e}_1 =$ unit vector in x-direction

$$\frac{\partial \Phi_j}{\partial n} = - i\omega n_j + Un_3\delta_{j5} - Un_2\delta_{j6} \quad \text{for } j = 2, 3, 4, 5, 6 \qquad (2\text{-}162)$$

$$F_j^{(m)} = \rho \sum_{k=2}^{6} S_{k_0} \iint_S (i\omega n_j + Un_3\delta_{j5} - Un_2\delta_{j6})\Phi_k ds \qquad (2\text{-}163)$$

$$= - \rho \sum_{k=2}^{6} S_{k_0} \iint_S (\Phi_{jn} + \frac{2U}{i\omega}\Phi_{3n}\delta_{j5} - \frac{2U}{i\omega}\Phi_{2n}\delta_{j6})\Phi_k ds \qquad (2\text{-}164)$$

where subscript n denotes the normal derivative

The motion-induced forces can be separated into two parts, ie the added mass term relating to the acceleration of the motion and damping term relating to the velocity of the motion, then:-

$$F_j^{(m)} = \sum_{k=2}^{6} S_{k_0} (\omega^2 A_{jk} + i\omega B_{jk}) \qquad (2\text{-}165)$$

where $A_{jk} = \text{Re}[- \frac{\rho}{\omega^2}\iint_S (\Phi_{jn} + \frac{2U}{i\omega}\Phi_{3n}\delta_{j5} - \frac{2U}{i\omega}\Phi_{2n}\delta_{j6})\Phi_k ds]$ (2-166)

and $B_{jk} = I_m[- \frac{\rho}{\omega}\iint_S (\Phi_{jn} + \frac{2U}{i\omega}\Phi_{3n}\delta_{j5} - \frac{2U}{i\omega}\Phi_{2n}\delta_{j6})\Phi_k ds]$ (2-167)

It is assumed that there is no coupling between the motion in

the horizontal and vertical planes for a slender ship so that $A_{jk} = B_{jk} = 0$ for j = odd numbers and k = even numbers or for j = even numbers and k = odd numbers. By applying the strip theory, equations (2-166) and (2-167) can be expressed in terms of a two-dimensional velocity potential in the following forms:-

$$A_{jk} = \text{Re}[- \frac{\rho}{\omega^2} \int_L dx \int_{S(x)} (\phi_{jn} + \frac{2U}{i\omega}\phi_{3n}\delta_{j5} - \frac{2U}{i\delta}\phi_{2n}\delta_{j6})\phi_k d\ell] \quad (2-168)$$

$$B_{jk} = \text{Im}[- \frac{\rho}{\omega} \int_L dx \int_{S(x)} (\phi_{jn} + \frac{2U}{i\omega}\phi_{3n}\delta_{j5} - \frac{2U}{i\omega}\phi_{2n}\delta_{j6})\phi_k d\ell] \quad (2-169)$$

where $\int_L$ is the lengthwise integral

and $\int_{S(x)}$ is the contourwise integral at section x

It is convenient to represent the sectional added mass and damping as:-

$$a_{jj}(x) = \text{Re}[- \frac{\rho}{\omega^2}\int_{S(x)} \phi_{jn}\phi_j \, d\ell] \quad (2-170)$$

$$b_{jj}(x) = \text{Im}[- \frac{\rho}{\omega}\int_{S(x)} \phi_{jn}\phi_j d\ell] \quad (2-171)$$

From this the hydrodynamic coefficients with the forward speed effect can be obtained. In this study, A_{33} and A_{53} are taken as examples of the process and the others are as listed in Table 2.13. They can be expressed by combining equations 2.168 and 2.170 as follows:-

$$A_{33} = \text{Re}[- \frac{\rho}{\omega^2}\int_L dx \int_{S(x)} (\phi_{3n} + \frac{2U}{i\omega}\phi_{3n}\delta_{35} - \frac{2U}{i\omega}\phi_{2n}\delta_{36}) \phi_3 d\ell]$$

$$= \text{Re}[-\frac{\rho}{\omega^2}\int_L dx \int_{S(x)} \phi_{3n} \cdot \phi_3 d\ell]$$

$$= \int_L a_{33}(x) dx \quad (2-172)$$

that is, there is no speed effect on A_{33}

Similarly,

$$A_{53} = Re \left[-\frac{\rho}{\omega^2} \int_L dx \int_{S(x)} (\phi_{5n} + \frac{2U}{i\omega}\phi_{3n}\delta_{55} - \frac{2U}{i\omega}\phi_{2n}\delta_{56})\phi_3 d\ell \right]$$

$$= Re \left[-\frac{\rho}{\omega^2} \int_L dx \int_{S(x)} (\phi_{5n}\phi_3 + \frac{2U}{i\omega}\phi_{3n}\phi_3) d\ell \right] \qquad (2-173)$$

From equation (2-162):-

$$\phi_{3n} = \frac{\partial\phi_3}{\partial n} = - i\omega n_3 \qquad (2-174)$$

$$\phi_{5n} = \frac{\partial\phi_5}{\partial n} = - i\omega n_5 + Un_3\delta_{55} \qquad (2-175)$$

$$= - i\omega n_5 + Un_3$$

Now, for a slender body $n_5 = -xn_3$

Therefore, $\phi_{5n} = - i\omega(- xn_3) + Un_3$

$$= i\omega(x + \frac{U}{i\omega})n_3$$

$$= - (x + \frac{U}{i\omega})\phi_{3n} \qquad (2-176)$$

$$A_{53} = Re \left[-\frac{\rho}{\omega^2} \int_L dx \int_{S(x)} (-x + \frac{U}{i\omega})\phi_3\phi_{3n} d\ell \right] \qquad (2-177)$$

$$= - \int xdx \{ -\frac{\rho}{\omega^2} Re \int_{S(x)} \phi_3\phi_{3n} d\ell \}$$

$$\qquad (2-178)$$

$$+ \frac{U}{\omega^2} \int_L dx \{ -\frac{\rho}{\omega} Im \int_{S(x)} \phi_3\phi_{3n} d\ell \}$$

$$= - \int xa_{33} dx + \int \frac{U}{\omega^2} b_{33} dx \qquad (2-179)$$

In the above equation the second term is caused by the speed effect.

A_{33}	no speed effect
B_{33}	no speed effect
A_{35}	$-\dfrac{U}{\omega^2}\int b_{33}dx$
B_{35}	$U\int a_{33}dx$
A_{55}	$\dfrac{U^2}{\omega^2}\int a_{33}dx$
B_{55}	$\dfrac{U^2}{\omega^2}\int b_{33}dx$
A_{53}	$\dfrac{U}{\omega^2}\int b_{33}dx$
B_{53}	$-U\int a_{33}dx$

Table (2-13) **Speed effect terms on the hydrodynamic
coefficients in the vertical plane motion**

6.   HYDROSTATIC RESTORING FORCE

Accurate estimation of the centre of gravity both in the
longitudinal and vertical directions is essential for correct
prediction of pitching and rolling moments. Correct estimation of the
hydrodstatic restoring forces are also important in the motion
predictions in the low frequency range.

The offsets of the model are shown in fig. 2.51 where the
mass of the structure was treated item by item as shown in fig. 2.52,
the vertical and longitudinal centres of gravity were measured using
the principle of a simply supported beam when one reaction was
'weighed' on a conventional weighing scale while the $\overline{GM}$ values were
obtained by an inclining experiment.

SIDE ELEVATION

SECTION 'C'-C'
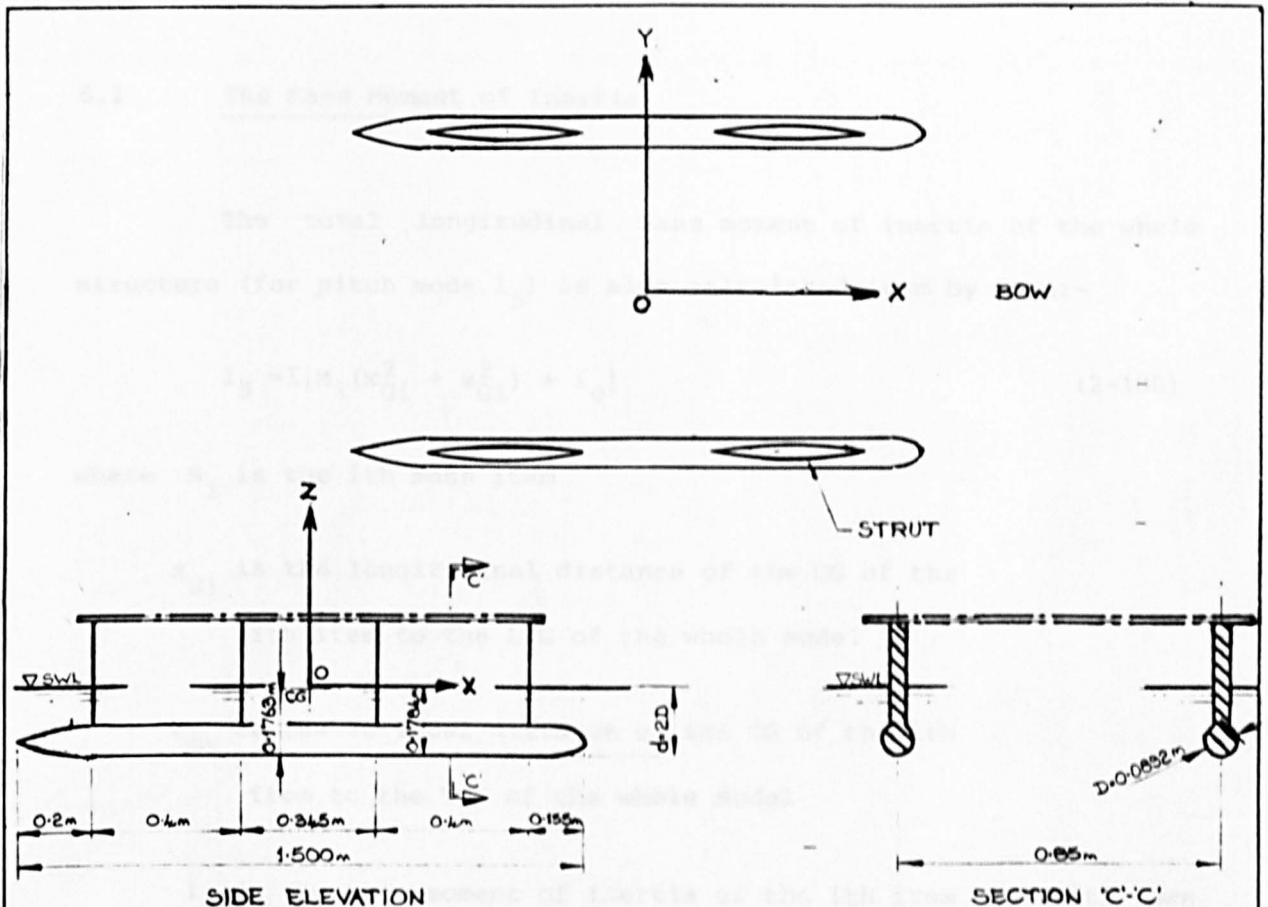
SWATH DETAILS AND DESCRIPTION OF CO-ORDINATE SYSTEM
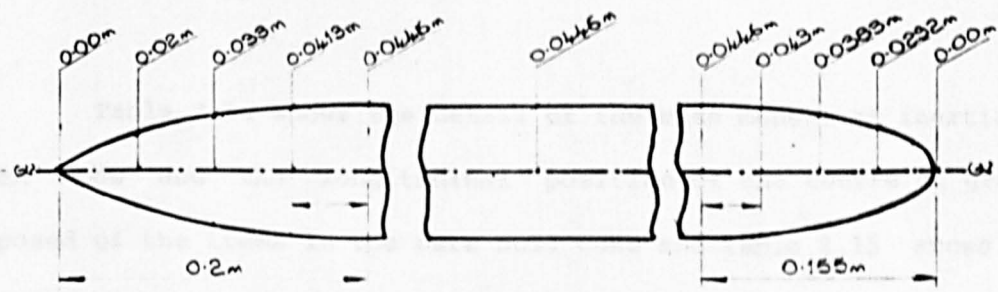
HULL OFFSETS
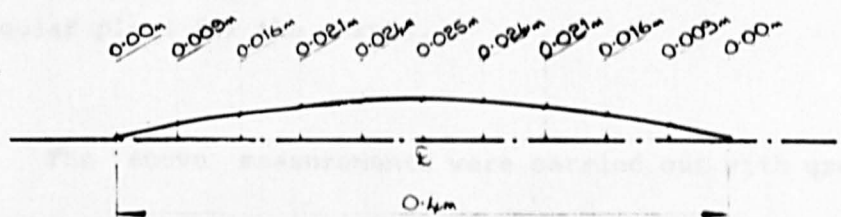
STRUT OFFSETS

THE STRUT IS SYMMETRIC TRANSVERSELY ABOUT AN AXIS IN THE
LONGITUDINAL 'X' AXIS

Fig. 2.51

6.1   The Mass Moment of Inertia

The total longitudinal mass moment of inertia of the whole structure (for pitch mode I_5) is also calculated item by item:-

$$I_5 = \Sigma[M_i(x_{Gi}^2 + z_{Gi}^2) + i_o]$$ (2-180)

where M_i is the ith mass item

x_{Gi} is the longitudinal distance of the CG of the

ith item to the LCG of the whole model

z_{Gi} is the vertical distance of the CG of the ith

item to the VCG of the whole model

i_o is the mass moment of inertia of the ith item about its own

axis parallel to the structural system axes Y, through the

item's own CG.

Table 2.14 shows the detail of the mass moment of inertia in pitch mode and the longitudinal position of the centre of gravity composed of the items in the bare hull case and Table 2.15 shows the details with the aft fins. The mass moment of inertia of each item about its own axis are approximated by a rod for the hulls and by a rectangular plate for the struts.

The above measurements were carried out with great care and checked by the hydrostatic computer program (POSH) [79]. Calculations and measurements were found to be in good agreement.

The hydrostatic restoring coefficients, which are frequency
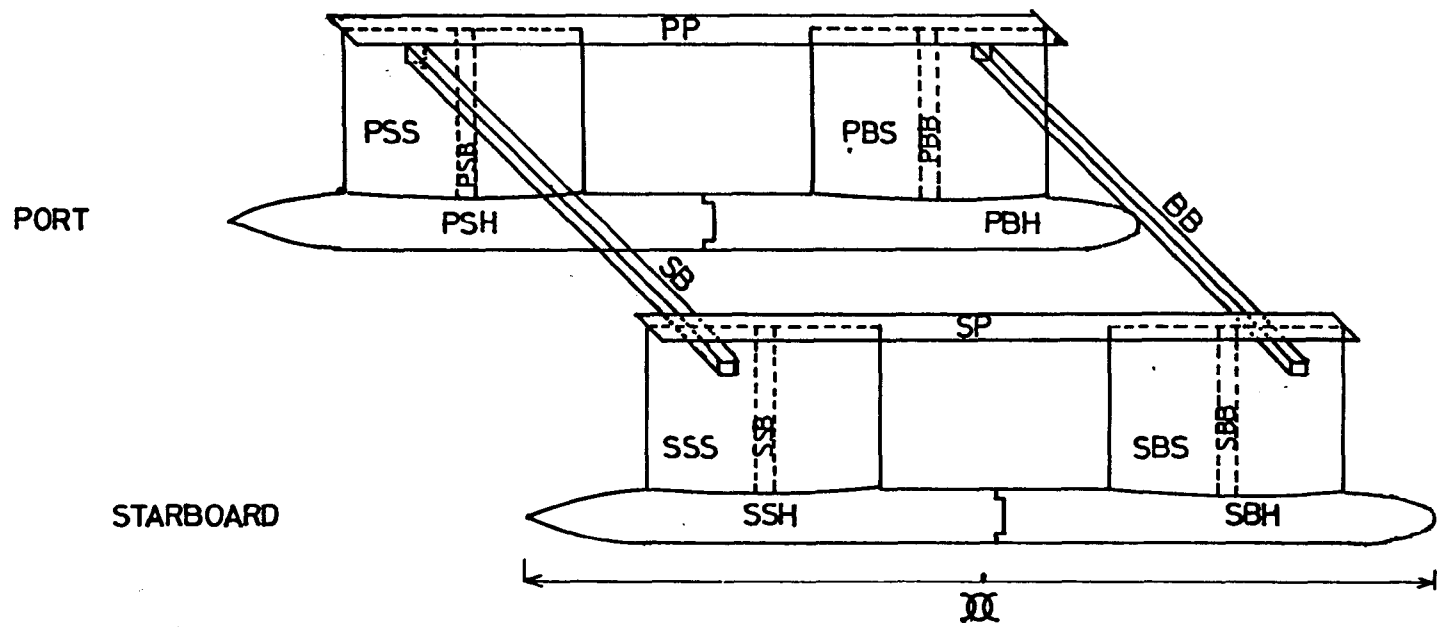
PORT

STARBOARD

SBH :	STARBOARD-BOW-HULL	
SBS :	—STRUT	
SBB :	—BALLAST	
SSH :	STARBOARD-STERN-HULL	
SSS :	—STRUT	
SSB :	—BALLAST	
SP :	STARBOARD-PLATE	
SF :	-FIN	
BB :	BOW-BAR	

PBH :	PORT-BOW-HULL
PBS :	—STRUT
PBB :	—BALLAST
PSH :	PORT-STERN-HULL
PSS :	—STRUT
PSB :	—BALLAST
PP :	PORT-PLATE
PF :	-FIN
SB :	STERN-BAR

Fig. 2.52

132.

The Longitudinal Mass Moment of Inertia (Bare Hull)

Name of Item in fig 2.52	Mass (M) (Kg)	$x_\otimes$ (m)	$Mx_\otimes$	x_G	z_G	$r_G^2 = x_G^2 + z_G^2$	i_o	Mr_G^2
SBH	2.500	0.385	0.963	0.363	-0.1317	0.1493	0.110	0.3732
SBS	1.179	0.395	0.466	0.373	0.0503	0.1415	0.0232	0.1668
SBB	0.382	0.395	0.151	0.373	-0.0383	0.1405	0.0024	0.0540
SP	0.722	0.030	0.022	0.008	0.1877	0.0350	-	0.0250
BB	1.241	0.435	0.540	0.413	0.1767	0.2020	-	0.2510
SSH	2.398	-0.335	-0.803	-0.357	-0.1317	0.1443	0.1333	0.3460
SSS	1.112	-0.350	-0.389	-0.372	0.0503	0.1405	0.0220	0.1560
SBS	1.408	-0.350	-0.493	-0.372	0.0480	0.1403	0.0090	0.1980
SB	1.237	-0.380	-0.470	-0.402	0.1767	0.1930	-	0.2390
PBH	2.386	0.385	0.919	0.363	-0.1317	0.1493	0.1060	0.3560
PBS	1.049	0.395	0.414	0.392	0.0503	0.1565	0.0210	0.1640
PBB	1.405	0.395	0.555	0.417	0.0540	0.1769	0.0090	0.2490
PP	0.699	0.030	0.021	0.008	0.1877	0.0350	-	0.0240
PSH	2.659	-0.335	-0.890	-0.357	-0.1317	0.1443	0.1310	0.3840
PSS	1.197	-0.350	-0.419	-0.372	0.0503	0.1405	0.0240	0.1680
PSB	0.328	-0.350	-0.115	-0.372	-0.0670	0.1425	0.0021	0.0470

Σ = 21.89   0.472   0.5912   2.9890

$x_{\otimes G} = 0.472/21.89 = 0.022$ (m)

$x_G = x_\otimes - x_{\otimes G}$

$I_5 = Mr_G^2 + i_o$

$= 2.989 + 0.5912$

$= 3.58$ (Kg.m^2)

Table 2.14

The Longitudinal Mass Moment of Inertia (With Aft Fins)

Name of Item in fig 2.52	Mass (M) (Kg)	$x_\otimes$ (m)	$Mx_\otimes$	x_G	z_G	$r_G^2 = x_G^2 + z_G^2$	i_o	Mr_G^2
SBH	2.500	0.385	0.963	0.369	-0.1317	0.1535	0.1100	0.3840
SBS	1.179	0.395	0.466	0.379	0.0503	0.1462	0.0232	0.1720
SBB	0.615	0.395	0.243	0.379	0.0337	0.1448	0.0390	0.0890
SP	0.722	0.030	0.022	0.014	0.1877	0.0350	-	0.0260
BB	1.241	0.435	0.540	0.419	0.1767	0.2068	-	0.2570
SSH	2.398	-0.335	-0.803	-0.351	-0.1317	0.1405	0.1333	0.3370
SSS	1.112	-0.350	-0.389	-0.366	0.0503	0.1365	0.0220	0.1518
SBS	1.091	-0.350	-0.381	-0.366	0.0223	0.1344	0.0690	0.1467
SB	1.237	-0.380	-0.470	-0.396	0.1767	0.1880	-	0.2326
PBH	2.386	0.385	0.919	0.369	-0.1317	0.1535	0.1060	0.3663
PBS	1.049	0.395	0.414	0.379	0.0503	0.1462	0.0210	0.1533
PBB	1.274	0.395	0.503	0.379	0.0333	0.1447	0.0080	0.1844
PP	0.699	0.030	0.021	0.014	0.1877	0.0354	-	0.0248
PSH	2.659	-0.335	-0.891	-0.351	-0.1317	0.1405	0.1310	0.3737
PSS	1.197	-0.350	-0.419	-0.366	0.0503	0.1365	0.0240	0.1634
PSB	0.362	-0.350	-0.127	-0.366	-0.0414	0.1357	0.0023	0.0491
SF	0.250	-0.502	-0.125	-0.524	-0.1317	0.2919	-	0.0730
PF	0.247	-0.502	-0.124	-0.524	-0.1317	0.2919	-	0.0720
$\sum =$	22.22		0.362				0.6790	3.2560

$$x_{\otimes G} = 0.362/22.22 = 0.01629 \ (m)$$

$$x_G = x_\otimes - x_{\otimes G}$$

$$I_5 = Mr_G^2 + i_o$$

$$= 3.256 + 0.679$$

$$= 3.935 \ (Kg \cdot m^2)$$

Table 2.15

and speed independent and are contributed by the inherent buoyancy effect, are:-

$$C_{33} = \rho g A_{wp} \qquad (2\text{-}181)$$

$$C_{35} = C_{53} = -\rho g M_{wp} \qquad (2\text{-}182)$$

$$C_{55} = \rho g I_{wp} - \Delta.\overline{BG}$$

$$= \rho g \nabla.(\frac{I_{wp}}{\nabla}) - \rho g \nabla \overline{BG} \qquad (2\text{-}183)$$

$$= \rho g \nabla(\overline{BM} - \overline{BG})$$

$$= \rho g \nabla.\overline{GM}_L$$

where A_{wp} is the waterplane area

   M_{wp} is the moment of waterplane area along the longitudinal direction

   I_{wp} is the moment of inertia of waterplane area along the longitudinal direction

   $\overline{BG}$ is the vertical distance between the centre of buoyancy and gravity

   $\overline{GM}_L$ is the metacentric height in the longitudinal direction

   ∇ is the volume displacement of the model

   Δ is the mass of the model

6.2   Inclining Experiment

The inclining mass (2.436Kg) were placed port and starboard of both aft end and forward end of the deck, as shown in fig. 2.53.

The distance apart of the transducers for the longitudinal case was S = 86cm and the distance apart of the transducers for the transverse case was S = 94cm.

6.2.1 $\overline{GM}_L$

The transducer readings were recorded as follows:-

1st Shift 0.426Kg (both P and S 2 x 0.213Kg	Aft to Fwd	Transducer Deflection	7.987 cm
2nd Shift 0.79Kg	Aft to Fwd	Transducer Deflection	12.2727 cm
3rd Shift 1.216Kg	Aft to Fwd	Transducer Deflection	20.259 cm
4th Shift 0.43Kg	Fwd to Aft	Transducer Deflection	7.792 cm
5th Shift 0.79Kg	Fwd to Aft	Transducer Deflection	12.2727 cm
6th Shift 1.22Kg	Fwd to Aft	Transducer Deflection	20.0649 cm

$$\overline{GM}_L = \frac{w_1 \cdot d}{(\Delta + W) \cdot \frac{\Delta T}{S}}$$

where w_1 is the mass of the item which was shifted

Δ is the mass of the model (before added mass)

W is the total inclining mass

d is the distance between the mass

ΔT is the difference between the transducers

S is the distance between the transducers

For example, first case $\Delta T = 7.987$cm

$$S = 86cm$$

$$d = 1.092m$$

$$w_1 = 0.426 \text{Kg}$$

$$W = 2.436 \text{Kg}$$

$$\Delta = 21.8 \text{Kg}$$

$$\overline{G_1'M_L} = \frac{0.426 \times 1.092}{(21.8) + 2.436) \times 7.987/86} = 0.20667 \text{(m)}$$

Correction of $\overline{GG'}$, due to shift in the elevation of ballast mass, as shown in fig. 2.53. For the first case (example):-

$$\overline{G_1G_1'} = \frac{0.426 \times 0.01}{(21.8 + 2.436)} = 0.000176 \text{(m)}$$

Therefore, $\overline{G_1M_L} = \overline{G_1'M_L} + \overline{G_1G_1'} = 0.20667 + 0.000176 = 0.20684 \text{(m)}$

The other cases are listed in Table 2.16.

Case	Inclining Mass	$\overline{G_1'M_L}$	$\overline{G_1G_1'}$	$\overline{G_1M_L}$
1	0.426	0.20667	0.00017577	0.20684
2	0.79	0.24943	0.001075	0.25050
3	1.216	0.23258	0.001154	0.23373
4	0.430	0.21184	0.0001774	0.21201
5	0.79	0.24943	0.001075	0.25050
6	1.22	0.23483	0.001154	0.2359

Average = 0.23158(m)

Table 2.16

Correction of CG due to 'Added Inclining Mass is:-

$$\overline{GG_1} = \frac{(0.79 \times 2) \times 0.2072 + 10.426 + 0.430) \times 0.2187}{21.8 + 2.436}$$

$$= 0.021224 \,(m)$$

$$\therefore \quad \overline{GM}_L = 0.23158 + 0.021224$$

$$= \underline{0.252804 \,(m)}$$

6.2.2 $\underline{\overline{GM}_T}$

The same procedure is used to find transverse $\overline{GM}_T$ as shown in Table 2.17.

Case	Shift	Transducer Records (cm)	$\overline{G_1'M_T}$ (m)	$\overline{G_1G_1'}$ (m)	$\overline{G_1M_T}$ (m)
1	0.426Kg P to S	4.8700	0.298	0.00017	0.29867
2	0.790Kg P to S	9.1550	0.294	0.00107	0.29557
3	1.216Kg P to S	14.0250	0.295	0.00115	0.29705
4	0.320Kg S to P	4.2857	0.342	0.00017	0.34257
5	0.790Kg S to P	9.1550	0.294	0.00107	0.29557
6	1.220Kg S to P	13.4410	0.308	0.00115	0.30985
Average $\overline{G_1M_T}$ = 0.30655(m)					

Table 2.17

$$\text{where } \overline{G_1 M_T} = \frac{w_1 \cdot d}{(\Delta + W) \cdot \frac{\Delta T}{S}}$$

d = 0.88m

W = 2.4366Kg

S = 0.94m

Δ = 21.8Kg

$$\overline{GM}_T = \overline{G_1M}_T + \overline{GG}_1$$

$$= 0.30655 + 0.021224$$

$$= \underline{0.32777\,(m)}$$

$\overline{GM}_L$ and $\overline{GM}_T$ compared with computer calculations [79]:-

Program		Inclining Experiment
$KM_L = 0.429$	$GM_L = 0.2527\,(m)$	$GM_L = 0.252804\,(m)$
$KM_T = 0.512$	$GM_T = 0.3357\,(m)$	$GM_T = 0.32777\,(m)$

where KG = 0.1763m was obtained by weighing the model on the scales and the KM values were calculated by a computer program.
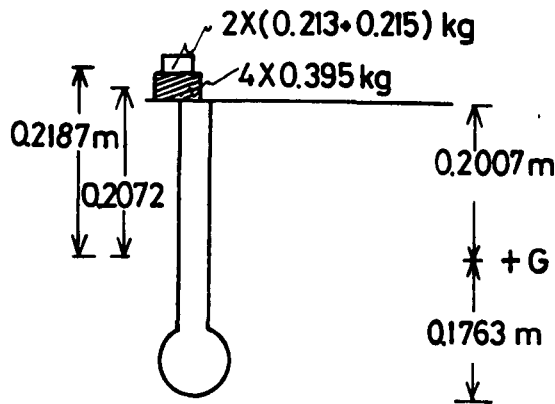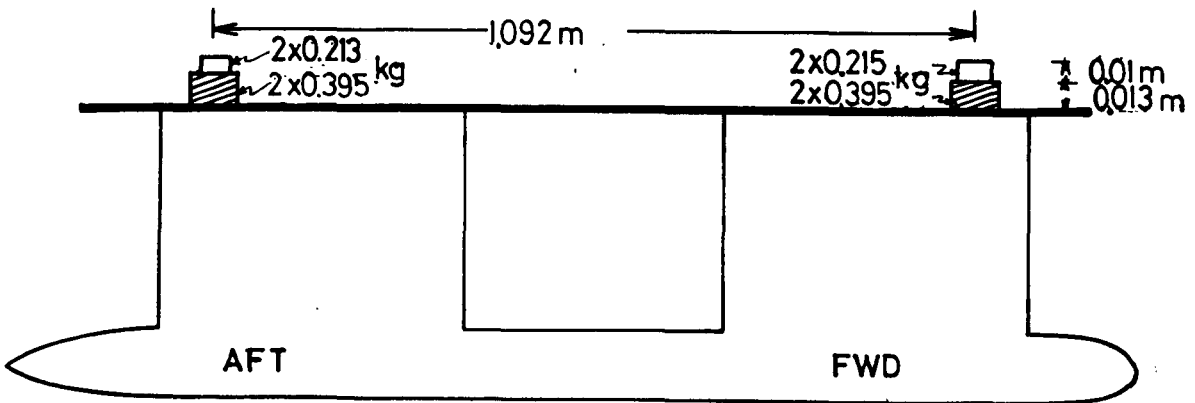
Fig. 2.53

7.   DESCRIPTION OF THE COMPUTATION

The computational procedure is explained in the flow chart shown in fig. 2.54. The frequency range of the calculation was chosen between 1.5 rad s^{-1} and 8.0 rad s^{-1} in twenty-seven equally spaced frequencies.

Strip theory is applied along the SWATH model length. The model has been divided into twenty-one sections, including the end sections which have zero area. Because of the symmetric geometric sections, as shown in fig. 2.55, the twenty-one sections reduce to nine different sections. Each section is symmetric about its transverse centreline in the X-Z plane. To use the Frank Close-fit method, sixteen straight line segments were taken for one-half of the demihull contours.

The input data included the x and y co-ordinates of these points, the depth of submergence, an indication as to whether the body was submerged or floating in the free surface, and the mode of the motion. Similar geometric sections will yield the same sectional added mass and damping coefficient in program DAMP and the same sectional wave-exciting forces in program WET but have different phase shifts because of their position relating to the origin. In program YREX and YRAD, Simpson's first integration rule is used for the integration of the sectional force and hydrodynamic coefficients for the bare hull case in potential flow.

The main program SWAFIN takes into account the speed effects, viscous effects and the contribution of the fins, both in the hydrodynamic coefficients and the wave-exciting forces and moments. It
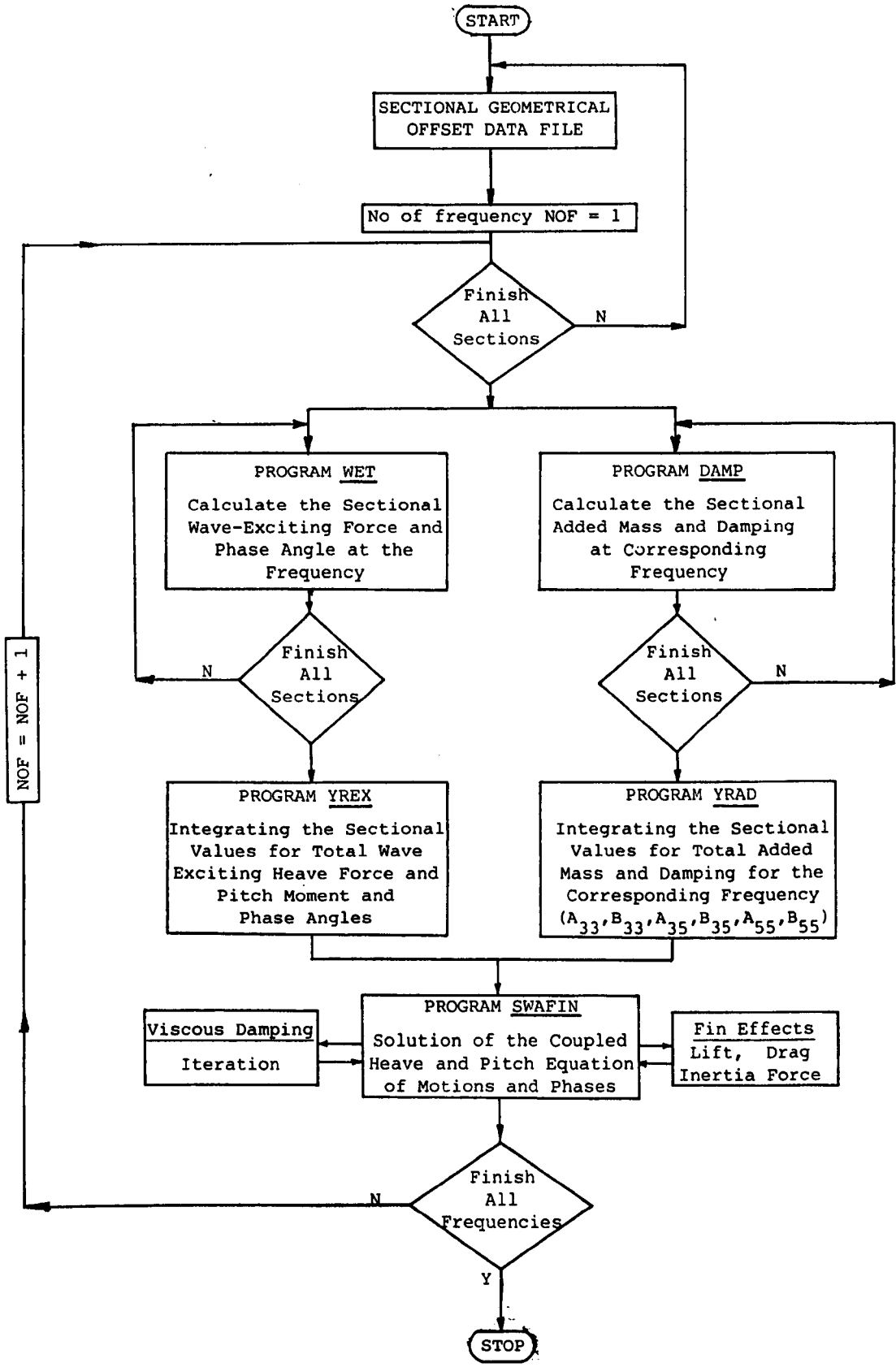
Fig. 2.54 Flowchart of the computer program
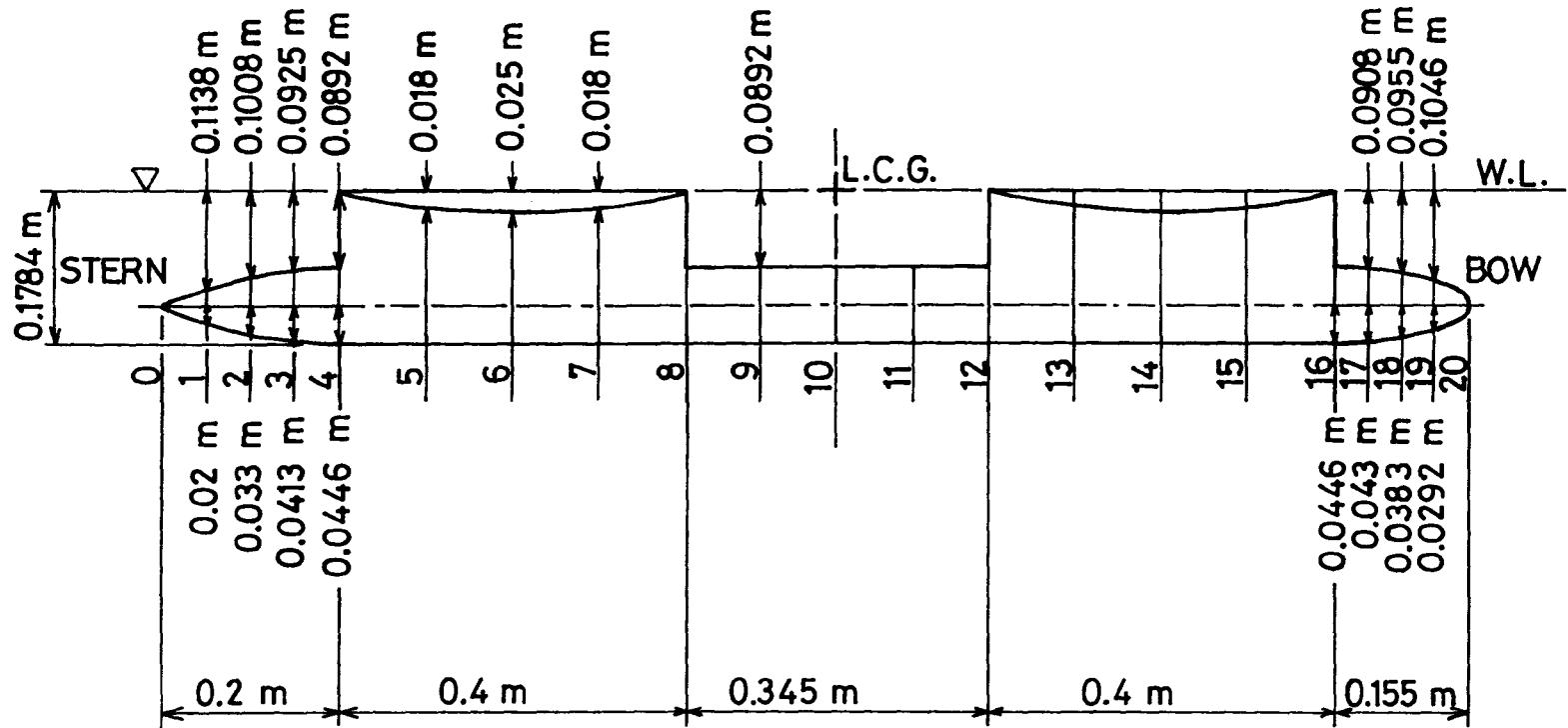
SECTIONS 4,8,9,10,11,12 & 16 ARE IDENTICAL.

SECTIONS 5,7,13 & 15 ARE IDENTICAL.

SECTIONS 6 & 14 ARE IDENTICAL.

Fig. 2.55

uses an inverse matrix method to solve for the coupled heave and pitch motions.

Assuming a linear relationship between the wave excitation and ship response, the equations of coupled heave and pitch motion are:-

$$(M + A_{33})\ddot{S}_3 + B_{33}\dot{S}_3 + C_{33}S_3 + A_{35}\ddot{S}_5 + B_{35}\dot{S}_5 + C_{35}S_5 = F_3 e^{-i\omega t} \quad (2\text{-}184)$$

$$A_{53}\ddot{S}_3 + B_{53}\dot{S}_3 + C_{53}S_3 + (I_5 + A_{55})\ddot{S}_5 + B_{55}\dot{S}_5 + C_{55}S_5 = F_5 e^{-i\omega t} \quad (2\text{-}185)$$

Since the right hand side is complex, the resulting motion displacement S is assumed to be complex and given by:-

$$S_3 = \text{Re}(\bar{S}_3 e^{-i\omega t}) \qquad \text{with} \quad \bar{S}_3 = S_{3R} + iS_{3I}$$

$$S_5 = \text{Re}(\bar{S}_5 e^{-i\omega t}) \qquad \text{with} \quad \bar{S}_5 = S_{5R} + iS_{5I}$$

$$F_3 = \text{Re}(\bar{F}_3 e^{-i\omega t}) \qquad \text{with} \quad \bar{F}_3 = F_{3R} + iF_{3I}$$

$$F_5 = \text{Re}(\bar{F}_5 e^{-i\omega t}) \qquad \text{with} \quad \bar{F}_5 = F_{5R} + iF_{5I}$$

$$(2\text{-}186)$$

where $\bar{S}$ is the complex amplitude of the motion displacement

and subscript R, I denotes the real and imaginery parts
     of the terms.

The motion displacement, velocity and acceleration are written, for example S_3, as:-

$$S_3 = \bar{S}_3 e^{-i\omega t}$$

$$\dot{S}_3 = -i\omega \bar{S}_3 e^{-i\omega t}$$

$$\ddot{S}_3 = -\omega^2 \bar{S}_3 e^{-i\omega t}$$

$$(2\text{-}187)$$

Substituting equation (2-187) into equations (2-184) and (2-185):-

$$\{[-\omega^2(M+A_{33})+C_{33}]-i\omega B_{33}\}\bar{S}_3+\{(-\omega^2 A_{35}+C_{35})-i\omega B_{35}\}\bar{S}_5 = \bar{F}_3 \qquad (2-188)$$

$$\{(-\omega^2 A_{53}+C_{53})-i\omega B_{53}\}\bar{S}_3+\{[-\omega^2(I_5+A_{55})+C_{55}]-i\omega B_{55}\}\bar{S}_5 = \bar{F}_5 \qquad (2-189)$$

$$\begin{bmatrix} c_{33}-\omega^2(M+A_{33}) & c_{35}-\omega^2 A_{35} & \omega B_{35} & \omega B_{35} \\ c_{33}-\omega^2 A_{53} & c_{55}-\omega^2(I_5+A_{55}) & \omega B_{53} & \omega B_{55} \\ -\omega B_{33} & -\omega B_{35} & c_{33}-\omega^2(M+A_{33}) & c_{35}-\omega^2 A_{35} \\ -\omega B_{53} & -\omega B_{55} & c_{53}-\omega^2 A_{53} & c_{55}-\omega^2(I_5+A_{55}) \end{bmatrix} \times \begin{bmatrix} S_{3R} \\ S_{5R} \\ S_{3I} \\ S_{5I} \end{bmatrix} = \begin{bmatrix} F_{3R} \\ F_{5R} \\ F_{3I} \\ F_{5I} \end{bmatrix}$$

$$(2.190)$$

Therefore, the amplitude of the motions are:-

$$S_3 = (S_{3R}^2 + S_{3I}^2)^{\frac{1}{2}}$$

$$(2-191)$$

$$S_5 = (S_{5R}^2 + S_{5I}^2)^{\frac{1}{2}}$$

and the phase angle

$$\alpha_3 = \tan^{-1}(\frac{S_{3I}}{S_{3R}})$$

$$(2-192)$$

$$\alpha_5 = \tan^{-1}(\frac{S_{5I}}{S_{5R}})$$

CHAPTER
3

The

Determination

of Fin Size

CHAPTER   3

THE DETERMINATION OF FIN SIZE

1.   INTRODUCTION

Dynamic stability and the minimisation of ship motions have received significant attention in recent years. Several studies on the applicability of appendages in the form of large lift-force producing devices for controlling or reducing ship motions have been carried out. Rudders have been used for a long time to steer ships or to keep their heading straight while the ship is moving through waves. Bilge keels and anti-rolling fins have been used in the reduction and control of roll motion. However, there has been comparatively few studies on the minimisation of vertical plane stability and motions.

Bessho [80] and Abkowitz [43] have presented studies of anti-pitching fins on ship motions. The analysis [43] reported that the pitching motion can be reduced to one-half by using a pair of fins at the bow with an area equal to between three and seven percent of a conventional ship waterplane area. In Reference [80], both the pure mathematical and experimental studies show the applicability of a pair, or pairs, of fins to cancel the wave-exciting force and moment for a container cargo ship.

In the study of SWATH vertical plane motion, because of the relatively small waterplane area of a SWATH compared to a mono-hull ship, small wave exciting forces will be generated at certain wave lengths. However, the motion is not necessarily reduced when the wave

exciting force vanishes at certain wave lengths because the damping coefficients also vanishes as a consequence. In addition, the small waterplane area which gives small restoring moment in the vertical plane will yield a pitch-instability when the ship speed exceeds a certain value. It is believed that the eddy damping and, hence, the righting moment could be increased by adding stabilising fins. The motion can be further reduced by using active control surfaces.

In general, there are at least four unknown parameters to be determined in the study of stationary fins, ie number of pairs of fins, fin areas, aspect ratio and locations. For different design purposes, the number of pairs may be chosen as a pair of forward fins at the bow or a pair of after fins at the stern only or both pairs.

The geometric aspect ratio of the fin which determines the lift-slope coefficient, also affects the lift-force, as discussed in Chapters 2 and 5.

In practice, the primary function of the aft fins is to provide pitch stability. In order to overcome the Munk moment (which causes the SWATH's bow down motion at higher speed) with a minimum fin area, a fin with a high lift curve slope, ie a higher aspect ratio which has an inherent minimum drag characteristic, is required. The position of the aft fin should be located as far aft as possible to obtain the largest righting moment arm relative to the longitudinal centre of gravity. In order to ensure sufficient stability and to avoid any unexpected error caused by a moving system, it is recommended [81] that a fixed aft fin should be used. Such fins can be seen in existing SWATH ships. On the contrary, for a conventional mono-hull ship, Reference [43] recommended that the anti-pitching fin

be located at the bow instead of the stern. This may be because the severe pitching motion of the monohull ship is associated with serious slamming at the bow and, therefore, it may be desirable that a greater increase in pitch damping can be achieved by forward fins.

For anti-heaving motion, the most favourable fin position seems to be the one nearest the longitudinal centre of gravity or with a pair of forward fins with a minimum destabilising effect on the pitch stability. Therefore, in contrast to the aft fin, the forward fin should have a low lift curve slope, ie lower aspect ratio fin section.

2. THEORETICAL ANALYSIS AND REVIEW [50,66]

The determination of the fin size and the location of the fins are based on the coupled heave and pitch motion equations. The fins must provide pitch and heave stability throughout the operational speeds, increase damping for the heave and pitch modes and create adequate separation between the natural periods of heave and pitch.

In order to simplify the demonstration of the procedure and for practical use, it is assumed that the locations and the planform of the fins are given. (In this study the AFT fins are put at 0.85 hull length, the FWD fins at 0.15 hull length, and the planform was assumed to be rectangular).

The initial fin size was determined using Routh's stability condition, as a first approximation for the lower bound of the numerical value $C_h S_p C_L \alpha$. These initial fin sizes were designated as

1.0. Other fins with the same geometric aspect ratio but different sizes were designated with the number indicating the projected fin area to the 1.0 initial fin. (For example 0.0 means a bare hull without fins and 2.0 means a fin area which is double that of the initial fin).

2.1   Equation of Motion

When a SWATH ship moves with a forward speed U, assume the vertical plane motion (heave, pitch and surge) is decoupled from the horizontal plane motion. Surge is ignored in the following calculations. The coupled heave and pitch equations of motion without external excitation can be expressed in the form:-

$$(M + A_{33}) \ddot{Z} + B_{33}\dot{Z} + C_{33}Z + A_{35}\ddot{\theta} + B_{35}\dot{\theta} + C_{35}\theta = 0 \qquad (3-1a)$$

$$A_{53}\ddot{Z} + B_{53}\dot{Z} + C_{53}Z + (I_5 + A_{55})\ddot{\theta} + B_{55}\dot{\theta} + C_{55}\theta = 0 \qquad (3-1b)$$

The equations are the same as in Chapter 2 except for the wave exciting force terms.

The origin of the co-ordinate system is located on the still water surface and the vertical axis passes through the centre of gravity. The axes OX, OY, OZ are directed towards the bow, port and upward, as shown in fig. 2.4 in the previous chapter. Z(t) is the heave motion displacement, (+ive) for upward and $\theta(t)$ is the pitch angular displacement, and (+ive) for bow down.

The coefficients of added mass and damping of geometrically slender bodies were calculated by a strip-theory synthesis (in which the flow at each cross-section is assumed to be locally two-dimensional) using the Frank Close-fit method [59] and curve-fitted into approximate formulae [62] (depending on the

draught, frequency) which are suitable for the circular section-aerofoil strut combination. To obtain the three-dimensional coefficients, the sectional hydrodynamic coefficients of the two-dimensional solution are integrated lengthwise. For the case of a ship with forward speed, Ogilvie and Tuck [78] presented a more consistent and rational theory for forward speed effects on the hydrodynamic coefficients which are derived on the basis of strip theory.

The other contributing factors are viscous damping effects on the bare hull and the fin effect, as shown in Chapter 2.

2.2   Solution of the Linearised Equation of Motion

Equation (3.1) will have an eigenvalue solution in the form:-

$$Z(t) = C_{1n} e^{\sigma_n t} \tag{3-2}$$

$$\theta(t) = C_{2n} e^{\sigma_n t} \tag{3-3}$$

where C_{1n} and C_{2n} are constants and σ_n are the eigen values or characteristic roots.

Substituting into equation (3-1), we obtain:-

$$[(M + A_{33})\sigma^2 + B_{33}\sigma + C_{33}]C_{1n} + (A_{35}\sigma^2 + B_{35}\sigma + C_{35})C_{2n} = 0 \tag{3-4a}$$

and

$$(A_{53}\sigma^2 + B_{53}\sigma + C_{53})C_{1n} + [(I_5 + A_{55})\sigma^2 + B_{55}\sigma + C_{55}]C_{2n} = 0 \tag{3-4b}$$

The characteristic equation becomes of the form:-

$$a\sigma^4 + b\sigma^3 + c\sigma^2 + d\sigma + e = 0 \tag{3-5}$$

where $a = (M + A_{33})(I_5 + A_{55}) - A_{53}A_{55}$

$b = (M + A_{53})B_{55} - A_{53}B_{35} + B_{33}(I_5 + A_{55}) - A_{35}B_{35}$

$c = (M + A_{33})C_{55} - A_{53}C_{35} + B_{33}B_{55} - B_{35}B_{53}$
$+ (I_5 + A_{55})C_{33} - A_{35}C_{53}$

$d = B_{33}C_{55} - B_{35}C_{35} + C_{33}B_{35} - C_{35}B_{53}$

$e = C_{33}C_{55} - C_{35}C_{53}$

It is clear from the stability equation (3-5) that there are four roots. The condition which will make the motion stable is that the real part of all roots must be negative.

Routh [82], in his development of dynamics, indicates certain conditions for the coefficients in order that the roots of a polynomial to indicate stability (ie have negative real parts) for the quartic of the form of equation (3-5), the conditions are [83]:

$$\frac{b}{a} > 0, \quad \frac{c}{a} > 0, \quad \frac{d}{a} > 0, \quad \frac{e}{a} > 0, \quad \frac{bcd - ad^2 - b^2e}{a^3} > 0 \qquad (3-6)$$

In order to solve the stability equation, the roots were found using the program JYNAG, using a routine from the NAG library. This routine is based on the method of Grant and Hitchins [84].

2.3.   Stability Characteristics

Let us examine the relationship between the stability root and simple oscillatory motion. The roots can be written as:-

$$\sigma_n = \sigma_{nR} \pm i\sigma_{nI} \qquad (3-7)$$

where n = 1, 2 ,3 ,4 , and σ_{nR} is the real part of the root and σ_{nI} is the imaginary part of the root. If the motion is convergent oscillatory and if σ_1 and σ_2 indicated the roots of the heave mode then:-

$$\sigma_1 = \sigma_{1R} + i\sigma_{1I} \qquad \text{and} \sigma_2 = \sigma_{1R} - i\sigma_{1I}$$
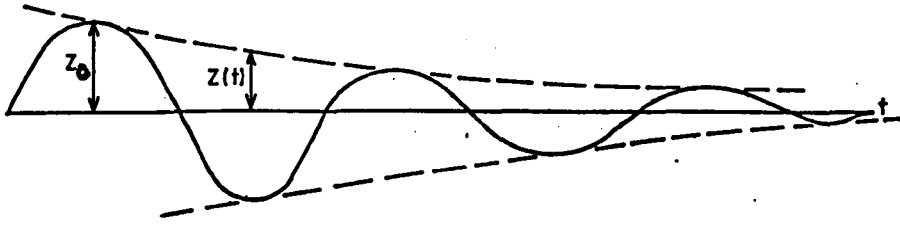
$$Z(t) = e^{\sigma_{1R}t}(C_1\cos\sigma_{1I}t + C_2\sin\sigma_{1I}t)$$

and
$$Z(t) = Z_o e^{\sigma_{1R}t}$$

where σ_{1I} is the circular oscillation frequency

σ_{1R} is the decay constant

The natural undamped oscillation frequency in the heave mode:-

$$\omega_{nH} = (\sigma_{1R}^2 + \sigma_{1I}^2)^{\frac{1}{2}} \qquad (3-8)$$

The natural period, $T = 2\pi/\omega$, gives:-

$$T_H = \frac{2\pi}{\left|\sigma_{1I}\right|} \text{ for heave mode} \qquad (3-9a)$$

and
$$T_p = \frac{2\pi}{\left|\sigma_{3I}\right|} \text{ for pitch mode} \qquad (3-9b)$$

The damping ratio γ = decaying constant/undamped natural frequency:-

$$\gamma_H = \frac{-\sigma_{1R}}{\omega_{nH}} = -\frac{\sigma_1 + \sigma_2}{2\sqrt{\sigma_1\sigma_2}} \text{ for heave mode} \qquad (3-10a)$$

and

$$\gamma_p = \frac{-\sigma_{3R}}{\omega_{np}} = -\frac{\sigma_3 + \sigma_4}{2\sqrt{\sigma_3\sigma_4}} \text{ for pitch mode} \qquad (3-10b)$$

Another measure of the degree of stability is the time to halve the amplitude of the disturbed motion. For instance, in heave

oscillation-:

$$Z(t) = Z_o e^{\sigma_{1R} t}$$

If we let $Z(t) = \frac{1}{2} \dot{Z}_o$

Then $\quad \dfrac{Z(t)}{Z_o} = e^{\sigma_{1R} t} = \dfrac{1}{2}$

$$T_H^{(\frac{1}{2})} = \frac{\ell n2}{|\sigma_{1R}|} \quad \text{for heave} \tag{3-11b}$$

$$T_P^{(\frac{1}{2})} = \frac{\ell n2}{|\sigma_{3R}|} \quad \text{for pitch} \tag{3-11b}$$

Clearly, if a stable motion becomes progressively less stable, the value $T^{(\frac{1}{2})}$ will become larger. All these numerical values which are related to the roots are listed in Tables 3.2 to 3.7.

2.4. Limited Speed - To Maintain Motion Stability Without Fins

According to Routh's stability condition:-

$$e = C_{33}C_{55} - C_{35}C_{53} > 0 \tag{3-12}$$

This implies that to satisfy the condition

$$C_{55} > 0$$

$$C_{55} = \rho g \nabla (\frac{Iw}{\nabla} - BG) - U^2 A_{33} - \rho A_o U^2 \int x \cdot B_m(x) dx$$

$$- \rho U^2 \sum_{i=1}^{n} A_i^f \ell_i (\frac{\partial C_L}{\partial \alpha})_i \tag{3-13}$$

For the SWATH without fins, the instability will start at the speed

U_{lim}, where:-

$$\dot{U}_{lim} < \left[\frac{\rho g \nabla (Iw/\nabla - BG) - C_{35}C_{53}/C_{33}}{A_{33} + \rho A_o \int x \cdot B_m(x) \, dx} \right]^{\frac{1}{2}}$$

since $\rho g \nabla.GM \gg C_{35}C_{53}/C_{33}$

$$U_{lim} \simeq \left[\frac{\rho g \nabla (Iw/\nabla - BG)}{A_{33} + \rho A_o \int x \cdot B_m(x) \, dx} \right]^{\frac{1}{2}} \qquad (3-14)$$

Beyond this speed, to maintain the stability, the SWATH needs stabilising fins.

The numerical value of U_{lim} calculated for SWATH1 and SWATH2 are $1.796ms^{-1}$ and $2.019ms^{-1}$ since SWATH2 has a larger GM_L than SWATH1, see Table 3.1.

2.5   Initial Fin Size

After determining U_{lim} for both SWATH1 and SWATH2, it is clearly necessary to fit fins to maintain stability up to a certain design speed. This speed was taken to be $3.0ms^{-1}$ in this study.

The initial fin size for the speed can be determined by the lower bound:-

$$\rho U^2 \sum_{i=1}^{n} A_i^f \ell_i (\frac{\partial C_L}{\partial \alpha})_i < \rho g (\frac{Iw}{\nabla} - BG) - U^2 (A_{33} + \rho A_o \int x B_m(x) \, dx)$$

$$C_h S_p \frac{\partial C_L}{\partial \alpha} > \frac{U^2 (A_{33} + \rho A_o \int x \cdot B_m(x) \, dx) - \rho g \nabla (Iw/\nabla - BG)}{\rho U^2 |\ell|} \qquad (3-15)$$

Assume

1. one identical fin size on each hull.
2. the geometric aspect ratio AR = 1.2.
3. this initial fin is located aft at 0.85 hull length.

PARAMETER	SWATH 1	SWATH2
Displacement (m^3)	0.022	0.025
Weight (Kg)	21.8	25.0
Length of Hull (m)	1.5	1.61
Hull Spacing (m)	0.855	0.855
Draft (m)	0.1784	0.223
Max Diameter of Hull (m)	0.0892	0.0892
VCG above Baseline (m)	0.1763	0.1763
VCB above Baseline (m)	0.064	0.075
Longitudinal GM (m)	0.2528	0.288
Waterplane Area Moment about the pitch axis (m^3) (Mw)	0.001	0.001
Waterplane Area Moment of Inertia about the pitch axis (m^4) (Iw)	0.008	0.010
Natural Heave Period (sec)	1.7	1.8
Natural Pitch Period (sec)	2.25	2.15
Distance Between Struts Centre to Centre (m)	0.745	0.855

Table 3.1

4. $\dfrac{\partial C_L}{\partial \alpha} = \dfrac{1.8\pi Ae}{1.8 + \sqrt{Ae^2 + 4}}$ where Ae is the effect aspect ratio

$= 2.AR$

5. neglect the drag force effects and strength consideration of the fins.

The initial fin sizes necessary to ensure pitch stability were found to be:-

	Chord (m)	Span (m)	Location (m)
SWATH 1	0.079	0.095	- 0.524 (aft LCG)
SWATH 2	0.072	0.087	- 0.562 (aft LCG)

2.6   The Lift-Curve Slope $\partial C_L/\partial \alpha$

The lift force L_f on the fin with a small angle of attack can be expressed by:-

$$L_f(t) = \tfrac{1}{2}\rho U^2 C_{hi} S_{pi} \frac{\partial C_L}{\partial \alpha} \alpha(t) \tag{3-16}$$

The lift-curve slope $\partial C_L/\partial \alpha$ can be derived from [69]:-

$$C_L = \left[\dfrac{C_o \cdot Ae}{\cos\Omega \sqrt{\dfrac{Ae^2}{\cos^4\Omega} + 4} + \dfrac{C_o}{\pi}}\right]\alpha + \dfrac{C_{DF}}{Ae}\alpha^2 \tag{3-17}$$

Neglecting the cross flow-drag effect gives,

$$\dfrac{\partial C_L}{\partial \alpha} = \dfrac{1.8\pi Ae}{\cos\Omega \sqrt{\dfrac{Ae^2}{\cos^4\Omega} + 4} + 1.8} \tag{3-18}$$

where C_o is the section lift-curve slope corrected from the experiment which is equal to 1.8π per radian
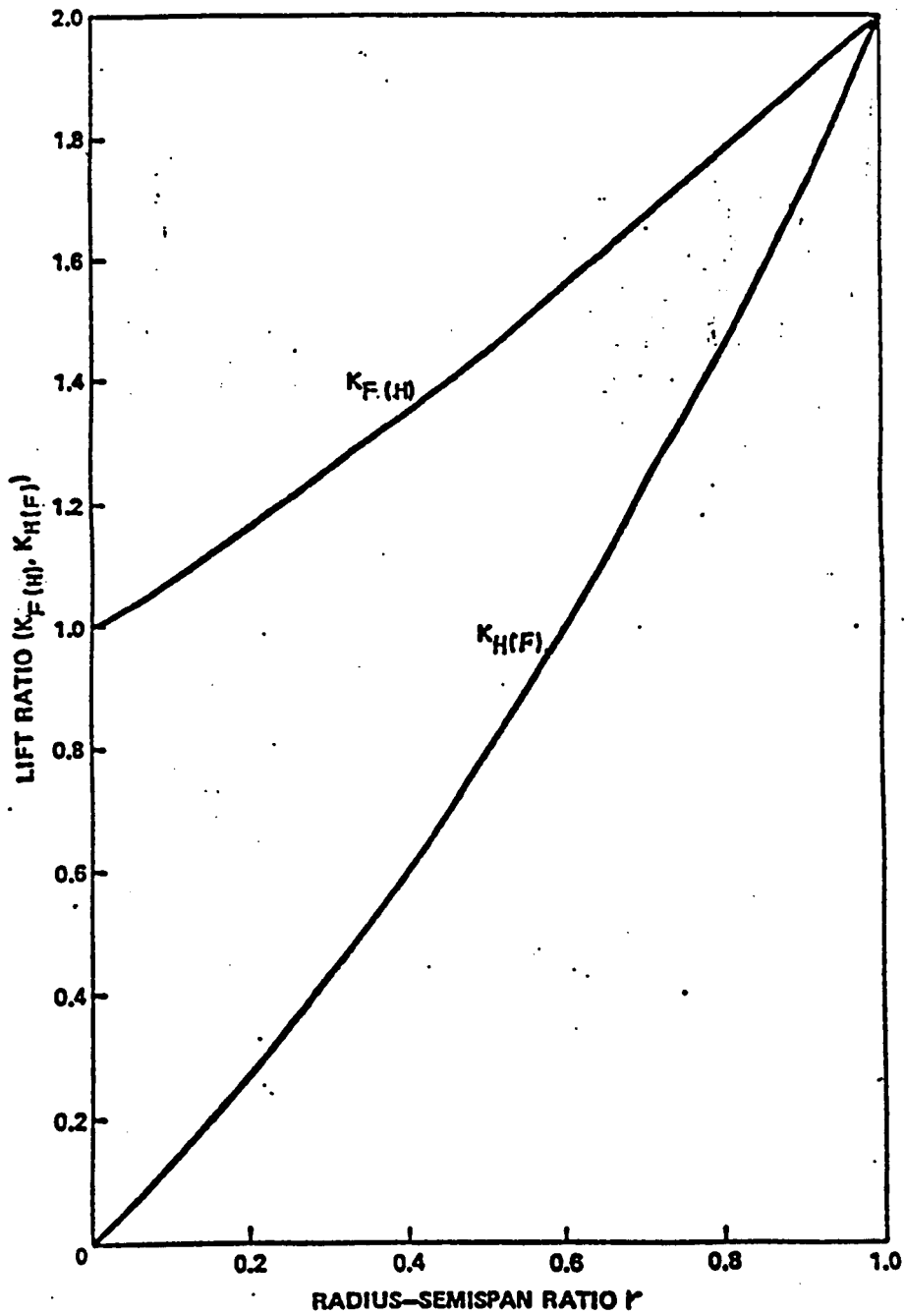
Fig. 3.1

Ae is the effect aspect ratio

C_{DF} is the cross flow-drag coefficient

Ω is the sweep angle of quarter-chord line

for $\Omega = 0.0$ (without sweep angle)

$$\left(\frac{\partial C_L}{\partial \alpha}\right)_o = \frac{1.8\pi Ae}{1.8 + \sqrt{Ae^2 + 4}} \quad \text{per radian} \tag{3-19}$$

2.7 Hull Body-Fin Interaction (According to Slender Body Theory [71,85])

$$\frac{\partial C_L}{\partial \alpha} = [K_{F(H)} + K_{H(F)}]\left(\frac{\partial C_L}{\partial \alpha}\right)_o \tag{3-20}$$

where $K_{F(H)} = \dfrac{\left(\dfrac{\partial C_L}{\partial \alpha}\right)_{F(H)}}{\left(\dfrac{\partial C_L}{\partial \alpha}\right)_o}$ \hfill (3-21a)

and $K_{H(F)} = \dfrac{\left(\dfrac{\partial C_L}{\partial \alpha}\right)_{H(F)}}{\left(\dfrac{\partial C_L}{\partial \alpha}\right)_o}$ \hfill (3-21b)

where H(F) is the lift on the hull induced by the fin and F(H) is the lift on the fin induced by the hull.
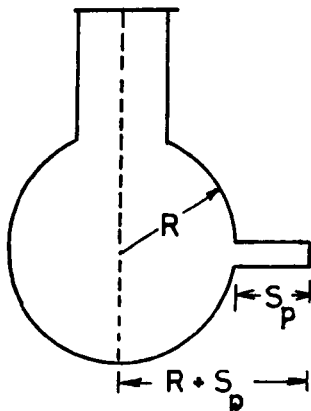
Fig. 3.2

The values of $K_{F(H)}$ and $K_{H(F)}$ are shown in fig. 3.1 and also can be expressed in terms of the ratio $r = R/R+S_p$ where R is the radius of the body to which the fin is attached and $(R+S_p)$ is the transverse distance from the hull body axis to the tip of the fin, as shown in fig. 3.2

Thus

$$K_{F(H)} = \frac{2}{\pi(1-r)^2}[(1+r^4)\{\tfrac{1}{2}\tan^{-1}\tfrac{1}{2}(\tfrac{1}{r}-r)+\tfrac{\pi}{4}\}$$

(3-22a)

$$-r^2\{(\tfrac{1}{r}-r)+2\tan^{-1}r\}]$$

and

$$K_{H(F)} = \frac{2}{(1-r^2)}\Big[(1-r^2)^2-\tfrac{2}{\pi}[(1+r^4)\{\tfrac{1}{2}\tan^{-1}\tfrac{1}{2}(\tfrac{1}{r}-r)+\tfrac{\pi}{4}\}$$

(3-22b)

$$-r^2\{(\tfrac{1}{r}-r)+2\tan^{-1}r\}]\Big]$$

Also the effect aspect ratio is:-

$$Ae = [(R+S_p)-\frac{R^2}{(R+S_p)}]/C_h$$

(3-23)

where S_p is the span of the fin

C_h is the chord of the fin.

3.   THE DESCRIPTION OF THE COMPUTER PROGRAM

The main program FSIZE is for the determination of the fin size. The eigenvalues from the heave-pitch coupled equations of motion were solved for the frequency dependent added mass coefficients by the subroutine AVMCOF where the approximate coefficient formulae were developed, based on a curve-fitting technique which was presented in Chapter 2. The damping coefficients are taken from the subroutine ADAMP.

The lift-curve slope coefficients ($C_{L\alpha}$) with the correction for the fin-body section effect for a given chord and span of fin geometry, as shown in section 2.7 of this chapter, are derived from the routine CCLAF. The motion equations are solved by a numerical NAG

routine built into JYNAG, containing C02AEF, X01AAF, X02AAF, C02AEZ, P01AAF, X02ACF, P0TAAZ, X01AAZ, X04AAF, DFLOAT, and S02ADF.

The input used in the program is listed as:-

GML   The longitudinal metacentric height (m)

WD   The weight of SWATH ship (Kg)

SL   The total length of SWATH ship (m)

VS1   The expected maximum speed to run (ms^{-1})

DISP   The displacement (volume) of the ship (m^3)

THICK   The maximum thickness of the design fin (m)

WI   The waterplane moment of inertia (m^3)

BG   The distance between CG and CB (m)

R( ) array   The radius of circular hull section (m)

TY( ) array The half-strut thickness (m)

SSAM   The total mass of SWATH ship (kg)

SI55   The mass moment of inertia (Kg m^2)

AWP   The waterplane area (m^2)

H   The draft (m)

FWAVE   The wave frequency (Hz)

AWAVE   The wave amplitude (m)

VS   The speed in ms^{-1}

4.   <u>NUMERICAL RESULTS</u>

The above theory was applied to the SWATH designs in this study with the computer program FSIZE on the VAX 11/730 computer at the University of Glasgow. The results of the calculations are presented in Tables 3.2 to 3.7 and figs. 3.4 to 3.8.

The relation between the real, imaginary stability roots and the damped and undamped natural frequency are shown in a vector diagram, fig. 3.3. This diagram expresses the physical meaning of figs. 3.4 to 3.8 for different speeds.

In Table 3.2, the column FIN SIZE, FWD means forward fin, AFT means afterwards fin, <u>0.0 FWD</u> means afterwards fin only and, for the FWD and AFT fins combination case, the total fin area was kept twice that of the 1.0 fin but divided into FWD and AFT fins of the same aspect ratio. In figs.3.4 to 3.8, the circle mark means AFT fin only and the asterisk, *, means the combination of FWD and AFT fins. The number beside the asterisk indicates the AFT fin size. The FWD fin size is two minus that number. For example, <u>*1.8</u> means 1.8 AFT fin size and 0.2 FWD fin size and <u>⊙ 0.6</u> means AFT fin only with area 0.6 times inertia fin size.

Tables 3.2 to 3.7 shows the damping ratio, natural period and half decay time for both heave and pitch mode for speeds of 2.0 ms^{-1}, 2.5ms^{-1} and 3.0ms^{-1}.

The results show that the roots of the heave mode σ_1 and σ_2 are in complex conjugate form for all the cases of calculation and, as shown in figs. 3.4 to 3.8, the real roots of heave are smaller than in
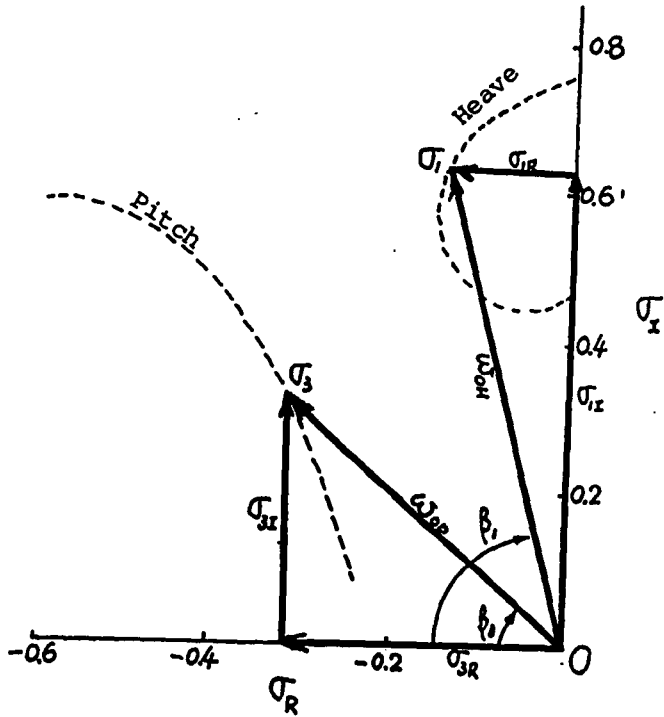
VECTOR DIAGRAM

STABILITY ROOT PLANE

$$\gamma_H = \cos\beta_1$$

$$\gamma_P = \cos\beta_3$$

$$\sigma_{1R} = \omega_{OH} \cdot \gamma_H$$

$$\sigma_{1I} = \omega_{OH}\sqrt{1 - \gamma_H^2} \quad \text{damped natural frequency of Heave mode}$$

$$\omega_{OH}^2 = \sigma_1\sigma_2 = |\sigma_1|^2 = |\sigma_2|^2 \quad \text{undamped natural frequency of Heave}$$

Fig. 3.3

pitch mode ($\sigma_{1R} < \sigma_{3R}$) and the imaginary roots of heave are greater than in pitch mode ($\sigma_{1I} > \sigma_{3I}$). This shows that heave mode has smaller natural period and damping ratio but a greater half-decay time than in pitch mode.

For the case of AFT fin only, the size from 0.8 to 2.0 appears to provide the necessary stability in pitch. The greater the fin size, the greater the absolute value of the real root for pitch but this is not true for the heave case.

At about 1.4 fin size, $|\sigma_R|$ has a maximum value and decreases as the fin size increases or decreases. For the AFT fin only, this 1.4 fin size provides the maximum damping ratio between the speeds 2.0ms^{-1} and 3.0ms^{-1}. By using the FWD and AFT fin combination, the pitch stability begins to decrease with the AFT fins less than 1.5 as the speed increases. Therefore, for the AFT fin only, a fin size of 1.4 was selected. For FWD and AFT fin combination, an AFT fin of 1.5 and a FWD fin of 0.5 was found to be the best choice.

STABILITY CHARACTERISTICS OF SWATH 1

Fin Size		Mode	Natural Period (sec)		
FWD	AFT	Heave(H) Pitch(P)	2.0m/sec	2.5m/sec	3.0m/sec
0.0	0.0	H	1.605	1.598	1.595
		P	—	—	—
0.0	0.2	H	1.621	1.623	1.633
		P	18.040	—	—
0.0	0.4	H	1.648	1.660	1.683
		P	6.932	—	—
0.0	0.6	H	1.684	1.709	1.750
		P	5.239	14.347	—
0.0	0.8	H	1.728	1.772	1.839
		P	4.418	6.543	26.237
0.0	1.0	H	1.782	1.853	1.958
		P	3.893	4.874	6.548
0.0	1.2	H	1.848	1.961	2.130
		P	3.506	3.999	4.566
0.0	1.4	H	1.932	2.125	2.416
		P	3.194	3.369	3.525
0.0	1.6	H	2.031	2.674	2.875
		P	2.939	2.528	2.868
0.0	1.8	H	2.083	2.374	2.582
		P	2.838	2.887	3.329
0.0	2.0	H	2.063	2.258	2.413
		P	2.894	3.133	3.896
0.1	1.9	H	2.064	2.521	2.833
		P	3.168	3.076	3.721
0.2	1.8	H	1.995	2.314	3.109
		P	3.678	3.967	3.953
0.3	1.7	H	1.944	2.178	2.649
		P	4.354	5.549	7.624
0.5	1.5	H	1.891	2.065	2.381
		P	7.220	—	—
0.7	1.3	H	1.872	2.025	2.291
		P	—	—	—
0.9	1.1	H	1.872	2.018	2.266
		P	—	—	—

TABLE 3-2

STABILITY CHARACTERISTICS OF SWATH 2

Fin Size		Mode	Natural Period (sec)		
FWD	AFT	Heave(H) Pitch(P)	2.0m/sec	2.5m/sec	3.0m/sec
0.0	0.0	H	1.675	1.671	1.672
		P	27.802	—	—
0.0	0.2	H	1.688	1.691	1.701
		P	6.472	—	—
0.0	0.4	H	1.710	1.721	1.742
		P	5.034	—	—
0.0	0.6	H	1.739	1.760	1.795
		P	4.335	8.244	—
0.0	0.8	H	1.775	1.810	1.864
		P	3.886	5.673	19.063
0.0	1.0	H	1.820	1.874	1.952
		P	3.555	4.593	6.784
0.0	1.2	H	1.874	1.955	2.072
		P	3.290	3.935	4.878
0.0	1.4	H	1.940	2.067	2.253
		P	3.064	3.443	3.877
0.0	1.6	H	2.015	2.252	2.601
		P	2.872	2.988	3.093
0.0	1.8	H	2.068	2.364	2.656
		P	2.768	2.801	3.021
0.0	2.0	H	2.065	2.273	2.476
		P	2.778	2.951	3.352
0.1	1.9	H	2.043	2.352	2.942
		P	3.048	3.166	3.190
0.2	1.8	H	1.988	2.187	2.543
		P	3.437	4.025	4.732
0.3	1.7	H	1.950	2.106	2.369
		P	3.900	5.240	8.780
0.5	1.5	H	1.909	2.032	2.232
		P	5.338	—	—
0.7	1.3	H	1.895	2.006	2.183
		P	10.805	—	—
0.9	1.1	H	1.897	2.004	2.171
		P	—	—	—

TABLE 3-3

Fin Size		Mode	Damping Ratio		
FWD	AFT	Heave(H) Pitch(P)	2.0m/sec	2.5m/sec	3.0m/sec
0.0	0.0	H	0.099	0.123	0.146
		P	—	—	—
0.0	0.2	H	0.160	0.201	0.242
		P	—	—	—
0.0	0.4	H	0.201	0.255	0.308
		P	0.407	—	—
0.0	0.6	H	0.286	0.301	0.366
		P	0.385	0.760	—
0.0	0.8	H	0.265	0.342	0.419
		P	0.388	0.535	0.930
0.0	1.0	H	0.290	0.379	0.471
		P	0.399	0.483	0.591
0.0	1.2	H	0.310	0.415	0.526
		P	0.416	0.465	0.506
0.0	1.4	H	0.322	0.451	0.597
		P	0.439	0.459	0.447
0.0	1.6	H	0.316	0.420	0.355
		P	0.480	0.524	0.705
0.0	1.8	H	0.273	0.296	0.279
		P	0.551	0.665	0.795
0.0	2.0	H	0.229	0.241	0.232
		P	0.619	0.739	0.860
0.1	1.9	H	0.352	0.437	0.411
		P	0.585	0.669	0.828
0.2	1.8	H	0.404	0.550	0.745
		P	0.598	0.650	0.643
0.3	1.7	H	0.429	0.563	0.708
		P	0.639	0.741	0.841
0.5	1.5	H	0.457	0.580	0.704
		P	0.791	1.182	4.736
0.7	1.3	H	0.473	0.591	0.708
		P	1.211	—	—
0.9	1.1	H	0.480	0.597	0.711
		P	—	—	—

TABLE 3-4

Fin Size		Mode	Damping Ratio		
FWD	AFT	Heave(H) Pitch(P)	2.0m/sec	2.5m/sec	3.0m/sec
0.0	0.0	H	0.110	0.134	0.157
		P	0.678	—	—
0.0	0.2	H	0.163	0.201	0.238
		P	0.334	—	—
0.0	0.4	H	0.198	0.246	0.294
		P	0.334	1.383	—
0.0	0.6	H	0.228	0.286	0.343
		P	0.345	0.591	—
0.0	0.8	H	0.253	0.320	0.387
		P	0.359	0.505	0.894
0.0	1.0	H	0.275	0.352	0.427
		P	0.376	0.477	0.629
0.0	1.2	H	0.292	0.381	0.471
		P	0.395	0.468	0.551
0.0	1.4	H	0.303	0.407	0.517
		P	0.418	0.469	0.510
0.0	1.6	H	0.310	0.427	0.454
		P	0.453	0.480	0.593
0.0	1.8	H	0.274	0.340	0.348
		P	0.509	0.590	0.708
0.0	2.0	H	0.239	0.277	0.287
		P	0.568	0.672	0.782
0.1	1.9	H	0.335	0.453	0.501
		P	0.546	0.604	0.714
0.2	1.8	H	0.374	0.494	0.625
		P	0.560	0.642	0.713
0.3	1.7	H	0.395	0.508	0.624
		P	0.592	0.718	0.871
0.5	1.5	H	0.419	0.525	0.631
		P	0.693	1.023	2.685
0.7	1.3	H	0.431	0.535	0.637
		P	0.887	—	—
0.9	1.1	H	0.437	0.538	0.638
		P	1.469		

TABLE 3-5

STABILITY CHARACTERISTICS OF SWATH 1

Fin Size		Mode	Half Decay Time (sec)		
FWD	AFT	Heave(H) Pitch(P)	2.0m/sec	2.5m/sec	3.0m/sec
0.0	0.0	H	1.783	1.428	1.191
		P	0.627	0.379	0.310
0.0	0.2	H	1.102	0.872	0.722
		P	2.316	0.467	0.354
0.0	0.4	H	0.884	0.695	0.573
		P	1.717	0.590	0.405
0.0	0.6	H	0.766	0.598	0.492
		P	1.384	1.354	0.496
0.0	0.8	H	0.694	0.538	0.440
		P	1.158	1.139	1.146
0.0	1.0	H	0.649	0.499	0.405
		P	0.987	0.974	0.986
0.0	1.2	H	0.626	0.474	0.380
		P	0.847	0.839	0.859
0.0	1.4	H	0.627	0.463	0.358
		P	0.720	0.720	0.779
0.0	1.6	H	0.673	0.637	0.835
		P	0.593	0.454	0.318
0.0	1.8	H	0.809	0.845	0.980
		P	0.474	0.357	0.281
0.0	2.0	H	0.968	1.003	1.117
		P	0.405	0.315	0.256
0.1	1.9	H	0.605	0.572	0.624
		P	0.485	0.377	0.277
0.2	1.8	H	0.478	0.387	0.307
		P	0.544	0.511	0.519
0.3	1.7	H	0.462	0.353	0.291
		P	0.578	0.555	0.541
0.5	1.5	H	0.406	0.320	0.265
		P	0.616	0.395	0.309
0.7	1.3	H	0.385	0.305	0.252
		P	0.465	0.288	0.298
0.9	1.1	H	0.377	0.299	0.247
		P	0.301	0.245	0.228

TABLE 3-6

STABILITY CHARACTERISTICS OF SWATH 2

Fin Size		Mode	Half Decay Time (sec)		
FWD	AFT	Heave(H) Pitch(P)	2.0m/sec	2.5m/sec	3.0m/sec
0.0	0.0	H	1.665	1.368	1.162
		P	3.324	0.417	0.317
0.0	0.2	H	1.128	0.911	0.766
		P	2.016	0.528	0.360
0.0	0.4	H	0.932	0.746	0.624
		P	1.569	0.877	0.412
0.0	0.6	H	0.820	0.652	0.543
		P	1.302	1.243	0.506
0.0	0.8	H	0.748	0.591	0.489
		P	1.114	1.070	1.056
0.0	1.0	H	0.703	0.550	0.453
		P	0.968	0.934	0.925
0.0	1.2	H	0.677	0.524	0.428
		P	0.845	0.819	0.815
0.0	1.4	H	0.673	0.512	0.411
		P	0.734	0.714	0.721
0.0	1.6	H	0.705	0.626	0.390
		P	0.624	0.602	0.671
0.0	1.8	H	0.801	0.721	0.788
		P	0.517	0.423	0.332
0.0	2.0	H	0.926	0.871	0.912
		P	0.444	0.359	0.295
0.1	1.9	H	0.635	0.511	0.560
		P	0.516	0.461	0.345
0.2	1.8	H	0.543	0.425	0.350
		P	0.561	0.530	0.514
0.3	1.7	H	0.500	0.394	0.327
		P	0.586	0.560	0.547
0.5	1.5	H	0.457	0.363	0.303
		P	0.612	0.489	0.307
0.7	1.3	H	0.437	0.350	0.292
		P	0.621	0.301	0.253
0.9	1.1	H	0.431	0.346	0.289
		P	0.358	0.252	0.223

TABLE 3-7

STABILITY ROOTS FOR VARIOUS FIN SIZE
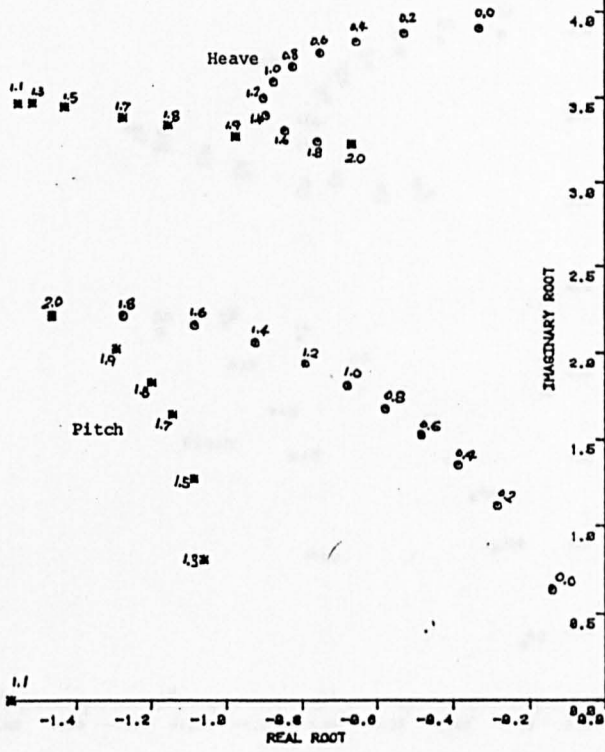
FOR SWATH[1] AT 1.7 M/SEC

STABILITY ROOTS FOR VARIOUS FIN SIZE

FOR SWATH[2] AT 1.7 M/SEC

Fig.3.4

Fig. 3.5

Fig. 3.6

168.

Fig.3.7
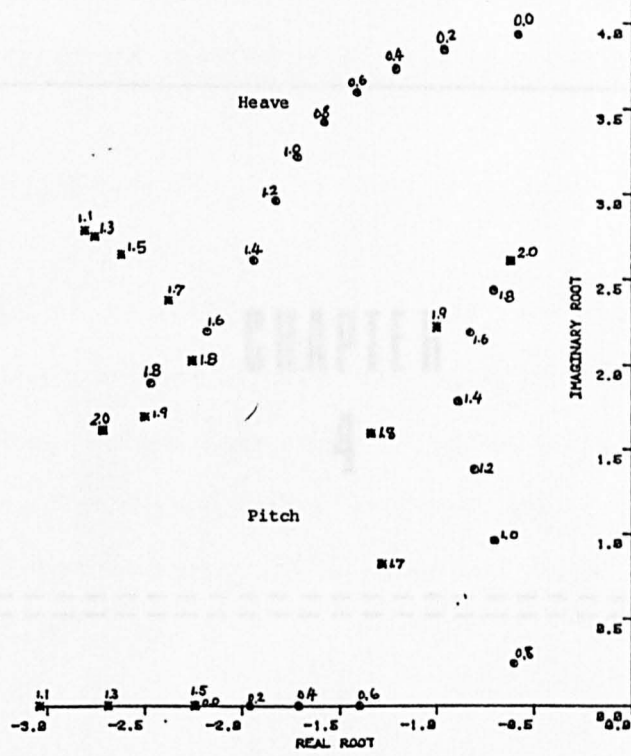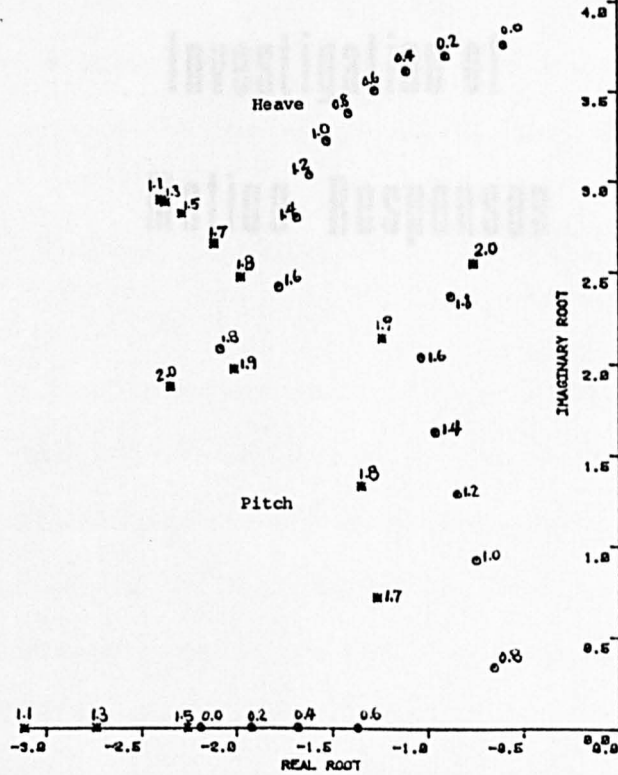
Fig. 3.8

CHAPTER
4

Experimental

Investigation of

Motion Responses

CHAPTER 4

EXPERIMENTAL INVESTIGATION OF MOTION RESPONSES

1. ## INTRODUCTION

In order to investigate the motion characteristics and to compare the calculation procedures developed for the prediction of the vertical plane motion responses, a series of model experiments were undertaken. The measurements included the trim and sinkage, heave and pitch motion responses at zero and forward speeds, both with and without aft fins.

The SWATH model was made in a simple geometric shape with twin circular hulls and two aerofoil type struts per hull. In the first stage the experiments were carried out in the head sea case with a range of forward speeds at $0.5ms^{-1}$, $1.0ms^{-1}$, $1.5ms^{-1}$ and $2.0ms^{-1}$, the corresponding Froude numbers being 0.13, 0.26, 0.39, and 0.52, respectively. (The Froude numbers are based on the hull length.)

In addition to the calm water tests, further vertical motion experiments were performed in a range of regular wave frequencies from 0.5Hz to 1.1Hz, which covers the wave length ratio, λ/L from 1 to 6. In order to identify the interference effects arising from the wavemaker and tank wall effects, the wave displacements were measured at three positions across the tank during the motion experiments. The model was also tested by altering the angle of attack of the aft fixed fins. The fixed angles were 0°, $\pm 2^{\circ}$ and $\pm 4^{\circ}$. The results obtained from the bare hull and the hull with fins were compared.

The results show that the SWATH model behaved very well in the head sea regular waves except at the low frequency range where the natural frequencies of heave and pitch synchronise with the waves. However, the resonance frequency range usually occurs in following seas. Having identified the importance of the motion response in following seas, extensive tests were carried out using the model with fins in following seas.

All the tests were carried out in the 76m x 4.6m x 2.4m model test tank at the University of Glasgow. The measured values from the tests were plotted, as well as tabulated, for detailed comparison between the theoretical predictions and the measurements. This tabulated data could also be utilised in future studies.

2.   DESCRIPTION OF THE MODEL

The SWATH model used during the tests was a simple geometric shape with a twin circular hull with two airfoil struts per hull. The hydrostatic data of the model is shown in Table 4.1. The twin strut type has a longer natural period of heave and roll compared with single strut type because it has nearly one-half the waterplane area of the single strut. The primary reason for choosing this particular design was because it was intended to be the prototype for a large SWATH vessel where a single strut would have been inappropriate from longitudinal stability considerations. It also provided a reasonably simple shape for theoretical analysis and calculations. (The computer program can deal with more general forms.)

The model was ballasted to a level draught which was double the diameter of the hull by using lead shot placed in the centre of

Weight	21.8Kg
Hull Length	1.5m
Strut Length	0.4m
Draft (2 x D)	0.1784m
Hull Diameter (D)	0.0892m
Hull spacing between centres of the hulls	0.855m
Waterplane Area (A_{wp})	$0.054m^2$
Longitudinal distance from nose of hull to forward strut end	0.155m
Longitudinal distance from tail of hull to rear strut end	0.2m
KM_L	0.429m
KM_T	0.512m
KG	0.1763m
VCB	0.064m
LCG	0.7275m (no fin) from Nose 0.7354m (with aft fin) from Nose
GM_L	0.2528m
GM_T	0.3278m
Aft fin position	1.25m (from Nose) 0.524m (from LCG)
Fin Chord	0.0935m
Fin Span	0.1124m

Table 4.1 Hydrostatic Data of the SWATH Model

each strut. At zero speed tests in waves the model was moored as shown in fig. 4.1 During the forward speed test the model was towed from the front struts at the still water draught of 0.1784m which is almost the same height as the vertical centre of gravity (= 0.1763m). The centre line of the model was towed in the centre of the tank.

In order to prevent yawing and rolling effects due to any asymmetry in the model or the wave system, the model was guided by four circular bars to maintain the course. These provided negligible restraint to vertical movement. The stiffness of the towing arrangement was progressively changed during the experiment so that the model surged about approximately the same mean position throughout.

Tests were carried out first for the bare hull without fin and then with fins fitted aft as in fig. 4.2a. Figure 4.2b shows the tests in a wave frequency of 0.8Hz at three different speeds. The size of the fin was calculated as shown in Reference [68]. Its offsets are shown in fig. 4.3. The tests were conducted initially with the fins in the zero-angle of attack position, ie the fin chord line parallel to the main hull axis and then changed to $\pm 2.0^{\circ}$ and $\pm 4.0^{\circ}$. A positive fin angle is defined as the case when the trailing edge is upward.

3.   **INSTRUMENTATION**

For the motion tests, the instrumentation was set to record the profiles of the regular wave trains as well as the heave and pitch motion of the model. The heave and pitch motions of the model were recorded with three gravity type LVDT (Linear Variable Differential Transformer) vertical displacement transducers, as shown in fig. 4.4. They were attached to the carriage with piano wires suspended over a
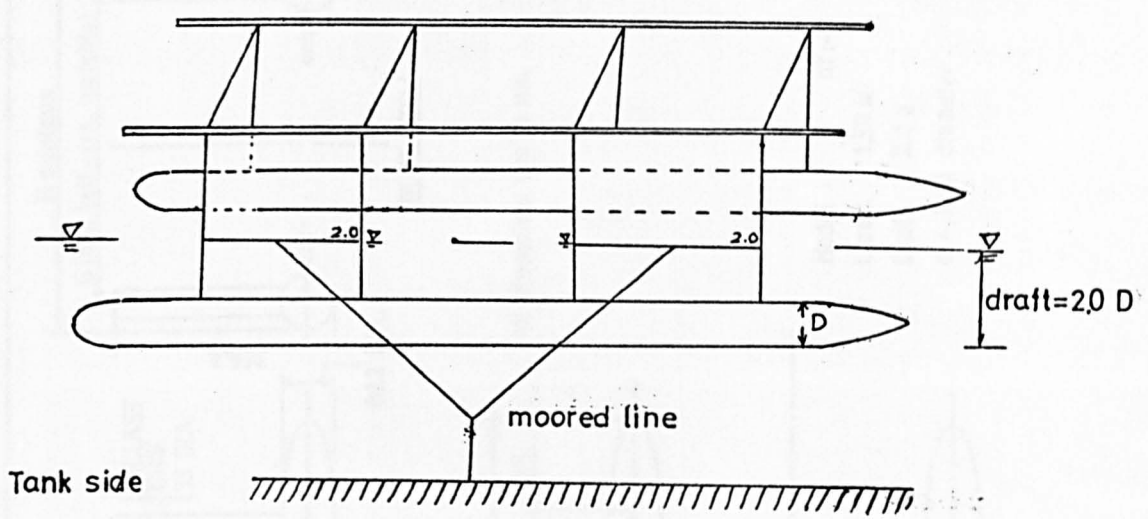
Model in zero speed test
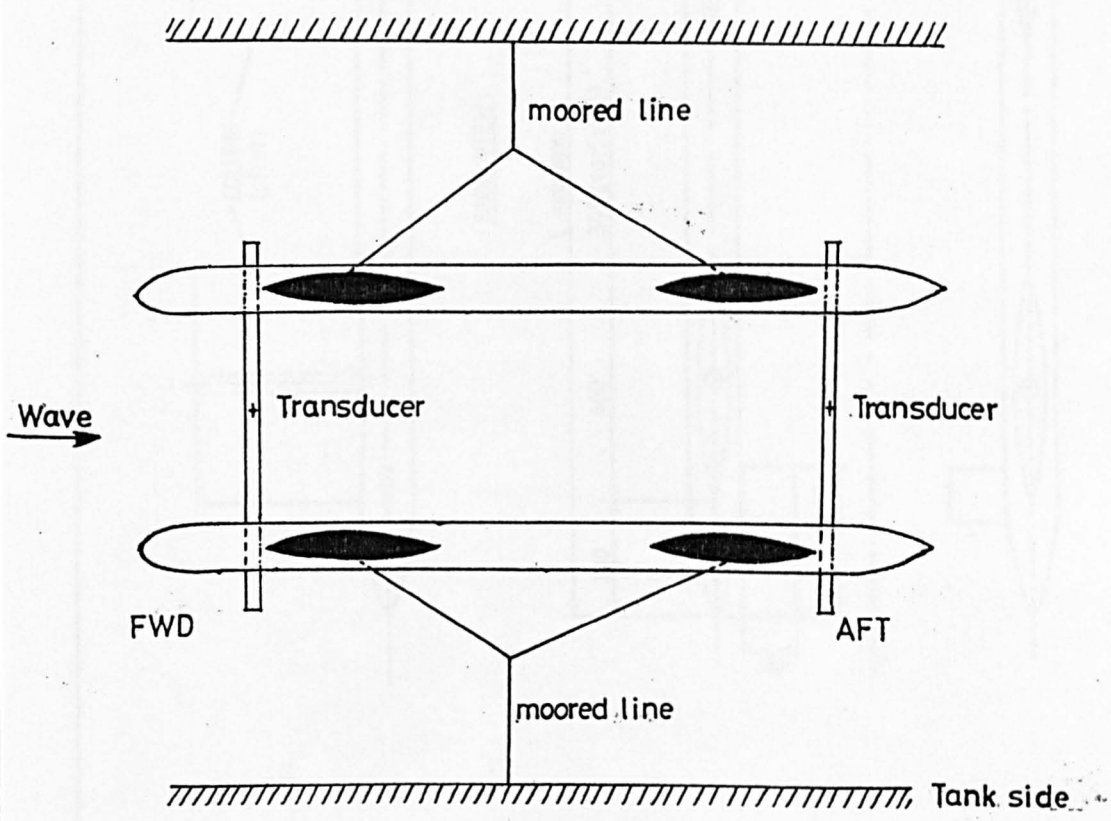
Fig. 4.1 Model Moored Position

COLUMN (strut)

BALLAST TANK 33 DIA.

HULL

364.4

89.2 DIA,

SIDE VIEW

B maximum

B (bet. hull-crs. variable)

FRONT VIEW

L maximum

| 200 | 400 | 345 (variable) | 400 | 155 |

50

100

171   93
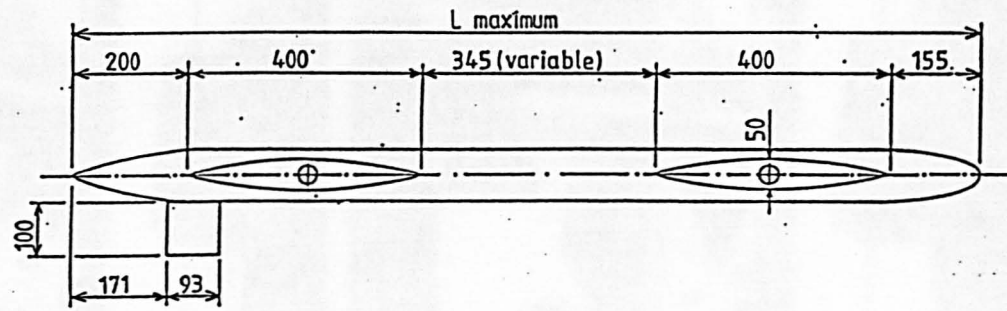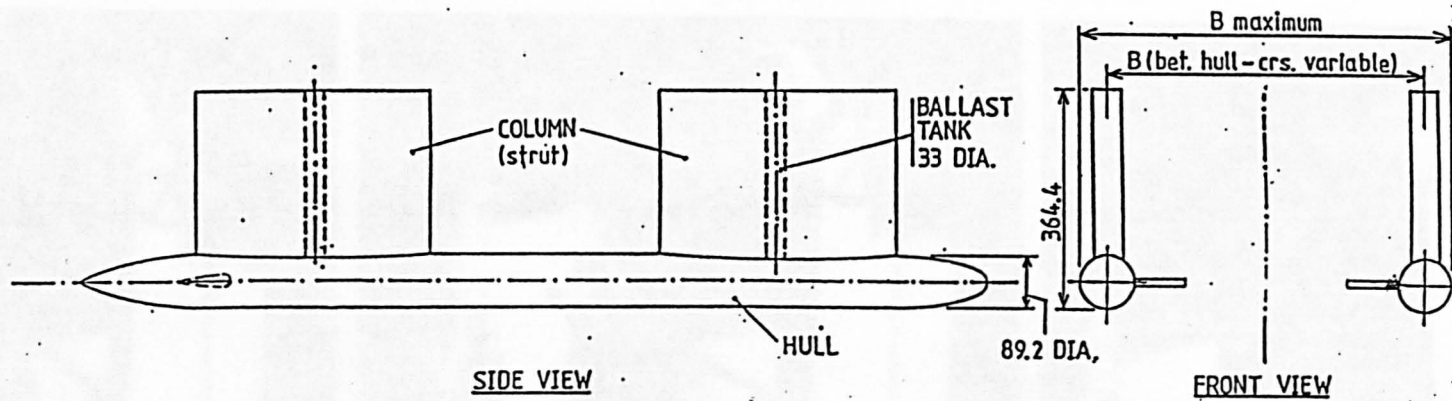
All dimensions are in mm.
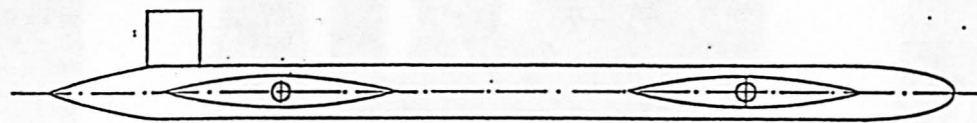
TOP VIEW

Model   at :-
L max.   1.50 m
Draft   2.0 d
d = Hull diameter
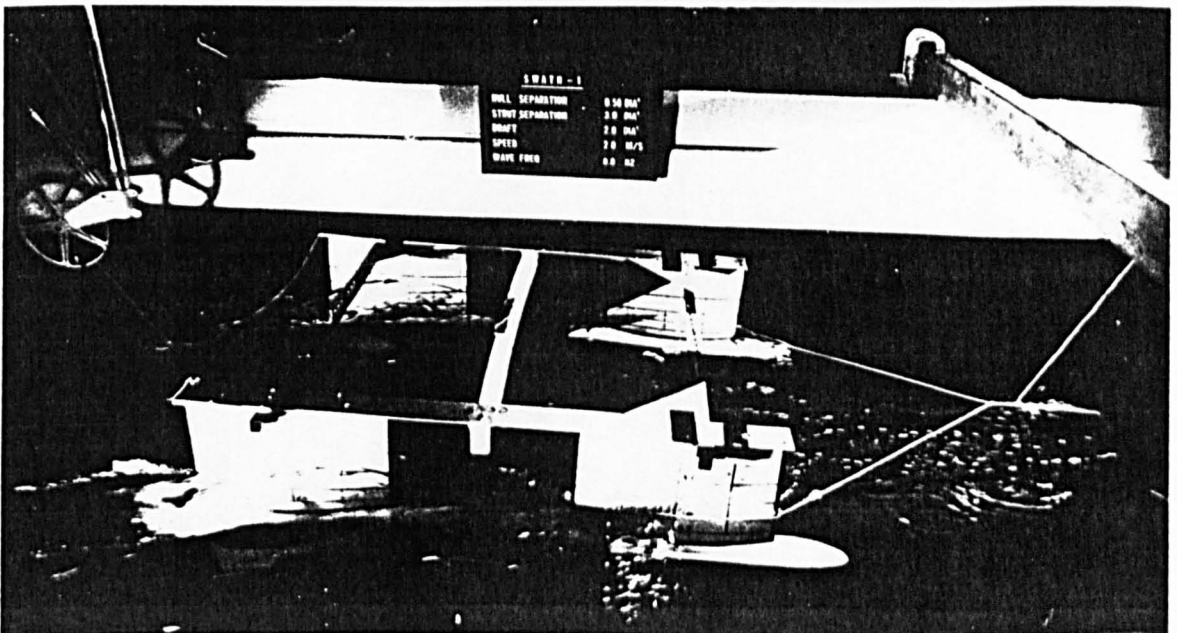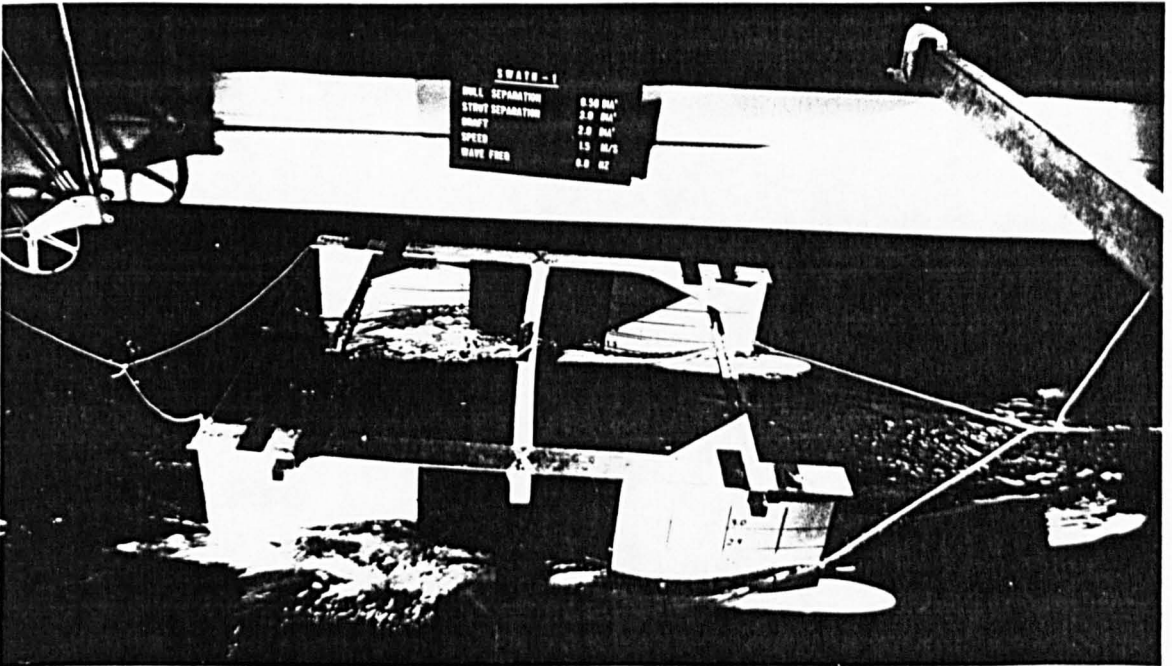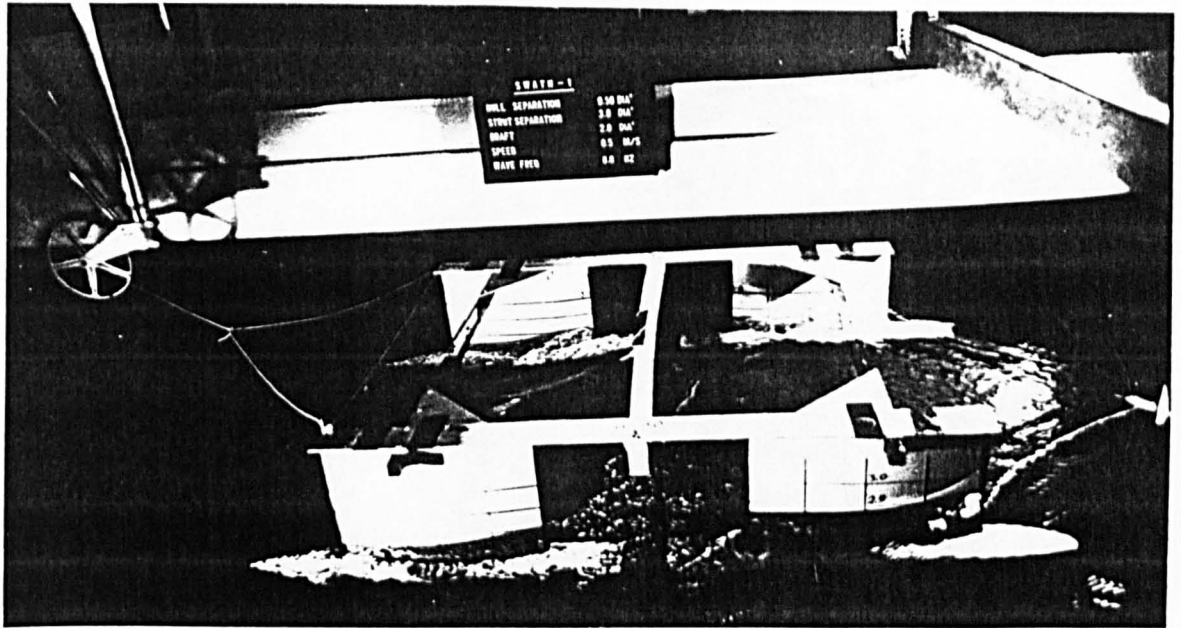
Fig. 4.2a

Fig. 4.2b Head Sea tests in a wave frequency of 0.8hz
at speeds 0.5, 1.5 and 2.0 ms⁻¹
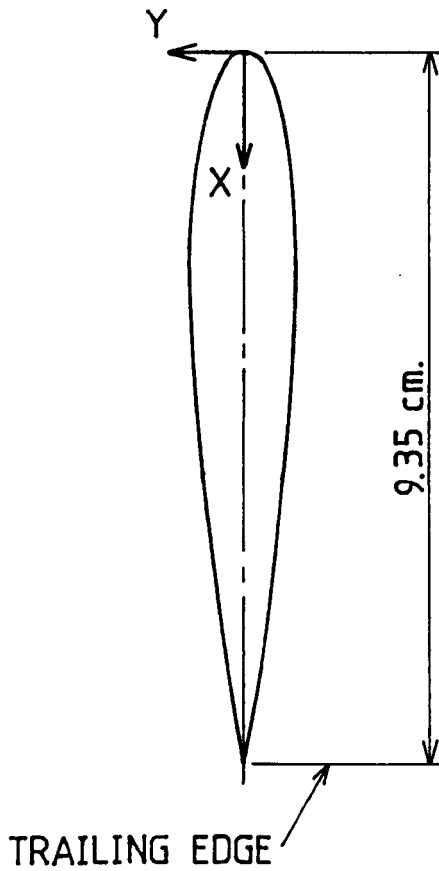
TABLE OF FIN OFFSETS		
CHORD C = 9.35 cm. SPAN S = 11.24 cm.		
$\frac{X}{C}$	X cm.	± Y cm.
0.0	0.000	0.000
0.05	0.467	0.415
0.1	0.935	0.547
0.15	1.870	0.670
0.2	2.338	0.694
0.3	2.805	0.701
0.4	3.740	0.678
0.5	4.675	0.619
0.6	5.610	0.533
0.7	6.545	0.428
0.8	7.480	0.306
0.9	8.415	0.169
1.0	9.350	0.000

OFFSETS FOR SWATH CONTROL SURFACE SECTIONS

Fig. 4.3
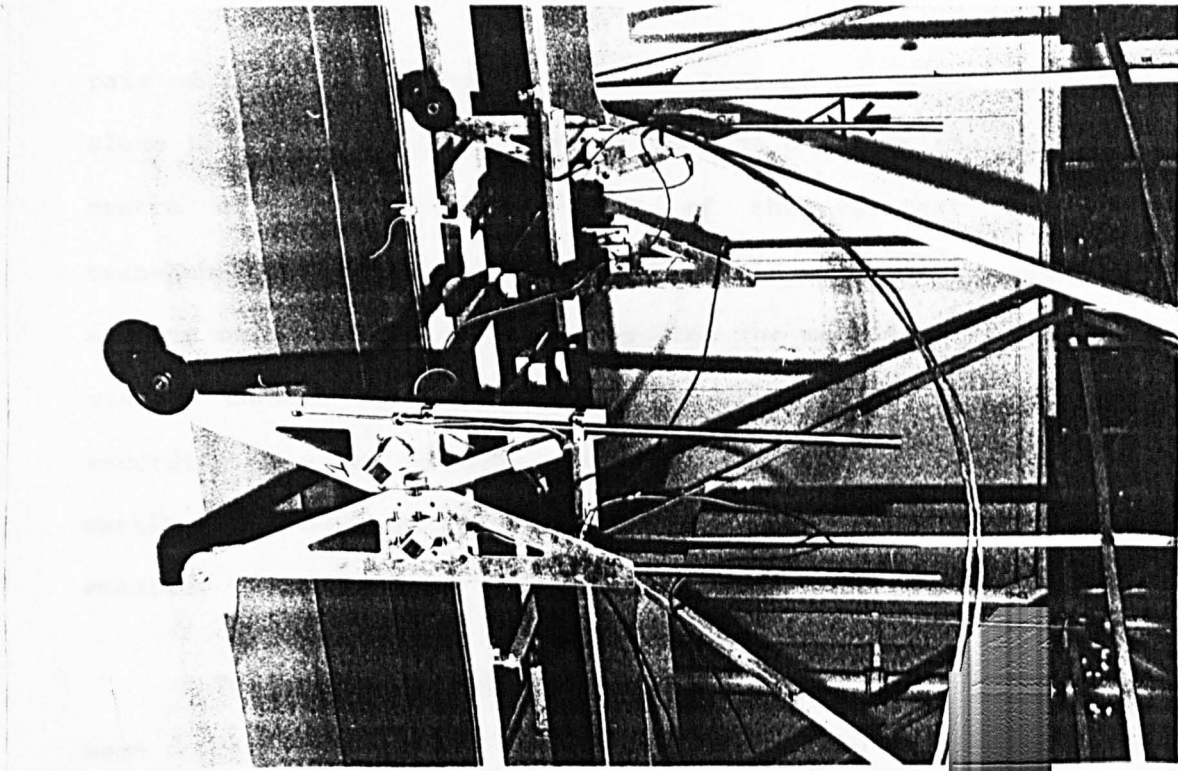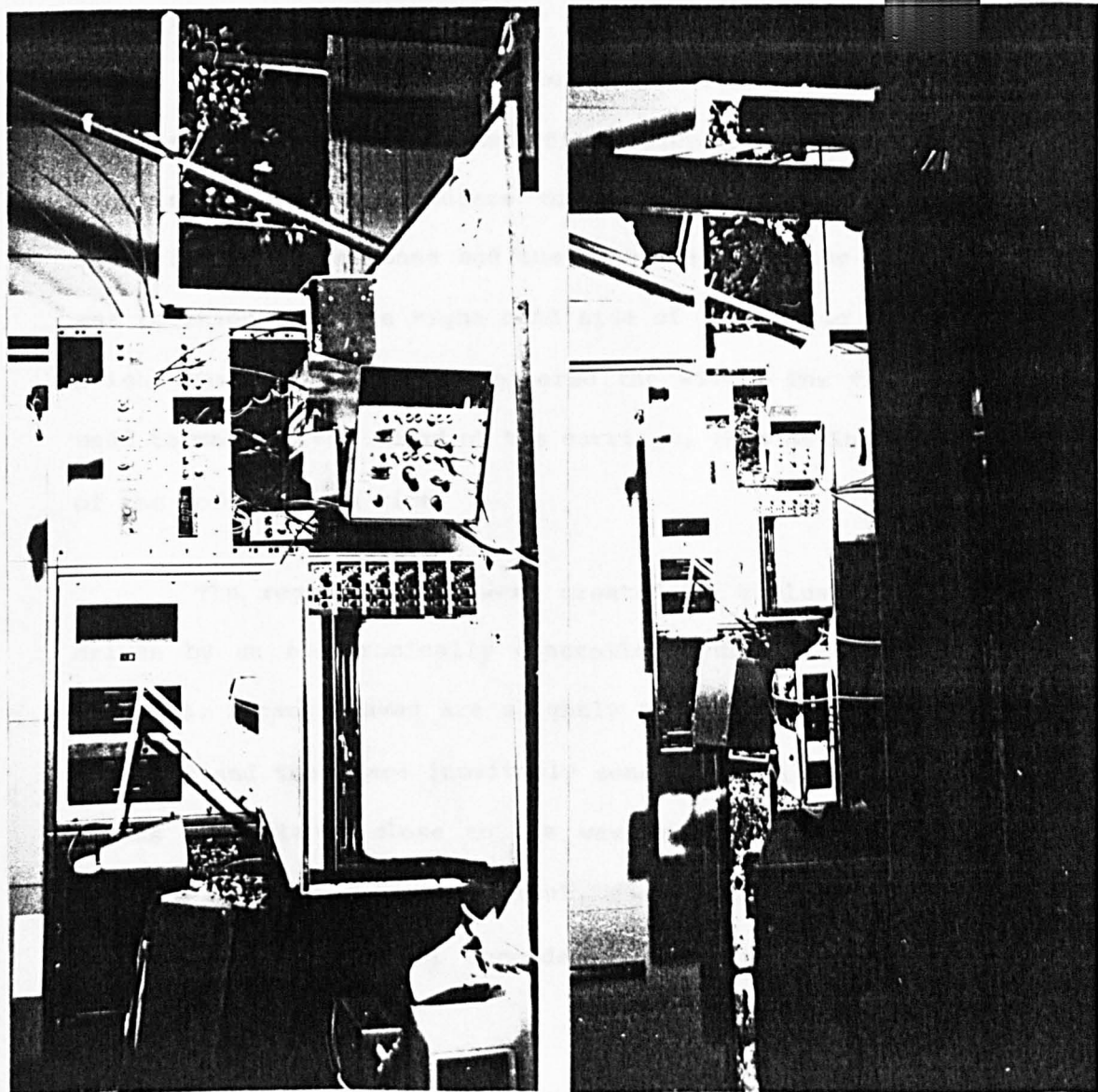
Fig. 4.4   LVDT Pen Recorder

pair of pulleys and connected to the deck of the model, two of them close to the centre of the struts and the other at the longitudinal centre of gravity. The weights of the vertical displacement transducers were balanced in order to avoid any inertia acceleration effects on the transducers arising from the motion of the model. The signals induced as a result of the motion were amplified before recording on a pen recorder, giving a trace of heave, pitch and the vertical displacement at LCG versus time. Figure 4.5 shows a typical example.

To record the model's motion responses, five channels were used on the carriage, one for the signal received from the transducer measuring the vertical motions at the position of the LCG of the model, two for the signals due to the heave and pitch motion responses received from a special amplifier which sums and differences the signals from the transducers to produce an output proportional to heave and pitch response and one connected with the wave probe which was positioned at the right hand side of the bow to measure the wave height where the model encountered the waves. The fifth channel was used to measure the speed of the carriage, thus giving the exact speed of the model versus time.

The regular waves were created by a plunger type wavemaker driven by an electronically controlled hydraulic pump, as shown in fig. 4.6. Because waves are slightly attenuated as they proceed down the tank and there are inevitably some tank wall effects, three wave probes were placed close to the wavemaker and at distances of B/4, B/3, B/2 from the side of the tank. The records from these probes were obtained on a separate recorder. A typical record is shown in fig. 4.7.

Fig. 4.5 A typical example of motion signal records
(at No FIN 0.7hz, 1.5 ms⁻¹)
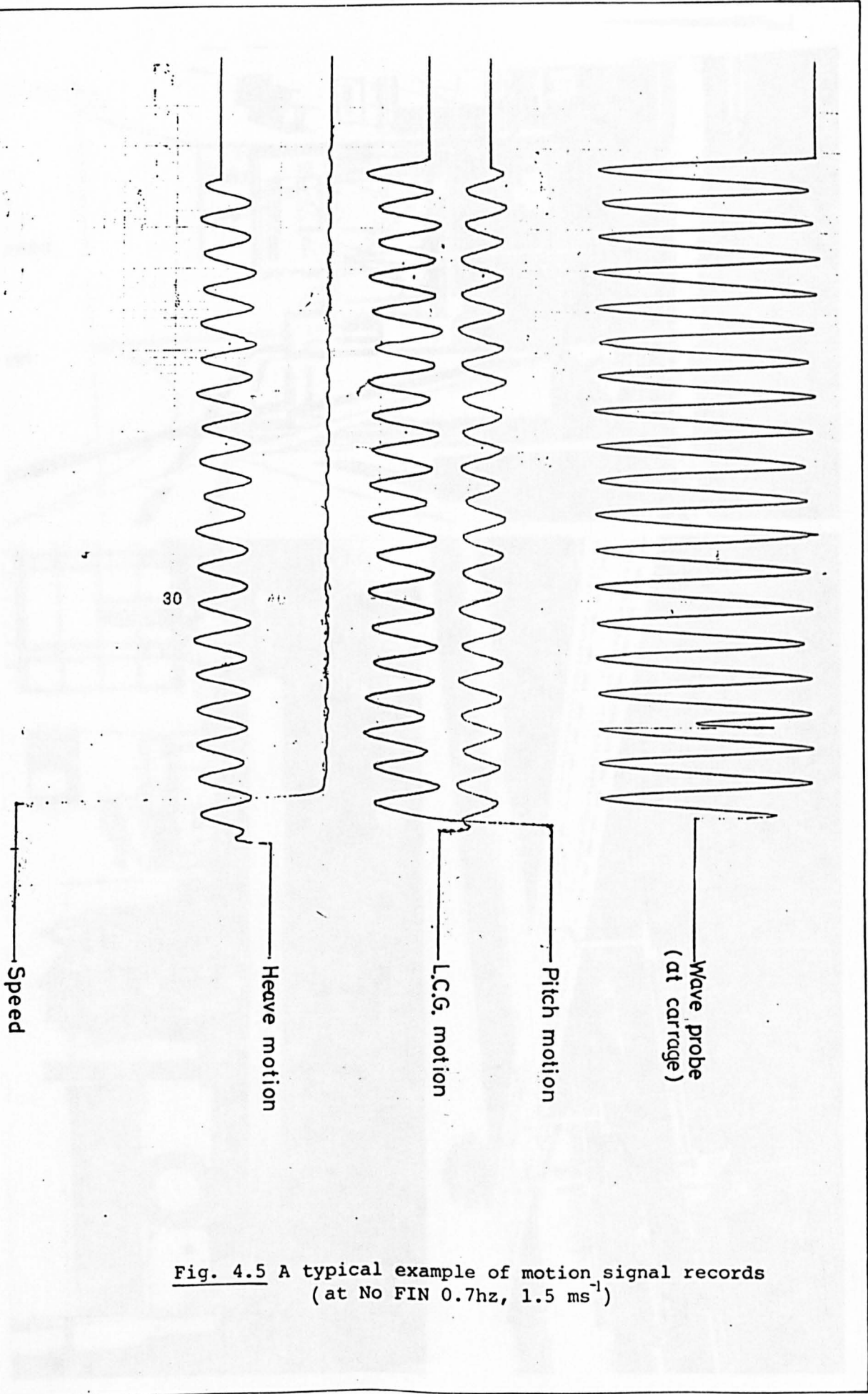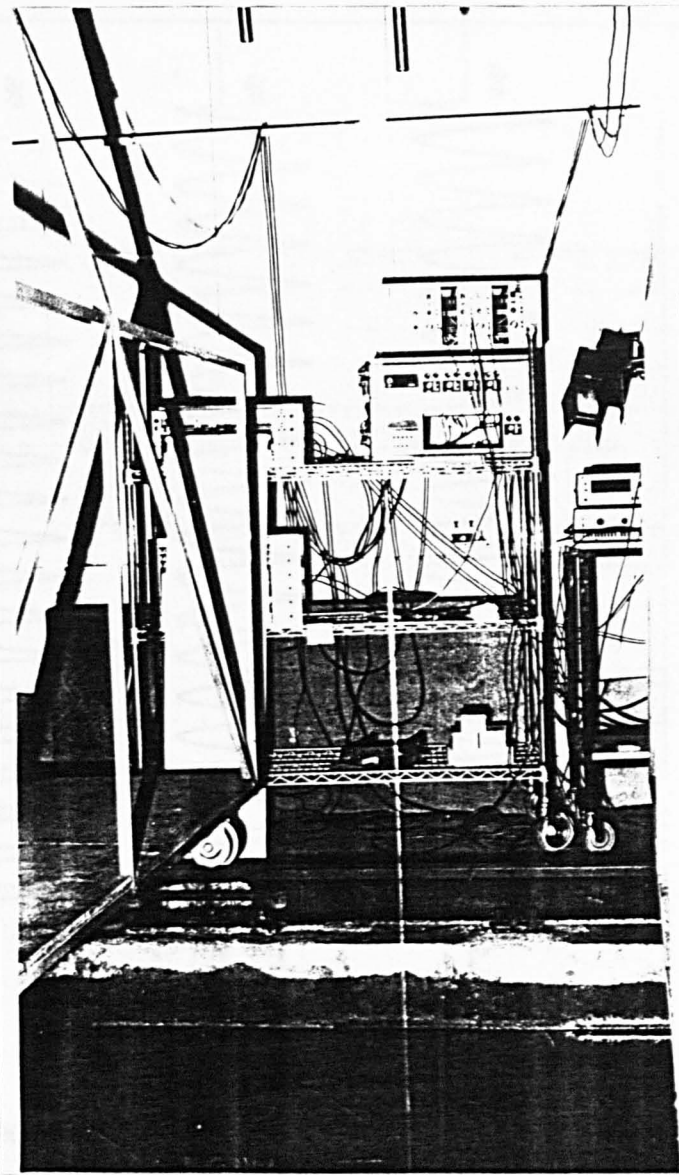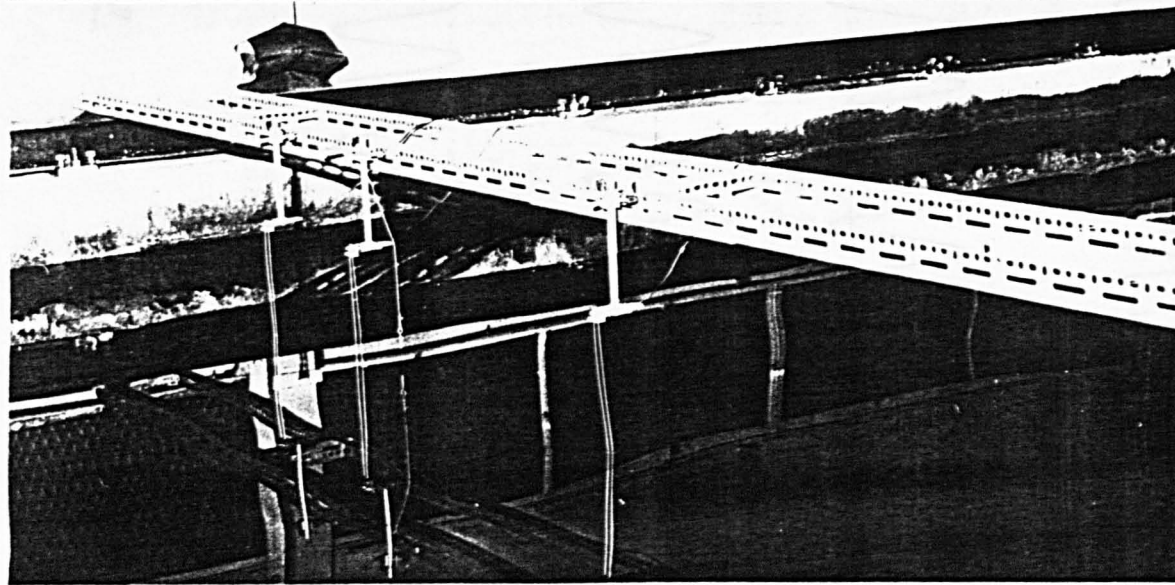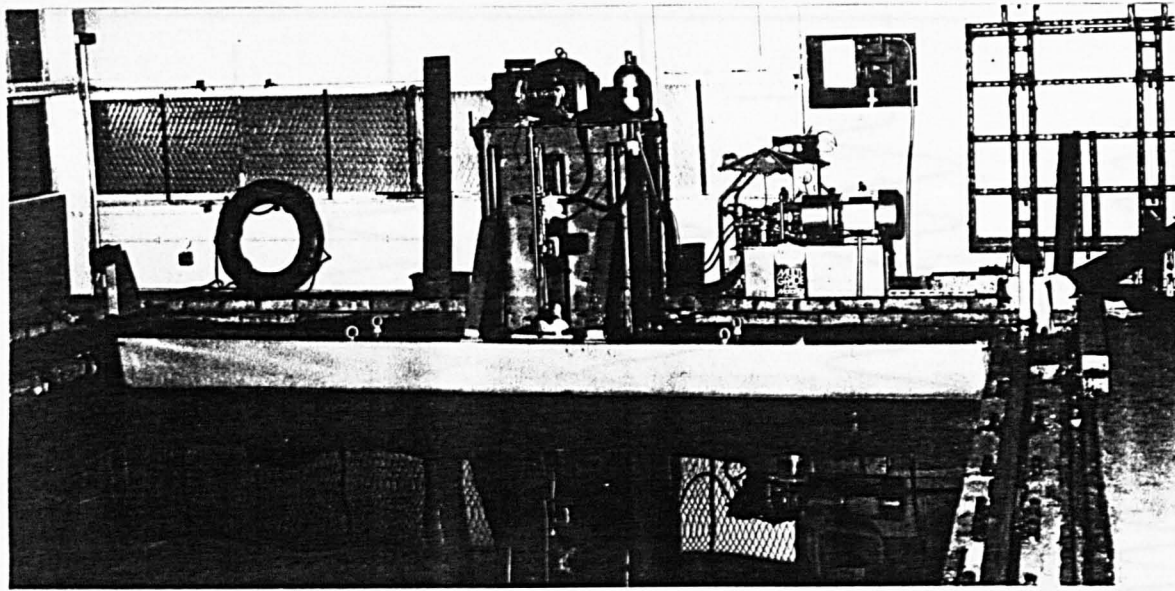
Fig. 4.6 Wave-maker, wave probe and wave signal processing unit
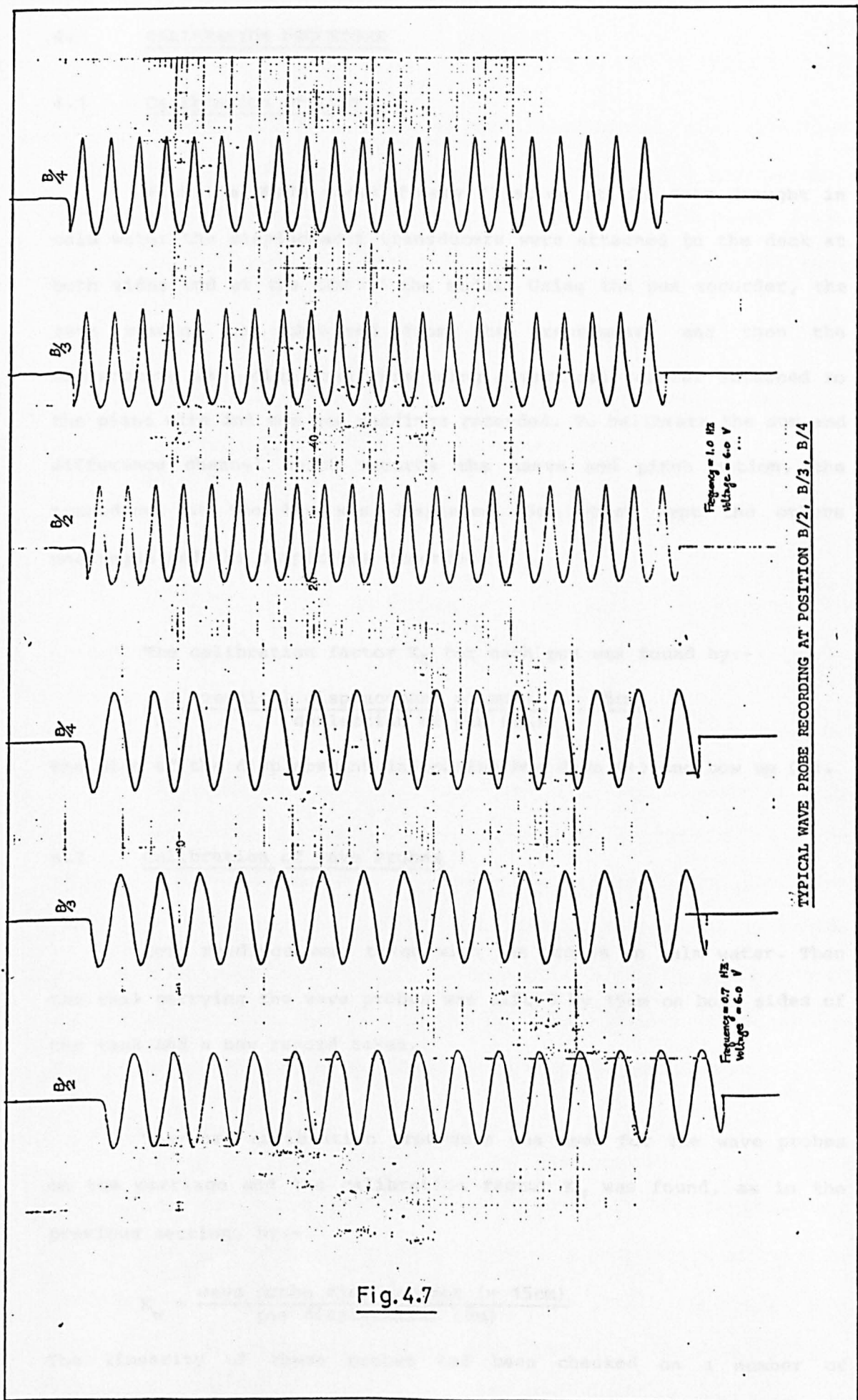
TYPICAL WAVE PROBE RECORDING AT POSITION B/2, B/3, B/4

Frequency = 1.0 Hz
Voltage = 6.0 V

Frequency = 0.7 Hz
Voltage = 6.0 V

Fig.4.7

4.   CALIBRATION PROCEDURE

4.1   Calibration of LVDT

With the SWATH model freely floating at the test draught in calm water the displacement transducers were attached to the deck at both sides and at the LCG of the model. Using the pen recorder, the zero reading was obtained from the transducers and then the transducers were displaced ±5cm using a vertical vernier attached to the piano wire and the new readings recorded. To calibrate the sum and difference channel which records the heave and pitch motion, the transducer at the bow was displaced ±5cm which kept the others unchanged and the output was recorded.

The calibration factor K_D for each pen was found by:-

$$K_D = \frac{\text{vertical displacement of model } (= \pm 5cm)}{\text{deflection of pen (cm)}}$$

the sign of the displacement indicating bow down (+) and bow up (-).

4.2   Calibration of Wave Probes

Zero readings were taken with the probes in calm water. Then the rail carrying the wave probes was lifted by 15cm on both sides of the tank and a new record taken.

The same calibration procedure was used for the wave probes on the carriage and the calibration factor K_w was found, as in the previous section, by:-

$$K_w = \frac{\text{wave probe displacement } (= 15cm)}{\text{pen displacement (cm)}}$$

The linearity of these probes had been checked on a number of occasions previously.

5.   DATA COLLECTION AND RECORD ANALYSIS

During the experiments, the transducer signals were amplified and recorded in analogue form on paper strip charts. The wave height, heave, pitch and LCG motion versus time were recorded. For each case, the record was analysed manually by taking the average of five wave readings.

The distance between the forward and aftward LVDT transducers was 78.5cm. The pitch angle θ was calculated by:-

$$\theta = \tan^{-1} \frac{\text{amplitude from the difference amplifier}}{78.5\text{cm}}$$

As well as the magnitude of the pitch oscillation the departure of the mean line from the at rest position was measured in order to give the trim angle under way.

The numerical values for the bare hull test in waves at zero speed, carried out in 1982 and 1984, are listed in Table 4.2 and the comparison with the theoretical results is plotted in fig. 5.10. The numerical values for the forward speed tests are recorded in Tables 4.3 to 4.26 and are plotted as response amplitudes versus wave frequencies in figs. 4.8 to 4.61. In all these figures the dimension for pitch amplitude/wave amplitude is in degrees per centimetre.

Owing to the limitation of the wavemaker, the wave frequencies only cover the range from 0.4Hz to 1.1Hz. Outside this range, good wave forms cannot be produced as a result of a combination of effects, including tank wall effects. Even within the range, tank wall effects are present as can be seen from the differences in wave height recorded on the probes at different distances from the tank

SWATH VERTICAL MODEL TEST RESULT - 1982

ZERO SPEED - WITHOUT FIN

Freq (Hz)	$\omega=2\pi f$ (rad sec)	Wave Amplitude (cm)	Heave Amp / Wave Amp (cm/cm)	Pitch Amp / Wave Amp (deg/cm)
0.3	1.885	5.220	0.9157	0.1877
0.4	2.513	3.144	1.1323	0.8018
0.5	3.142	4.610	1.2104	0.2734
0.6	3.770	6.220	1.0531	0.1603
0.7	4.398	5.047	0.1805	0.2361
0.8	5.026	5.707	0.2050	0.2329
0.9	5.655	6.145	0.1601	0.2134
1.0	6.283	4.900	0.1051	0.1427
1.1	6.912	5.385	0.0609	0.0650
1.2	7.539	4.950	0.0474	0.0282
1.3	8.168	3.070	0.0303	0.1094

SWATH VERTICAL MODEL TEST RESULT - 1984

ZERO SPEED WITHOUT FIN

0.580	3.644	3.546	1.650	0.297
0.660	4.147	3.995	0.145	0.178
0.715	4.492	4.280	0.165	0.226
0.740	4.649	4.027	0.219	0.258
0.820	5.152	3.628	0.226	0.267
0.831	5.220	3.554	0.224	0.264
0.857	5.385	3.881	0.191	0.258
0.946	5.944	4.443	0.155	0.196
1.005	6.315	4.598	0.118	0.159
1.060	6.660	4.239	0.077	0.104
1.171	7.358	3.669	0.035	0.040

Table 4.2

side. To compare the difference, the heave and pitch amplitude both per wave amplitude at B/2 and at carriage are listed in the tables. The terms in the last column described as 'LCG Motion/Wave B/2', which is the oscillation motion at the position of LCG, show a very good agreement with the 'heave motion/wave B/2' terms.

6.   DISCUSSION OF THE RESULTS FOR THE HEAD SEA CASE

Figures 4.8 and 4.9 show the sinkage and trim against the speed in the calm water test. It is clear that, for the bare hull case, both sinkage and trim increased as the speed goes up. The phenomena, as explained earlier, of the bow trim down is caused by the Munk moment which is proportional to the heave added mass times the square of the model speed. As fig. 4.9 shows, the fixed fin (zero degree angle) has significant effect on the trim problem. The higher the speed, the more trim angle can be reduced. The maximum reduction can be reached when the fin angle is equal to $+2^{\circ}$ and there is almost no trim at the higher speed. However, for fin angles -2° and -4°, the trim was even worse than for fixed fin because in these cases the lift force increased the Munk moment. Nevertheless, they are much better than the bare hull. For fin angle $+4^{\circ}$, too much anti-Munk moment was induced, the bow rising up linearly proportional to the speed.

When the model moved in waves, the trim and sinkage was measured for four speeds both with and without fins and were plotted against wave frequency as shown in figs. 4.10 to 4.21. The speed effects can be seen clearly from these diagrams. As the speed increased both the sinkage and trim also increased. Figures 4.12, 4.14, 4.16, 4.18 and 4.20 also show that the change of the fixed fin angles did not affect the sinkage very much. At the highest speed,

2.0ms^{-1}, there is a considerable change in sinkage compared to the other speeds and stays nearly constant when the fin angles are changed. However, this did not seem to be true for the trim, when compared in figs. 4.13, 4.15, 4.17, 4.19 and 4.21. It was found that at the lower speed of 0.5ms^{-1} the trim is the same for fin angles at 0°, -2° and -4° and the trim is reduced to zero when the fin angles are at +2° and +4°. As the speed increased the lift generated by fins becomes effective. The bow down movement due to the Munk moment can be counteracted by the positive fin angle and, therefore, the trim is reduced. This can be seen in fig. 4.17 for +2°. When the fin angle increased to +4° too much lift was induced and, hence, the bow rose up, as shown in fig. 4.21. Also, it is significant to note that the wave frequency has very little effect on the trim and sinkage.

In figs. 4.22 to 4.29, the trim and sinkage were plotted in a different way. The comparison was made based on the same speed as the fin angles changed. When the speed is low, at 0.5ms^{-1}, although the sinkage and trim are small, the aft fin has no contribution as shown in figs. 4.22 and 4.23. As the speed increased to 1.0ms^{-1}, as shown in fig. 4.24, the fin becomes effective and the sinkage can be reduced. However, this does not seem to be true for the trim as can be seen in fig. 4.25. At all the other fin angles the trim is worse than in the bare hull case, except for fin angle at +4°. This can be explained by the fact that if the speed is not high enough to generate the necessary lift to counter the Munk moment, then the aft fin becomes an extra appendage which induces drag at the stern. In addition, since the fins are attached at the centre of the lower hull, whereas the pitch centre is located about the water surface, the moment will increase the trim considerably. Until the speed is increased (1.5ms^{-1} and 2.0ms^{-1}) the moment which is generated by the lift can reduce the

trim and sinkage significantly as can be seen in figs. 4.26 to 4.29. Obviously, in figs. 4.27 and 4.29, too much righting moment was generated by the fin at an angle of $+4^{\circ}$ thus making the bow rise.

In figs. 4.30 to 4.41 the heave and pitch motions, which were plotted against wave frequency for the bare hull and different fin angles, decrease and the peak point shifts to the lower frequency when the speed increases. The speed effect can be seen in these figures. When the speed increased the encounter frequency also increased and, therefore, when the motion response was plotted against the wave frequency instead of the encounter frequency both the heave and pitch motion response curves shifted to a lower frequency as the speed increased.

In figs 4.42, 4.44, 4.46 and 4.48, the comparison of the heave responses were plotted for various fin angles at the same speed. Fins operate most effectively near the synchronous range and have little influence at higher or lower frequencies. The significant reductions happened at the higher speeds of $1.5ms^{-1}$ and $2.0ms^{-1}$, see figs. 4.46 and 4.48. The heave motion was reduced by 50% compared with the bare hull at the low frequency range. The results also reveal that further reduction of the heave motion can be made by changing the fixed fin angles at the low frequency range.

The pitch motion responses are plotted in a similar way as shown in figs. 4.43, 4.45, 4.47 and 4.49. Again, a significant reduction was found at the low frequency range with the higher speed. A turn over point occurs at a frequency of about 0.55Hz. When wave frequencies are higher than this the pitch motion becomes worse than the bare hull case. In other words, the effect of the fin is mainly

due to increased damping forces which has considerable significance at nearly resonant conditions. In SWATH designs the heave and pitch motions are small at the higher frequencies and, consequently, this will not be a great problem for a SWATH ship designer.

Finally, the pitching and heaving motion in regular waves is presented in the form of the response amplitude operators versus the encounter frequencies as shown in figs. 4.50 to 4.61, where the original speeds had been marked. If the effect is purely dependent on encounter frequency all the points may be expected to be located on a single curve. The experimental results are seen to follow this pattern to an acceptable degree.

In figs. 4.62 and 4.63 comparisons are presented for no fin, a fixed fin at 0° and a fixed fin angle $+2^\circ$. It is clear that the presence of the fins greatly reduces the maximum pitch response, the average at the peak being about 42% lower than for the bare hull. The advantage of the non-zero angle of the fins is less great in the quoted case, the reduction being 32% lower than the bare hull. In heave the influence of the fins consists mainly of a shift of the response curve towards lower frequencies and about 21% reduction from the fixed fin at 0° and 19% reduction for the fixed fin angle at 2°.

7.   DISCUSSION OF THE RESULTS FOR THE FOLLOWING SEA CASE

In the following sea model tests, the instrumental facilities are the same as in the previous sections. The natural frequency in heave and pitch mode, both with and without fins, at zero speed have been measured and listed in Table 4.27.

SWATH VERTICAL MOTION TEST

SPEED V=0.5m/sec   WITHOUT FIN

FREQ. (hz)	WAVE AMPLITUDE (cm)				HEAVE AMP (cm)	PITCH ANG (deg)	HEAVE A. WAVE B/2	HEAVE A. WAVE CAR	PITCH ANG WAVE B/2	PITCH ANG WAVE CAR	TRIM (deg)	SINKAGE (cm)	LCG MOT WAVE B/2
	B/2	B/3	B/4	CAR.									
0.40	1.894	1.994	2.206	1.919	2.607	1.818	1.376	1.359	0.960	0.947	0.120	0.288	1.362
0.45	2.376	2.578	2.571	2.466	4.125	1.040	1.736	1.673	0.430	0.422	0.150	0.247	1.720
0.50	2.930	3.003	2.945	2.996	7.619	1.246	2.600	2.543	0.766	0.749	0.188	0.200	2.629
0.55	3.030	3.271	3.382	3.025	3.123	0.389	1.031	1.032	0.411	0.412	0.120	0.165	1.014
0.60	3.885	3.895	3.715	4.271	0.734	0.389	0.189	0.172	0.100	0.091	0.165	0.073	0.179
0.70	4.530	5.000	4.635	4.487	0.606	0.690	0.134	0.135	0.152	0.154	0.000	0.000	0.137
0.80	4.670	4.665	4.430	4.320	0.678	0.690	0.145	0.157	0.148	0.160	0.000	0.000	0.146
0.90	4.635	4.834	4.620	4.490	0.504	0.735	0.109	0.112	0.159	0.164	0.188	0.000	0.105
1.00	3.885	3.955	3.815	3.953	0.276	0.528	0.071	0.070	0.136	0.134	0.269	0.000	0.066
1.10	4.225	4.320	4.085	3.858	0.129	0.231	0.031	0.033	0.055	0.060	0.295	0.289	0.027

TABLE 4-3

SWATH VERTICAL MOTION TEST

SPEED V=1.0m/sec   WITHOUT FIN

FREQ. (hz)	WAVE AMPLITUDE (cm)				HEAVE AMP (cm)	PITCH ANG (deg)	HEAVE A. WAVE B/2	HEAVE A. WAVE CAR	PITCH ANG WAVE B/2	PITCH ANG WAVE CAR	TRIM (deg)	SINKAGE (cm)	LCG MOT WAVE B/2
	B/2	B/3	B/4	CAR.									
0.40	1.970	2.074	2.279	1.982	2.543	1.454	1.291	1.283	0.738	0.734	0.927	0.514	1.288
0.45	2.424	2.633	2.500	2.252	5.641	2.630	2.327	2.505	1.085	1.075	0.897	0.572	2.355
0.50	2.863	2.940	2.905	3.010	6.060	2.852	2.117	2.013	0.996	0.948	1.204	0.597	2.066
0.55	3.106	3.271	3.529	2.937	1.502	1.026	0.484	0.511	0.330	0.349	0.898	0.576	0.478
0.60	4.165	4.200	4.060	3.934	0.476	0.317	0.114	0.121	0.076	0.081	0.868	0.622	0.111
0.70	4.295	4.467	4.553	4.426	0.386	0.343	0.089	0.087	0.080	0.077	0.805	0.471	0.086
0.80	4.090	4.101	3.884	3.807	0.413	0.536	0.101	0.108	0.131	0.141	0.751	0.507	0.101
0.90	4.772	4.980	4.754	4.345	0.338	0.706	0.071	0.077	0.148	0.162	1.020	0.398	0.069
1.00	5.045	5.200	4.955	4.385	0.181	0.494	0.036	0.041	0.098	0.113	1.288	0.254	0.036
1.10	4.225	4.467	4.218	3.636	0.061	0.238	0.014	0.016	0.056	0.065	1.395	0.145	0.010

TABLE 4-4

SWATH VERTICAL MOTION TEST

SPEED V=1.5m/sec   WITHOUT FIN

FREQ.	WAVE			AMPLITUDE	HEAVE AMP	PITCH ANG	HEAVE A.	HEAVE A.	PITCH ANG	PITCH ANG	TRIM	SINKAGE	LCG MOTI
(hz)			(cm)		(cm)	(deg)	WAVE B/2	WAVE CAR	WAVE B/2	WAVE CAR	(deg)	(cm)	WAVE B/2
	B/2	B/3	B/4	CAR.									
0.40	1.894	1.994	2.206	1.924	3.886	2.056	2.052	2.020	1.086	1.069	2.422	0.494	2.029
0.45	2.500	2.712	2.574	2.288	4.935	2.899	1.974	2.157	1.160	1.257	2.153	0.654	1.979
0.50	2.863	2.940	2.835	2.965	1.850	1.124	0.646	0.624	0.393	0.379	2.247	0.670	0.616
0.55	3.030	3.271	3.382	2.991	0.580	0.425	0.191	0.194	0.140	0.142	2.362	0.520	0.183
0.60	4.235	4.200	4.125	3.893	0.330	0.165	0.078	0.085	0.039	0.042	2.010	0.495	0.088
0.70	4.295	4.467	4.553	4.251	0.442	0.414	0.103	0.104	0.096	0.097	1.958	0.869	0.102
0.80	4.225	4.248	3.883	3.791	0.369	0.479	0.087	0.097	0.113	0.126	2.011	0.797	0.085
0.90	5.163	5.415	5.180	4.467	0.287	0.440	0.056	0.064	0.085	0.099	2.516	0.656	0.059
1.00	4.975	4.980	4.754	4.049	0.127	0.351	0.026	0.031	0.071	0.087	2.038	0.725	0.025
1.10	4.363	4.687	4.486	3.489	0.054	0.176	0.012	0.015	0.040	0.050	2.092	0.652	0.014

TABLE 4-5

SWATH VERTICAL MOTION TEST

SPEED V=2.0m/sec   WITHOUT FIN

FREQ.	WAVE			AMPLITUDE	HEAVE AMP	PITCH ANG	HEAVE A.	HEAVE A.	PITCH ANG	PITCH ANG	TRIM	SINKAGE	LCG MOTI
(hz)			(cm)		(cm)	(deg)	WAVE B/2	WAVE CAR	WAVE B/2	WAVE CAR	(deg)	(cm)	WAVE B/2
	B/2	B/3	B/4	CAR.									
0.40	1.894	1.994	2.206	1.982	3.059	1.333	1.615	1.543	0.704	0.673	3.406	1.934	1.597
0.45	2.424	2.632	2.426	2.189	2.632	1.358	1.086	1.202	0.560	0.620	3.406	2.058	1.082
0.50	2.863	3.015	2.905	2.861	1.077	0.713	0.376	0.376	0.249	0.249	3.247	2.016	0.301
0.55	3.030	3.271	3.382	2.919	0.502	0.365	0.166	0.172	0.120	0.125	3.585	2.037	0.164
0.60	4.165	4.200	4.060	3.893	0.330	0.234	0.079	0.085	0.056	0.060	3.002	2.430	0.074
0.70	4.599	5.000	4.705	4.426	0.385	0.350	0.084	0.087	0.076	0.079	3.519	2.900	0.095
0.80	4.953	5.000	4.705	4.176	0.369	0.377	0.075	0.088	0.076	0.090	3.519	2.700	0.079
0.90	5.375	5.580	5.180	4.569	0.246	0.325	0.046	0.054	0.060	0.071	3.017	2.460	0.053
1.00	5.180	5.270	4.955	3.693	0.129	0.235	0.025	0.035	0.045	0.064	2.949	2.319	0.027
1.10	4.635	4.907	4.553	3.155	0.054	0.094	0.012	0.017	0.020	0.030	3.110	2.319	0.014

TABLE 4-6

SWATH VERTICAL MOTION TEST

SPEED V=0.5m/sec   FIN ANGLE= 0.0 DEGREE

FREQ.	WAVE		AMPLITUDE		HEAVE AMP	PITCH ANG	HEAVE A.	HEAVE A.	PITCH ANG	PITCH ANG	TRIM	SINKAGE	LCG MOTI
(hz)			(cm)		(cm)	(deg)	WAVE B/2	WAVE CAR	WAVE B/2	WAVE CAR	(deg)	(cm)	WAVE B/2
	B/2	B/3	B/4	CAR.									
0.40	2.650	2.920	2.750	2.745	3.496	1.680	1.319	1.274	0.634	0.612	0.314	0.255	1.308
0.45	3.020	3.230	3.160	3.200	5.814	2.010	1.925	1.817	0.666	0.628	0.289	0.255	1.922
0.50	3.240	3.470	3.380	3.280	5.225	1.380	1.613	1.593	0.426	0.421	0.315	0.146	1.618
0.55	3.870	4.100	4.030	3.863	2.960	0.270	0.765	0.766	0.070	0.070	0.182	0.292	0.770
0.60	4.560	4.730	4.410	4.355	1.219	1.020	0.267	0.279	0.224	0.234	0.053	0.219	0.267
0.70	4.210	5.130	5.140	4.691	0.686	1.000	0.163	0.146	0.238	0.213	0.105	0.036	0.158
0.80	4.930	5.210	4.940	4.373	0.599	0.810	0.122	0.137	0.164	0.185	0.420	0.036	0.116
0.90	4.560	5.130	5.000	4.568	0.442	0.750	0.097	0.097	0.164	0.164	0.420	0.146	0.088
1.00	3.210	3.420	3.310	3.591	0.152	0.460	0.047	0.042	0.143	0.128	0.401	0.055	0.031
1.10	3.420	3.790	3.610	3.309	0.027	0.170	0.008	0.008	0.050	0.051	0.496	0.219	0.009

TABLE 4-7

SWATH VERTICAL MOTION TEST

SPEED V=1.0m/sec   FIN ANGLE= 0.0 DEGREE

FREQ.	WAVE		AMPLITUDE		HEAVE AMP	PITCH ANG	HEAVE A.	HEAVE A.	PITCH ANG	PITCH ANG	TRIM	SINKAGE	LCG MOTI
(hz)			(cm)		(cm)	(deg)	WAVE B/2	WAVE CAR	WAVE B/2	WAVE CAR	(deg)	(cm)	WAVE B/2
	B/2	B/3	B/4	CAR.									
0.40	2.650	2.840	2.660	2.590	3.978	1.430	1.501	1.536	0.540	0.552	1.680	0.365	1.449
0.45	2.870	3.080	3.020	3.190	5.869	1.790	2.045	1.840	0.624	0.561	1.365	0.474	2.011
0.50	3.020	3.230	3.230	3.345	2.883	0.270	0.955	0.862	0.089	0.081	1.576	0.365	0.952
0.55	3.680	3.870	3.830	3.820	1.683	0.420	0.457	0.441	0.114	0.110	1.496	0.401	0.457
0.60	4.490	4.530	4.270	4.164	1.200	0.720	0.267	0.288	0.160	0.173	1.522	0.401	0.267
0.70	4.780	5.050	5.070	4.760	0.734	0.960	0.154	0.154	0.201	0.202	1.522	0.401	0.152
0.80	5.000	5.130	4.930	4.309	0.391	0.850	0.078	0.091	0.170	0.197	1.707	0.292	0.083
0.90	3.790	4.100	3.970	3.640	0.172	0.530	0.045	0.047	0.140	0.145	1.605	0.146	0.042
1.00	3.930	4.260	4.120	3.670	0.057	0.380	0.015	0.016	0.097	0.104	1.680	0.140	0.011
1.10	3.500	3.790	3.680	3.500	0.070	0.210	0.020	0.020	0.060	0.060	1.627	0.130	0.025

TABLE 4-8

SWATH VERTICAL MOTION TEST

SPEED V=1.5m/sec   FIN ANGLE= 0.0 DEGREE

FREQ. (hz)	WAVE AMPLITUDE (cm)				HEAVE AMP (cm)	PITCH ANG (deg)	HEAVE A. WAVE B/2	HEAVE A. WAVE CAR	PITCH ANG WAVE B/2	PITCH ANG WAVE CAR	TRIM (deg)	SINKAGE (cm)	LCG MOTI WAVE B/2
	B/2	B/3	B/4	CAR.									
0.40	2.330	2.530	2.460	2.550	2.577	0.356	1.106	1.011	0.153	0.140	1.129	0.766	1.142
0.45	2.780	2.970	2.870	3.080	1.913	0.420	0.688	0.621	0.151	0.136	1.103	0.730	0.701
0.50	3.300	3.370	3.360	3.485	1.581	0.454	0.479	0.454	0.138	0.130	0.998	0.730	0.492
0.55	3.900	4.090	3.990	3.780	1.233	0.725	0.316	0.326	0.186	0.192	1.050	0.803	0.326
0.60	4.500	4.570	4.370	4.260	1.004	0.859	0.223	0.235	0.191	0.202	1.155	0.730	0.232
0.70	4.950	5.370	5.420	4.930	0.683	1.034	0.138	0.138	0.209	0.210	1.287	0.949	0.138
0.80	5.180	5.290	5.050	4.540	0.313	0.840	0.060	0.069	0.162	0.185	1.443	1.022	0.061
0.90	3.790	4.180	3.970	4.000	0.102	0.496	0.027	0.026	0.131	0.124	1.129	0.438	0.031
1.00	4.740	4.810	4.710	3.725	0.000	0.390	0.000	0.000	0.082	0.105	1.313	0.547	0.000
1.10	4.370	4.660	4.560	3.740	0.091	0.210	0.021	0.024	0.048	0.056	1.313	0.511	0.023

TABLE 4-9

SWATH VERTICAL MOTION TEST

SPEED V=2.0m/sec   FIN ANGLE= 0.0 DEGREE

FREQ. (hz)	WAVE AMPLITUDE (cm)				HEAVE AMP (cm)	PITCH ANG (deg)	HEAVE A. WAVE B/2	HEAVE A. WAVE CAR	PITCH ANG WAVE B/2	PITCH ANG WAVE CAR	TRIM (deg)	SINKAGE (cm)	LCG MOTI WAVE B/2
	B/2	B/3	B/4	CAR.									
0.40	2.480	2.720	2.640	2.570	1.989	0.331	0.802	0.774	0.133	0.129	1.050	2.044	0.801
0.45	2.700	2.930	2.910	2.930	1.427	0.598	0.529	0.487	0.221	0.204	1.076	2.117	0.539
0.50	3.380	3.550	3.490	3.654	1.229	0.770	0.364	0.336	0.228	0.211	0.688	2.000	0.370
0.55	3.970	4.230	4.190	3.944	1.086	0.910	0.274	0.275	0.229	0.231	0.767	2.153	0.274
0.60	4.630	4.630	4.520	4.411	0.922	0.980	0.199	0.209	0.212	0.222	0.793	2.153	0.196
0.70	4.730	5.210	5.170	4.585	0.540	0.961	0.114	0.118	0.203	0.210	1.050	2.007	0.123
0.80	4.880	4.820	4.750	4.190	0.247	0.664	0.051	0.059	0.136	0.158	1.365	2.190	0.061
0.90	4.520	4.970	4.860	4.015	0.121	0.410	0.027	0.030	0.091	0.102	1.182	1.934	0.028
1.00	4.660	5.050	4.930	3.773	0.000	0.290	0.000	0.000	0.062	0.077	1.208	1.952	0.000
1.10	5.030	5.370	5.150	3.180	0.045	0.150	0.009	0.014	0.030	0.047	1.247	1.715	0.009

TABLE 4-10

. SWATH VERTICAL MOTION TEST

SPEED V=0.5m/sec   FIN ANGLE=-2.0 DEGREE

FREQ. (hz)	WAVE AMPLITUDE (cm)				HEAVE AMP (cm)	PITCH ANG (deg)	HEAVE A. WAVE B/2	HEAVE A. WAVE CAR	PITCH ANG WAVE B/2	PITCH ANG WAVE CAR	TRIM (deg)	SINKAGE (cm)	LCG MOTI WAVE B/2
	B/2	B/3	B/4	CAR.									
0.40	1.985	2.088	2.052	2.101	2.607	1.636	1.313	1.241	0.824	0.779	0.477	0.000	1.321
0.45	2.574	2.706	2.618	2.294	4.531	2.000	1.760	1.975	0.777	0.872	0.477	0.000	1.791
0.50	3.015	3.170	3.113	2.899	5.279	1.182	1.751	1.821	0.392	0.408	0.393	0.000	1.781
0.55	3.309	3.479	3.396	3.119	2.248	0.224	0.679	0.721	0.068	0.072	0.337	0.000	0.684
0.60	3.603	3.789	3.608	4.596	0.954	0.491	0.265	0.208	0.136	0.107	0.365	0.038	0.262
0.70	3.971	4.330	4.316	4.257	0.607	0.738	0.153	0.143	0.186	0.173	0.393	0.076	0.151
0.80	4.118	4.330	3.962	3.642	0.565	0.738	0.137	0.155	0.179	0.203	0.604	0.077	0.137
0.90	3.824	4.175	4.033	3.881	0.383	0.644	0.100	0.099	0.168	0.166	0.561	0.058	0.101
1.00	4.779	5.026	4.670	4.128	0.150	0.581	0.031	0.036	0.122	0.141	0.631	0.192	0.028
1.10	0.000	0.000	0.000	0.000	0.000	0.000	0.000	0.000	0.000	0.000	0.000	0.000	0.000

TABLE 4-11

SWATH VERTICAL MOTION TEST

SPEED V=1.0m/sec   FIN ANGLE=-2.0 DEGREE

FREQ. (hz)	WAVE AMPLITUDE (cm)				HEAVE AMP (cm)	PITCH ANG (deg)	HEAVE A. WAVE B/2	HEAVE A. WAVE CAR	PITCH ANG WAVE B/2	PITCH ANG WAVE CAR	TRIM (deg)	SINKAGE (cm)	LCG MOT. WAVE B/2
	B/2	B/3	B/4	CAR.									
0.40	1.912	2.041	2.052	2.055	2.779	0.693	1.453	1.352	0.362	0.337	2.385	0.153	1.471
0.45	2.574	2.784	2.689	2.459	3.305	0.553	1.284	1.344	0.215	0.225	2.189	0.229	1.299
0.50	2.941	3.170	3.113	2.044	2.489	0.393	0.846	0.875	0.134	0.138	2.189	0.076	0.858
0.55	3.162	3.402	3.255	3.202	1.431	0.250	0.453	0.447	0.079	0.078	2.189	0.114	0.462
0.60	3.529	3.711	3.425	3.504	0.985	0.536	0.279	0.281	0.152	0.153	2.189	0.114	0.286
0.70	3.824	4.253	4.245	4.101	0.626	0.811	0.164	0.153	0.212	0.198	2.189	0.137	0.168
0.80	3.971	4.021	3.750	3.606	0.304	0.658	0.077	0.084	0.166	0.182	2.216	0.192	0.080
0.90	3.676	4.175	4.033	3.670	0.158	0.561	0.043	0.043	0.153	0.153	2.245	0.140	0.044
1.00	4.191	4.716	4.599	3.716	0.048	0.436	0.011	0.013	0.104	0.117	2.385	0.077	0.012
1.10	0.000	0.000	0.000	0.000	0.000	0.000	0.011	0.000	0.075	0.000	0.000	0.000	0.000

TABLE 4-12

SWATH VERTICAL MOTION TEST

SPEED V=1.5m/sec   FIN ANGLE=-2.0 DEGREE

FREQ. (hz)	WAVE AMPLITUDE (cm)				HEAVE AMP (cm)	PITCH ANG (deg)	HEAVE A. WAVE B/2	HEAVE A. WAVE CAR	PITCH ANG WAVE B/2	PITCH ANG WAVE CAR	TRIM (deg)	SINKAGE (cm)	LCG MOTI WAVE B/2
	B/2	B/3	B/4	CAR.									
0.40	1.800	1.895	1.893	1.723	1.362	0.177	0.757	0.790	0.098	0.103	2.132	0.305	0.765
0.45	2.280	2.447	2.403	2.152	0.892	0.407	0.391	0.414	0.179	0.189	2.109	0.460	0.400
0.50	2.550	2.763	2.621	2.259	0.702	0.488	0.275	0.311	0.191	0.216	2.245	0.500	0.279
0.55	2.835	3.079	2.913	2.701	0.804	0.480	0.284	0.298	0.169	0.178	2.076	0.346	0.290
0.60	3.075	3.237	2.985	2.902	0.673	0.587	0.219	0.232	0.191	0.202	2.020	0.346	0.226
0.70	3.150	3.474	3.350	3.232	0.438	0.671	0.139	0.136	0.213	0.208	2.076	0.462	0.142
0.80	3.897	3.943	3.608	3.463	0.246	0.559	0.063	0.071	0.143	0.161	2.383	0.519	0.065
0.90	3.824	4.125	4.104	3.624	0.100	0.477	0.026	0.028	0.125	0.132	2.371	0.519	0.026
1.00	3.971	4.716	4.528	3.569	0.029	0.312	0.007	0.008	0.079	0.007	2.398	0.462	0.008
1.10	0.000	0.000	0.000	0.000	0.000	0.000	0.000	0.000	0.000	0.000	0.000	0.000	0.000

TABLE 4-13

SWATH VERTICAL MOTION TEST

SPEED V=2.0m/sec   FIN ANGLE=-2.0 DEGREE

FREQ. (hz)	WAVE AMPLITUDE (cm)				HEAVE AMP (cm)	PITCH ANG (deg)	HEAVE A. WAVE B/2	HEAVE A. WAVE CAR	PITCH ANG WAVE B/2	PITCH ANG WAVE CAR	TRIM (deg)	SINKAGE (cm)	LCG MO WAVE B/2
	B/2	B/3	B/4	CAR.									
0.40	1.950	2.053	2.039	1.875	1.165	0.084	0.597	0.621	0.043	0.045	2.581	2.000	0.634
0.45	2.475	2.605	2.549	2.254	1.072	0.232	0.433	0.475	0.094	0.103	2.609	1.923	0.455
0.50	2.850	3.047	2.985	2.511	0.899	0.421	0.315	0.358	0.148	0.167	2.553	1.885	0.330
0.55	3.000	3.158	3.058	2.946	0.755	0.565	0.252	0.256	0.188	0.192	2.609	1.885	0.265
0.60	3.375	3.474	3.277	3.188	0.662	0.589	0.196	0.208	0.175	0.185	2.497	1.923	0.206
0.70	3.600	3.868	3.932	3.583	0.481	0.674	0.134	0.134	0.187	0.188	2.469	1.846	0.145
0.80	4.118	4.330	3.962	3.193	0.233	0.504	0.057	0.073	0.122	0.158	2.357	2.019	0.070
0.90	3.824	4.098	3.892	2.743	0.096	0.363	0.025	0.035	0.095	0.132	2.483	2.000	0.024
1.00	4.044	4.639	4.387	3.073	0.058	0.191	0.014	0.019	0.047	0.062	2.595	1.962	0.015
1.10	0.000	0.000	0.000	0.000	0.000	0.000	0.000	0.000	0.000	0.000	0.000	0.000	0.000

TABLE 4-14

SWATH VERTICAL MOTION TEST

SPEED V=0.5m/sec   FIN ANGLE= 2.0 DEGREE

FREQ.	WAVE		AMPLITUDE		HEAVE AMP	PITCH ANG	HEAVE A.	HEAVE A.	PITCH ANG	PITCH ANG	TRIM	SINKAGE	LCG MOT
(hz)			(cm)		(cm)	(deg)	WAVE B/2	WAVE CAR	WAVE B/2	WAVE CAR	(deg)	(cm)	WAVE B/2
	B/2	B/3	B/4	CAR.									
0.40	1.912	2.188	2.071	1.867	2.428	1.264	1.270	1.300	0.661	0.677	0.258	0.156	1.298
0.45	2.059	2.266	2.214	2.106	4.350	1.625	2.113	2.066	0.789	0.772	0.172	0.117	2.129
0.50	2.822	3.125	3.000	2.816	5.081	0.894	1.800	1.804	0.317	0.317	0.090	0.161	1.852
0.55	3.193	3.511	3.389	2.832	2.366	0.203	0.741	0.835	0.064	0.072	0.069	0.154	0.733
0.60	3.639	3.830	3.606	4.133	1.046	0.565	0.287	0.253	0.155	0.137	0.114	0.115	0.281
0.70	4.158	4.548	4.543	3.982	0.646	0.050	0.155	0.162	0.204	0.213	0.043	0.092	0.149
0.80	3.550	3.672	3.396	3.211	0.491	0.661	0.138	0.153	0.186	0.206	0.226	0.000	0.137
0.90	3.550	4.063	3.892	3.798	0.350	0.667	0.099	0.092	0.188	0.176	0.155	0.000	0.100
1.00	3.920	4.609	4.316	3.688	0.150	0.522	0.038	0.041	0.133	0.142	0.226	0.211	0.036
1.10	0.000	0.000	0.000	0.000	0.000	0.000	0.020	0.000	0.090	0.000	0.080	0.000	0.000

TABLE 4-15

SWATH VERTICAL MOTION TEST

SPEED V=1.0m/sec   FIN ANGLE= 2.0 DEGREE

FREQ.	WAVE		AMPLITUDE		HEAVE AMP	PITCH ANG	HEAVE A.	HEAVE A.	PITCH ANG	PITCH ANG	TRIM	SINKAGE	LCG MOT
(hz)			(cm)		(cm)	(deg)	WAVE B/2	WAVE CAR	WAVE B/2	WAVE CAR	(deg)	(cm)	WAVE B/2
	B/2	B/3	B/4	CAR.									
0.40	1.931	2.074	2.091	1.858	3.273	1.258	1.695	1.762	0.651	0.677	0.912	0.615	1.673
0.45	2.525	2.713	2.668	2.212	4.943	1.692	1.958	2.235	0.670	0.765	0.855	0.577	1.941
0.50	2.896	3.191	3.029	2.699	2.529	0.319	0.873	0.937	0.110	0.118	0.941	0.615	0.870
0.55	3.193	3.431	3.317	3.009	1.443	0.294	0.313	0.479	0.092	0.097	1.015	0.577	0.451
0.60	3.564	3.830	3.606	3.363	1.000	0.565	0.281	0.297	0.159	0.168	0.998	0.523	0.286
0.70	4.084	4.548	4.543	3.920	0.644	0.030	0.158	0.164	0.203	0.212	1.026	0.538	0.162
0.80	3.846	4.063	3.679	3.459	0.302	0.663	0.079	0.087	0.172	0.192	1.131	0.442	0.082
0.90	3.846	4.297	4.033	3.633	0.152	0.587	0.039	0.042	0.153	0.161	1.244	0.340	0.040
1.00	3.920	4.609	4.316	3.578	0.048	0.381	0.012	0.013	0.097	0.106	1.230	0.231	0.011
1.10	0.000	0.000	0.000	0.000	0.000	0.000	0.000	0.000	0.000	0.000	0.000	0.000	0.000

TABLE 4-16

SWATH VERTICAL MOTION TEST

SPEED V=1.5m/sec   FIN ANGLE= 2.0 DEGREE

FREQ. (hz)	WAVE		AMPLITUDE (cm)		HEAVE AMP (cm)	PITCH ANG (deg)	HEAVE A. WAVE B/2	HEAVE A. WAVE CAR	PITCH ANG WAVE B/2	PITCH ANG WAVE CAR	TRIM (deg)	SINKAGE (cm)	LCG MOTI(WAVE B/2
	B/2	B/3	B/4	CAR.									
0.40	1.931	2.074	2.019	1.867	2.612	0.556	1.353	1.399	0.288	0.298	0.285	0.769	1.367
0.45	2.515	2.656	2.618	2.204	1.611	0.126	0.641	0.731	0.050	0.057	0.328	0.726	0.704
0.50	2.885	3.047	2.972	2.628	1.202	0.356	0.417	0.457	0.123	0.135	0.393	0.763	0.425
0.55	3.180	3.359	3.255	2.973	0.867	0.702	0.273	0.292	0.221	0.236	0.561	0.931	0.285
0.60	3.550	3.672	3.467	3.248	0.809	0.682	0.228	0.249	0.192	0.209	0.382	0.801	0.235
0.70	3.994	4.375	4.387	4.044	0.599	0.884	0.150	0.148	0.221	0.219	0.337	0.863	0.155
0.80	3.235	3.170	3.042	2.651	0.216	0.490	0.067	0.081	0.151	0.185	0.617	0.769	0.070
0.90	3.309	3.634	3.396	2.936	0.087	0.411	0.026	0.029	0.124	0.139	0.590	0.807	0.026
1.00	3.529	3.866	3.750	3.092	0.106	0.275	0.030	0.034	0.078	0.089	0.547	0.750	0.029
1.10	0.000	0.000	0.000	0.000	0.000	0.000	0.000	0.000	0.000	0.000	0.000	0.000	0.000

TABLE 4-17

SWATH VERTICAL MOTION TEST

SPEED V=2.0m/sec   FIN ANGLE= 2.0 DEGREE

FREQ. (hz)	WAVE		AMPLITUDE (cm)		HEAVE AMP (cm)	PITCH ANG (deg)	HEAVE A. WAVE B/2	HEAVE A. WAVE CAR	PITCH ANG WAVE B/2	PITCH ANG WAVE CAR	TRIM (deg)	SINKAGE (cm)	LCG MOTI(WAVE B/2
	B/2	B/3	B/4	CAR.									
0.40	1.923	2.031	2.052	1.914	1.035	0.151	0.538	0.541	0.079	0.079	0.000	2.328	0.558
0.45	2.424	0.000	2.633	2.500	2.162	1.023	0.296	0.422	0.473	0.122	0.137	0.150	2.222
0.50	3.003	3.203	3.113	2.549	1.046	0.463	0.348	0.410	0.154	0.181	0.140	2.061	0.356
0.55	3.254	3.437	3.255	3.035	0.855	0.617	0.263	0.281	0.190	0.203	0.140	1.985	0.274
0.60	3.624	3.828	3.608	3.407	0.718	0.682	0.198	0.211	0.188	0.200	0.056	2.061	0.209
0.70	3.994	4.375	4.387	3.827	0.511	0.709	0.128	0.133	0.178	0.185	0.056	2.023	0.134
0.80	3.603	3.711	3.538	3.128	0.229	0.469	0.064	0.073	0.130	0.150	0.295	2.115	0.069
0.90	3.529	4.021	3.821	3.174	0.125	0.361	0.035	0.039	0.102	0.114	0.253	2.135	0.039
1.00	3.971	4.407	4.245	3.009	0.096	0.116	0.024	0.032	0.029	0.039	0.281	2.038	0.024
1.10	0.000	0.000	0.000	0.000	0.000	0.000	0.000	0.000	0.000	0.000	0.000	0.000	0.000

TABLE 4-18

SWATH VERTICAL MOTION TEST

SPEED V=0.5m/sec   FIN ANGLE=-4.0 DEGREE

FREQ.	WAVE		AMPLITUDE		HEAVE AMP	PITCH ANG	HEAVE A.	HEAVE A.	PITCH ANG	PITCH ANG	TRIM	SINKAGE	LCG MOTI
(hz)			(cm)		(cm)	(deg)	WAVE B/2	WAVE CAR	WAVE B/2	WAVE CAR	(deg)	(cm)	WAVE B/2
	B/2	B/3	B/4	CAR.									
0.40	1.634	1.915	1.818	1.802	2.272	1.459	1.390	1.261	0.893	0.810	0.678	0.015	1.396
0.45	1.856	2.074	2.121	1.982	4.059	1.829	2.187	2.048	0.985	0.923	0.521	0.037	2.207
0.50	2.302	2.473	2.424	2.590	4.688	1.014	2.036	1.810	0.440	0.392	0.625	0.037	2.067
0.55	2.673	2.872	2.879	2.847	2.136	0.182	0.799	0.750	0.068	0.064	0.547	0.074	0.825
0.60	3.045	3.112	3.030	3.315	0.758	0.360	0.249	2.229	0.118	0.109	0.599	0.074	0.249
0.70	3.342	3.670	3.788	3.604	0.535	0.689	0.160	0.148	0.206	0.191	0.501	0.109	0.164
0.80	3.267	3.351	3.258	2.630	0.429	0.551	0.131	0.163	0.169	0.209	0.672	0.091	0.134
0.90	3.267	3.431	3.409	3.306	0.306	0.543	0.094	0.093	0.166	0.164	0.769	0.116	0.097
1.00	3.639	3.750	3.712	3.387	0.117	0.428	0.032	0.034	0.118	0.126	0.698	0.164	0.029
1.10	0.000	0.000	0.000	0.000	0.000	0.000	0.000	0.000	0.000	0.000	0.000	0.000	0.000

TABLE 4-19

SWATH VERTICAL MOTION TEST

SPEED V=1.0m/sec   FIN ANGLE=-4.0 DEGREE

FREQ.	WAVE		AMPLITUDE		HEAVE AMP	PITCH ANG	HEAVE A.	HEAVE A.	PITCH ANG	PITCH ANG	TRIM	SINKAGE	LCG MOTI
(hz)			(cm)		(cm)	(deg)	WAVE B/2	WAVE CAR	WAVE B/2	WAVE CAR	(deg)	(cm)	WAVE B/2
	B/2	B/3	B/4	CAR.									
0.40	1.838	2.053	1.966	1.932	3.094	1.158	1.683	1.601	0.630	0.599	2.781	0.109	1.755
0.45	2.206	2.368	2.330	2.345	4.268	1.132	1.935	1.820	0.513	0.483	2.859	0.145	2.014
0.50	2.647	2.842	2.767	2.773	2.431	0.315	0.918	0.877	0.119	0.114	2.781	0.109	0.961
0.55	3.015	3.158	3.058	3.091	1.404	0.272	0.466	0.454	0.090	0.008	2.755	0.159	0.489
0.60	3.382	3.632	3.422	3.391	0.964	0.523	0.285	0.284	0.155	0.154	2.676	0.145	0.299
0.70	3.639	3.910	3.939	3.802	0.531	0.822	0.146	0.140	0.226	0.216	2.830	0.091	0.153
0.80	3.713	3.830	3.712	3.225	0.209	0.606	0.056	0.065	0.163	0.188	2.922	0.145	0.058
0.90	3.713	4.069	4.015	3.568	0.157	0.536	0.042	0.044	0.144	0.150	2.817	0.055	0.042
1.00	3.936	4.229	4.091	3.536	0.000	0.377	0.000	0.000	0.096	0.107	3.001	0.127	0.000
1.10	0.000	0.000	0.000	0.000	0.000	0.000	0.000	0.000	0.000	0.000	0.000	0.000	0.000

TABLE 4-20

199.

SWATH VERTICAL MOTION TEST

SPEED V=1.5m/sec   FIN ANGLE=-4.0 DEGREE

FREQ. (hz)	WAVE AMPLITUDE (cm)				HEAVE AMP (cm)	PITCH ANG (deg)	HEAVE A. WAVE B/2	HEAVE A. WAVE CAR	PITCH ANG WAVE B/2	PITCH ANG WAVE CAR	TRIM (deg)	SINKAGE (cm)	LCG MOTI WAVE B/2
	B/2	B/3	B/4	CAR.									
0.40	1.838	2.053	1.947	1.947	1.875	0.240	0.981	0.882	0.131	0.123	2.661	0.326	1.006
0.45	2.279	2.368	2.330	2.455	2.656	0.620	1.165	1.082	0.272	0.253	3.043	0.399	1.215
0.50	2.721	2.842	2.840	2.818	1.352	0.344	0.497	0.480	0.126	0.122	2.807	0.254	0.517
0.55	3.015	3.237	3.204	3.155	1.051	0.546	0.349	0.333	0.181	0.173	2.755	0.254	0.367
0.60	3.529	3.711	3.495	3.400	0.870	0.715	0.247	0.256	0.203	0.210	2.728	0.326	0.255
0.70	3.936	4.309	4.318	3.964	0.511	0.789	0.130	0.129	0.203	0.201	2.908	0.364	0.135
0.80	3.936	3.898	3.788	3.351	0.208	0.597	0.053	0.062	0.152	0.178	3.001	0.345	0.057
0.90	3.861	4.229	4.242	3.640	0.068	0.481	0.018	0.019	0.125	0.132	3.264	0.418	0.015
1.00	4.010	4.309	4.242	3.514	0.000	0.323	0.000	0.000	0.081	0.092	3.093	0.309	0.000
1.10	0.000	0.000	0.000	0.000	0.000	0.000	0.000	0.000	0.000	0.000	0.000	0.000	0.000

TABLE 4-21

SWATH VERTICAL MOTION TEST

SPEED V=2.0m/sec   FIN ANGLE=-4.0 DEGREE

FREQ. (hz)	WAVE AMPLITUDE (cm)				HEAVE AMP (cm)	PITCH ANG (deg)	HEAVE A. WAVE B/2	HEAVE A. WAVE CAR	PITCH ANG WAVE B/2	PITCH ANG WAVE CAR	TRIM (deg)	SINKAGE (cm)	LCG MOTI WAVE B/2
	B/2	B/3	B/4	CAR.									
0.40	1.912	2.132	2.019	1.982	1.169	0.270	0.611	0.590	0.141	0.136	3.220	1.884	0.628
0.45	2.279	2.447	2.308	2.330	1.268	0.256	0.556	0.544	0.112	0.110	3.193	1.884	0.572
0.50	2.647	2.921	2.813	2.660	0.906	0.593	0.342	0.341	0.224	0.223	3.273	2.029	0.352
0.55	3.088	3.237	3.173	3.109	0.870	0.647	0.282	0.280	0.209	0.208	3.193	2.029	0.292
0.60	3.529	3.711	3.462	3.618	0.689	0.722	0.195	0.190	0.204	0.200	3.193	2.210	0.205
0.70	3.897	4.263	4.183	3.875	0.498	0.702	0.128	0.128	0.180	0.181	3.034	1.993	0.136
0.80	3.897	4.026	3.750	3.360	0.232	0.490	0.060	0.069	0.126	0.145	3.193	2.029	0.057
0.90	3.713	4.069	3.939	3.423	0.088	0.330	0.024	0.026	0.089	0.096	3.762	2.127	0.021
1.00	3.861	4.229	4.242	3.153	0.037	0.214	0.009	0.012	0.055	0.068	3.802	2.109	0.006
1.10	0.000	0.000	0.000	0.000	0.000	0.000	0.000	0.000	0.000	0.000	0.000	0.000	0.000

TABLE 4-22

SWATH VERTICAL MOTION TEST

SPEED V=0.5a/sec   FIN ANGLE= 4.0 DEGREE

FREQ. (hz)	WAVE AMPLITUDE (cm)				HEAVE AMP (cm)	PITCH ANG (des)	HEAVE A. WAVE B/2	HEAVE A. WAVE CAR	PITCH ANG WAVE B/2	PITCH ANG WAVE CAR	TRIM (des)	SINKAGE (cm)	LCG MOTI WAVE B/2
	B/2	B/3	B/4	CAR.									
0.40	1.776	2.038	1.950	1.954	2.390	1.056	1.345	1.222	0.594	0.540	-0.027	0.309	1.355
0.45	2.173	2.364	2.325	2.236	3.996	1.339	1.839	1.787	0.616	0.599	-0.090	0.282	1.877
0.50	2.602	2.771	2.700	2.493	4.842	0.791	1.861	1.942	0.304	0.317	-0.106	0.257	1.896
0.55	3.061	3.260	3.225	3.139	2.324	0.397	0.759	0.740	0.129	0.126	-0.211	0.221	0.775
0.60	3.367	3.505	3.300	3.246	1.007	0.864	0.299	0.310	0.257	0.266	-0.118	0.221	0.301
0.70	4.810	5.210	5.220	4.930	0.694	1.010	0.144	0.141	0.210	0.205	-0.092	0.146	0.136
0.80	4.520	4.500	4.560	4.420	0.591	0.800	0.131	0.134	0.177	0.181	0.053	0.109	0.128
0.90	4.740	5.130	5.000	4.745	0.435	0.780	0.092	0.092	0.165	0.164	0.000	0.054	0.088
1.00	4.950	5.370	5.150	4.818	0.192	0.650	0.039	0.040	0.131	0.135	-0.066	0.109	0.034
1.10	4.810	5.050	4.890	4.500	0.055	0.270	0.011	0.012	0.056	0.060	0.171	0.219	0.013

TABLE 4-23

SWATH VERTICAL MOTION TEST

SPEED V=1.0a/sec   FIN ANGLE= 4.0 DEGREE

FREQ. (hz)	WAVE AMPLITUDE (cm)				HEAVE AMP (cm)	PITCH ANG (des)	HEAVE A. WAVE B/2	HEAVE A. WAVE CAR	PITCH ANG WAVE B/2	PITCH ANG WAVE CAR	TRIM (des)	SINKAGE (cm)	LCG MOTI WAVE B/2
	B/2	B/3	B/4	CAR.									
0.40	1.803	2.031	2.000	2.011	2.663	0.659	1.477	1.324	0.366	0.328	-0.394	0.761	1.442
0.45	2.220	2.364	2.325	2.324	3.916	0.823	1.764	1.685	0.371	0.354	0.396	0.699	1.778
0.50	2.822	3.125	3.000	2.932	2.440	0.227	0.865	0.832	0.080	0.077	0.388	0.806	0.893
0.55	3.061	3.211	3.195	3.074	1.305	0.418	0.426	0.425	0.137	0.136	0.291	0.809	0.435
0.60	4.520	4.740	4.520	4.391	1.205	0.740	0.267	0.274	0.164	0.168	0.208	0.565	0.271
0.70	4.810	5.130	5.220	4.927	0.753	1.010	0.157	0.153	0.210	0.205	0.262	0.584	0.160
0.80	4.520	4.580	4.560	4.282	0.382	0.830	0.085	0.089	0.184	0.194	0.394	0.493	0.086
0.90	4.440	4.820	4.630	4.455	0.197	0.670	0.044	0.044	0.151	0.150	0.538	0.383	0.044
1.00	4.660	4.890	4.710	4.318	0.055	0.440	0.012	0.013	0.094	0.102	0.630	0.328	0.011
1.10	4.300	4.670	4.560	3.864	0.064	0.240	0.015	0.016	0.056	0.062	0.525	0.292	0.018

TABLE 4-24

SWATH VERTICAL MOTION TEST

SPEED V=1.5m/sec   FIN ANGLE= 4.0 DEGREE

FREQ. (hz)	WAVE			AMPLITUDE (cm)	HEAVE AMP (cm)	PITCH ANG (deg)	HEAVE A. WAVE B/2	HEAVE A. WAVE CAR	PITCH ANG WAVE B/2	PITCH ANG WAVE CAR	TRIM (deg)	SINKAGE (cm)	LCG MOTI WAVE B/2
	B/2	B/3	B/4	CAR.									
0.40	1.880	2.109	2.071	1.978	1.685	0.254	0.896	0.852	0.135	0.128	-0.682	1.007	0.864
0.45	2.163	2.344	2.286	2.345	1.289	0.433	0.596	0.550	0.200	0.185	-0.682	1.051	0.578
0.50	2.668	2.891	2.786	2.773	1.110	0.568	0.416	0.400	0.213	0.205	-0.709	1.014	0.403
0.55	3.029	3.203	3.143	3.197	0.928	0.733	0.330	0.290	0.242	0.229	-0.656	1.123	0.290
0.60	4.520	4.660	4.490	4.218	0.971	0.960	0.215	0.230	0.212	0.227	-0.604	1.168	0.215
0.70	5.030	5.370	5.370	5.055	0.710	1.070	0.141	0.140	0.213	0.212	-0.630	1.095	0.142
0.80	4.810	4.890	4.710	4.391	0.383	0.820	0.080	0.087	0.170	0.187	-0.630	0.912	0.082
0.90	4.300	4.730	4.560	3.725	0.122	0.540	0.028	0.033	0.126	0.145	-0.342	0.890	0.027
1.00	5.030	5.370	5.220	4.290	0.000	0.380	0.000	0.000	0.076	0.089	-0.355	1.000	0.000
1.10	4.440	4.730	4.480	3.673	0.085	0.200	0.019	0.023	0.045	0.054	-0.342	0.930	0.018

TABLE 4-25

SWATH VERTICAL MOTION TEST

SPEED V=2.0m/sec   FIN ANGLE= 4.0 DEGREE

FREQ. (hz)	WAVE			AMPLITUDE (cm)	HEAVE AMP (cm)	PITCH ANG (deg)	HEAVE A. WAVE B/2	HEAVE A. WAVE CAR	PITCH ANG WAVE B/2	PITCH ANG WAVE CAR	TRIM (deg)	SINKAGE (cm)	LCG MOTI WAVE B/2
	B/2	B/3	B/4	CAR.									
0.40	2.840	3.230	3.030	3.127	1.884	0.399	0.663	0.602	0.140	0.128	-1.189	2.390	0.677
0.45	3.210	3.460	3.380	3.373	1.608	0.590	0.501	0.477	0.184	0.175	-1.295	2.258	0.545
0.50	3.720	4.020	4.010	3.946	1.518	0.820	0.408	0.385	0.220	0.208	-1.295	2.174	0.420
0.55	3.860	4.170	4.080	3.825	1.087	0.840	0.282	0.284	0.218	0.219	-1.322	2.174	0.280
0.60	4.440	4.490	4.300	3.935	0.862	0.850	0.194	0.219	0.191	0.216	-1.338	2.135	0.200
0.70	4.370	4.720	4.730	4.454	0.588	0.860	0.134	0.132	0.197	0.193	-1.430	2.260	0.138
0.80	3.860	3.940	3.720	3.318	0.245	0.490	0.063	0.073	0.127	0.147	-1.312	2.262	0.062
0.90	5.030	5.440	5.260	4.180	0.146	0.430	0.029	0.035	0.005	0.102	-1.050	2.263	0.026
1.00	5.100	5.450	5.150	3.945	0.057	0.290	0.011	0.014	0.057	0.073	-1.129	2.117	0.011
1.10	0.000	0.000	0.000	0.000	0.000	0.000	0.000	0.000	0.000	0.000	0.000	0.000	0.000

TABLE 4-26
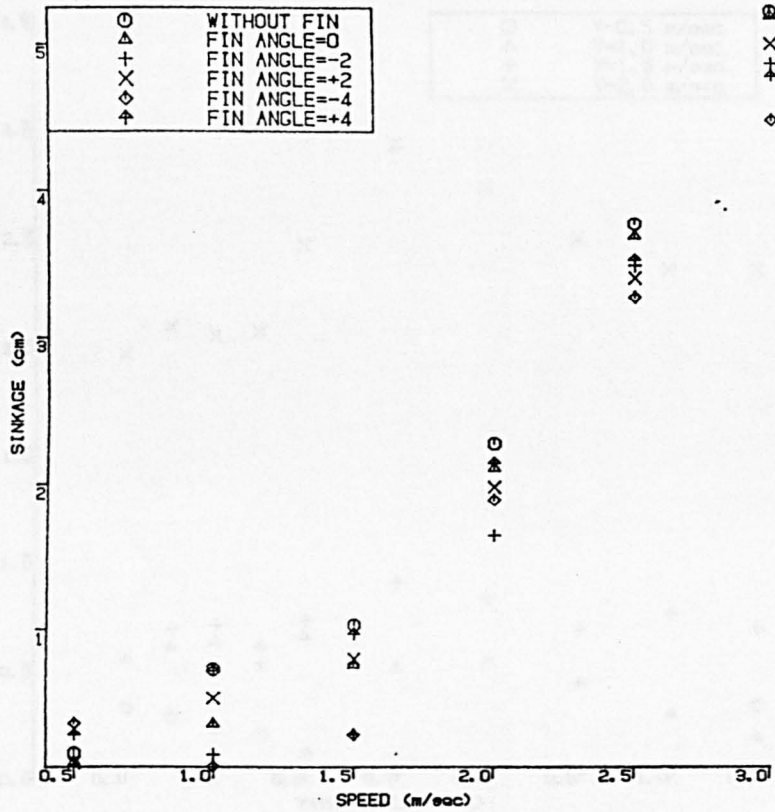
SWATH SINKAGE IN CALM WATER

Fig. 4.8
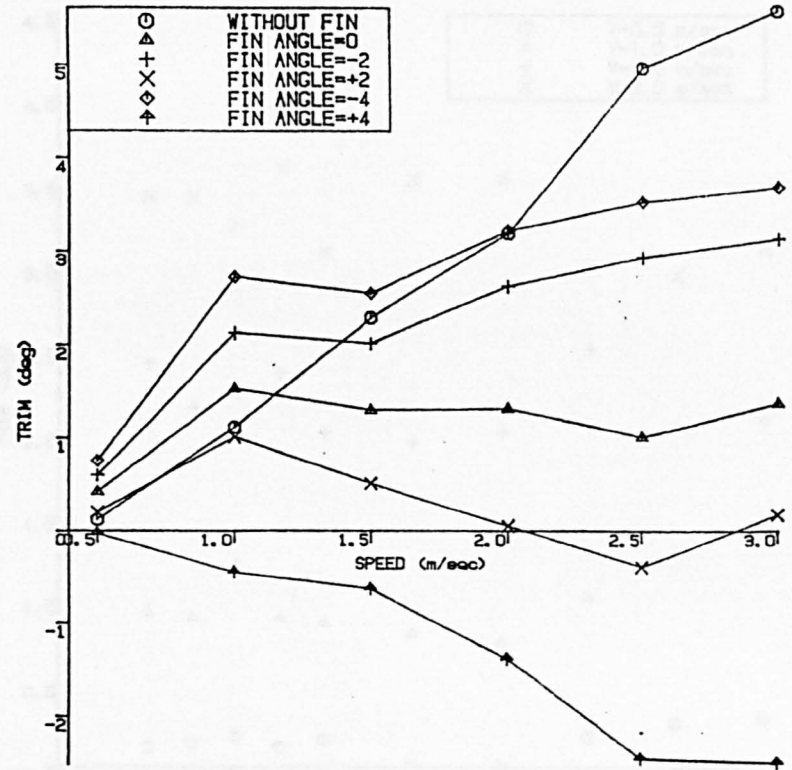
SWATH TRIM IN CALM WATER
(+) FOR BOW DOWN

Fig.4.9

202.
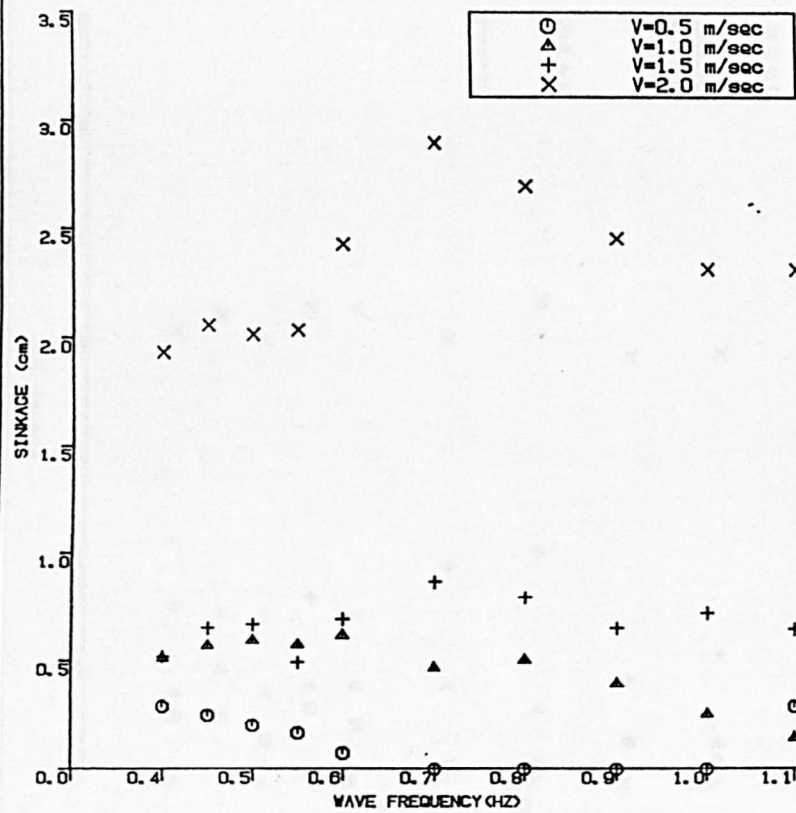
SWATH SINKAGE IN WAVES
WITHOUT FIN

Fig.4.10
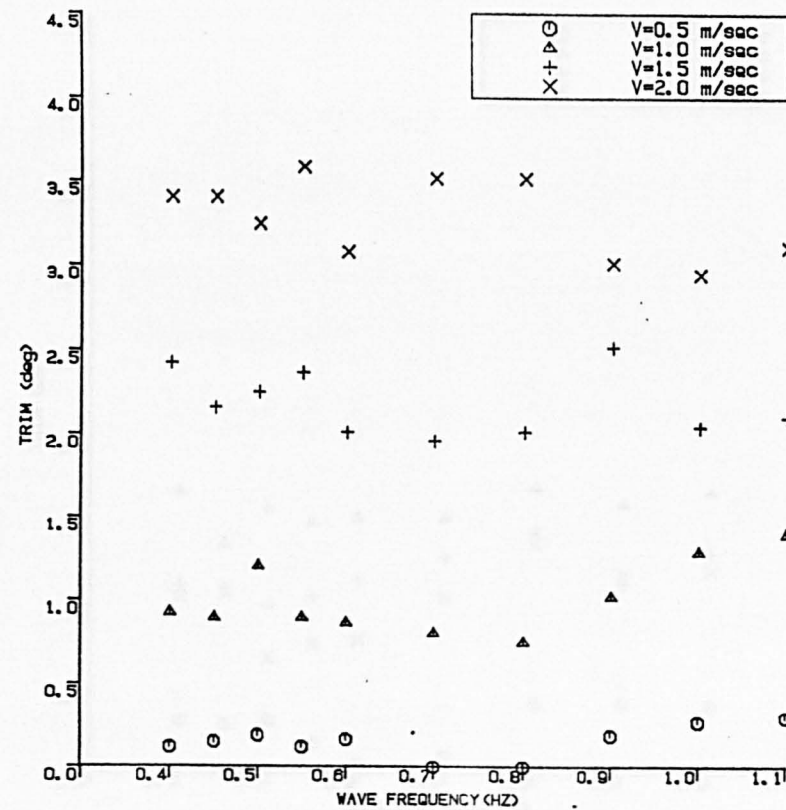
SWATH TRIM IN WAVES
·WITHOUT FIN

Fig.4·11
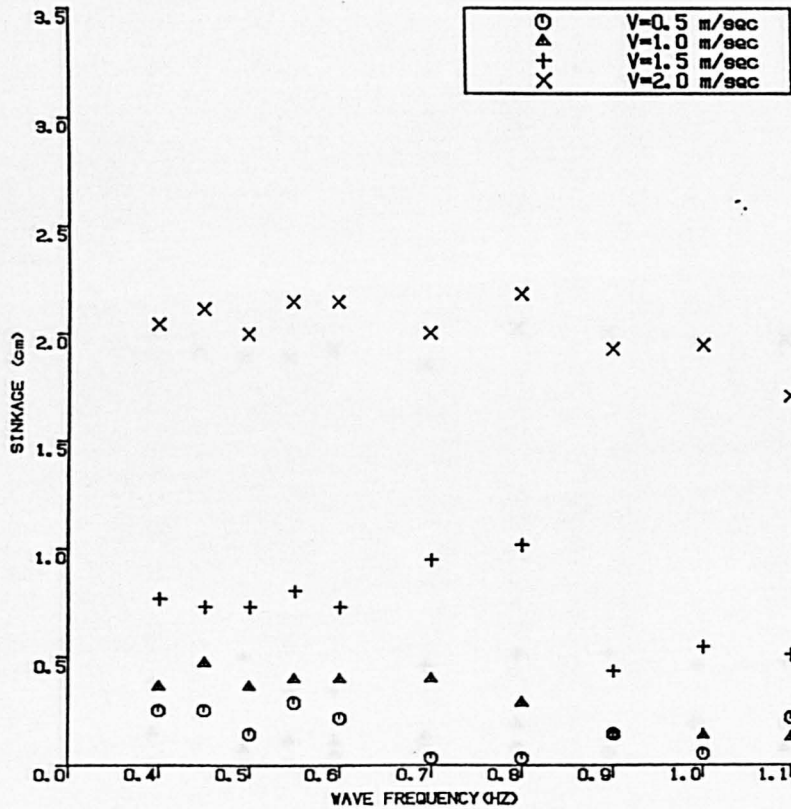
SWATH SINKAGE IN WAVES
FIN ANGLE=0.0 deg

Fig. 4.12
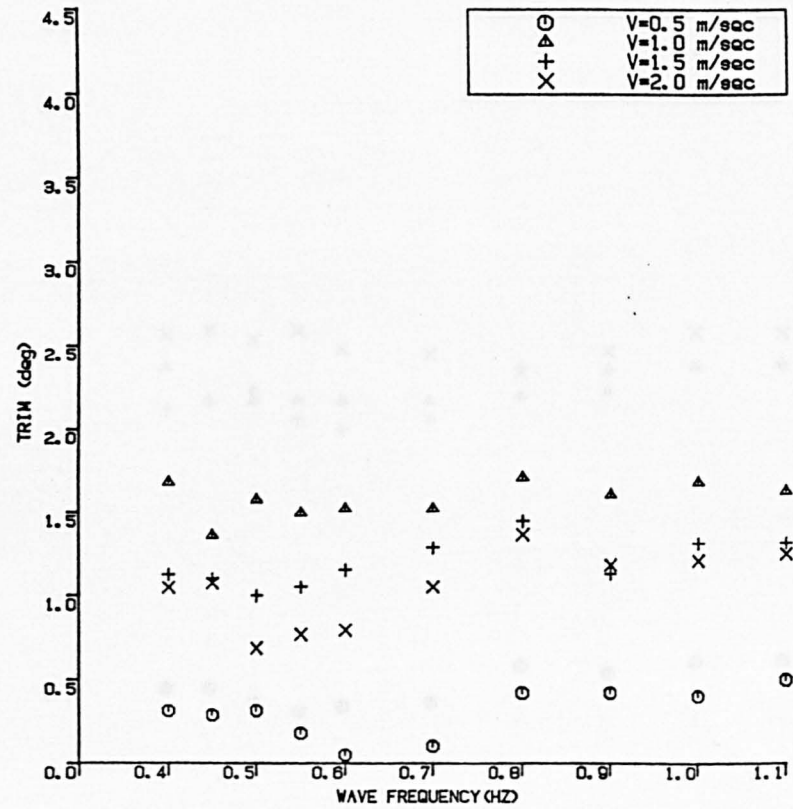
SWATH TRIM IN WAVES
FIN ANGLE=0.0 deg

Fig. 4.13
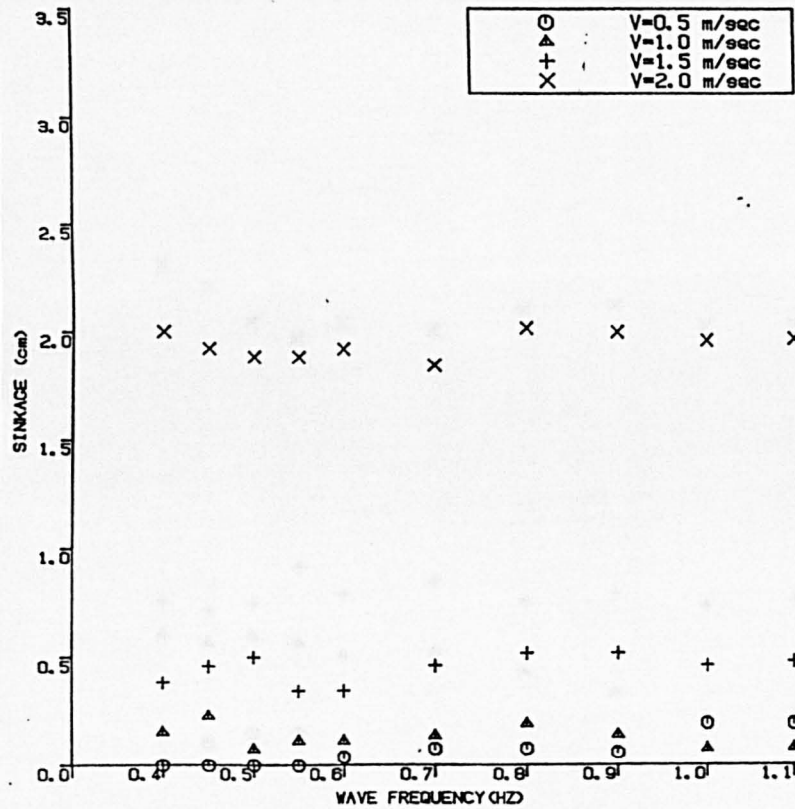
SWATH SINKAGE IN WAVES
FIN ANGLE=-2.0 deg

Fig. 4.14
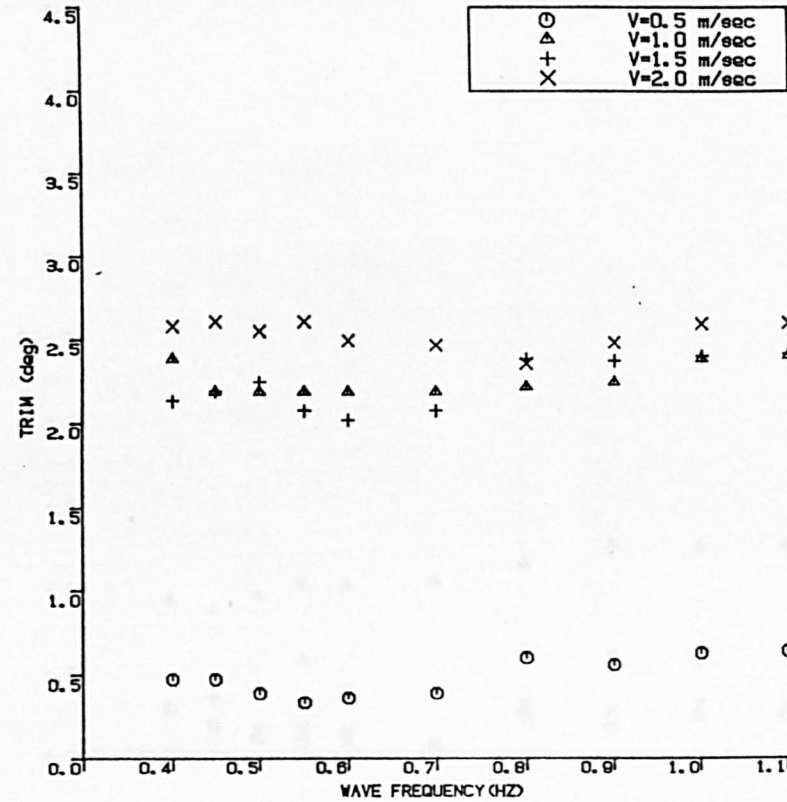
SWATH TRIM IN WAVES
FIN ANGLE=-2.0 deg

Fig. 4.15
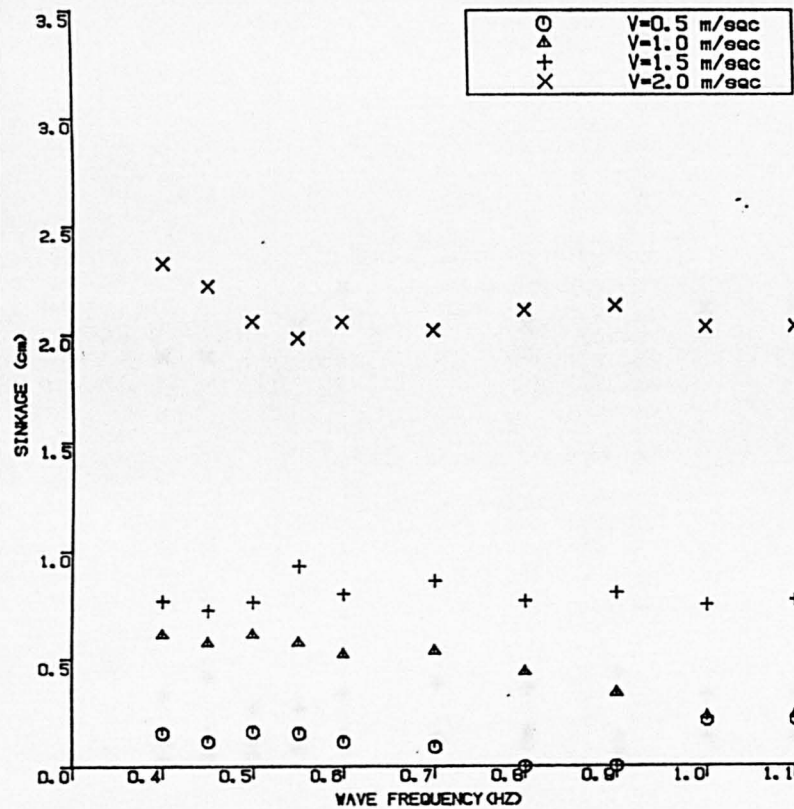
SWATH SINKAGE IN WAVES
FIN ANGLE=+2.0 deg

Fig.4.16
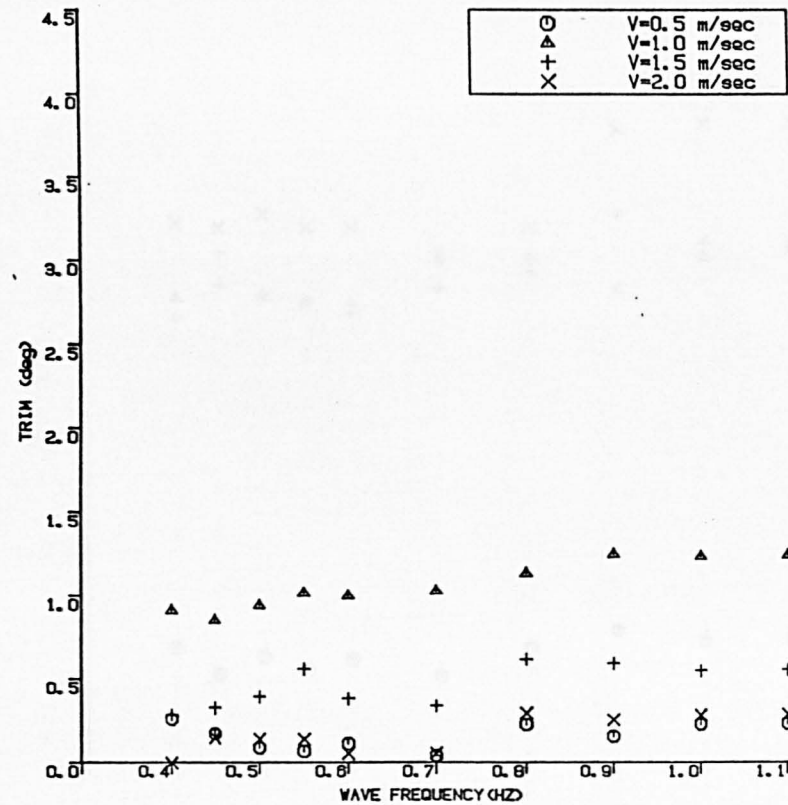
SWATH TRIM IN WAVES
FIN ANGLE=+2.0 deg

Fig.4.17
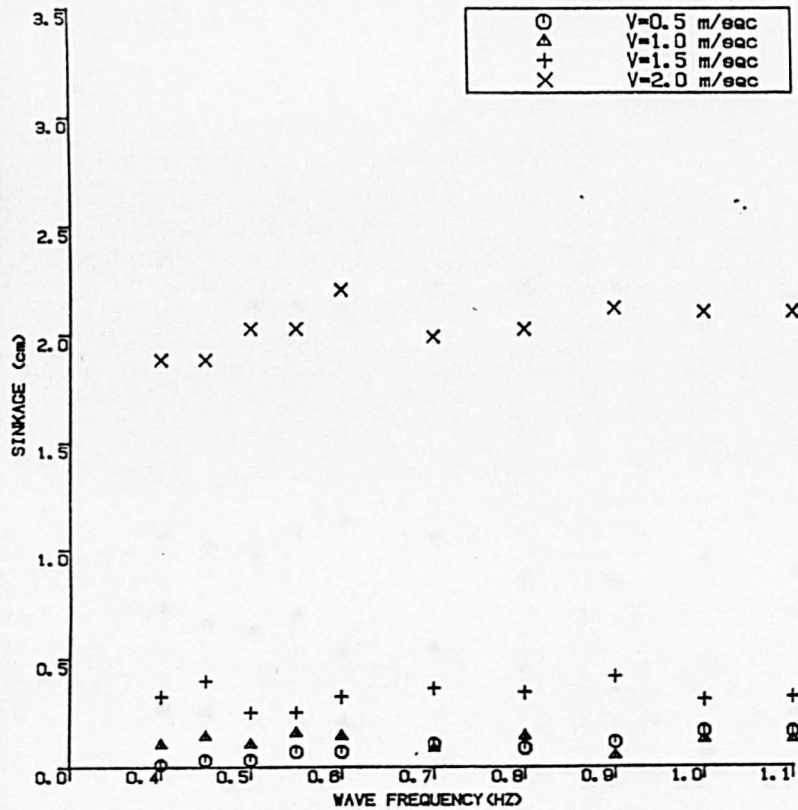
SWATH SINKAGE IN WAVES
FIN ANGLE=-4.0 deg

Fig.4.18
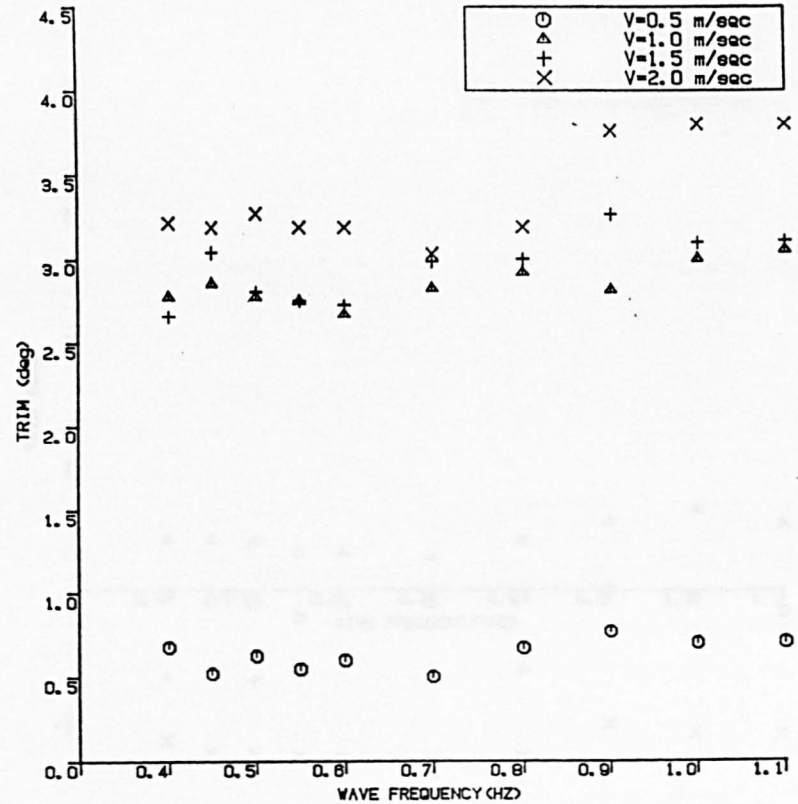
SWATH TRIM IN WAVES
FIN ANGLE=-4.0 deg

Fig.4.19
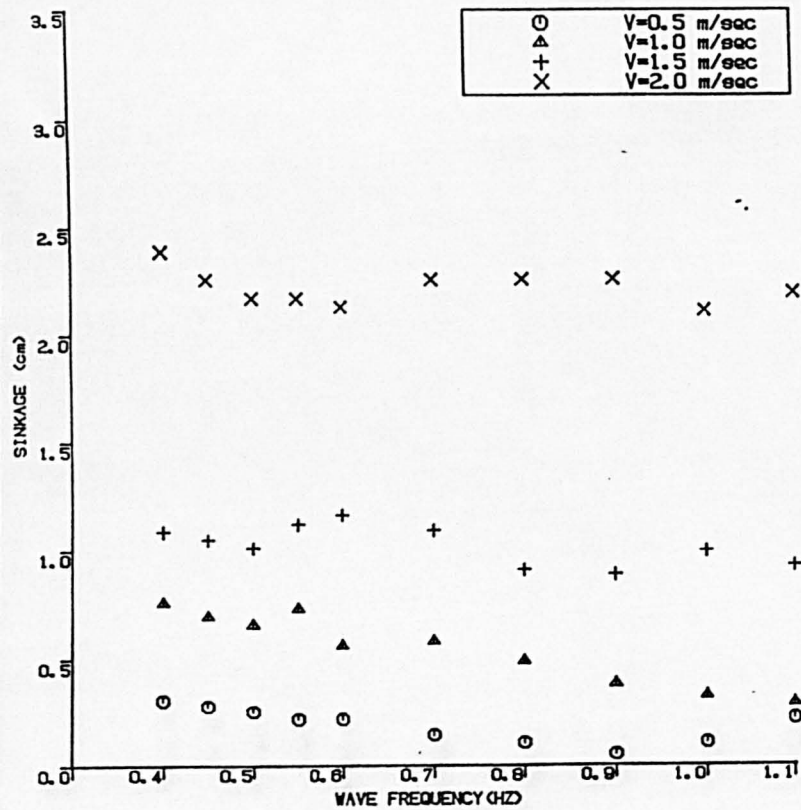
SWATH SINKAGE IN WAVES
FIN ANGLE=+4.0 deg

Fig. 4·20
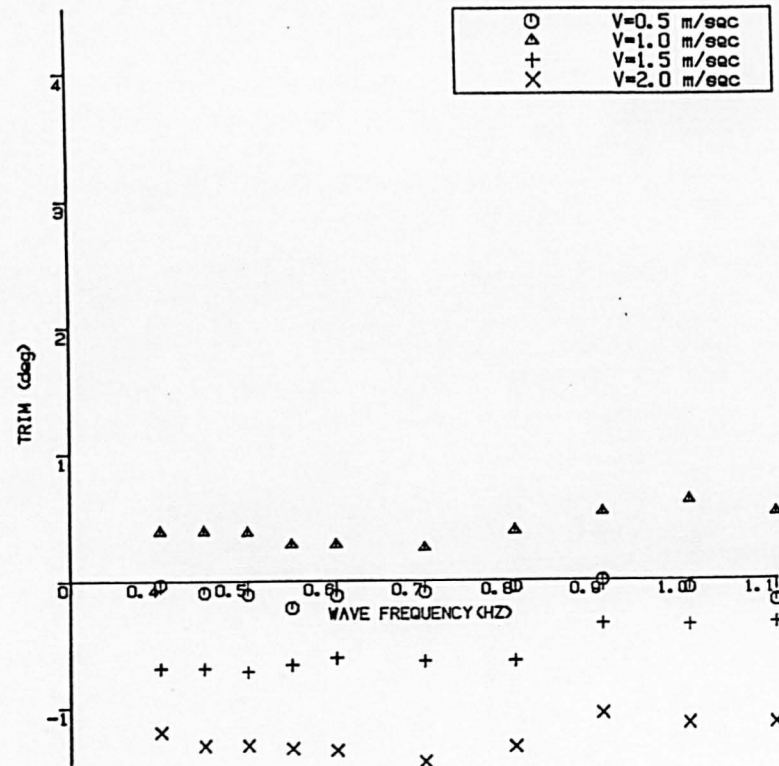
SWATH TRIM IN WAVES
FIN ANGLE=+4.0 deg

Fig. 4·21
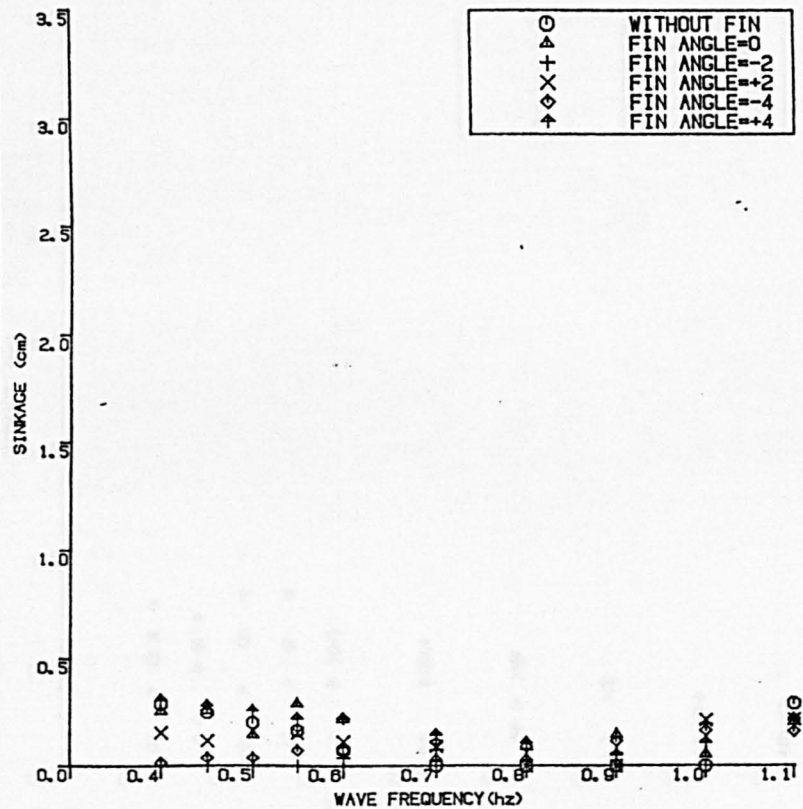
SWATH SINKAGE IN WAVES
SPEED V=0.5 m/sec

Fig. 4.22
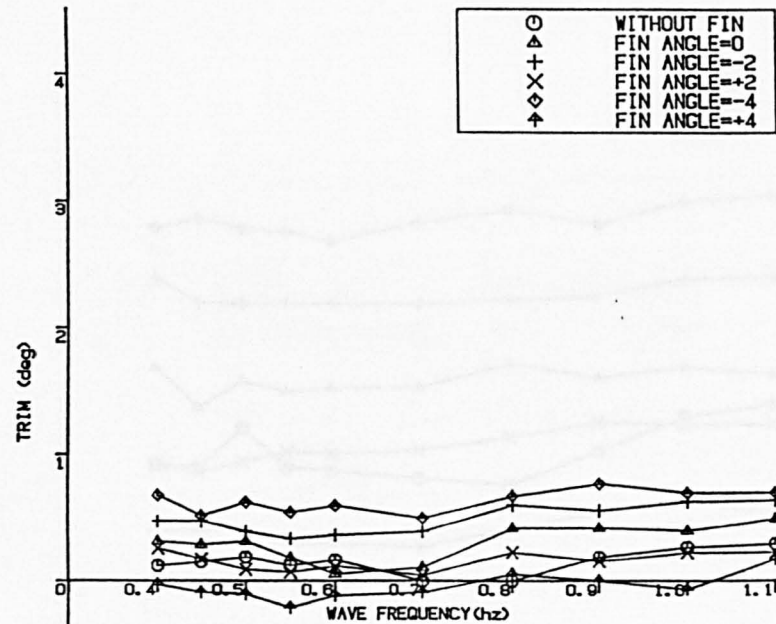
SWATH TRIM IN WAVES
SPEED V=0.5 m/sec

Fig. 4.23
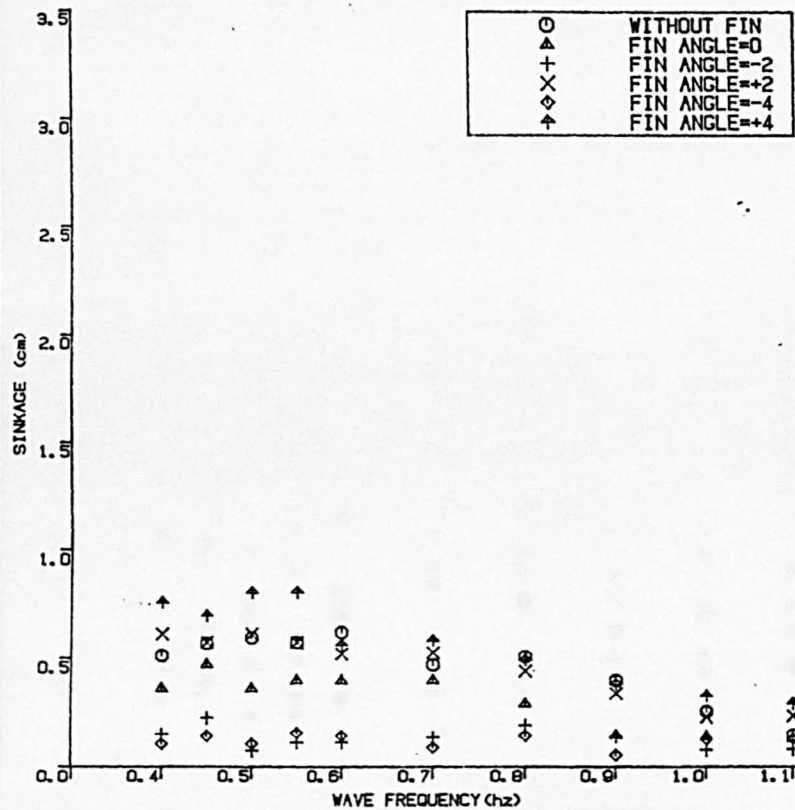
SWATH SINKAGE IN WAVES
SPEED V=1.0 m/sec

Fig. 4.24
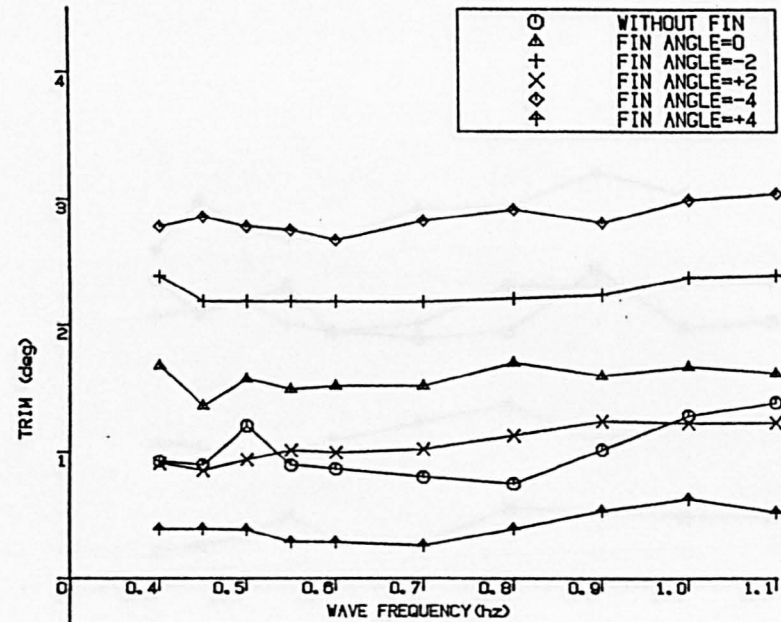
SWATH TRIM IN WAVES
SPEED V=1.0 m/sec

Fig. 4.25
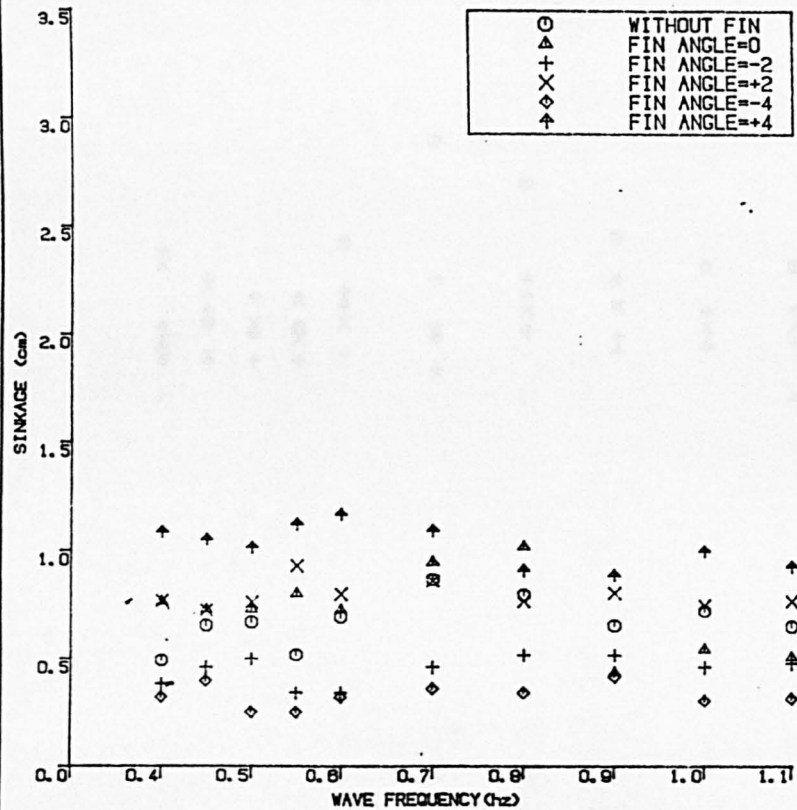
SWATH SINKAGE IN WAVES
SPEED V=1.5 m/sec

Fig. 4·26
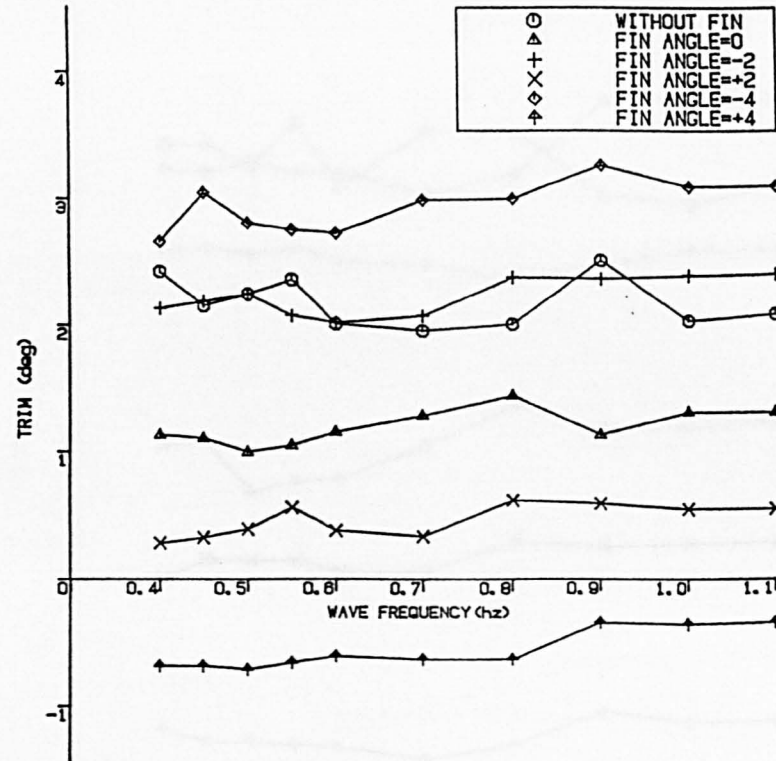
SWATH TRIM IN WAVES
SPEED V=1.5 m/sec

Fig. 4·27
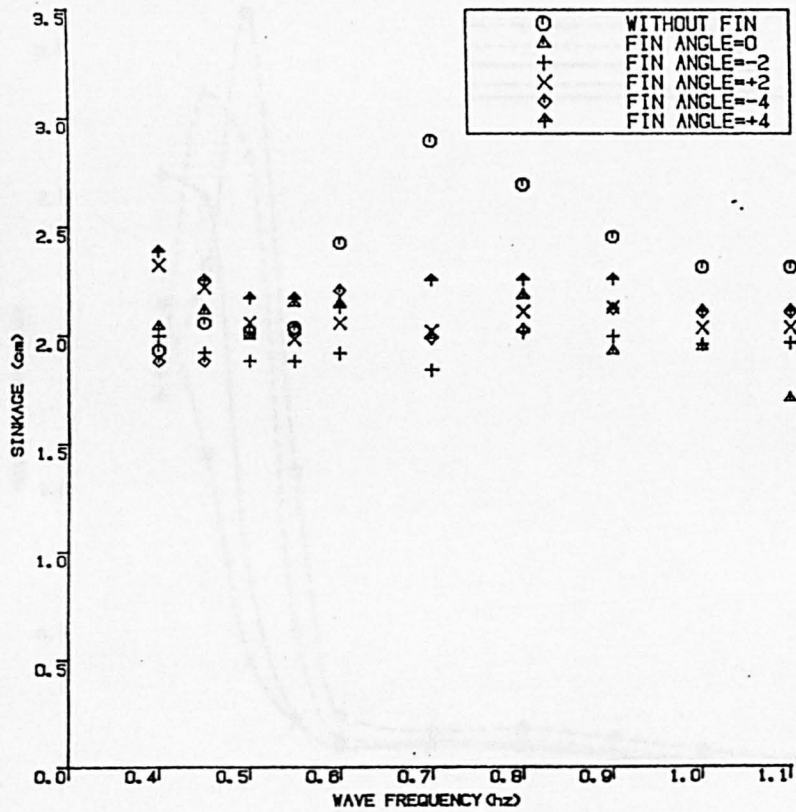
SWATH SINKAGE IN WAVES
SPEED V=2.0 m/sec

Fig. 4.28
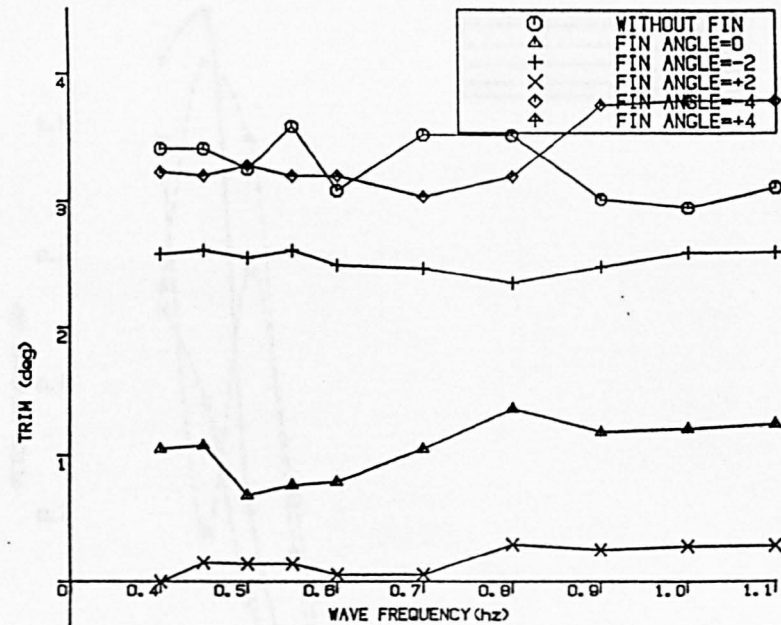
SWATH TRIM IN WAVES
SPEED V=2.0 m/sec

Fig. 4.29
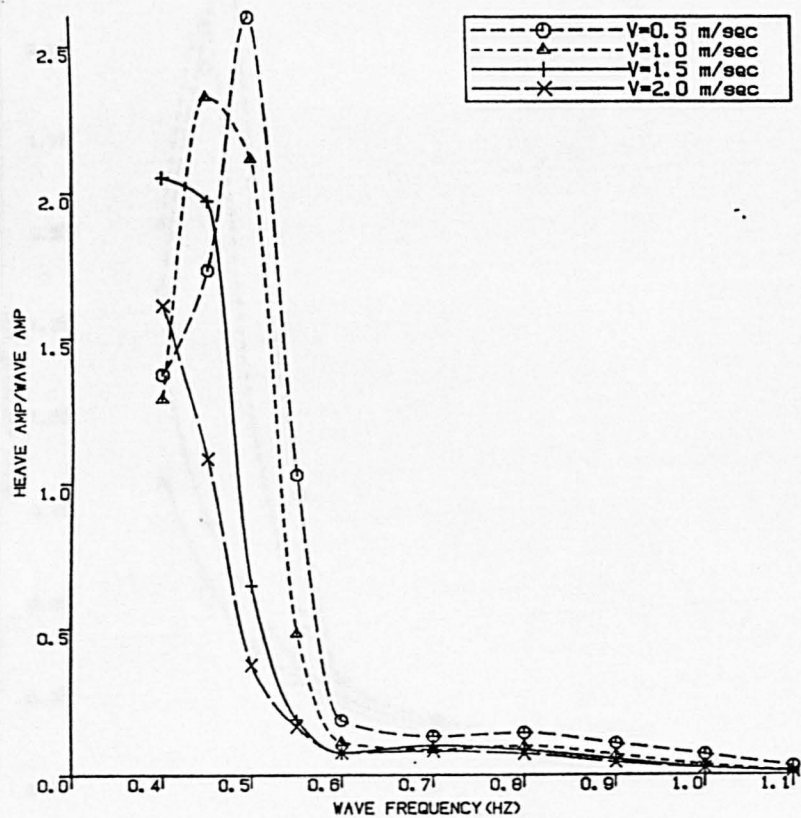
SWATH HEAVE MOTION TEST
WITHOUT FIN

Fig. 4.30
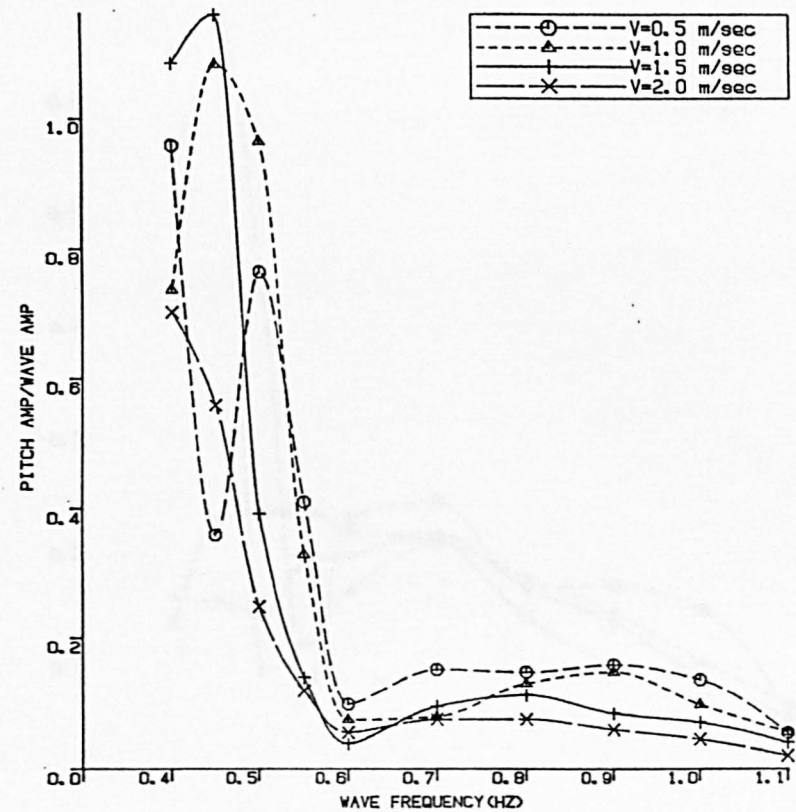
SWATH PITCH MOTION TEST
WITHOUT FIN

Fig. 4.31
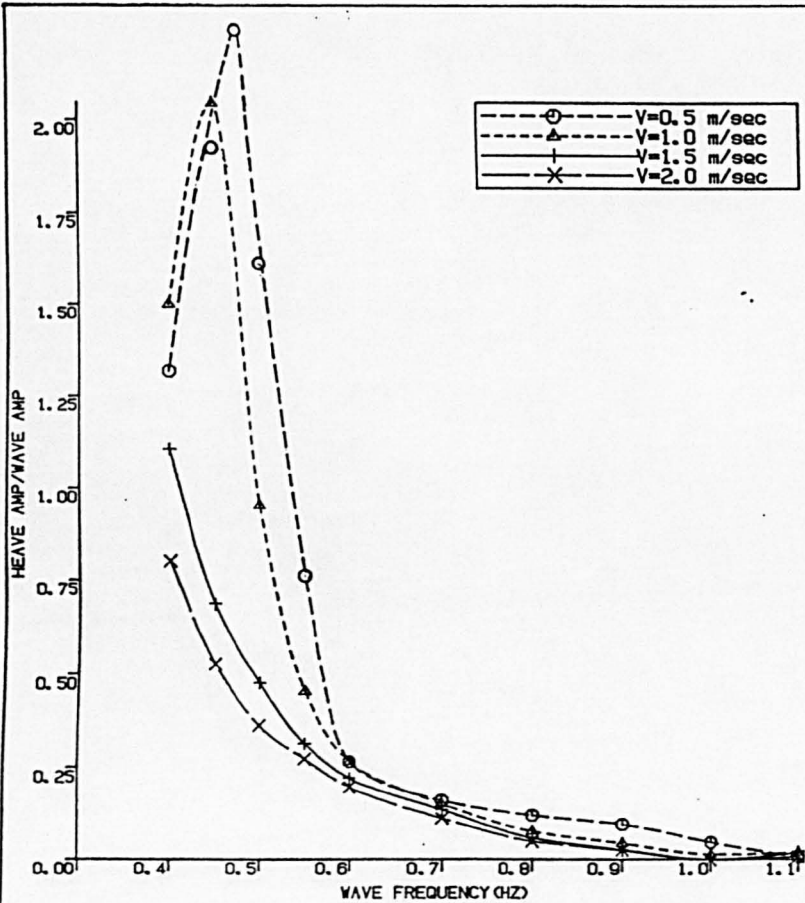
SWATH HEAVE MOTION TEST
FIN ANGLE=0. 0 deg

Fig. 4.32
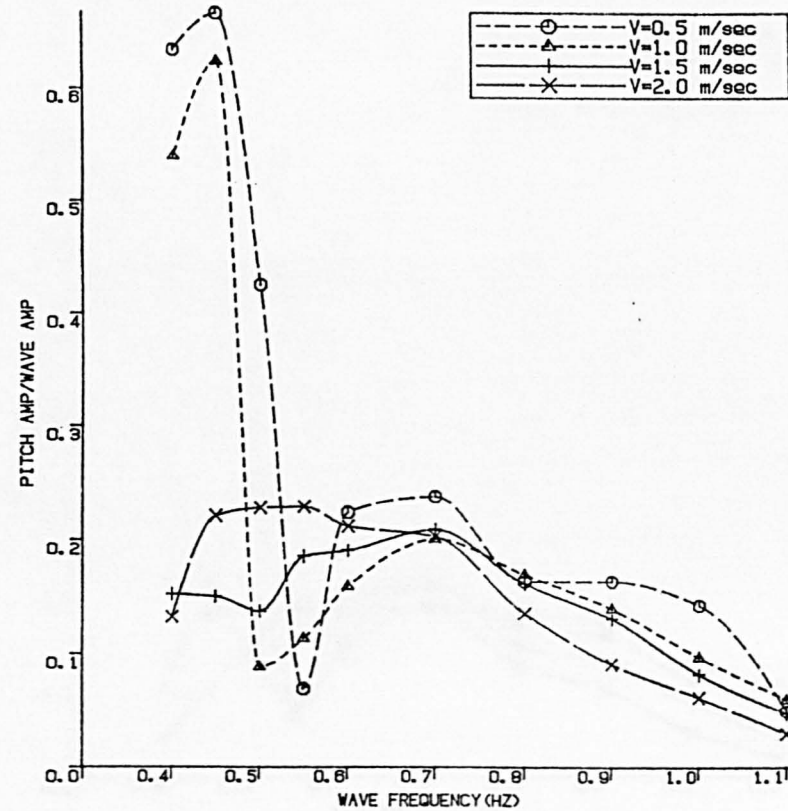
SWATH PITCH MOTION TEST
FIN ANGLE=0. 0

Fig.4.33

214.
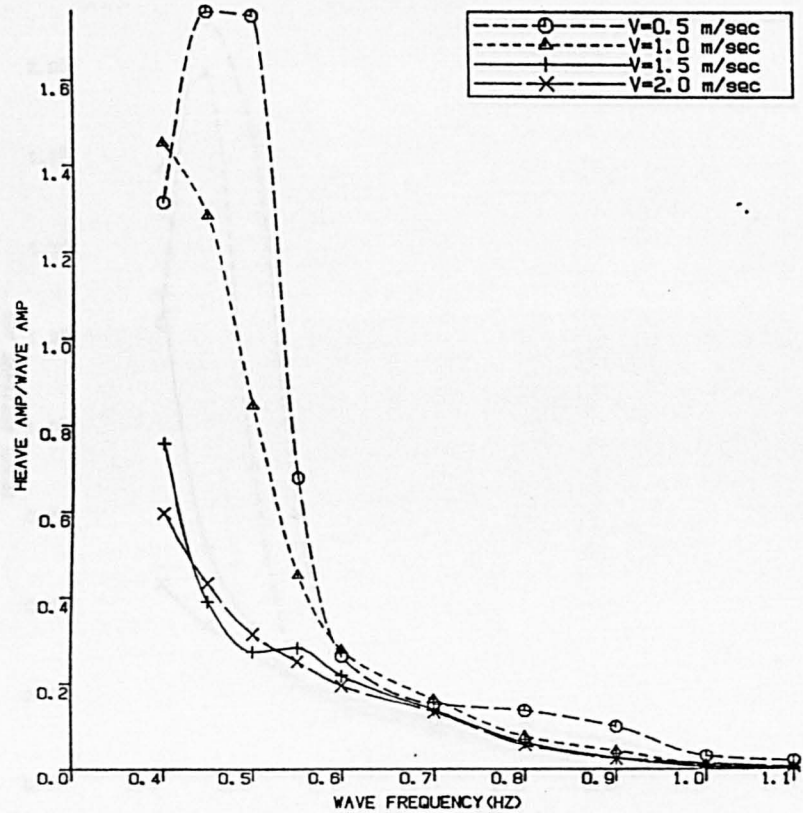
SWATH HEAVE MOTION TEST
FIN ANGLE=-2.0 deg

Fig. 4.34
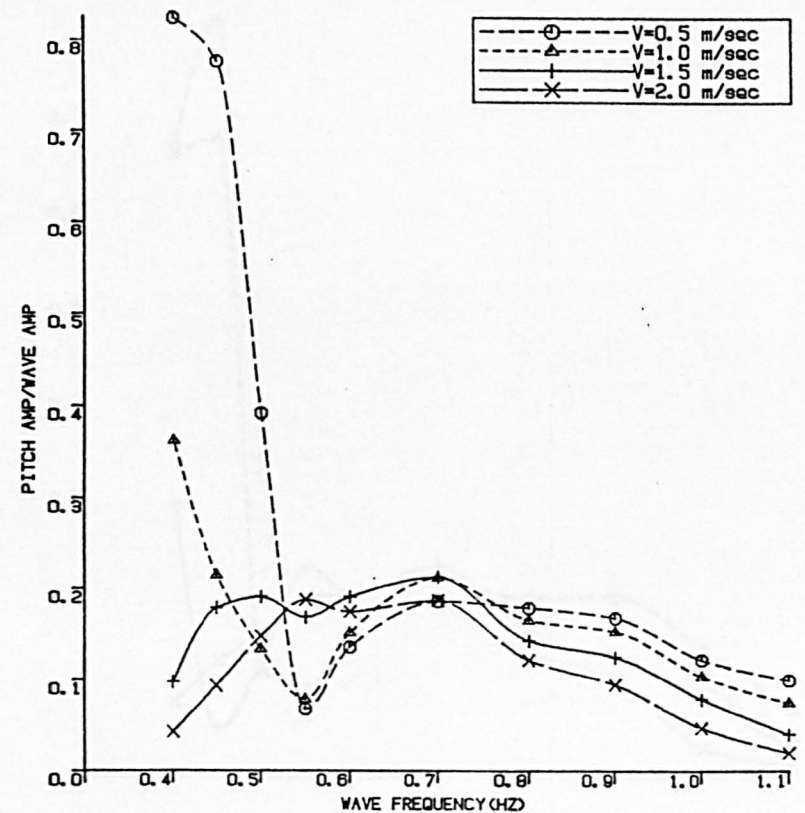
SWATH PITCH MOTION TEST
FIN ANGLE=-2.0 deg

Fig.4.35
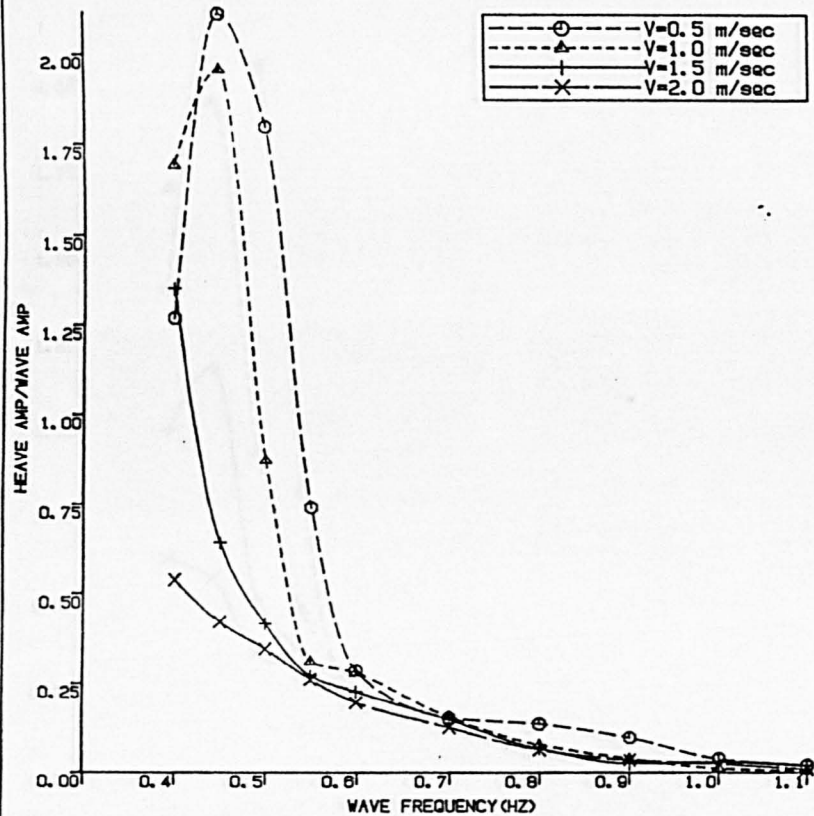
SWATH HEAVE MOTION TEST
FIN ANGLE=+2.0 deg

Fig. 4.36
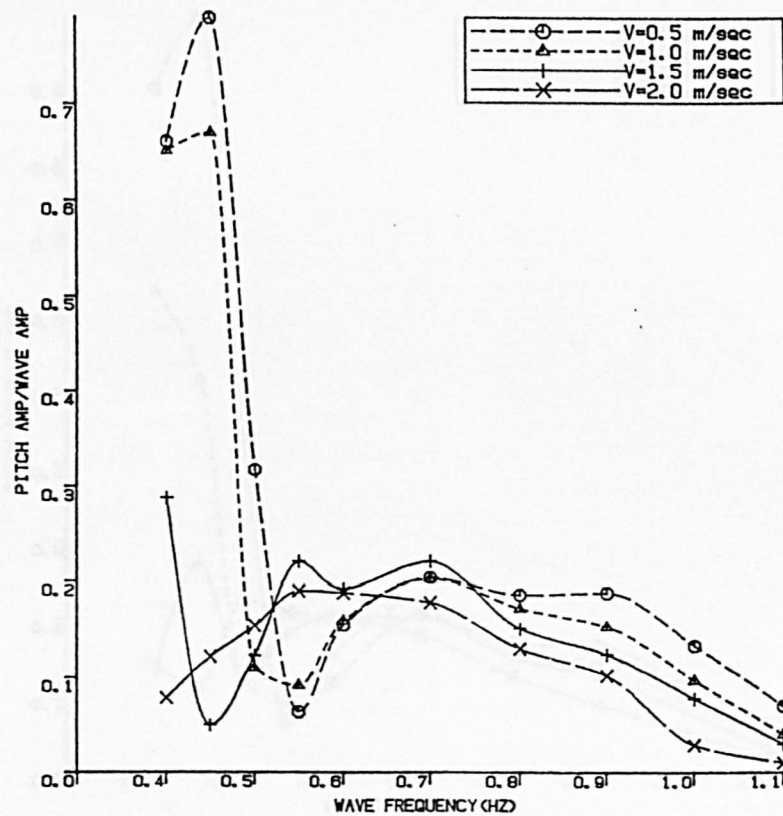
SWATH PITCH MOTION TEST
FIN ANGLE=+2.0 deg

Fig. 4.37
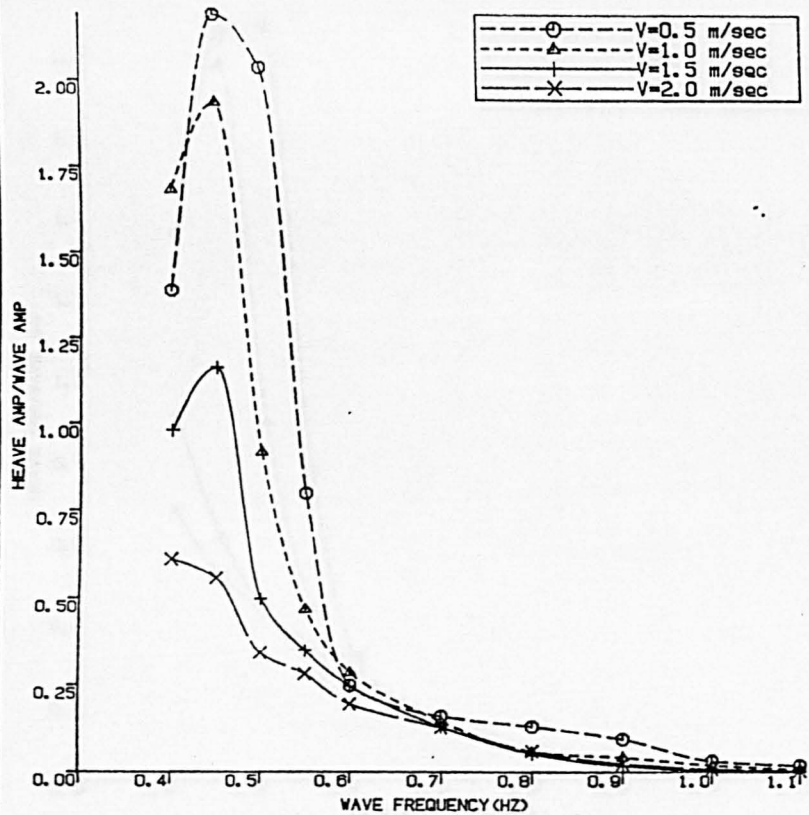
SWATH HEAVE MOTION TEST
FIN ANGLE=-4.0 deg

Fig. 4.38
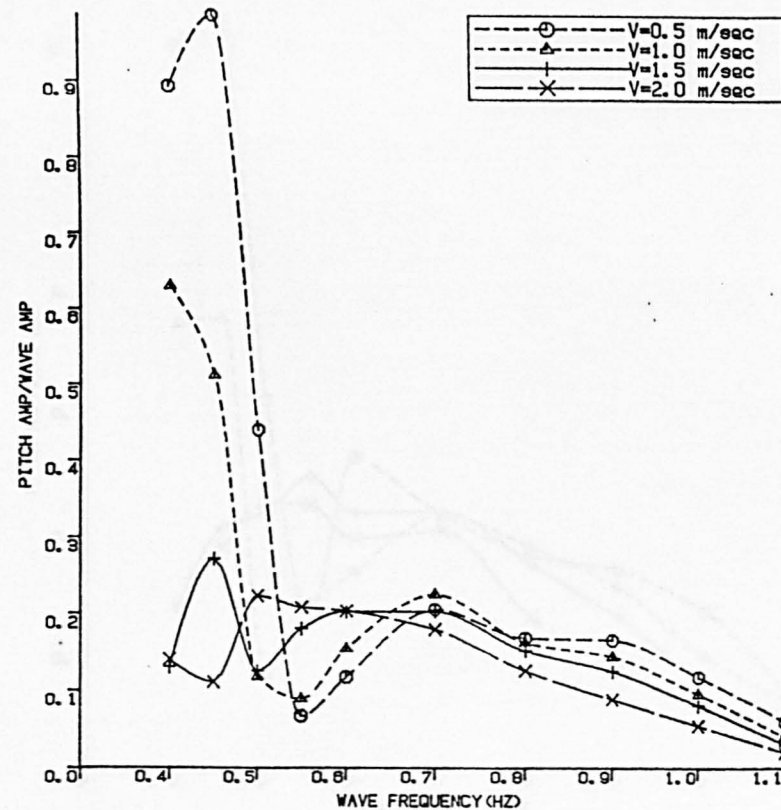
SWATH PITCH MOTION TEST
FIN ANGLE=-4.0 deg

Fig. 4.39

217.
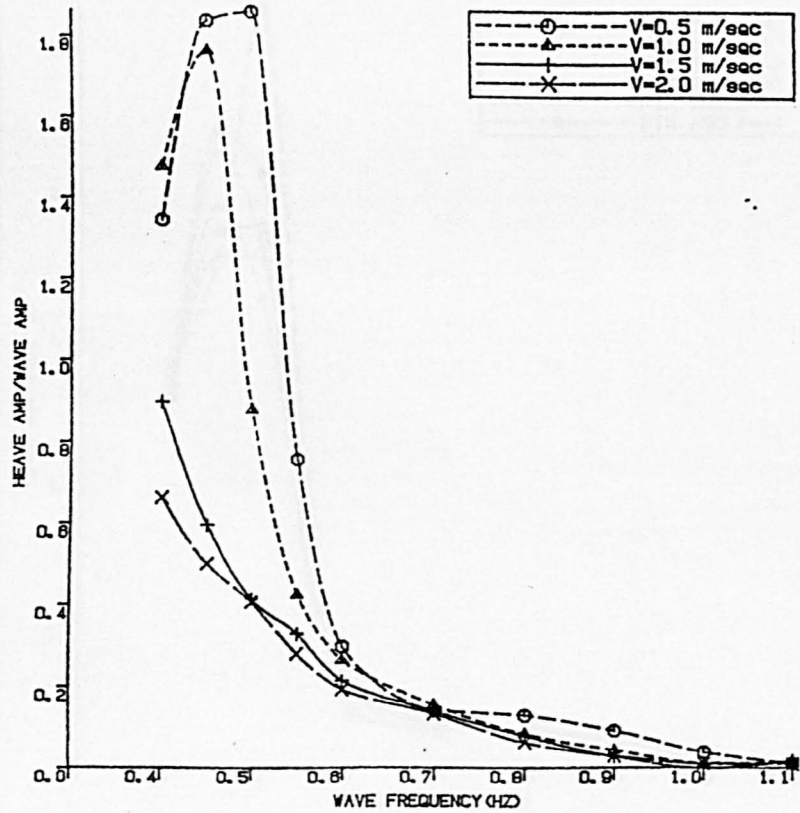
SWATH HEAVE MOTION TEST
FIN ANGLE=+4

Fig. 4.40
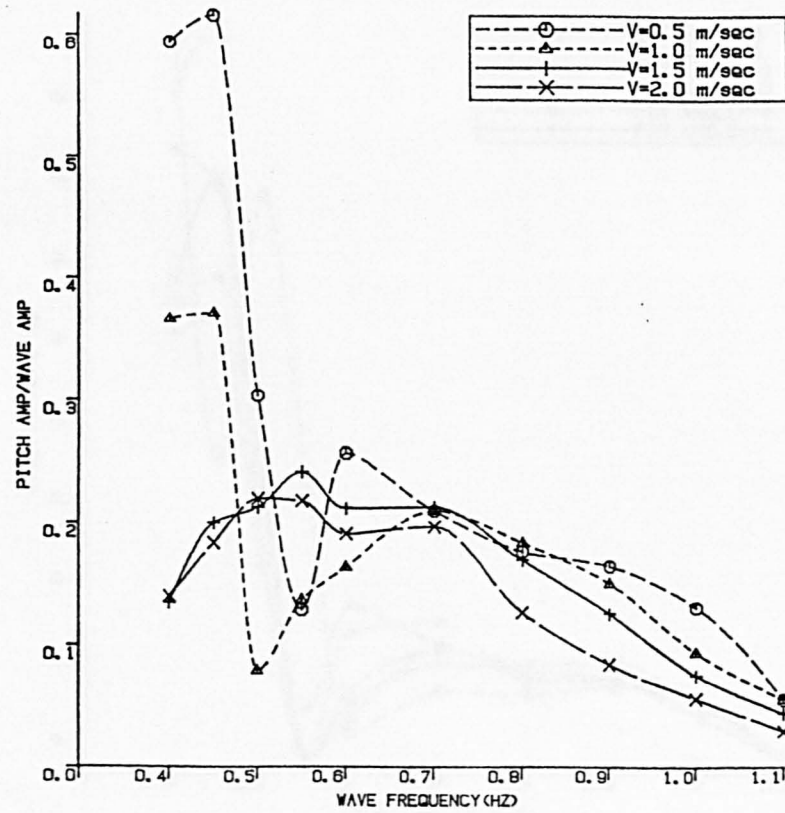
SWATH PITCH MOTION TEST
FIN ANGLE=+4.0 deg

Fig. 4.41
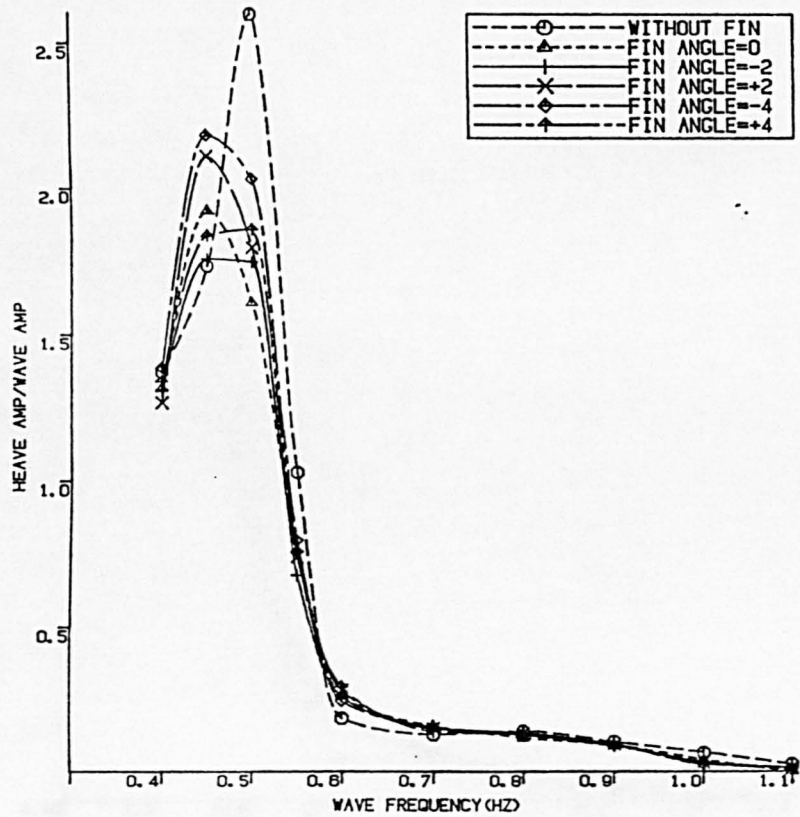
SWATH HEAVE MOTION TEST
SPEED V=0.5 m/sec

Fig. 4.42
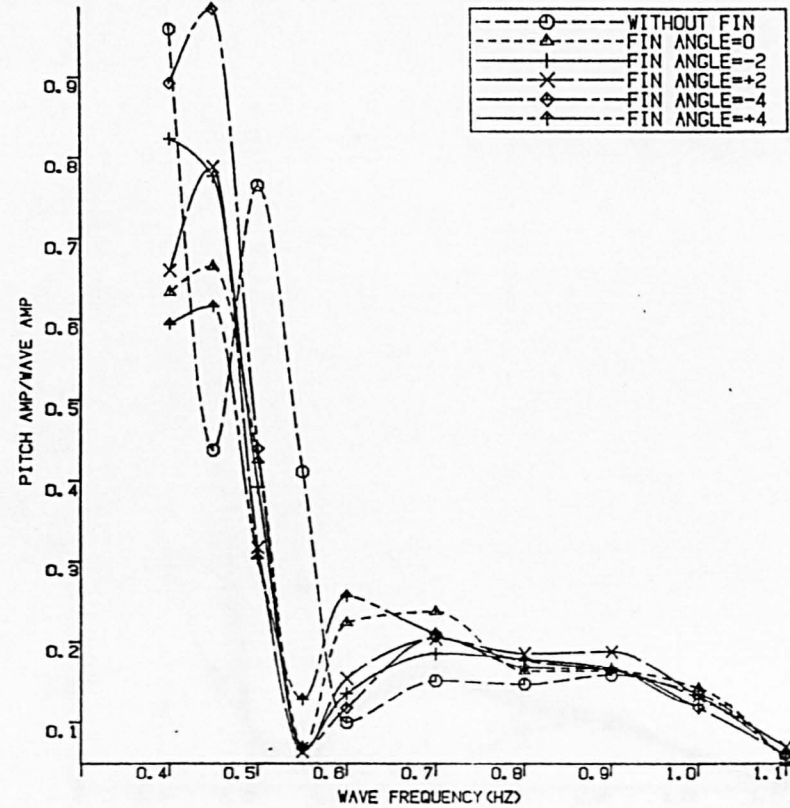
SWATH PITCH MOTION TEST
SPEED V=0.5 m/sec

Fig. 4.43
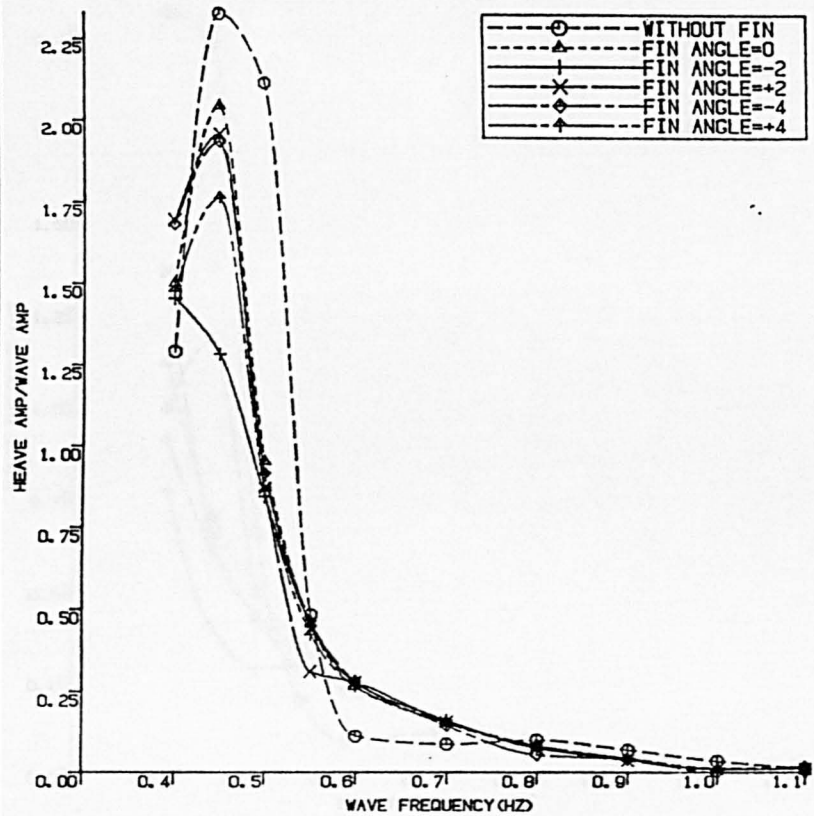
SWATH HEAVE MOTION TEST
SPEED V=1.0 m/sec

Fig. 4.44
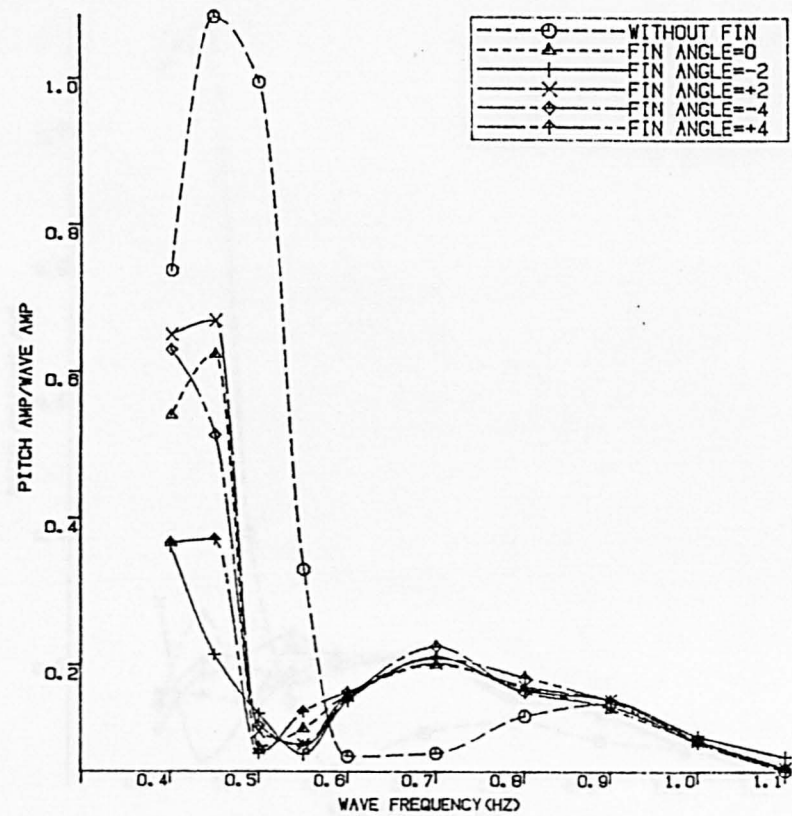
SWATH PITCH MOTION TEST
SPEED V=1.0 m/sec

Fig. 4.45
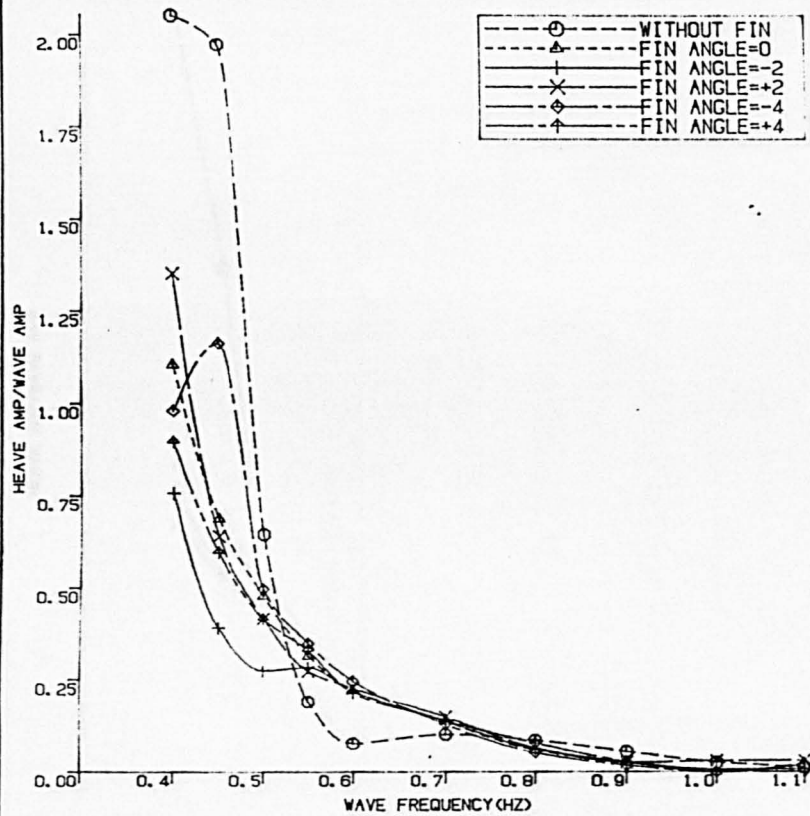
SWATH HEAVE MOTION TEST
SPEED V=1.5 m/sec

Fig. 4.46
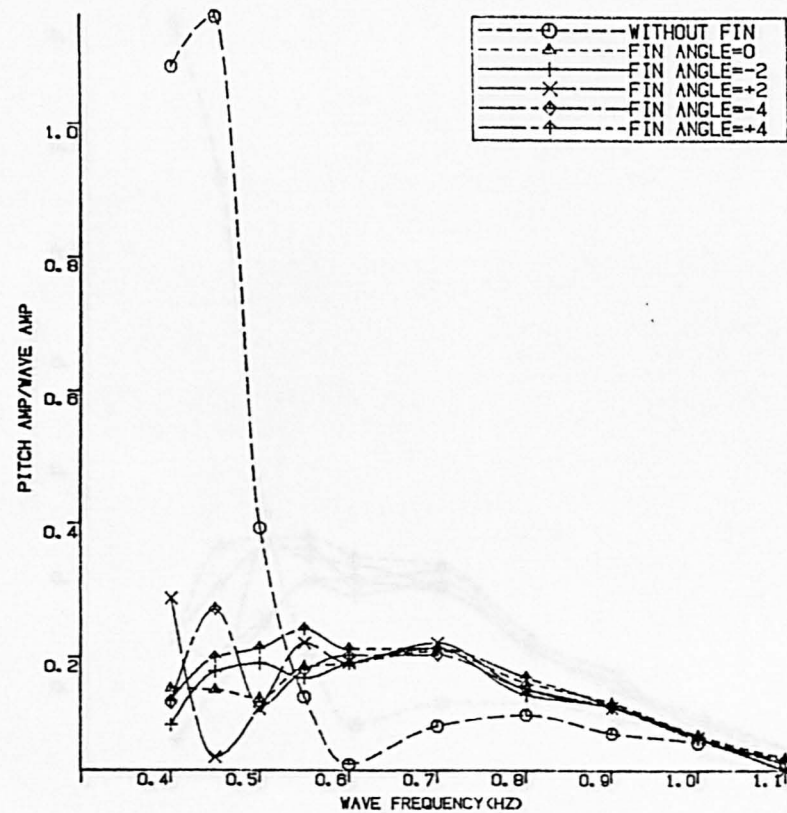
SWATH PITCH MOTION TEST
SPEED V=1.5 m/sec

Fig. 4.47
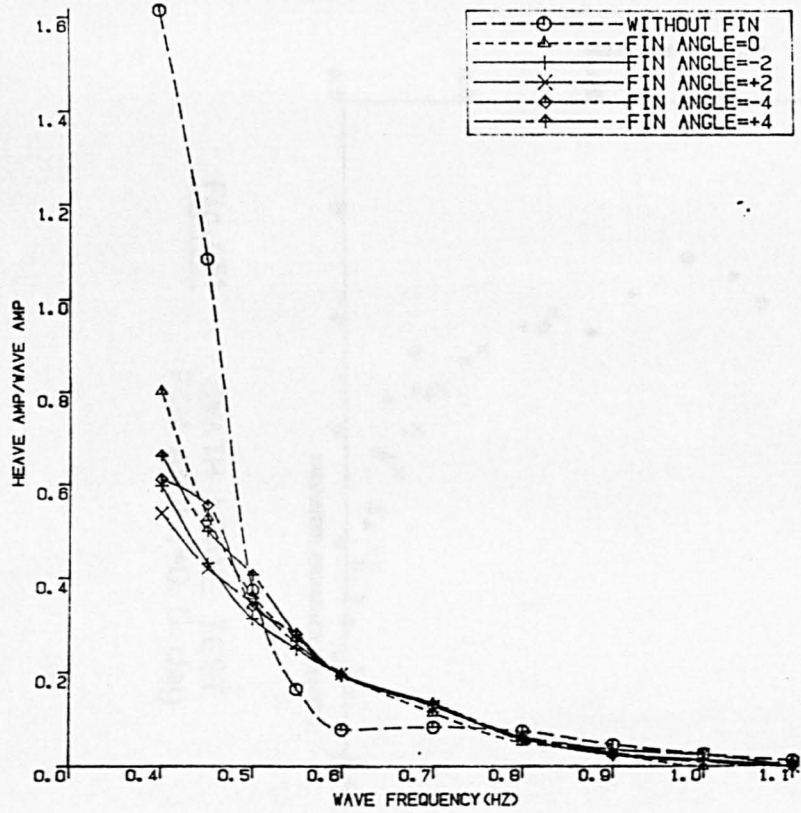
SWATH HEAVE MOTION TEST
SPEED V=2.0 m/sec

Fig. 4.48
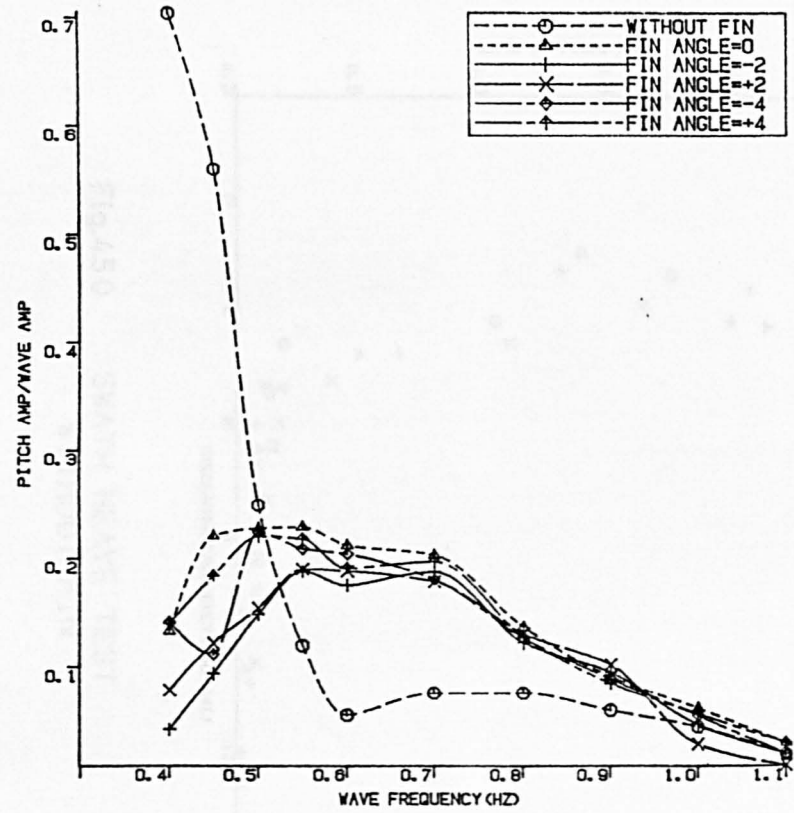
SWATH PITCH MOTION TEST
SPEED V=2.0 m/sec

Fig. 4.49
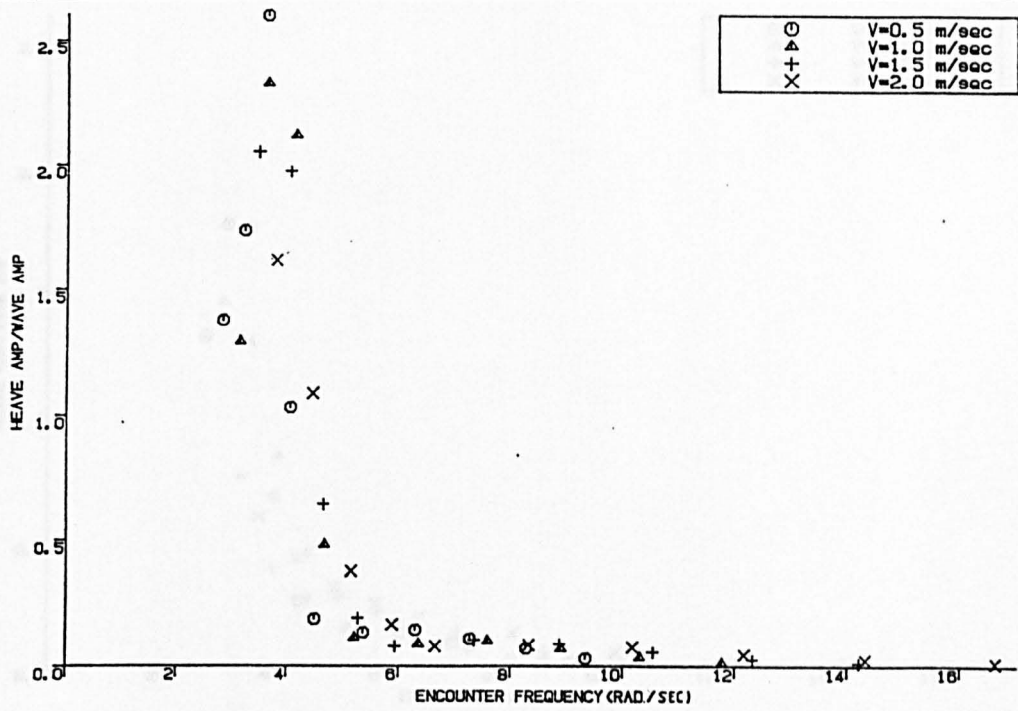
Fig.4.50   SWATH HEAVE TEST
WITHOUT FIN
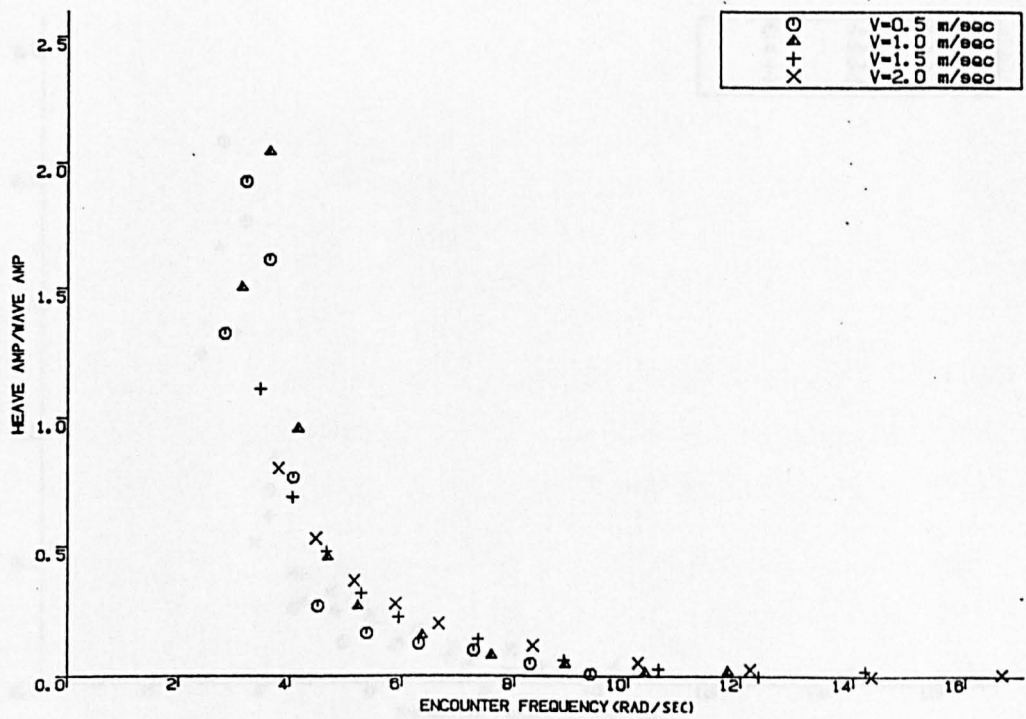
Fig.4.51   SWATH HEAVE TEST
FIN ANGLE=0.0 deg
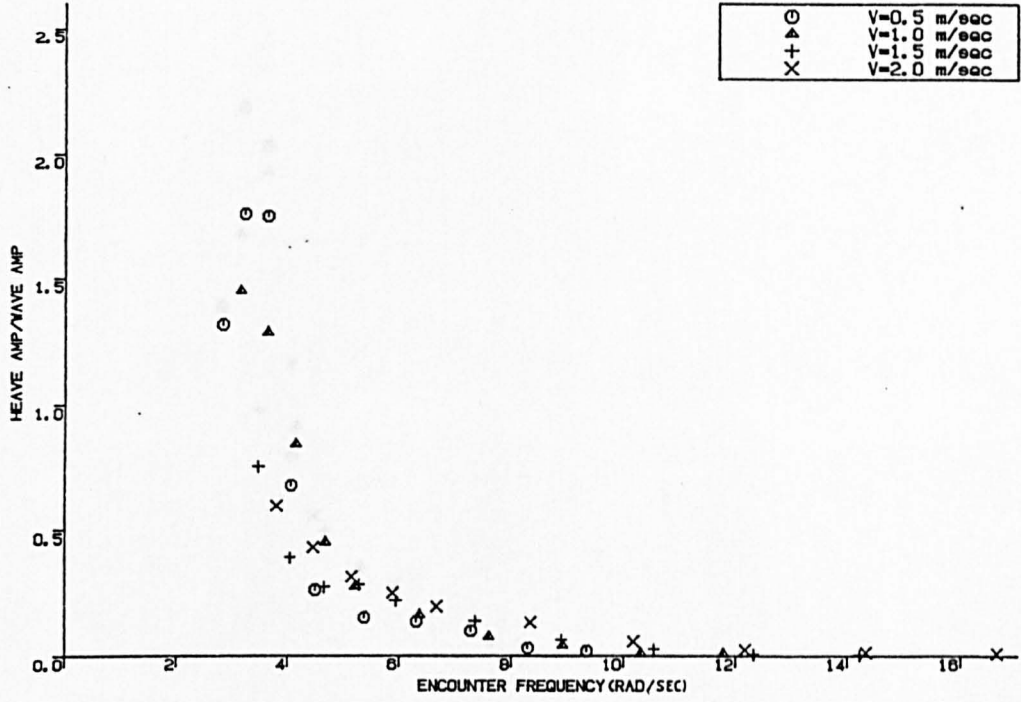
Fig.4.52   SWATH HEAVE TEST
FIN ANGLE=-2.0 deg
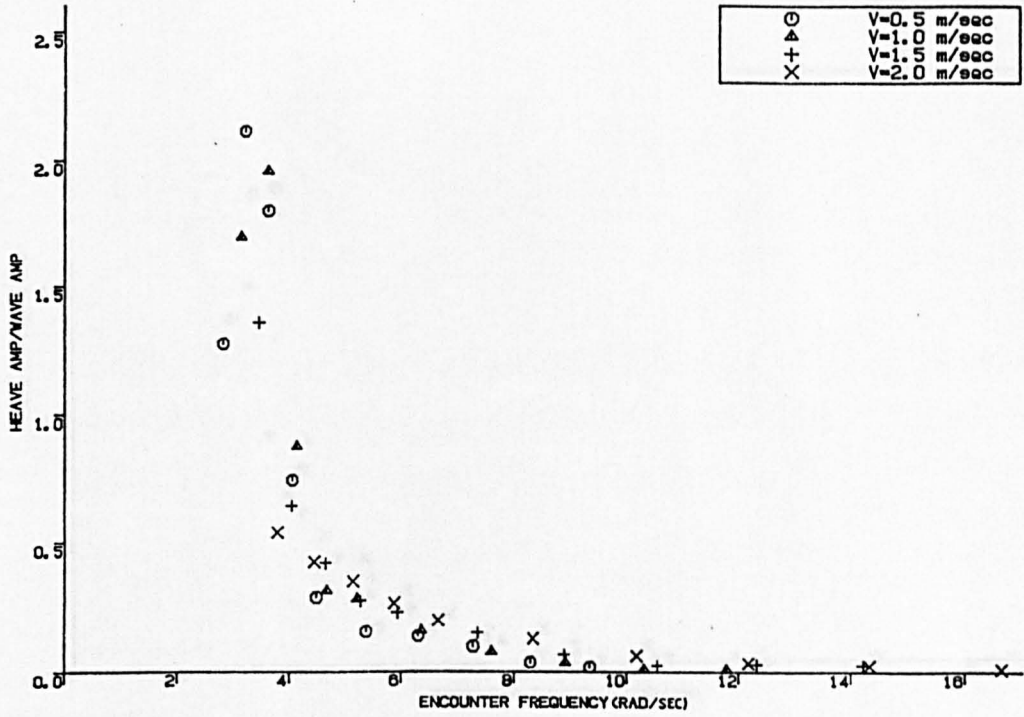
Fig. 4.53   SWATH HEAVE TEST
FIN ANGLE=+2.0 deg
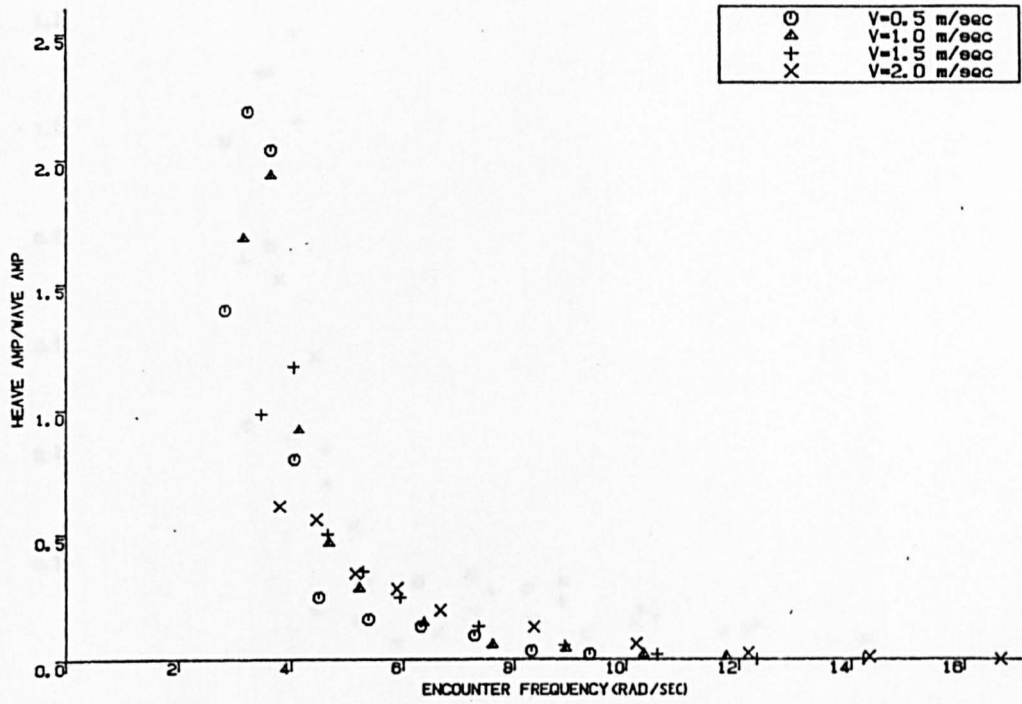
Fig.4.54   SWATH HEAVE TEST
FIN ANGLE=-4.0 deg
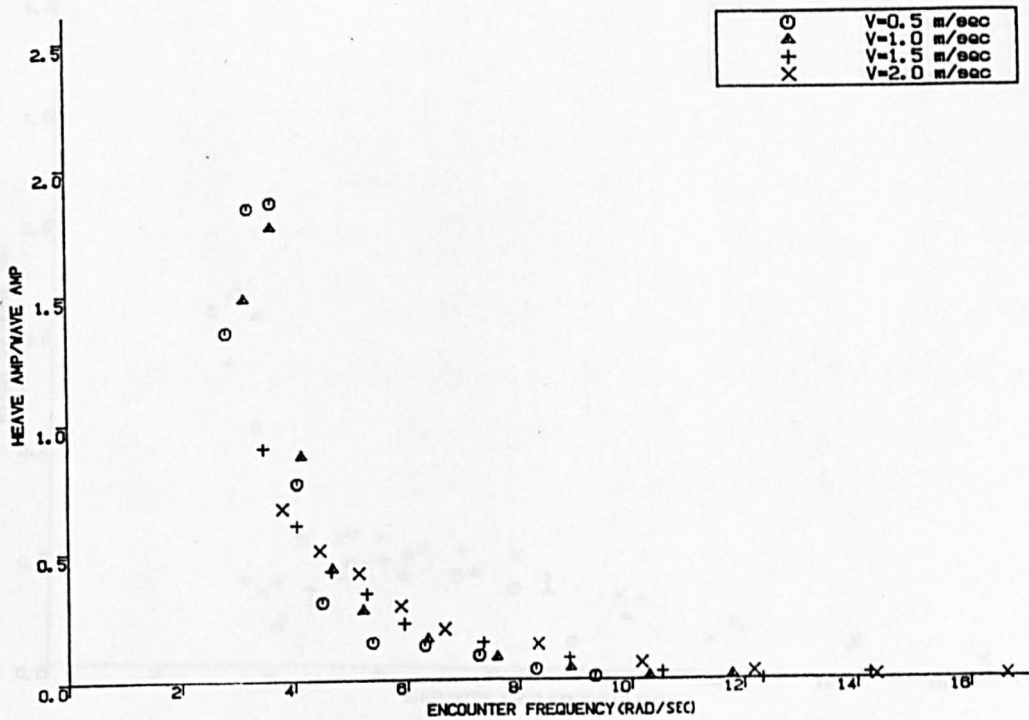
Fig.4.55   SWATH HEAVE TEST
FIN ANGLE=+4.0 deg
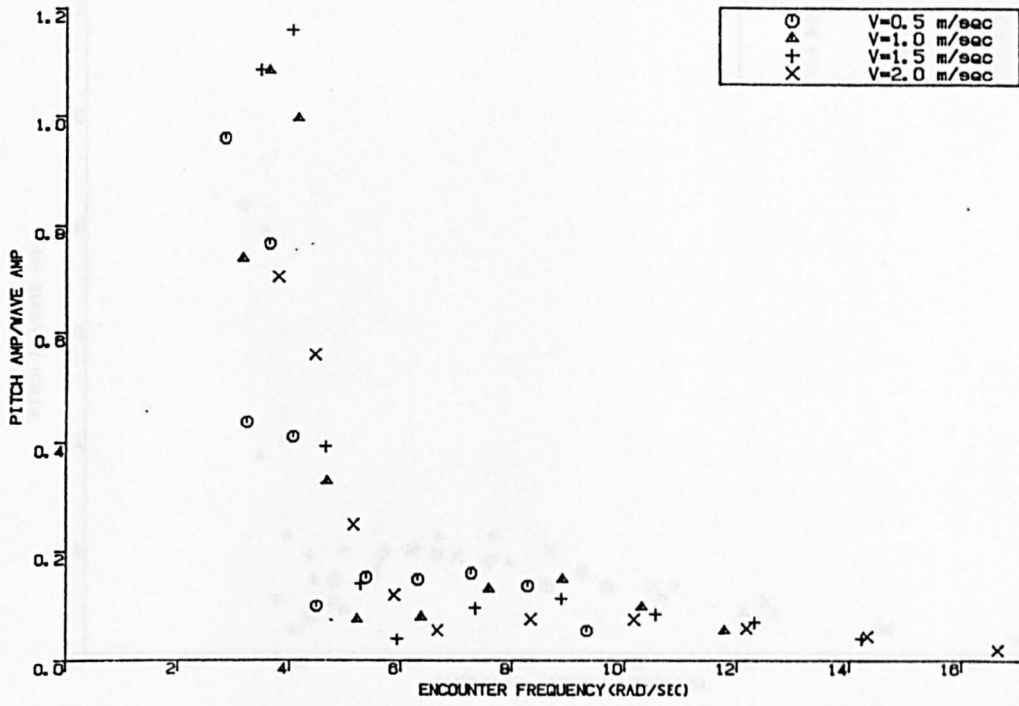
Fig. 4.56   SWATH PITCH TEST
              WITHOUT FIN
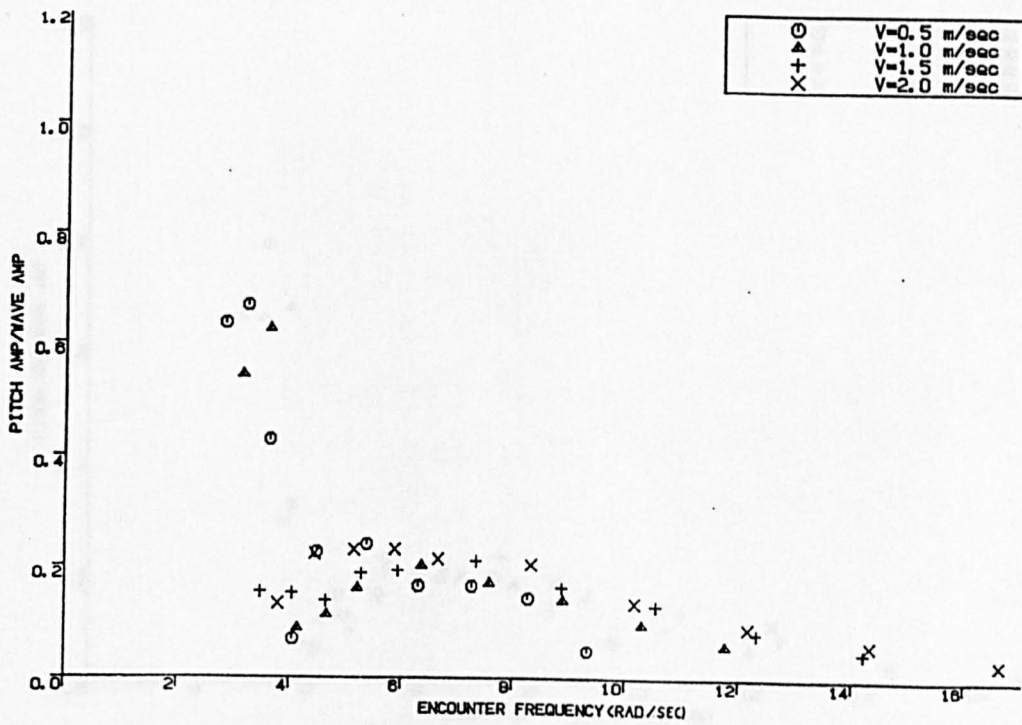
Fig. 4.57   SWATH PITCH TEST
   FIN ANGLE=0.0 deg
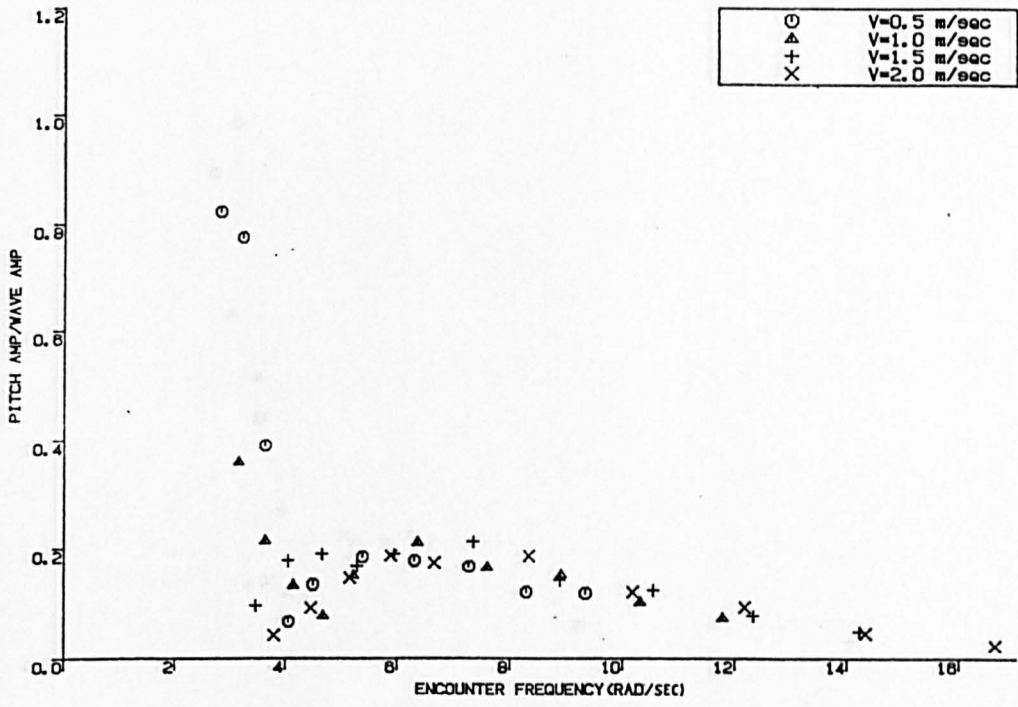
Fig. 4.58   SWATH PITCH TEST
FIN ANGLE=-2.0 deg
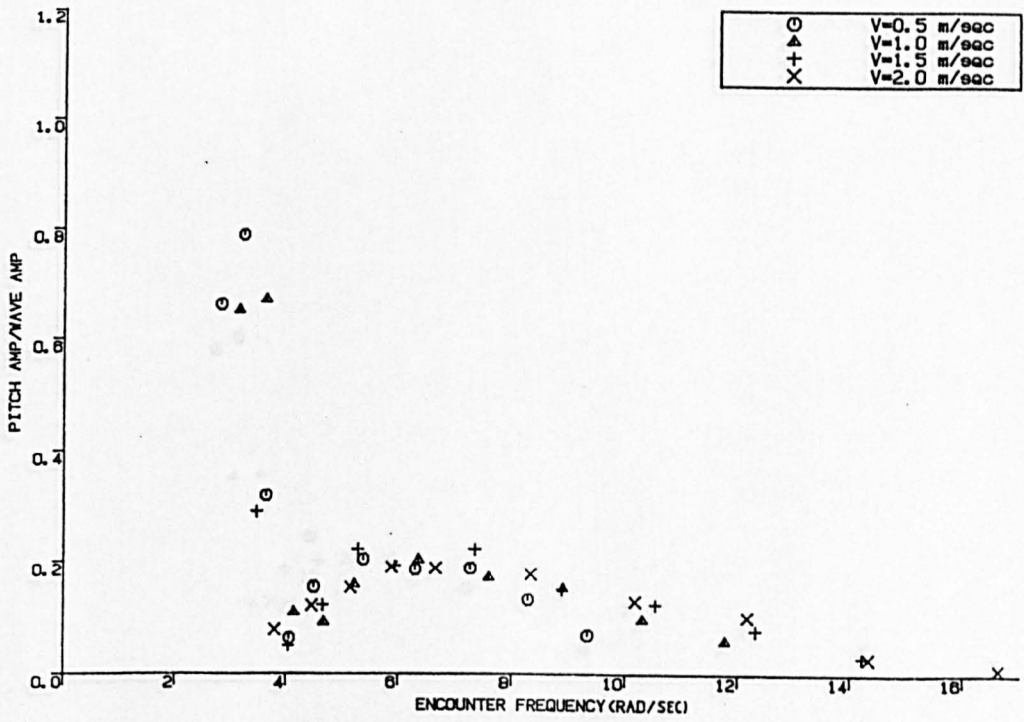
Fig. 4.59   SWATH PITCH TEST
FIN ANGLE=+2.0 deg
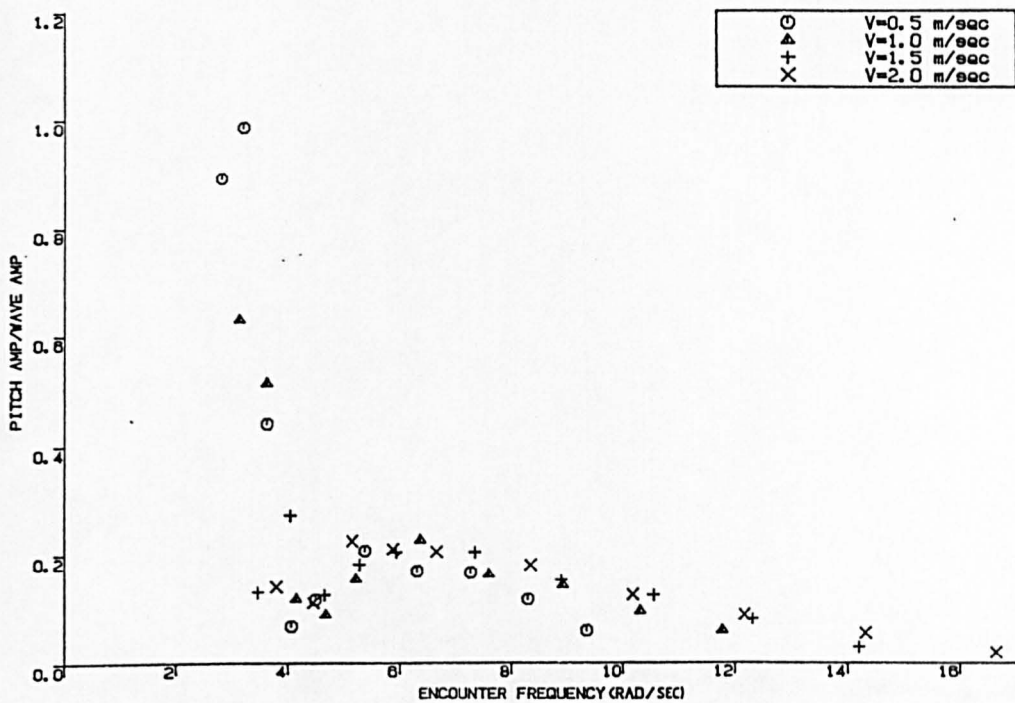
Fig. 4.60 SWATH PITCH TEST
FIN ANGLE=-4.0 deg
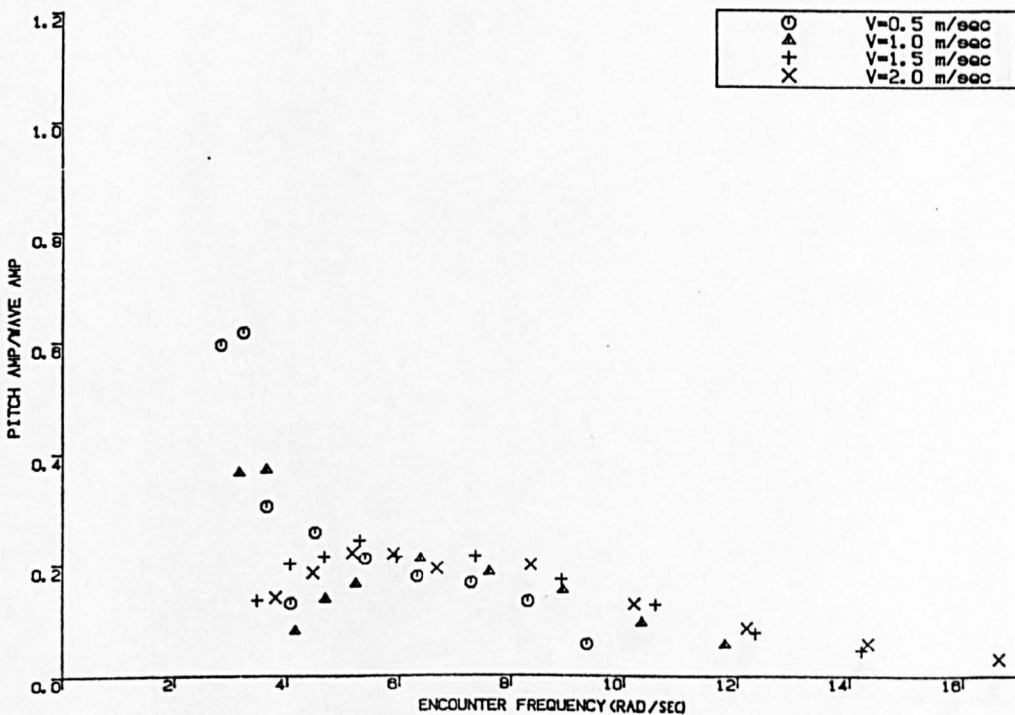

Fig. 4.61 SWATH PITCH TEST
FIN ANGLE=+4.0 deg
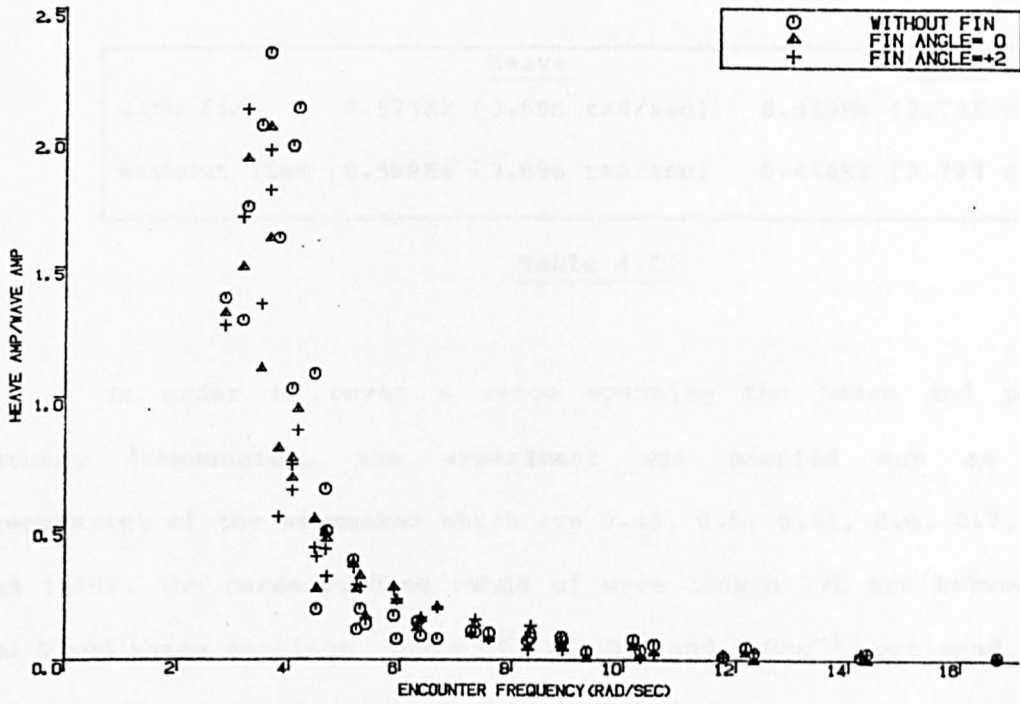
Fig. 4.62   SWATH HEAVE MOTION
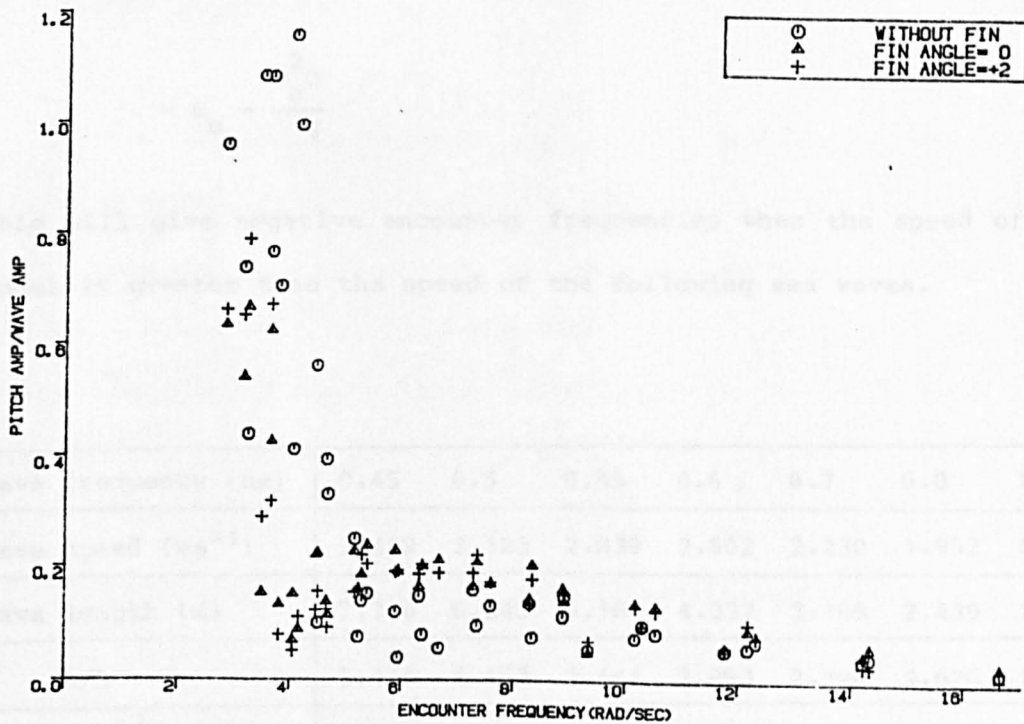
Fig. 4.63   SWATH PITCH MOTION

	Heave	Pitch
with fins	0.571Hz (3.588 rad/sec)	0.435Hz (2.733 rad/sec)
without fins	0.588Hz (3.696 rad/sec)	0.444Hz (2.793 rad/sec)

<u>Table 4.27</u>

In order to cover a range spanning the heave and pitch natural frequencies, the experiment was carried out at the frequencies of the wavemaker which are 0.45, 0.5, 0.55, 0.6, 0.7, 0.8 and 1.0Hz. The corresponding range of wave length λ/L are between 1 and 5 and three carriage speeds of 0.4, 0.6 and 0.8ms^{-1} were used. The corresponding encounter frequencies are given by:-

$$\omega = \omega_o - \frac{\omega_o^2 U}{g} \cos\mu \qquad (\mu = 0^\circ \text{ for following sea})$$

$$= \omega_o - \frac{\omega_o^2 U}{g}$$

This will give negative encounter frequencies when the speed of the model is greater than the speed of the following sea waves.

Wave frequency (hz)		0.45	0.5	0.55	0.6	0.7	0.8	1.0
Wave speed (ms^{-1})		3.469	3.123	2.839	2.602	2.230	1.952	1.561
Wave length (m)		7.710	6.245	5.161	4.337	3.186	2.439	1.561
λ/L		5.140	4.163	3.441	2.891	2.124	1.626	1.041
Encounter frequency (rads^{-1})	At (ms^{-1}) 0.4	2.501	2.739	2.969	3.190	3.609	3.996	4.673
	0.6	2.338	2.538	2.725	2.901	3.215	3.481	3.869
	0.8	2.175	2.337	2.482	2.611	2.821	2.966	3.064

<u>Table 4.28</u>

All the experimental results are listed in Tables 4.29 to 4.40 and the motion response per wave amplitude are plotted against non-dimensional encounter frequency, $\omega\sqrt{L/g}$, in figs. 4.64 to 4.77.

During the tests it was found that a very large surge force occurred, the waves forcing the model to surge forward and backward, making the measurement very difficult. After a series of tests, reasonable mooring and guidelines were used and these guidelines were designed not to inhibit the motion response.

Figures 4.64 to 4.67 recorded the speed effect on each case, ie without fins and with fixed fins at different angles in the heave mode. It was found that increase in the speed reduces the heave motion considerably in all cases. This is expected because of the effect of the viscous damping increase.

The comparison between without fin and fixed aft fin at different angles at certain speeds is plotted in figs. 4.68, 4.69 and 4.79. Contrary to expectation, at very low speeds - 0.4ms^{-1} and 0.6ms^{-1} - fixed aft fins made the heave motion worse. When the speed is increased to 0.8ms^{-1} there is a tendancy that all four cases approach the same value. This leads to the conclusion that the aft fins with fixed angles cannot necessarily reduce the heave motion in a following sea at low speeds. It must be remembered that the original fin size determination was based on retaining pitch stability as well as the heave and pitch damping for motion in waves at higher speeds.

Figures 4.71 to 4.74 shows the pitch motion response for each case at different speeds. As can be seen from the figures, the peak of the response curves shift to the left hand side as the speed

232.

increased.

The wave orbital speeds as shown in Table 4.28 are much higher than the model speed and the resultant speed makes the incident wave come from the reverse direction of the fin which, when the tail of the fin becomes the leading edge, yields the negative lift force and generates the destabilising pitch moment although the fins are expected to increase the eddy damping. As figs. 4.75, 4.76 and 4.77 show, the pitch response with fixed fin at 0° cannot be reduced from the result for the case without fin but a fixed fin angle of $+2^O$ (which is tail edge up) is slightly better than a fixed fin at 0°.

The local velocity over the surface of the aft fin was taken as the vector sum of the forward velocity of the model and the horizontal component of the water particle velocity:-

$$V_f = U - kc_w a_o e^{kh} \cos(kx - \omega t)$$

$$= U - V_w$$

and the change of angle of attack in wave $\delta\alpha$ was given by:-

$$\delta\alpha = \frac{V_w}{U - V_w}$$

Without moveable control of the aft fin the exciting force cannot be reduced.

The above data gathered represents a useful and reliable database for continuing the study into the behaviour of active controlled fins. It also shows that in head seas the presence of a fixed fin is generally beneficial both for heave and more especially for pitch.

SWATH VERTICAL MOTION TEST
FOLLOWING SEA CASE

SPEED V=0.4m/sec   WITHOUT FIN

FREQ.	WAVE			AMPLITUDE	HEAVE AMP	PITCH ANG	HEAVE A.	HEAVE A.	PITCH ANG	PITCH ANG
(hz)				(cm)	(cm)	(des)	WAVE B/2	WAVE CAR	WAVE B/2	WAVE CAR
	B/2	B/3	B/4	CAR.						
0.45	2.679	2.713	2.689	2.321	2.230	1.086	0.832	0.961	0.405	0.468
0.50	2.908	3.032	2.972	2.964	2.480	2.523	0.853	0.837	0.868	0.851
0.55	2.679	2.872	2.830	2.679	2.336	2.030	0.872	0.872	0.758	0.758
0.60	2.556	2.633	2.547	2.571	1.916	1.295	0.750	0.745	0.507	0.504
0.70	3.061	3.271	3.325	3.232	2.092	2.803	0.683	0.647	0.916	0.867
0.80	3.520	3.910	3.750	3.250	2.341	1.346	0.665	0.720	0.382	0.414
1.00	3.367	3.910	3.750	3.545	0.937	0.868	0.278	0.264	0.258	0.245

TABLE 4-29

SWATH VERTICAL MOTION TEST
FOLLOWING SEA CASE

SPEED V=0.6m/sec   WITHOUT FIN

FREQ.	WAVE			AMPLITUDE	HEAVE AMP	PITCH ANG	HEAVE A.	HEAVE A.	PITCH ANG	PITCH ANG
(hz)				(cm)	(cm)	(des)	WAVE B/2	WAVE CAR	WAVE B/2	WAVE CAR
	B/2	B/3	B/4	CAR.						
0.45	2.908	3.032	2.972	2.661	2.400	1.068	0.825	0.902	0.367	0.401
0.50	2.908	3.032	3.042	2.759	2.147	1.686	0.738	0.778	0.580	0.611
0.55	2.219	2.394	2.406	2.080	1.580	1.071	0.712	0.760	0.483	0.515
0.60	2.602	2.713	2.618	2.688	2.012	1.819	0.773	0.749	0.699	0.677
0.70	2.985	3.191	3.255	2.973	2.040	3.644	0.683	0.686	1.221	1.226
0.80	3.750	4.149	3.962	3.652	1.313	2.938	0.350	0.360	0.783	0.804
1.00	2.985	3.989	3.962	3.443	2.329	1.537	0.780	0.639	0.515	0.422

TABLE 4-30

SWATH VERTICAL MOTION TEST
FOLLOWING SEA CASE

SPEED V=0.8m/sec   WITHOUT FIN

FREQ.	WAVE		AMPLITUDE		HEAVE AMP	PITCH ANG	HEAVE A.	HEAVE A.	PITCH ANG	PITCH ANG
(hz)			(cm)		(cm)	(deg)	WAVE B/2	WAVE CAR	WAVE B/2	WAVE CAR
	B/2	B/3	B/4	CAR.						
0.45	2.526	2.633	2.618	2.366	1.940	0.877	0.768	0.820	0.347	0.371
0.50	2.908	3.032	2.972	2.821	2.079	1.155	0.715	0.737	0.397	0.409
0.55	3.138	3.351	3.255	3.188	2.056	1.890	0.655	0.645	0.602	0.593
0.60	2.602	2.633	2.618	2.795	1.464	1.836	0.563	0.524	0.706	0.657
0.70	2.908	3.191	3.255	3.205	1.048	3.108	0.360	0.327	1.069	0.970
0.80	3.520	3.830	3.679	3.170	0.754	4.377	0.214	0.238	1.243	1.381
1.00	3.750	4.309	4.033	2.259	1.175	2.323	0.313	0.520	0.619	1.028

TABLE 4-31

SWATH VERTICAL MOTION TEST
FOLLOWING SEA CASE

SPEED V=0.4m/sec   FIN ANGLE= 0.0 DEGREE

FREQ.	WAVE		AMPLITUDE		HEAVE AMP	PITCH ANG	HEAVE A.	HEAVE A.	PITCH ANG	PITCH ANG
(hz)			(cm)		(cm)	(deg)	WAVE B/2	WAVE CAR	WAVE B/2	WAVE CAR
	B/2	B/3	B/4	CAR.						
0.45	2.857	2.925	2.920	2.618	2.443	1.132	0.855	0.933	0.396	0.432
0.50	2.452	2.576	2.635	2.552	2.241	1.390	0.914	0.878	0.567	0.545
0.55	2.885	3.030	3.041	3.233	2.656	2.040	0.921	0.822	0.707	0.631
0.60	3.389	3.485	3.311	3.629	3.045	3.039	0.898	0.839	0.897	0.837
0.70	4.038	4.318	4.257	4.605	2.175	4.596	0.539	0.472	1.138	0.998
0.80	4.000	4.125	3.982	3.724	1.813	2.544	0.453	0.487	0.636	0.683
1.00	4.143	4.725	4.513	4.301	1.037	1.700	0.250	0.241	0.410	0.395

TABLE 4-32

SWATH VERTICAL MOTION TEST
FOLLOWING SEA CASE

SPEED V=0.6m/sec   FIN ANGLE=0.0 DEGREE

FREQ. (hz)	WAVE AMPLITUDE (cm)				HEAVE AMP (cm)	PITCH ANG (deg)	HEAVE A. WAVE B/2	HEAVE A. WAVE CAR	PITCH ANG WAVE B/2	PITCH ANG WAVE CAR
	B/2	B/3	B/4	CAR.						
0.45	2.571	2.700	2.655	2.309	1.959	1.370	0.762	0.848	0.533	0.593
0.50	2.452	2.652	2.703	2.543	2.090	1.802	0.852	0.822	0.735	0.709
0.55	2.885	3.030	3.041	3.247	2.506	2.116	0.869	0.772	0.733	0.652
0.60	3.462	3.485	3.378	3.534	2.697	3.209	0.779	0.763	0.927	0.908
0.70	4.038	4.242	4.324	4.078	2.996	5.417	0.742	0.735	1.342	1.328
0.80	4.214	4.500	4.181	3.797	1.642	3.229	0.390	0.432	0.766	0.850
1.00	4.286	5.025	4.646	3.626	1.720	2.816	0.401	0.474	0.657	0.777

TABLE 4-33

SWATH VERTICAL MOTION TEST
FOLLOWING SEA CASE

SPEED V=0.8m/sec   FIN ANGLE=0.0 DEGREE

FREQ. (hz)	WAVE AMPLITUDE (cm)				HEAVE AMP (cm)	PITCH ANG (deg)	HEAVE A. WAVE B/2	HEAVE A. WAVE CAR	PITCH ANG WAVE B/2	PITCH ANG WAVE CAR
	B/2	B/3	B/4	CAR.						
0.45	2.571	2.625	2.655	2.358	2.126	1.072	0.827	0.902	0.417	0.455
0.50	2.596	2.803	2.838	2.741	1.967	1.720	0.758	0.718	0.663	0.628
0.55	2.740	2.955	2.905	3.164	2.139	2.350	0.781	0.676	0.858	0.743
0.60	3.462	3.485	3.378	3.716	2.049	2.787	0.592	0.551	0.805	0.750
0.70	3.822	4.167	4.189	4.509	1.406	3.587	0.368	0.312	0.939	0.796
0.80	4.214	4.425	4.181	4.106	0.980	4.705	0.233	0.239	1.117	1.146
1.00	4.286	4.950	4.646	3.902	1.159	4.284	0.270	0.297	1.000	1.098

TABLE 4-34

SWATH VERTICAL MOTION TEST
FOLLOWING SEA CASE

SPEED V=0.4m/sec   FIN ANGLE=-2.0 DEGREE

| FREQ.	WAVE			AMPLITUDE	HEAVE AMP	PITCH ANG	HEAVE A.	HEAVE A.	PITCH ANG	PITCH ANG
(hz)				(cm)	(cm)	(deg)	WAVE B/2	WAVE CAR	WAVE B/2	WAVE CAR
	B/2	B/3	B/4	CAR.						
0.45	2.296	2.394	2.357	2.180	1.888	0.942	0.822	0.866	0.410	0.432
0.50	2.679	2.793	2.714	2.559	2.260	1.376	0.844	0.883	0.514	0.538
0.55	2.908	3.032	3.000	2.874	2.872	3.072	0.988	0.999	1.056	1.069
0.60	3.061	3.191	3.071	3.090	2.792	3.048	0.912	0.904	0.996	0.986
0.70	3.520	3.750	3.714	3.910	2.456	4.888	0.698	0.628	1.389	1.250
0.80	2.296	2.633	2.571	2.369	1.312	1.023	0.571	0.554	0.446	0.432
1.00	1.684	1.915	1.857	1.802	0.424	0.574	0.252	0.235	0.341	0.319

TABLE 4-35

SWATH VERTICAL MOTION TEST
FOLLOWING SEA CASE

SPEED V=0.6m/sec   FIN ANGLE=-2.0 DEGREE

FREQ.	WAVE			AMPLITUDE	HEAVE AMP	PITCH ANG	HEAVE A.	HEAVE A.	PITCH ANG	PITCH ANG
(hz)				(cm)	(cm)	(deg)	WAVE B/2	WAVE CAR	WAVE B/2	WAVE CAR
	B/2	B/3	B/4	CAR.						
0.45	2.449	2.553	2.500	2.162	1.824	1.035	0.745	0.844	0.423	0.479
0.50	2.526	2.713	2.714	2.432	2.016	1.537	0.798	0.829	0.608	0.632
0.55	2.908	3.032	3.071	2.919	2.352	2.445	0.809	0.806	0.841	0.838
0.60	3.061	3.191	3.071	3.081	2.432	3.120	0.795	0.789	1.019	1.013
0.70	3.520	3.670	3.714	3.586	2.600	5.066	0.739	0.725	1.439	1.413
0.80	2.526	2.793	2.643	2.559	1.200	2.135	0.475	0.469	0.845	0.834
1.00	1.913	2.154	2.071	2.378	1.004	0.972	0.525	0.422	0.508	0.409

TABLE 4-36

SWATH VERTICAL MOTION TEST
FOLLOWING SEA CASE

SPEED V=0.8m/sec.   FIN ANGLE=-2.0 DEGREE

FREQ.	WAVE				HEAVE AMP	PITCH ANG	HEAVE A.	HEAVE A.	PITCH ANG	PITCH ANG
(hz)	AMPLITUDE (cm)				(cm)	(deg)	WAVE B/2	WAVE CAR	WAVE B/2	WAVE CAR
	B/2	B/3	B/4	CAR.						
0.45	2.449	2.553	2.429	2.351	1.884	1.388	0.769	0.801	0.567	0.590
0.50	2.602	2.793	2.714	2.495	1.840	1.737	0.707	0.737	0.668	0.696
0.55	2.985	3.032	3.071	3.045	2.056	2.409	0.689	0.675	0.807	0.791
0.60	3.061	3.191	3.143	3.495	1.716	2.681	0.561	0.491	0.876	0.767
0.70	3.673	3.830	3.857	4.054	1.400	3.704	0.381	0.345	1.008	0.914
0.80	2.449	2.793	2.643	2.126	0.904	3.143	0.369	0.425	1.283	1.478
1.00	1.990	2.314	2.143	1.306	0.600	2.200	0.302	0.459	1.106	1.685

TABLE 4-37

SWATH VERTICAL MOTION TEST
FOLLOWING SEA CASE

SPEED V=0.4m/sec   FIN ANGLE= 2.0 DEGREE

FREQ.	WAVE				HEAVE AMP	PITCH ANG	HEAVE A.	HEAVE A.	PITCH ANG	PITCH ANG
(hz)	AMPLITUDE (cm)				(cm)	(deg)	WAVE B/2	WAVE CAR	WAVE B/2	WAVE CAR
	B/2	B/3	B/4	CAR.						
0.45	2.372	2.473	2.406	2.451	1.964	0.891	0.828	0.801	0.376	0.364
0.50	2.602	2.713	2.689	2.765	2.176	1.298	0.836	0.787	0.499	0.469
0.55	2.832	3.032	2.972	3.176	2.752	2.619	0.972	0.866	0.925	0.825
0.60	2.908	3.032	2.972	3.265	2.464	2.338	0.847	0.755	0.804	0.716
0.70	3.367	3.590	3.679	4.010	1.848	3.722	0.549	0.461	1.105	0.928
0.80	2.602	2.872	2.618	2.608	1.456	1.178	0.560	0.558	0.453	0.452
1.00	1.990	2.154	2.123	2.059	0.556	0.664	0.279	0.270	0.334	0.322

TABLE 4-38

SWATH VERTICAL MOTION TEST
FOLLOWING SEA CASE

SPEED V=0.6m/sec   FIN ANGLE= 2.0 DEGREE

FREQ.	WAVE		AMPLITUDE		HEAVE AMP	PITCH ANG	HEAVE A.	HEAVE A.	PITCH ANG	PITCH ANG
(hz)			(cm)		(cm)	(des)	WAVE B/2	WAVE CAR	WAVE B/2	WAVE CAR
	B/2	B/3	B/4	CAR.						
0.45	2.372	2.473	2.406	2.471	1.920	0.873	0.809	0.777	0.368	0.353
0.50	2.679	2.793	2.759	2.765	2.104	1.316	0.785	0.761	0.491	0.476
0.55	2.908	3.032	3.042	3.137	2.272	1.878	0.781	0.724	0.646	0.599
0.60	2.985	3.032	2.972	3.206	2.236	2.493	0.749	0.697	0.835	0.778
0.70	3.291	3.511	3.538	3.618	2.712	4.621	0.824	0.750	1.404	1.277
0.80	2.679	2.872	2.689	2.618	1.412	2.247	0.527	0.539	0.837	0.856
1.00	1.913	2.234	2.123	2.451	0.984	1.020	0.514	0.401	0.533	0.416

TABLE 4-39

SWATH VERTICAL MOTION TEST
FOLLOWING SEA CASE

SPEED V=0.8m/sec   FIN ANGLE= 2.0 DEGREE

FREQ.	WAVE		AMPLITUDE		HEAVE AMP	PITCH ANG	HEAVE A.	HEAVE A.	PITCH ANG	PITCH ANG
(hz)			(cm)		(cm)	(des)	WAVE B/2	WAVE CAR	WAVE B/2	WAVE CAR
	B/2	B/3	B/4	CAR.						
0.45	2.372	2.473	2.406	2.725	1.800	1.184	0.759	0.661	0.499	0.434
0.50	2.602	2.793	2.689	2.824	1.840	1.633	0.707	0.652	0.628	0.578
0.55	2.908	3.032	2.972	3.235	1.912	2.081	0.657	0.591	0.716	0.643
0.60	2.908	3.032	2.972	3.539	1.720	2.356	0.591	0.486	0.810	0.666
0.70	3.245	3.399	3.396	3.980	1.192	3.024	0.367	0.299	0.932	0.760
0.80	2.526	2.713	2.547	2.392	0.720	2.848	0.285	0.301	1.127	1.191
1.00	1.990	2.394	2.264	1.353	0.400	1.815	0.201	0.296	0.912	1.341

TABLE 4-40
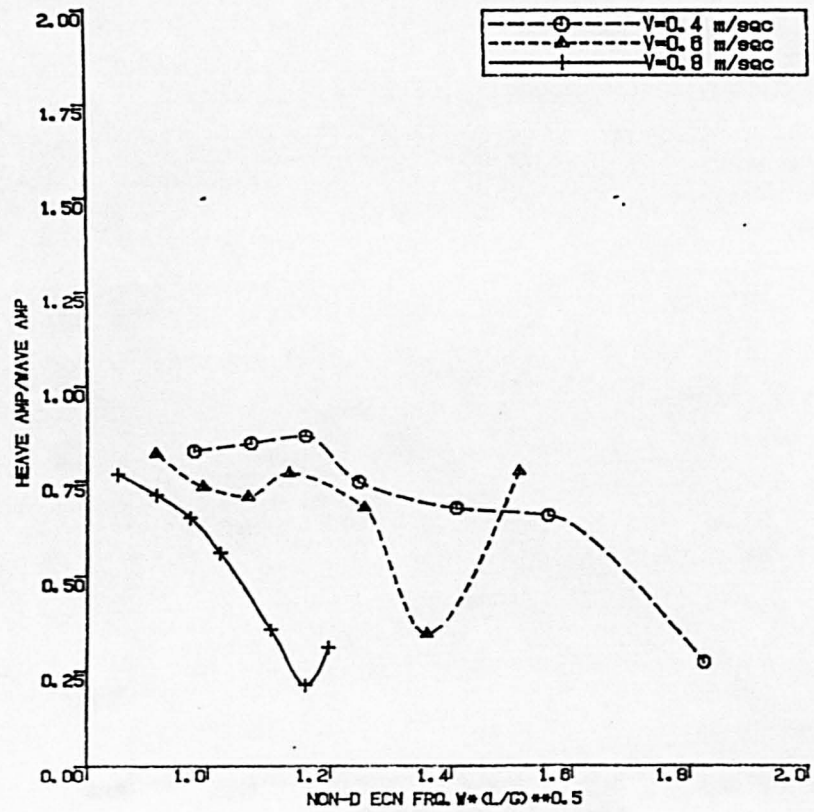
SWATH HEAVE IN FOLLOWING SEAS
WITHOUT FIN

Fig. 4.64
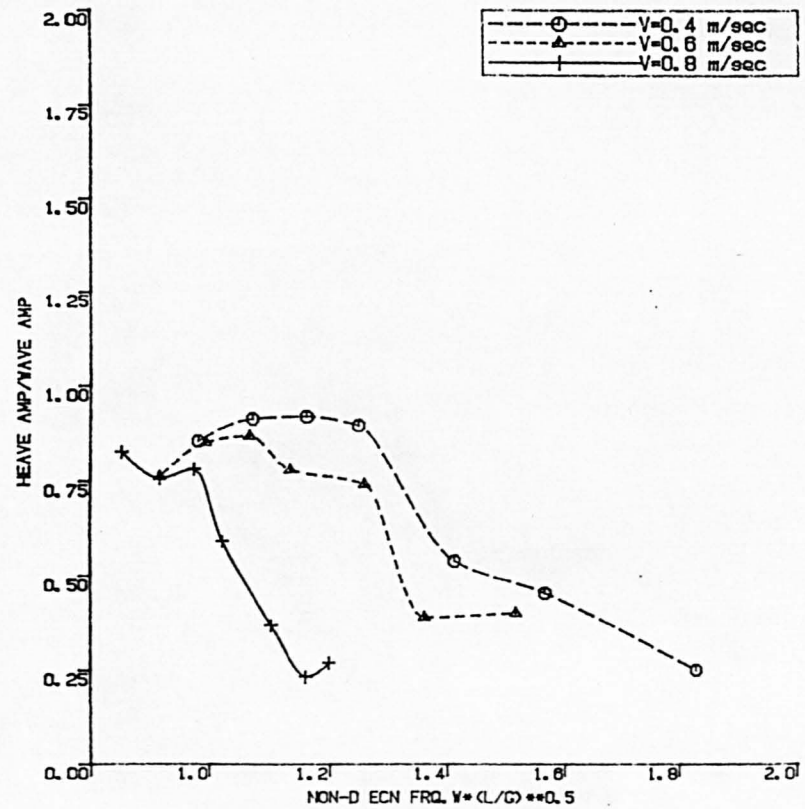
SWATH HEAVE IN FOLLOWING SEAS
FIN ANGLE=0.0 deg

Fig. 4.65
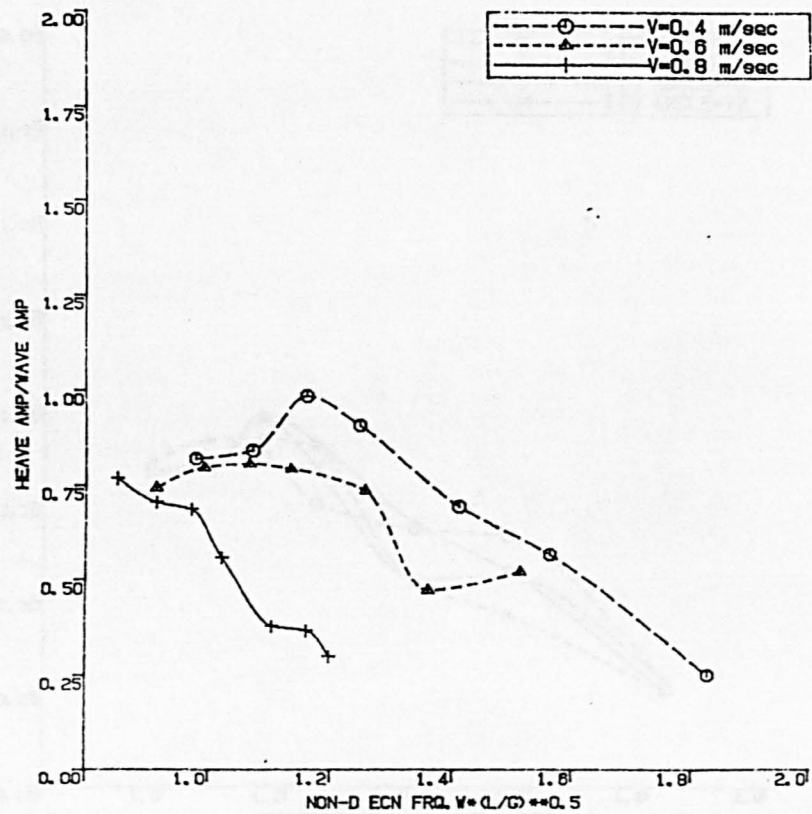
SWATH HEAVE IN FOLLOWING SEAS
FIN ANGLE=-2.0 deg

Fig. 4.66
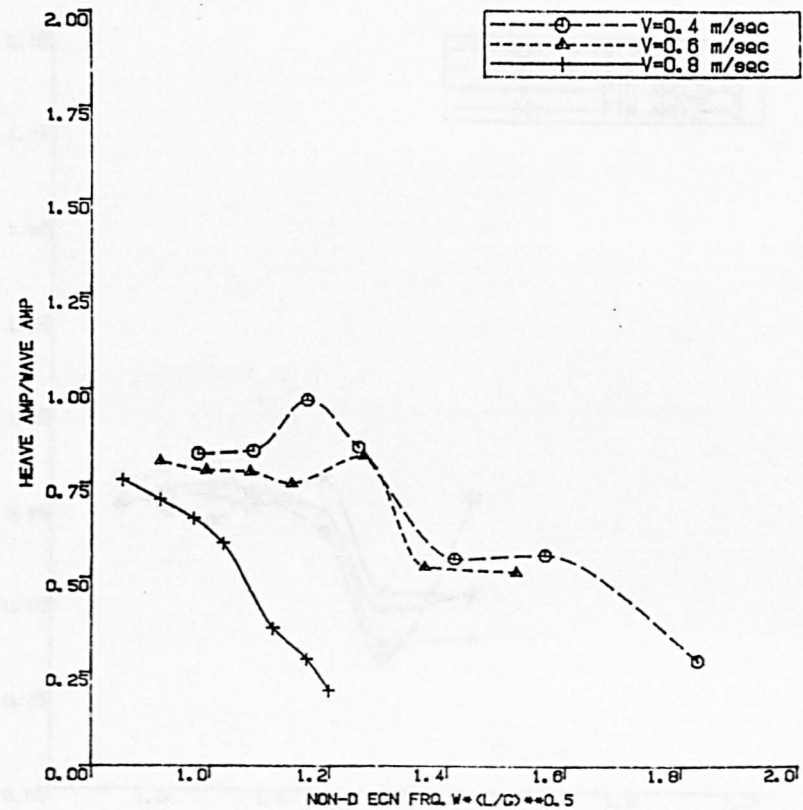
SWATH HEAVE IN FOLLOWING SEAS
FIN ANGLE=+2.0 deg

Fig.4.67
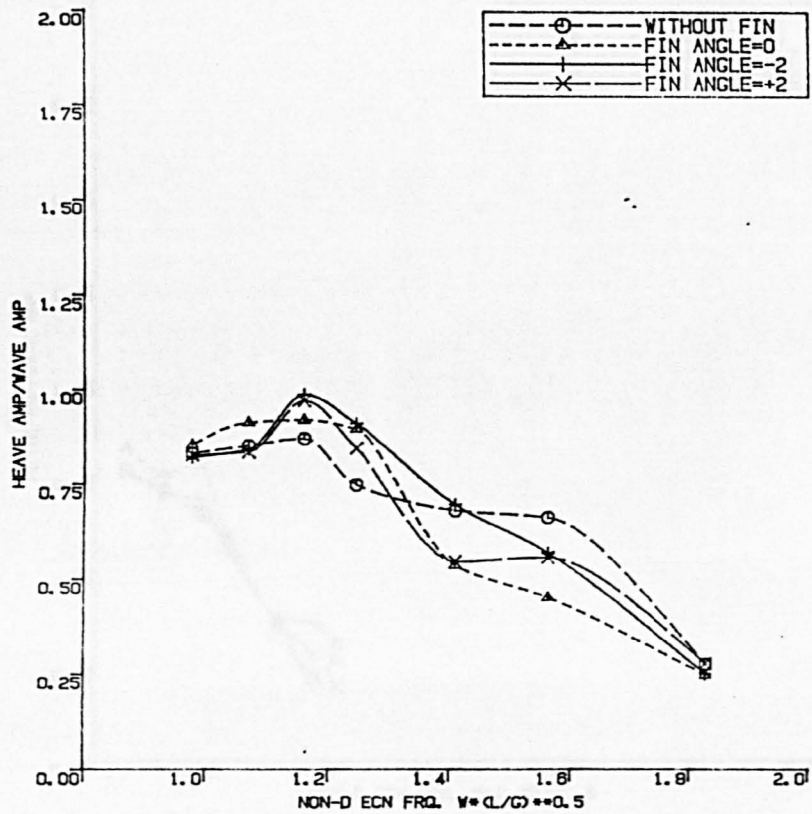
SWATH HEAVE IN FOLLOWING SEAS
V=0.4 m/sec

Fig.4.68
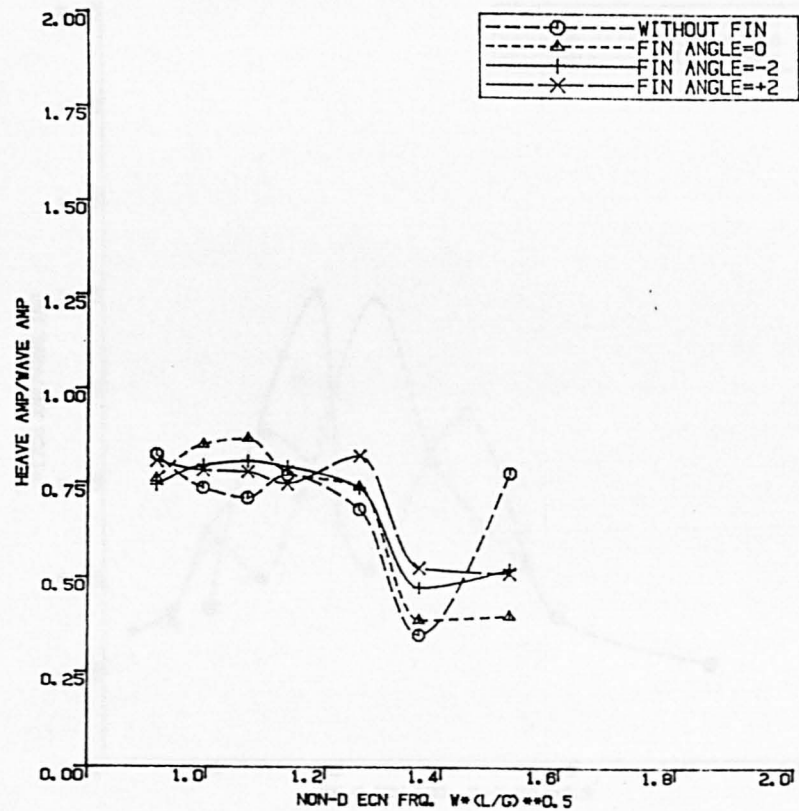
SWATH HEAVE IN FOLLOWING SEAS
V=0.6 m/sec

Fig.4.69
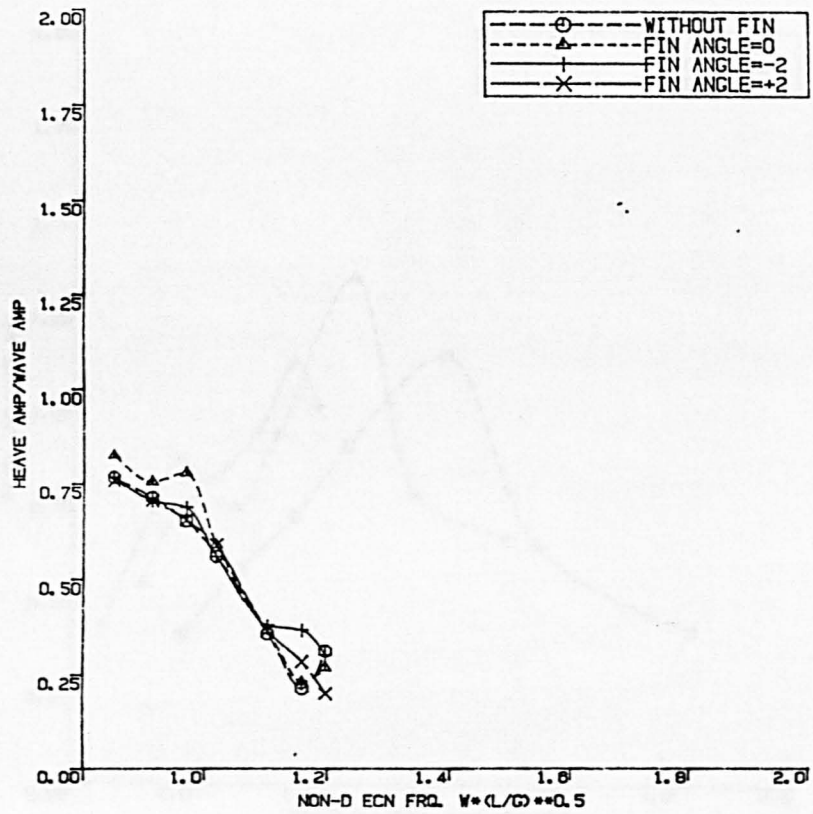
SWATH HEAVE IN FOLLOWING SEAS
V=0.8 m/sec

Fig. 4.70
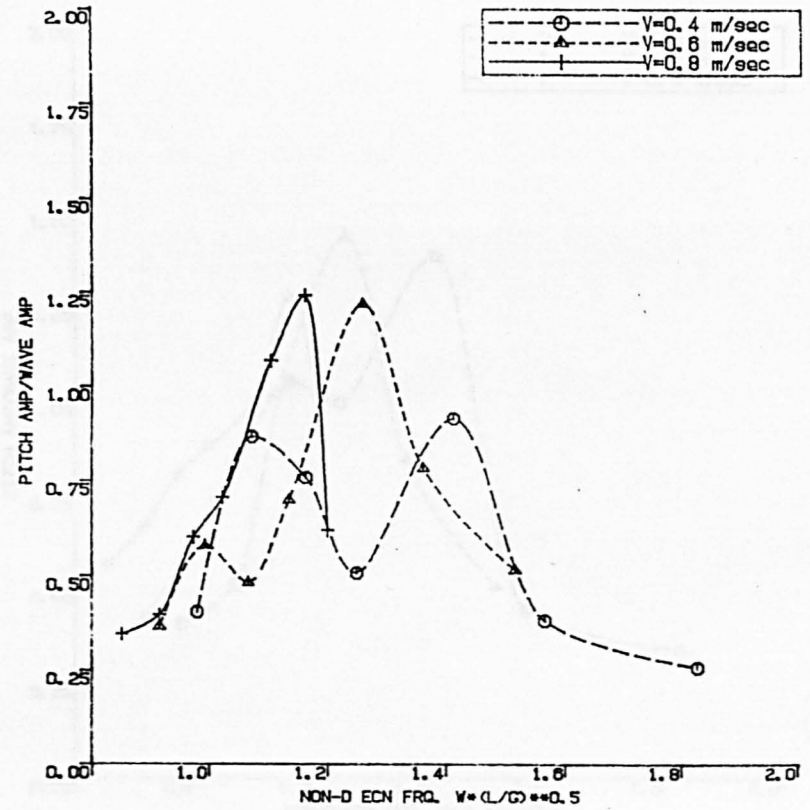
SWATH PITCH IN FOLLOWING SEAS
WITHOUT FIN

Fig. 4.71
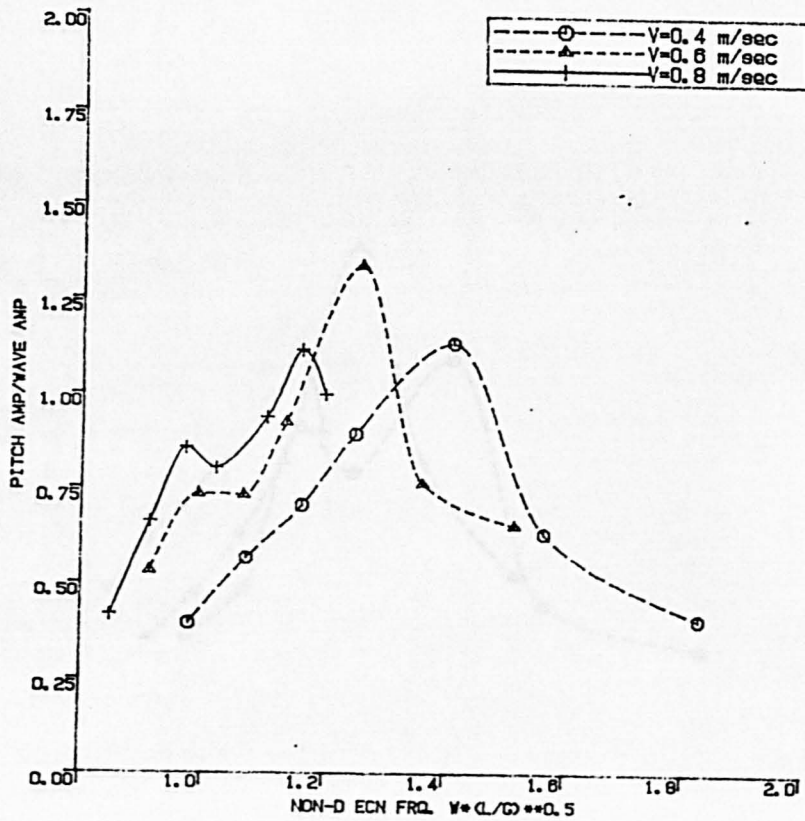
SWATH PITCH IN FOLLOWING SEAS
FIN ANGLE=0.0 deg

Fig.4.72
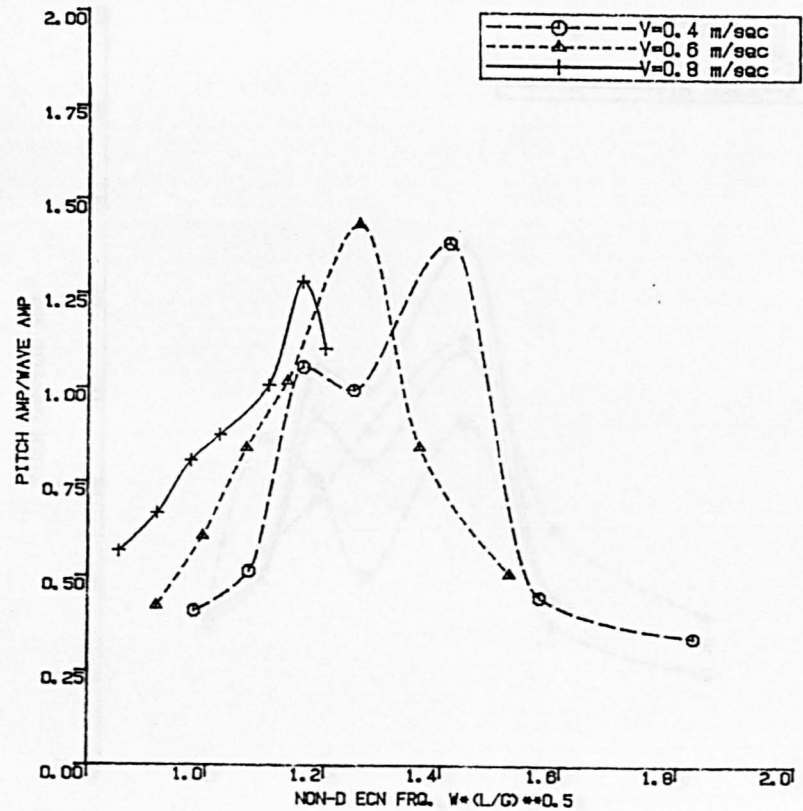
SWATH PITCH IN FOLLOWING SEAS
FIN ANGLE=-2.0 deg

Fig.4.73

243.
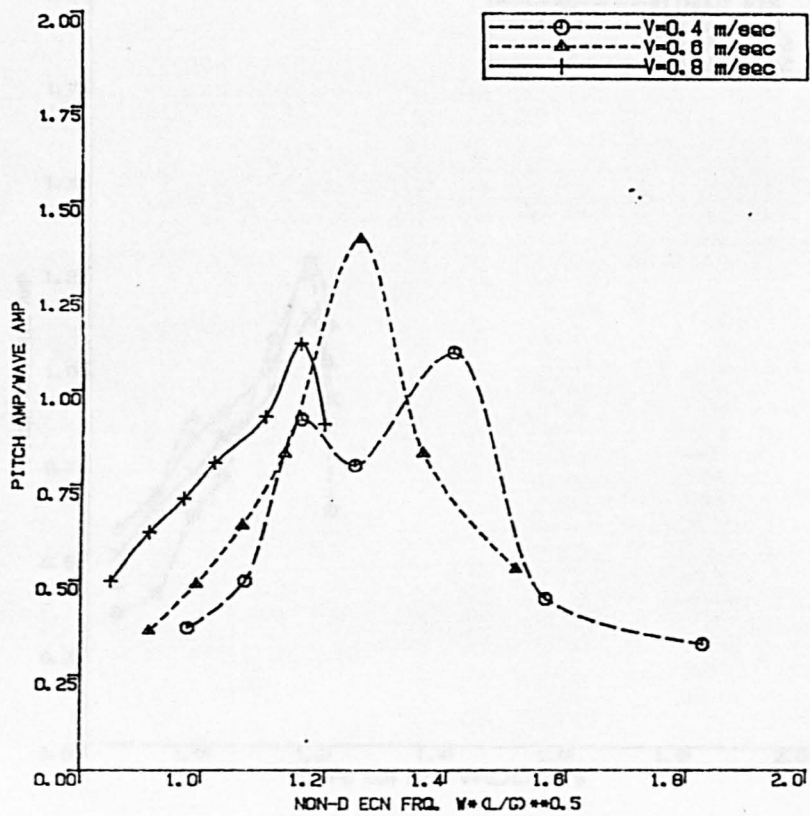
SWATH PITCH IN FOLLOWING SEAS
FIN ANGLE=+2.0 deg
Fig. 4.74
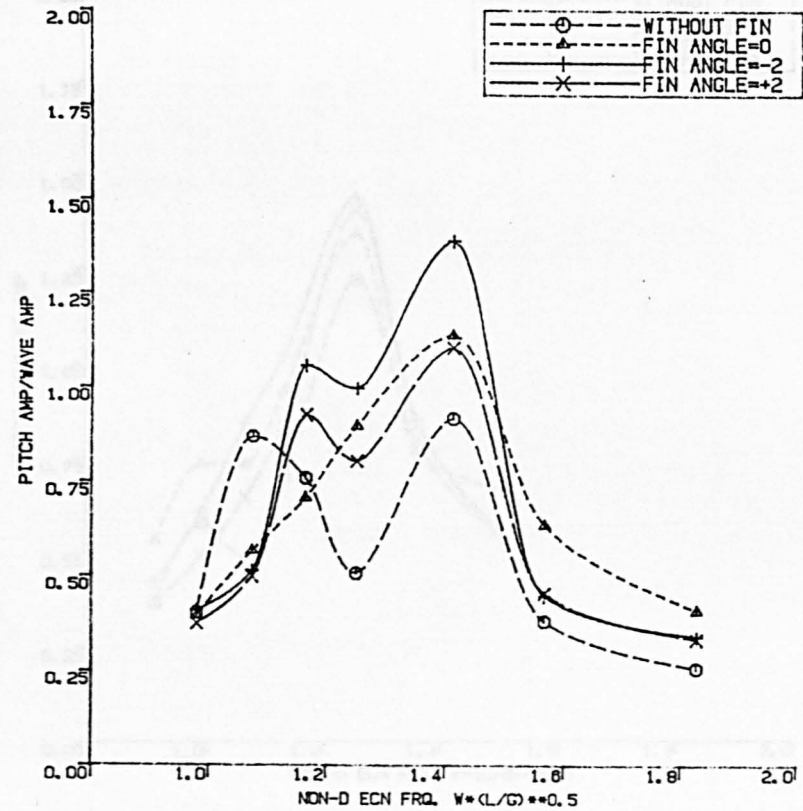
SWATH PITCH IN FOLLOWING SEAS
V=0.4 m/sec
Fig. 4.75
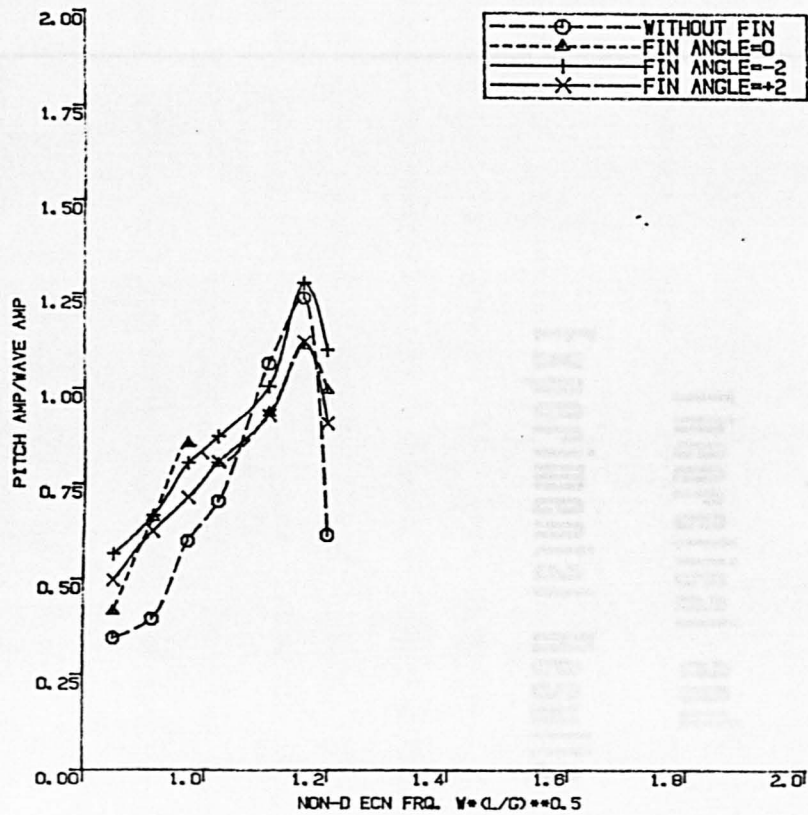
SWATH PITCH IN FOLLOWING SEAS
V=0.8 m/sec

Fig.4.76
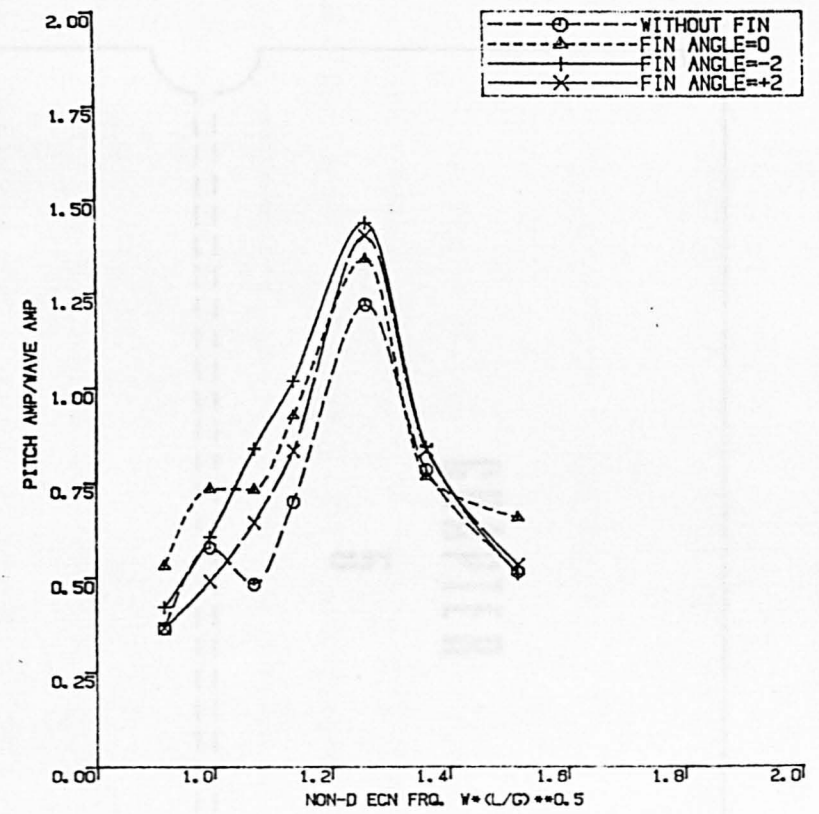
SWATH PITCH IN FOLLOWING SEAS
V=0.6 m/sec

Fig.4.77

CHAPTER
5

Comparison of
Theoretical and
Experimental Results

CHAPTER 5

COMPARISON OF THEORETICAL AND EXPERIMENTAL RESULTS

1.   THE HYDRODYNAMIC COEFFICIENTS

The values of the three dimensional hydrodynamic coefficients in heave motion against the non-dimensional frequency are as plotted in figures 5.1 to 5.7. The hydrodynamic coefficients are non-dimensionalised by the factors as defined in Table 5.1 where the non-dimensional frequencies are defined as $\omega\sqrt{L/g}$.

In fig. 5.1, the heave added mass $\bar{A}_{33}$ and the pitch added mass $\bar{A}_{55}$ for zero forward speed are plotted. The results are also compared with Lee's theoretical prediction [49] and the forced pitch and heave oscillation experiments [72] for a single strut model 'SWATH 6A'. From the results it can be seen that there are considerable discrepancies between the experimental and theoretically predicted results for $\bar{A}_{33}$. The theory underestimates the values especially at the lower frequencies. In Reference [49] a comparison is given of the theoretical predictions for both demi-hull and twin-hull methods. These show that there is a dip in $\bar{A}_{33}$ for the twin-hull method which was considered to be caused by a blockage effect between the hulls. However, except for the dip, the agreement between the demi-hull method and the experimental results is quite good. Therefore, only a demi-hull section has been used for further calculations in this study.

The values of $\bar{A}_{33}$, $\bar{A}_{35}$, $\bar{A}_{55}$, $\bar{B}_{33}$, $\bar{B}_{35}$, $\bar{B}_{55}$ for forward speeds

taking the speed effect into consideration, as described in the previous chapter are shown in figs. 5.2 to 5.7. In each figure comparisons are made of the solutions incorporating the potential flow assumption, viscous effects and the contribution by the aft fins.

According to the theory, there is no speed effect on $\bar{A}_{33}$. Figude 5.2 shows that the results are the same at two speeds ($F_n = 0.26$, 0.52). However, the experimental results for SWATH 6A in Reference [72], as shown in the same figure, indicated some speed effects existed but it is not significant. As would be expected from the theory fig. 5.3 shows that the coupled heave-pitch added mass $\bar{A}_{35}$ varies with speed significantly because of the term $U/\omega^2\int b_{33}dx$, and the contribution of the fin effect $2\ell(m^{(f)} + a_{33}^{(f)})$. Since the viscosity only affects the damping, there is no effect on the added mass as shown in the figures. In the comparisons in fig. 5.4, the speed effect dominates in the lower frequencies range for $\bar{A}_{55}$. The large difference between these two speeds confirmed the speed effect term $U^2/\omega^2.A_{33}$, which is significant only at lower frequencies.

Figure 5.5 presents the heave damping coefficient $\bar{B}_{33}$. For the bare hull the values shown in the figure are small under the potential flow assumption. Taking the viscosity into account, the speed-dependent term, $\rho A_o U\int B_m dx$, increases in proportion to the speed. At resonance, the non-linear viscous damping increases rapidly with amplitude of motion and thus limits the size of peak. The results also show the significant effects caused by the aft fins.

The heave-pitch coupled damping $\bar{B}_{35}$ is plotted in fig. 5.6. There is a great speed effect on $\bar{B}_{35}$, owing to the term UA_{33}, where the added mass A_{33} is relatively much larger than the damping term

and, therefore, in fig. 5.7, the speed-dependent term $U^2/\omega^2 B_{33}$ only has a slight contribution to the pitch damping $\bar{B}_{55}$. It is interesting to note that frequency has very little effect on $\bar{B}_{35}$ and $\bar{B}_{55}$. This phenomena has been confirmned by the experimental results in Reference [72].

It should be mentioned that the values in the figures presented here are dependent on the coefficients of drag and the lift-curve slope. The results presented for viscous effects uses $A_o = 0.07$ and $C_{DH} = 0.5$. For the aft fins, the lift-curve slope $C_{L\alpha}$ has been taken as 3.3268.

2. THE MOTION RESPONSES

2.1. The Motion Responses for the Bare Hull

The heave and pitch motion responses at zero speed which have been predicted by the strip theory under the potential flow assumption are presented in fig. 5.8. The model test results given in the comparison were obtained in 1982 and 1984. The respective test results show reasonable agreement with theory throughout the whole range of frequencies, although there are some discrepancies around resonance. The same results are compared with predictions based on Morison's equation approach [86], where the motions were considered uncoupled and the horizontal forces acting on the struts were included as shown in fig. 5.9. There is much better agreement between the Morison's approach and the experimental results even at the resonance frequency. In fig. 5.10, predictions based on the strip theory, taking into account the cross-flow drag effect, are shown. Different drag coefficients are compared in the same figure. The peak response value

Hydrodynamic Coefficients	Factor Divided	Non-dimensional Coefficients
A_{33}	$\rho \nabla$	$\bar{A}_{33}$
A_{35}	$\rho \nabla L$	$\bar{A}_{35}$
A_{55}	$\rho \nabla L^2$	$\bar{A}_{55}$
B_{33}	$\rho \nabla \sqrt{g/L}$	$\bar{B}_{33}$
B_{35}	$\rho \nabla \sqrt{gL}$	$\bar{B}_{35}$
B_{55}	$\rho \nabla L \sqrt{gL}$	$\bar{B}_{55}$

Table 5.1

The Non-dimensional hydrodynamic coefficients in Figs. 5.1 to 5.7
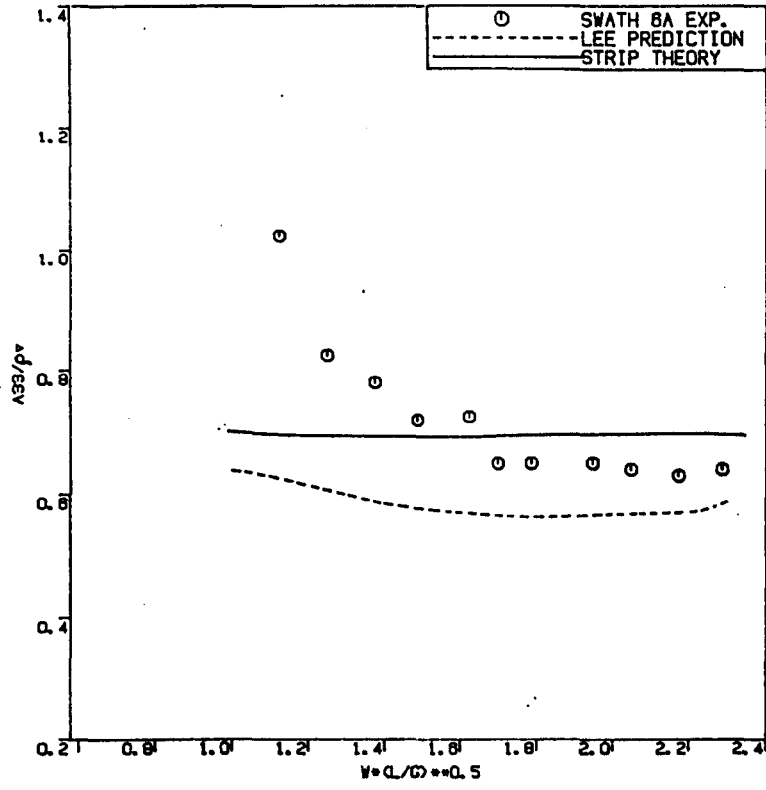
COMPARISON $\overline{A33}$ WITH TEST
AT Fn=0
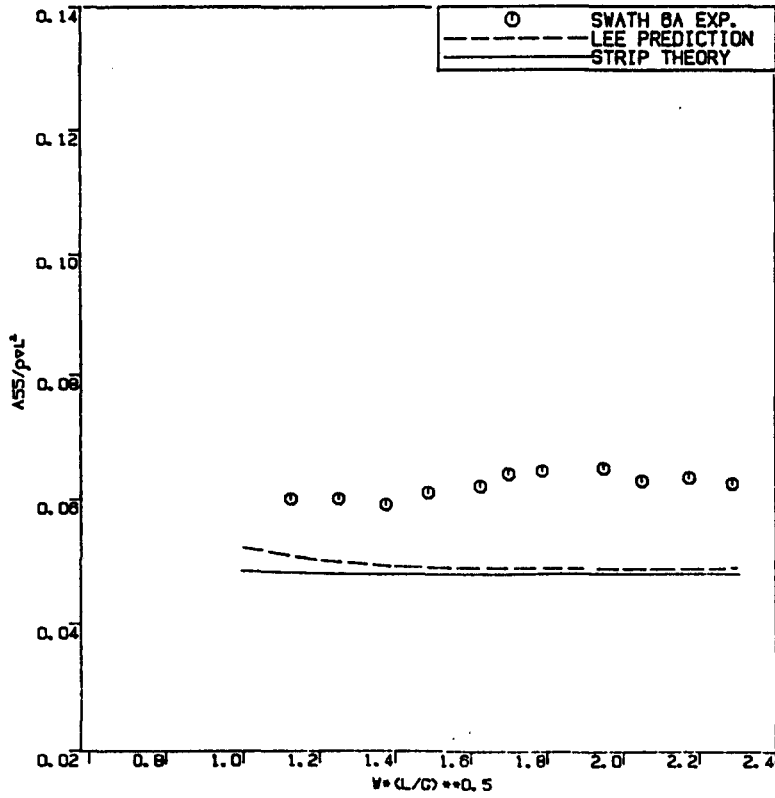
COMPARISON $\overline{A55}$ WITH TEST
AT Fn=0

FIG. 5.1
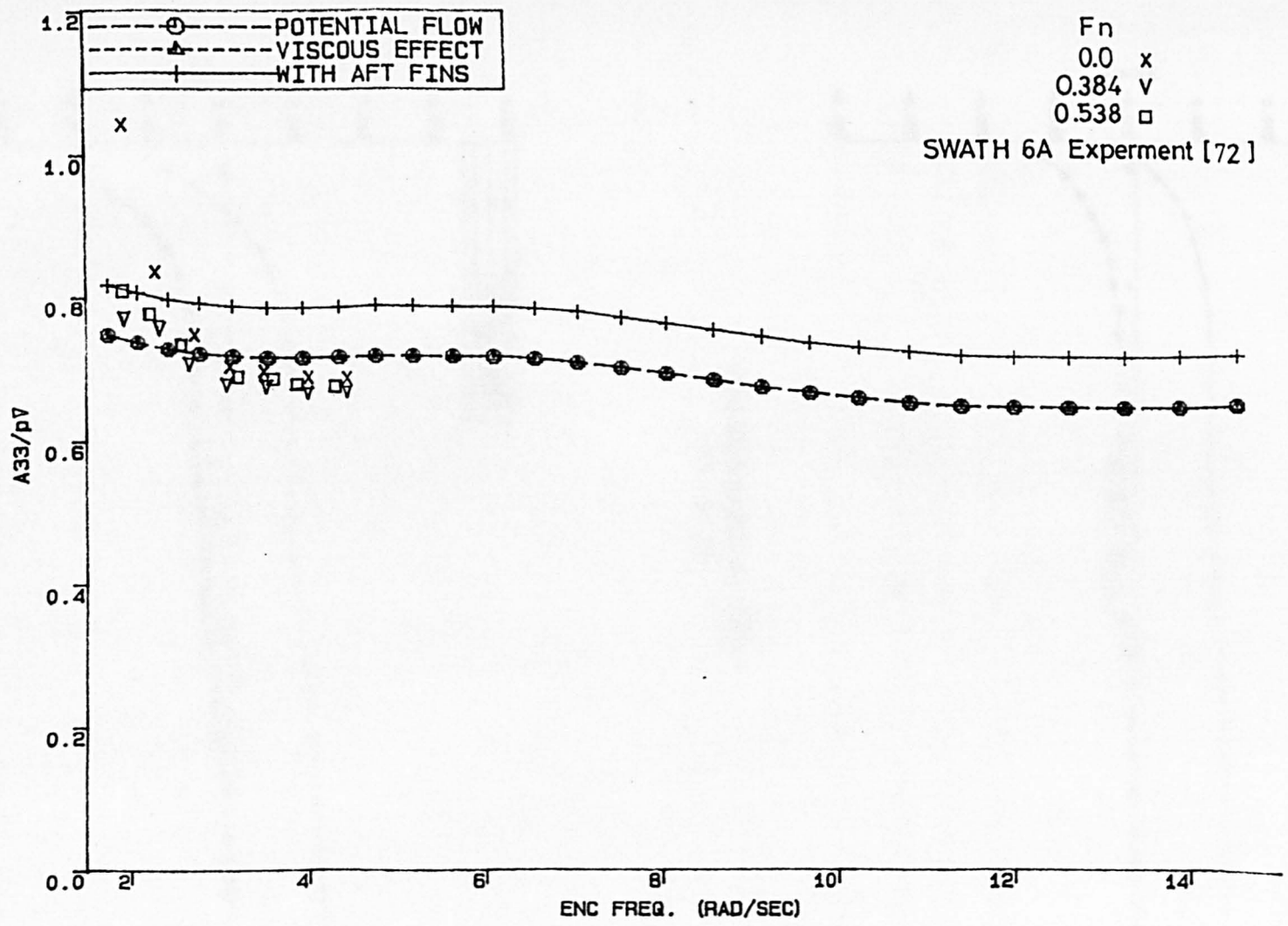
FIG. 5.2 NON-DIMENSION $\overline{A33}$

Fn=0.26
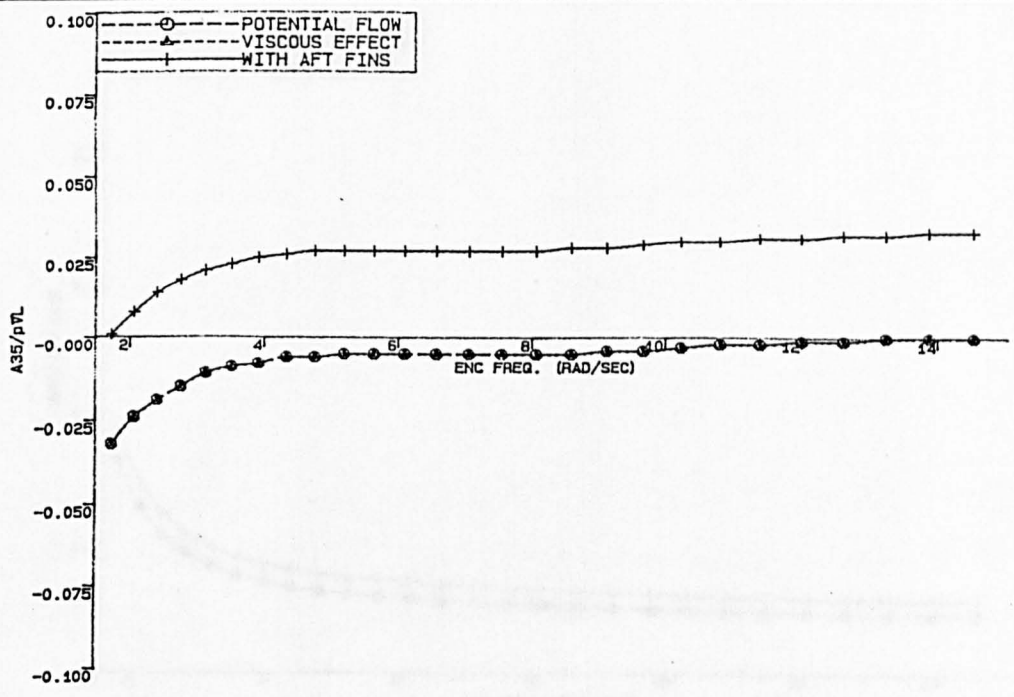
NON-DIMENSION $\overline{A35}$
Fn=0.26
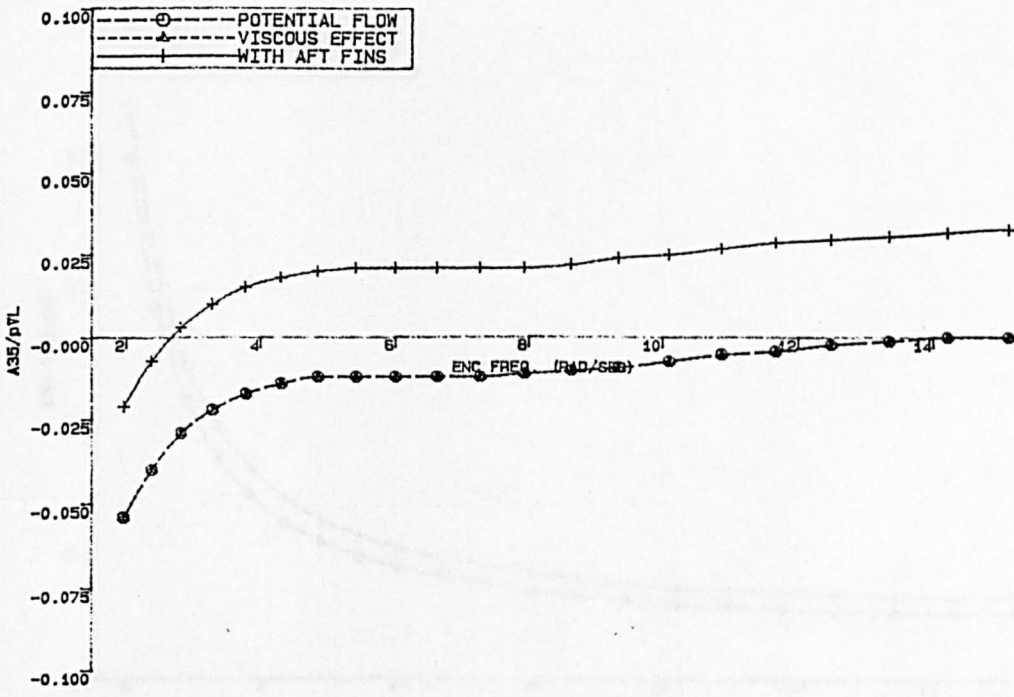
NON-DIMENSION $\overline{A35}$
Fn=0.52
FIG. 5.3
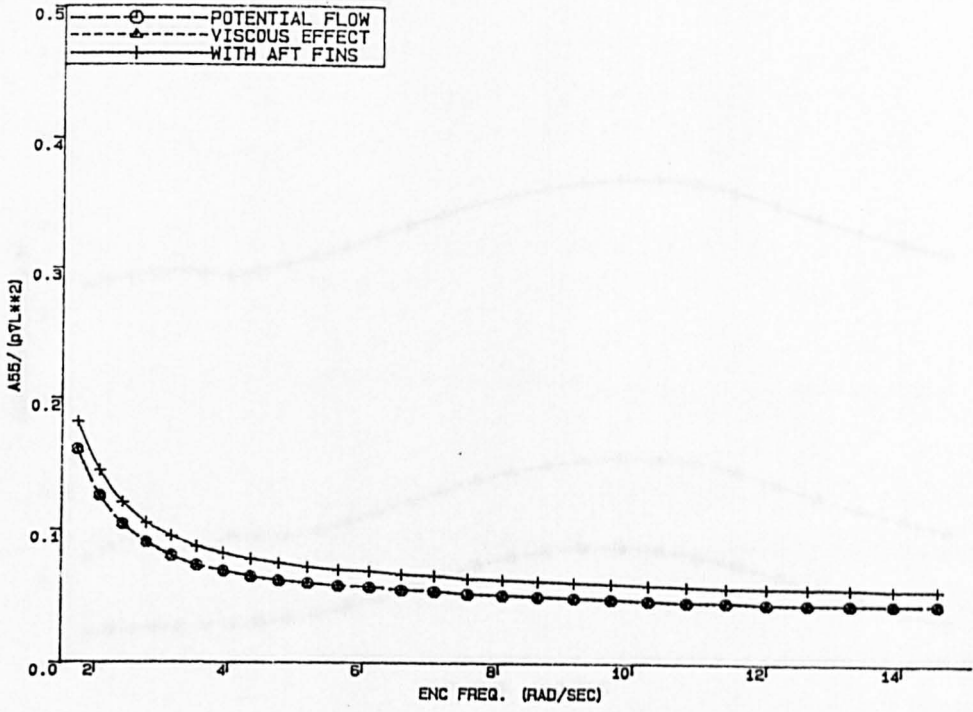
NON-DIMENSION $\overline{A55}$
Fn=0.26
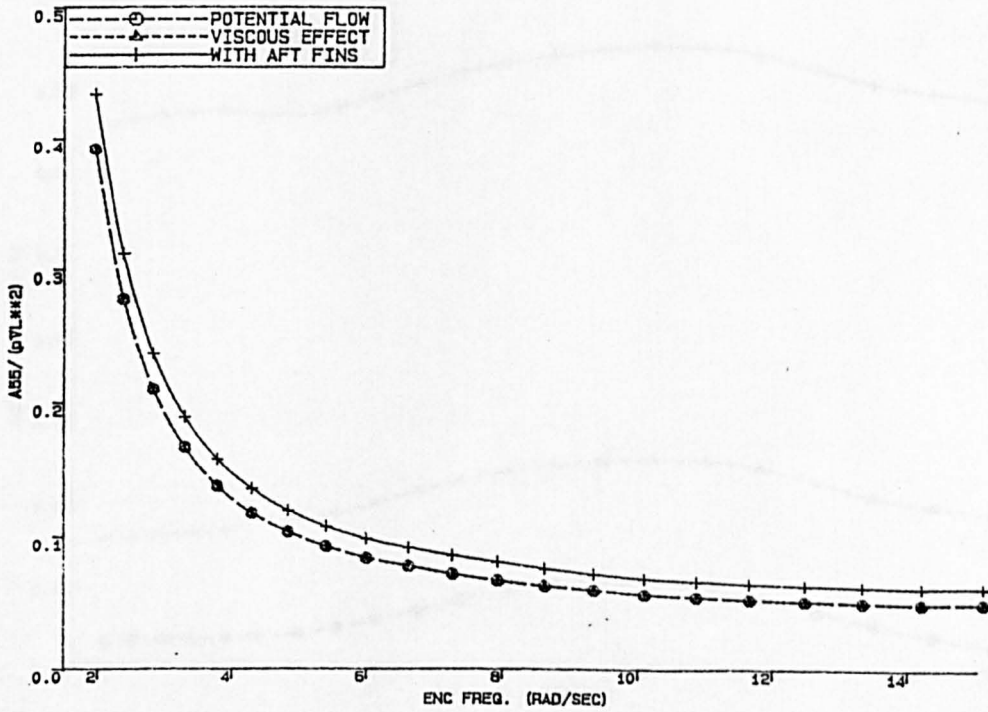
NON-DIMENSION $\overline{A55}$
Fn=0.52

FIG. 5.4
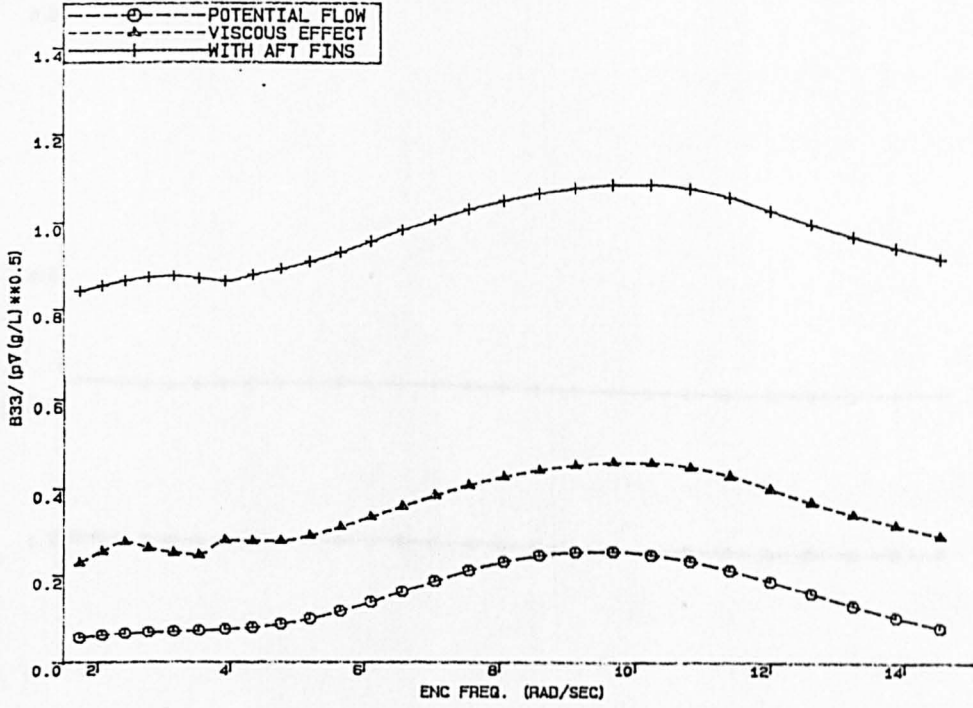
NON-DIMENSION B̄33
Fn=0.26
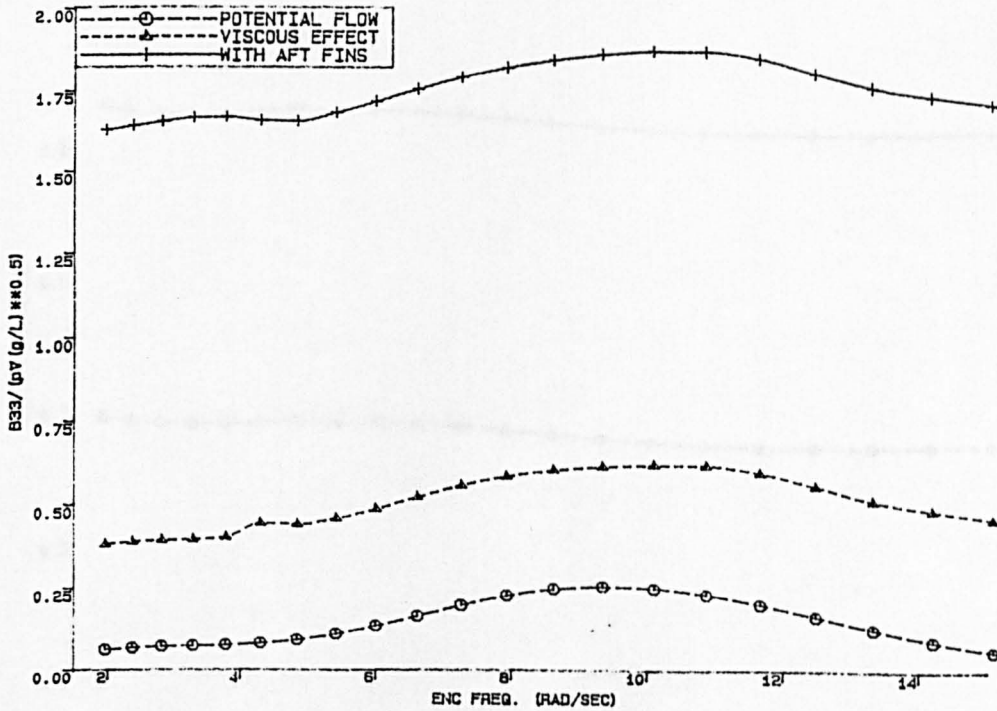
NON-DIMENSION B̄33
Fn=0.52

FIG. 5.5
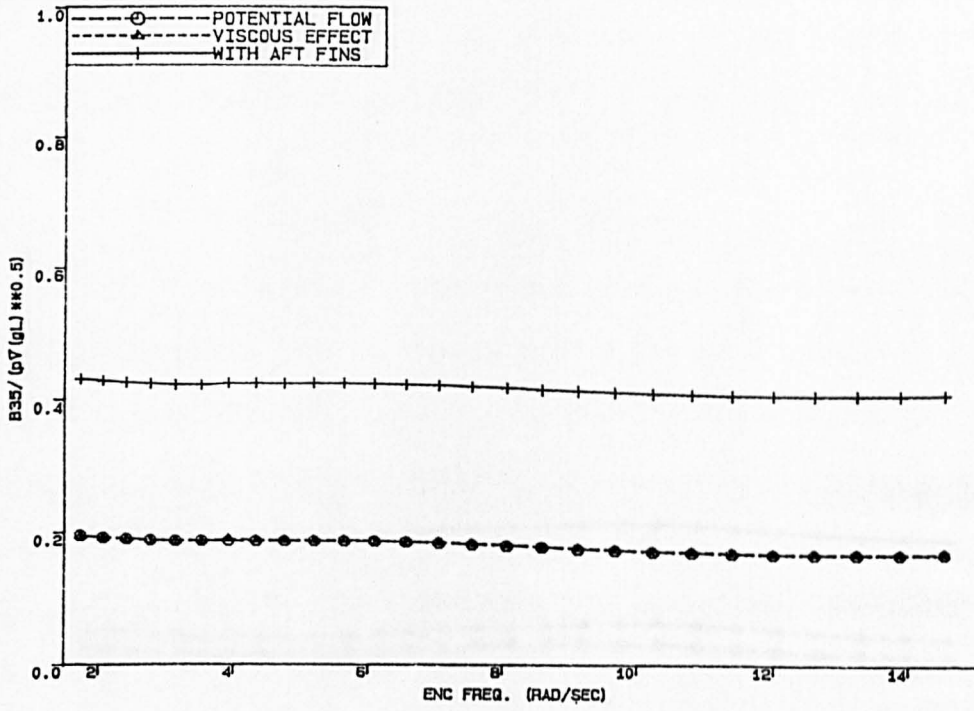
NON-DIMENSION $\overline{B35}$
Fn=0.26
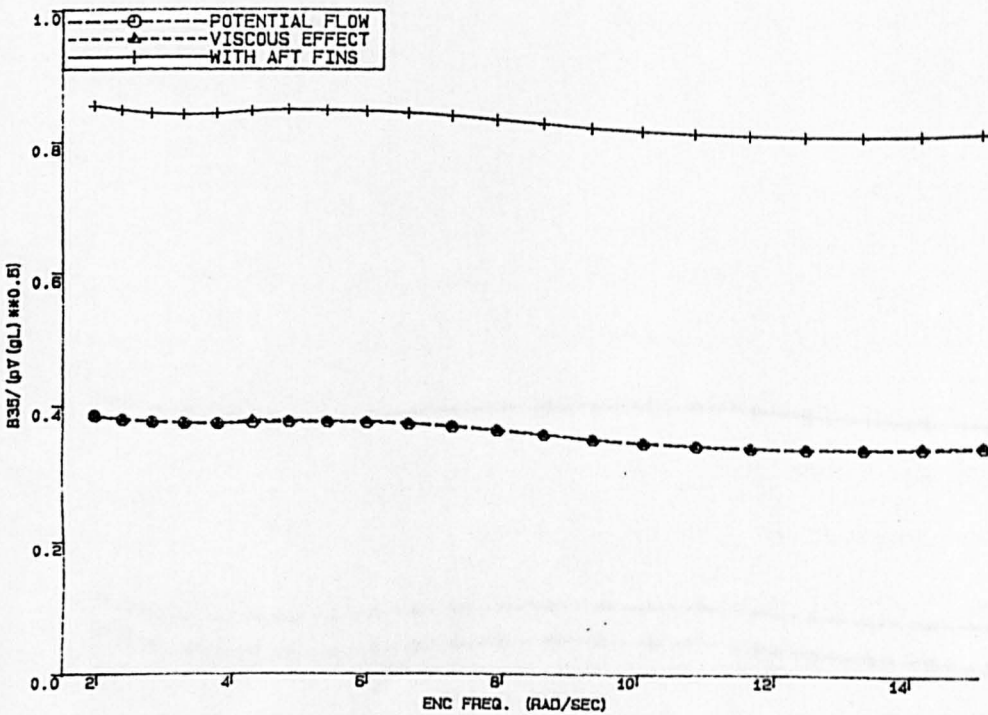
NON-DIMENSION $\overline{B35}$
Fn=0.52

FIG. 5.6
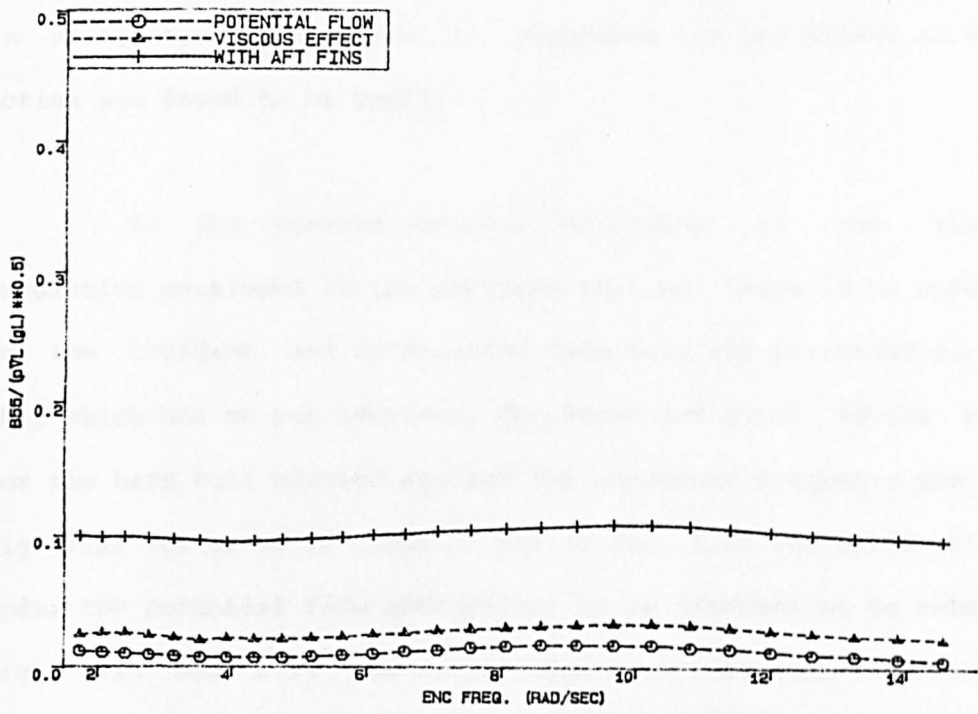
NON-DIMENSION $\overline{B55}$
Fn=0.26
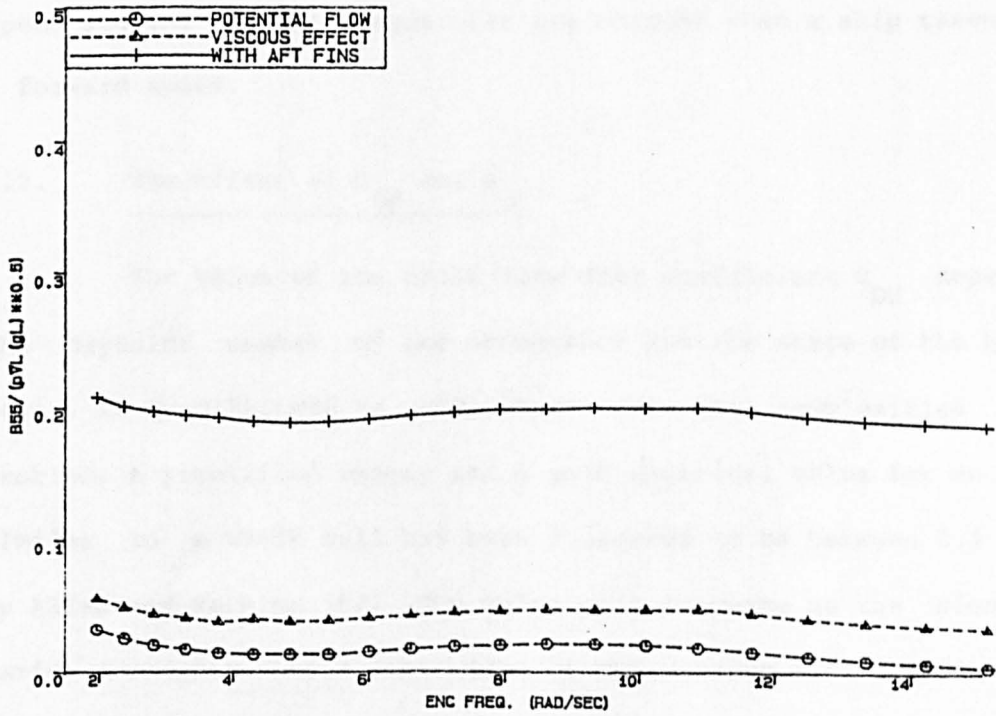
NON-DIMENSION $\overline{B55}$
Fn=0.52

FIG. 5.7

in heave can be reduced at resonance but the effect on the pitch motion was found to be small.

In the forward motion, according to the theoretical prediction mentioned in the previous section, there is no speed effect on the incident and diffraction wave velocity potential for a SWATH ship which has no end sections. The heave and pitch motion responses for the bare hull plotted against the encounter frequency are shown in fig. 5.11 for speed at 1.0ms^{-1}, and in fig. 5.12 for speed at 2.0ms^{-1}, under the potential flow assumption. It is interesting to note that in figs. 5.13 and 5.14 the comparisons were made both with and without considering the speed effects on the hydrodynamic coefficients. There is not much difference at the higher frequencies but the peak response would remain at the left (lower frequency) if no correction had been made to the added mass and damping coefficients. This confirmed the fact that the body motion-induced velocity potential is changed with speed and the natural frequencies are changed when a ship travels with a forward speed.

2.2. The Effect of C_{DH} and A_o

The value of the cross-flow drag coefficient C_{DH} depends on the Reynolds number of the cross-flow and the state of the boundary layer. It is difficult to understand all the complexities of the problem. A simplified theory and a good empirical value for an airship similar to a SWATH hull had been suggested to be between 0.4 and 0.7 by Allen and Perkins [87]. The value will increase as the slenderness ratio increases while the value of the viscous lift coefficient A_o, for a circular or polygonal cross-section was recommended to be about 0.07.
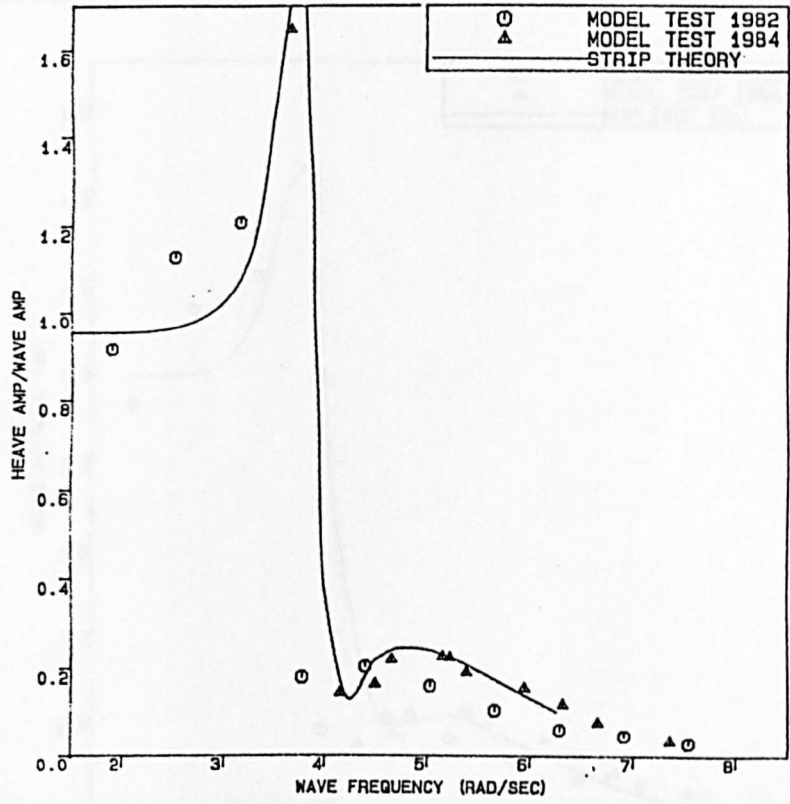
SWATH HEAVE IN HEAD SEAS
V=0.0
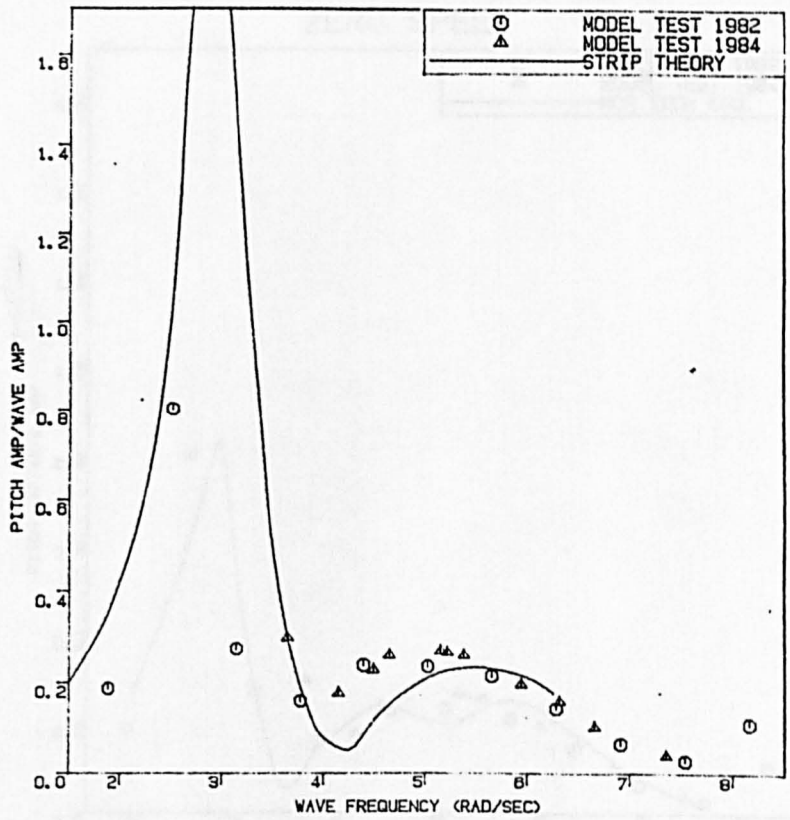
SWATH PITCH IN HEAD SEAS
ZERO SPEED

FIG. 5.8
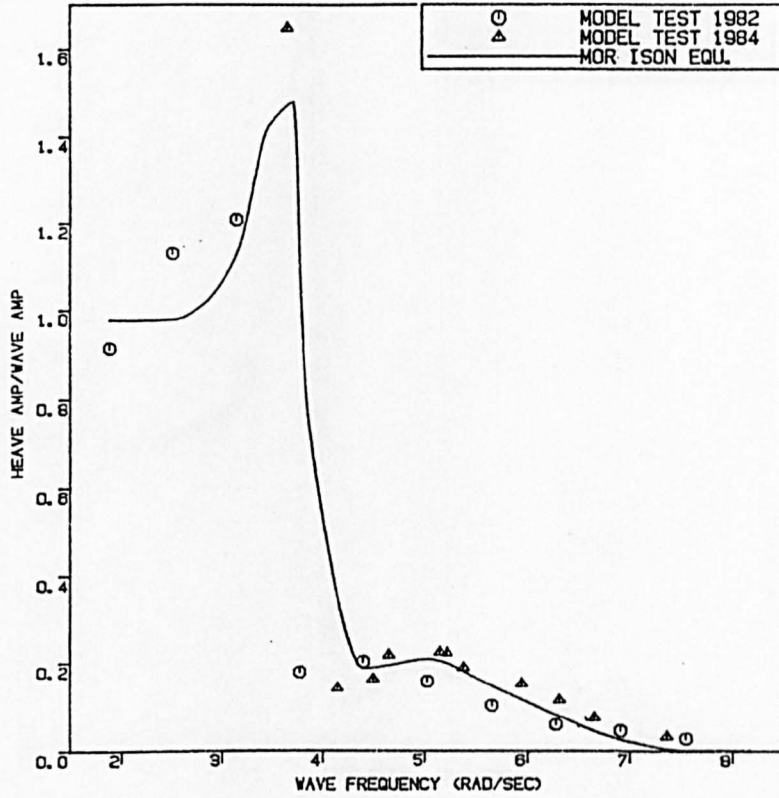
SWATH HEAVE IN HEAD SEAS
ZERO SPEED
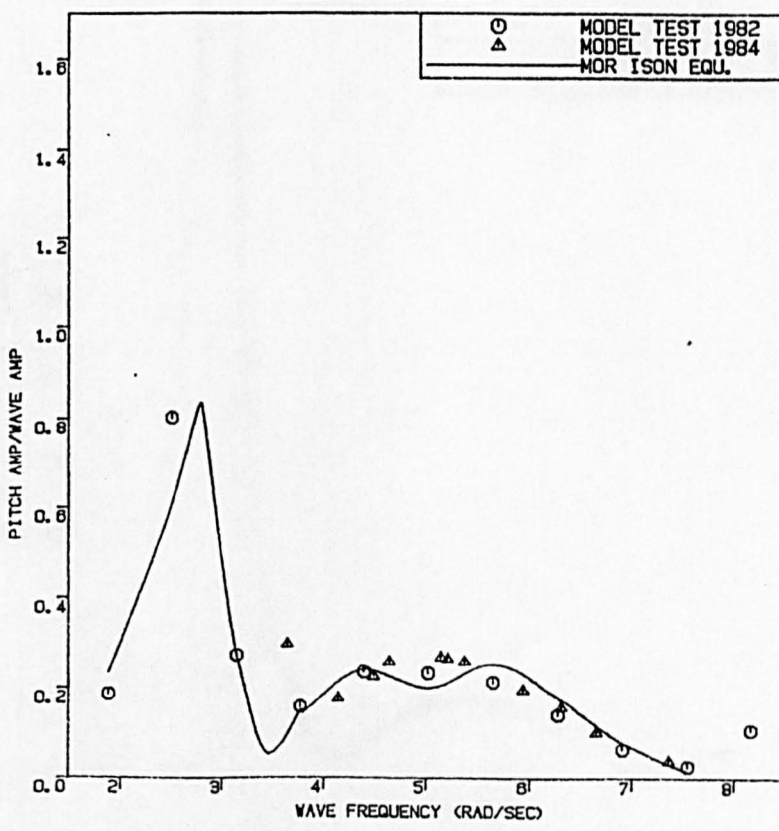
SWATH PITCH IN HEAD SEAS
ZERO SPEED

FIG. 5.9
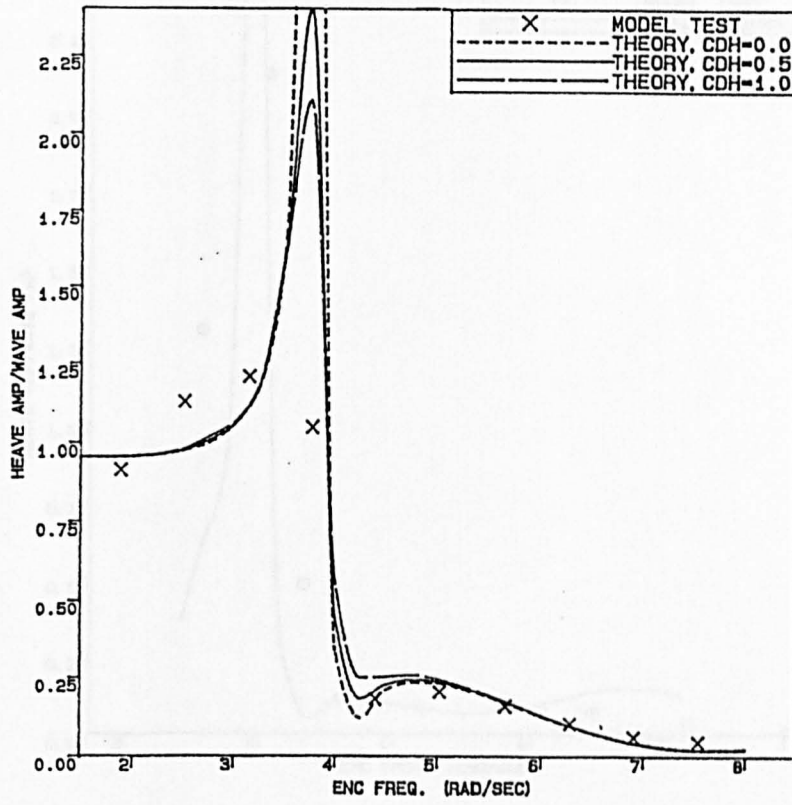
SWATH BARE HULL HEAVE
ZERO SPEED
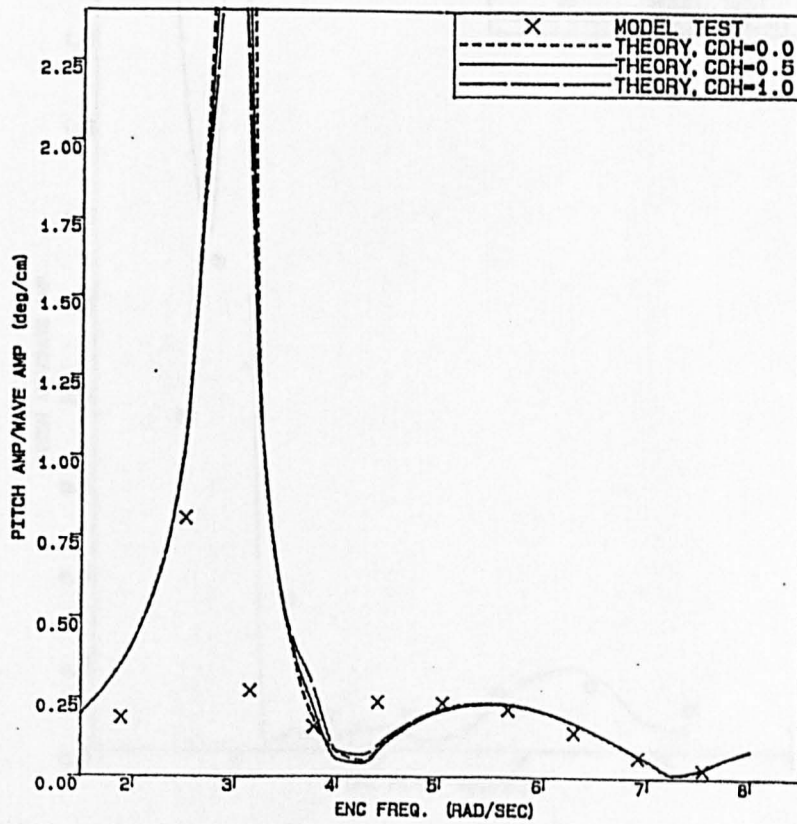
SWATH BARE HULL PITCH
ZERO SPEED
FIG. 5.10
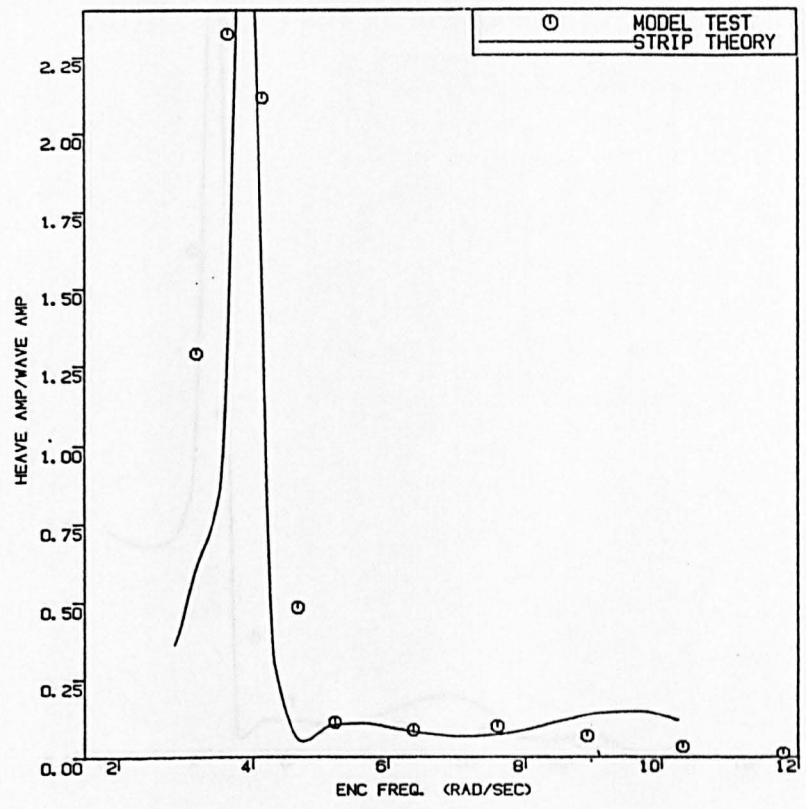
SWATH BARE HULL V=1.0 m/sec
HEAVE IN HEAD SEAS
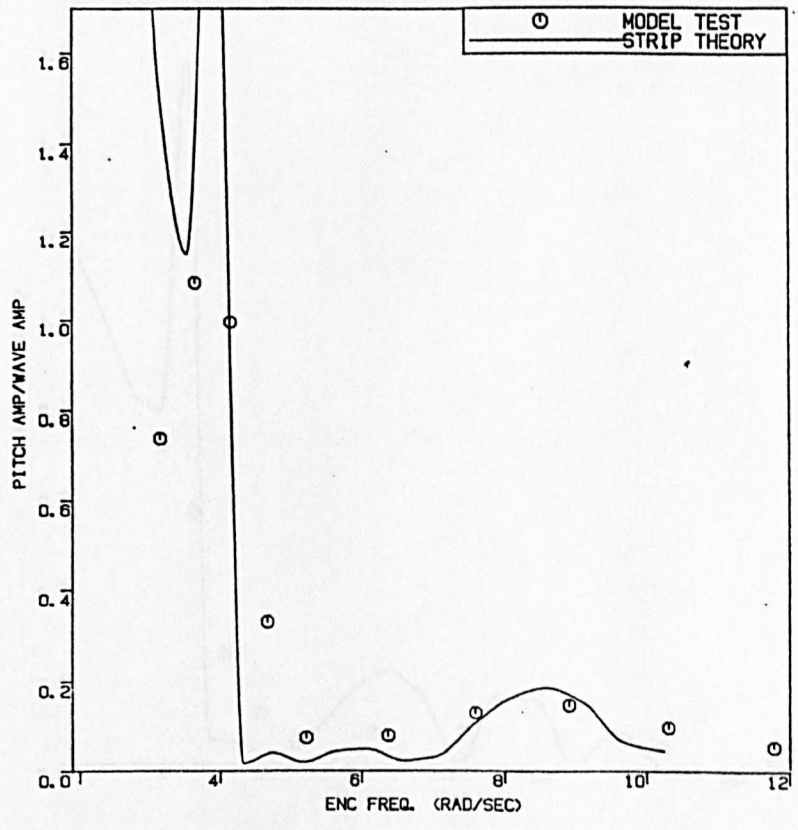
SWATH BARE HULL V=1.0 m/sec
PITCH IN HEAD SEAS

FIG. 5.11
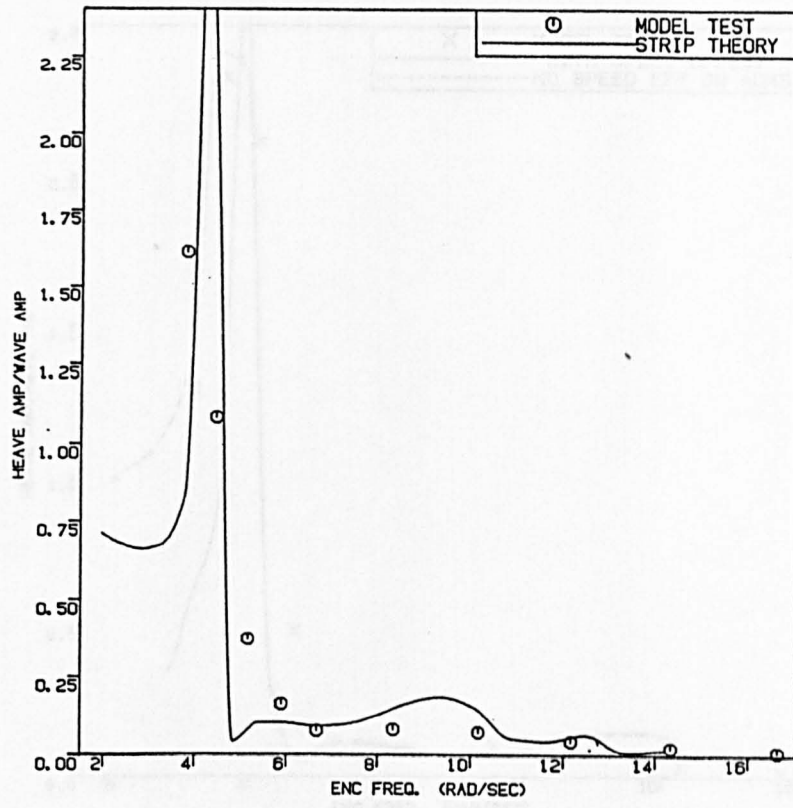
SWATH BARE HULL V=2.0 m/sec
HEAVE IN HEAD SEAS
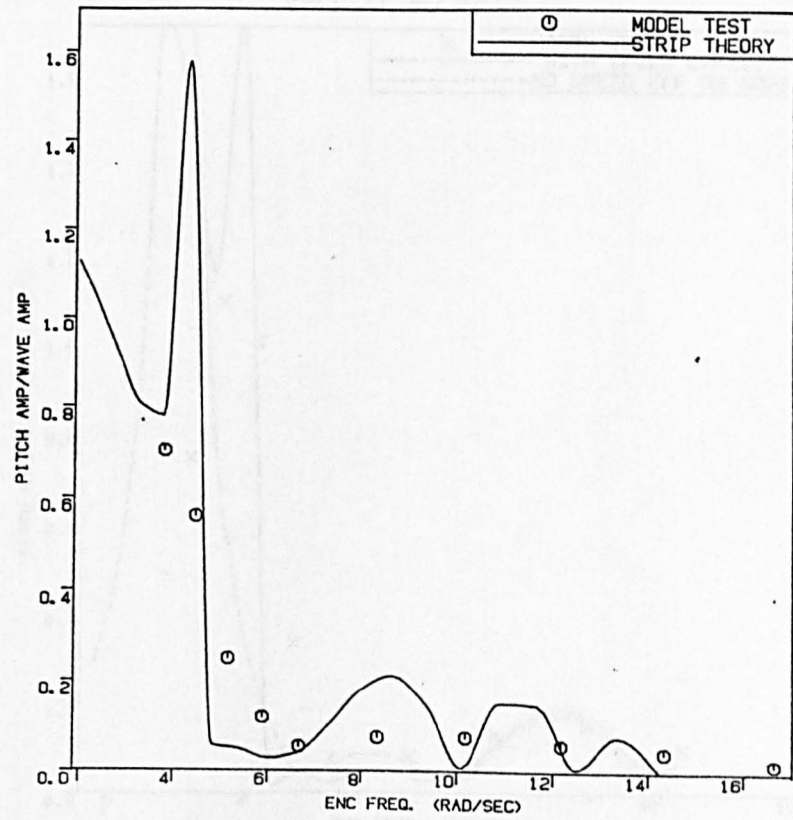


SWATH BARE HULL V=2.0 m/sec
PITCH IN HEAD SEAS

FIG. 5.12
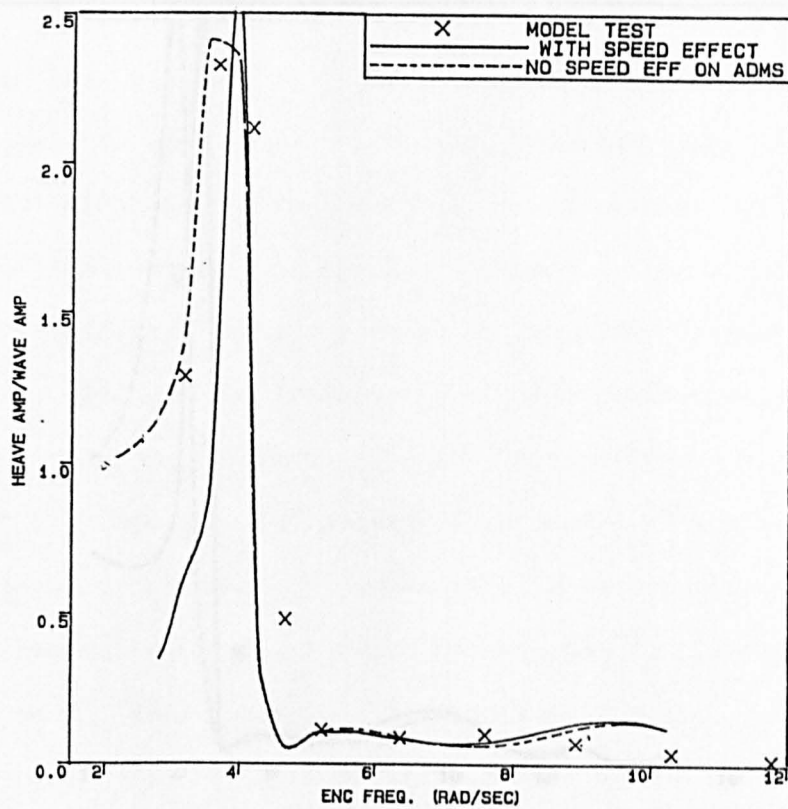
BARE HULL HEAVE
V=1.0 M/SEC
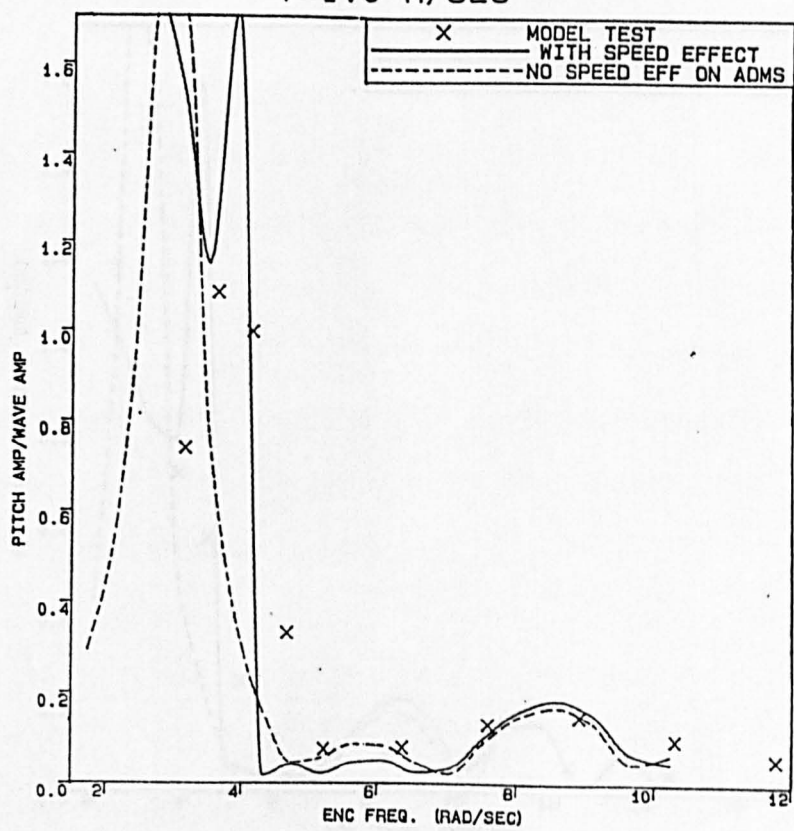
BARE HULL PITCH
V=1.0 M/SEC
FIG. 5.13
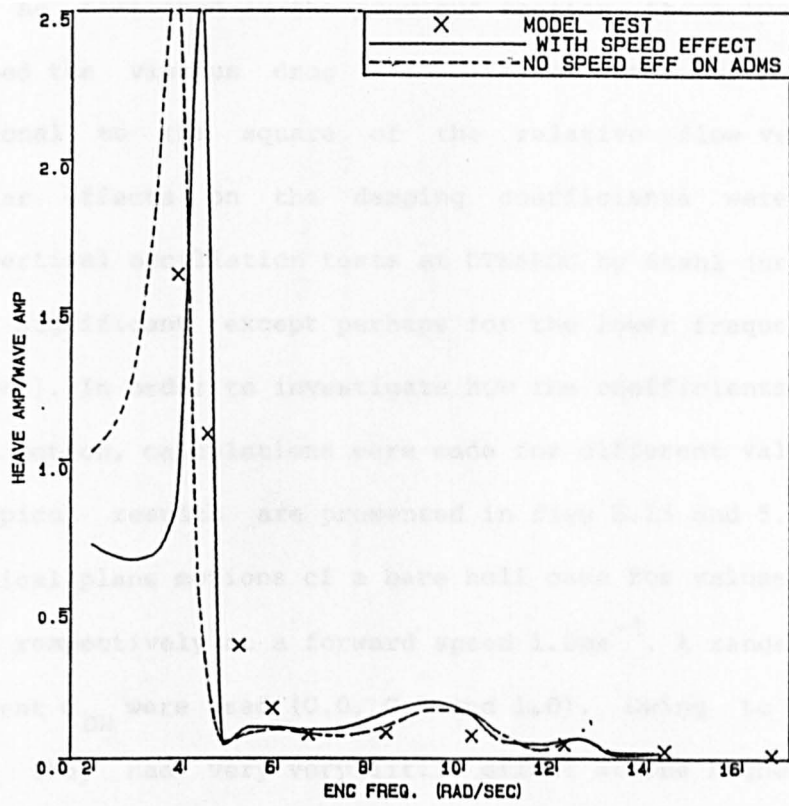
BARE HULL HEAVE
V=2.0 M/SEC
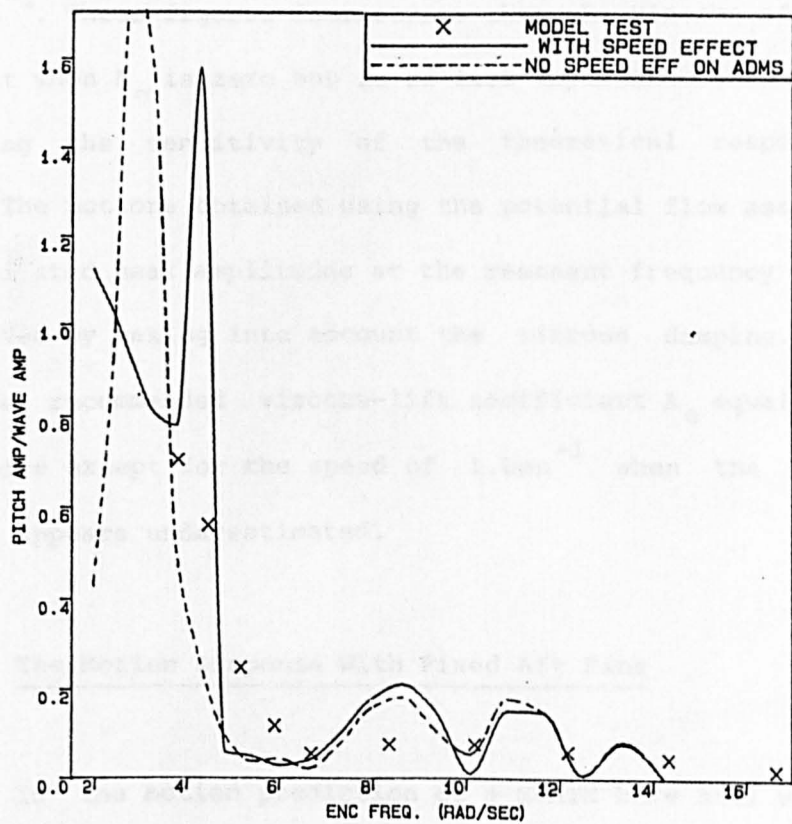
BARE HULL PITCH
V=2.0 M/SEC
FIG. 5.14

As mentioned in the previous section, these two coefficients determined the viscous drag and lift effects. Both effects are proportional to the square of the relative flow velocity. These non-linear effects on the damping coefficients were found by forced-vertical oscillation tests at DTNSRDC by Stahl (unpublished) to be not significant except perhaps for the lower frequencies at high speeds [49]. In order to investigate how the coefficients affect the vertical motion, calculations were made for different values of A_o and C_{DH}. Typical results are presented in figs 5.15 and 5.16 which show the vertical plane motions of a bare hull case for values of $A_o = 0.0$ and 0.07 respectively at a forward speed $1.0ms^{-1}$. A range of hull drag coefficient C_{DH} were used (0.0, 0.5 and 1.0). Owing to the viscous damping, they had very very little effect at the higher frequencies but it will be noted how the higher reduce the peaks at the low frequencies. Figures 5.17 and 5.18 present the vertical plane motion at $2.0ms^{-1}$. These figures demonstrate that the viscous effect is very important when A_o is zero but is of less importance when A_o equal 0.07 indicating the sensitivity of the theoretical response to these values. The motions obtained using the potential flow assumption yield over-estimated peak amplitudes at the resonant frequency and these can be improved by taking into account the viscous damping. It appears that the recommended viscous-lift coefficient A_o equal to 0.07 is a good choice except for the speed of $1.0ms^{-1}$ when the heave motion response appears underestimated.

2.3.   The Motion Response With Fixed Aft Fins

In the motion prediction of a SWATH bare hull with fixed aft fins, two factors received special attention - the drag coefficient and lift-curve slope. In order to avoid possible confusion with the
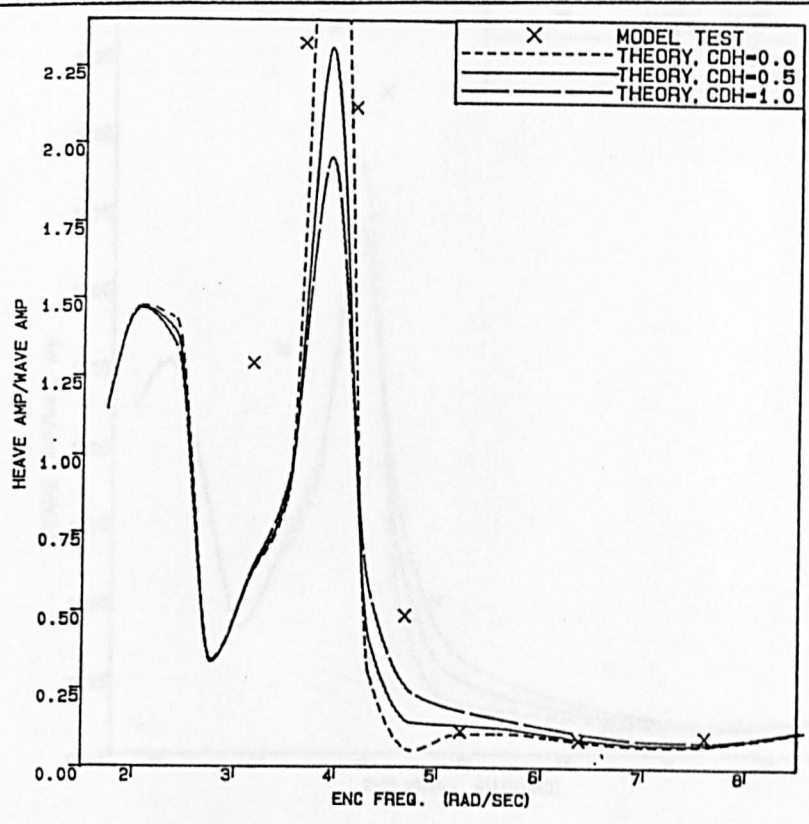
BARE HULL HEAVE AO=0.0
Fn=0.26 (V=1.0 m/s)
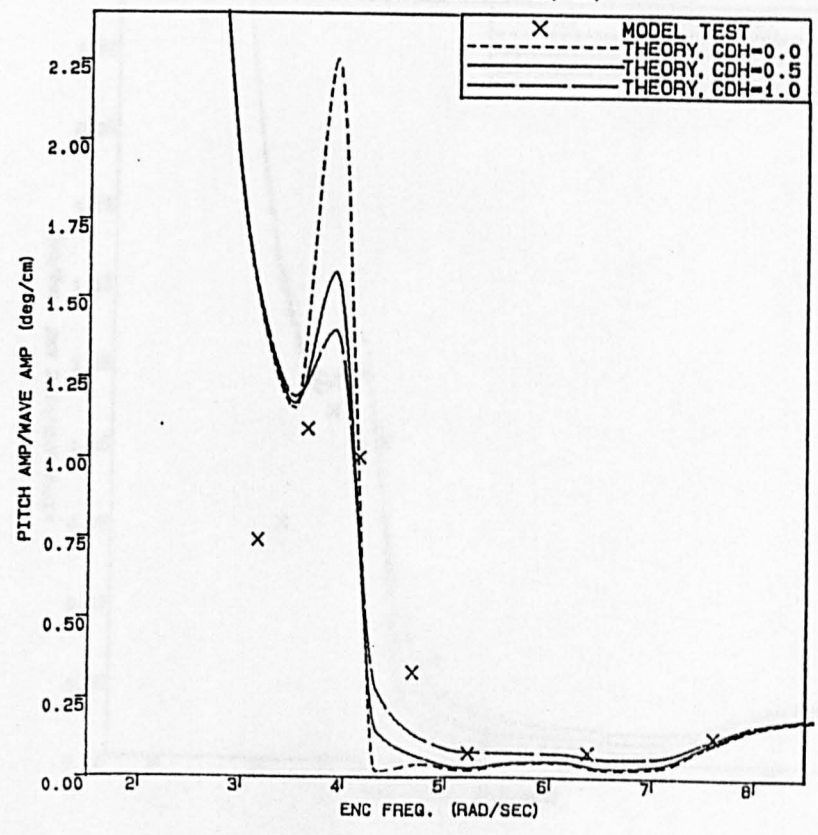

BARE HULL PITCH AO=0.0
Fn=0.26 (V=1.0 m/s)

FIG. 5.15
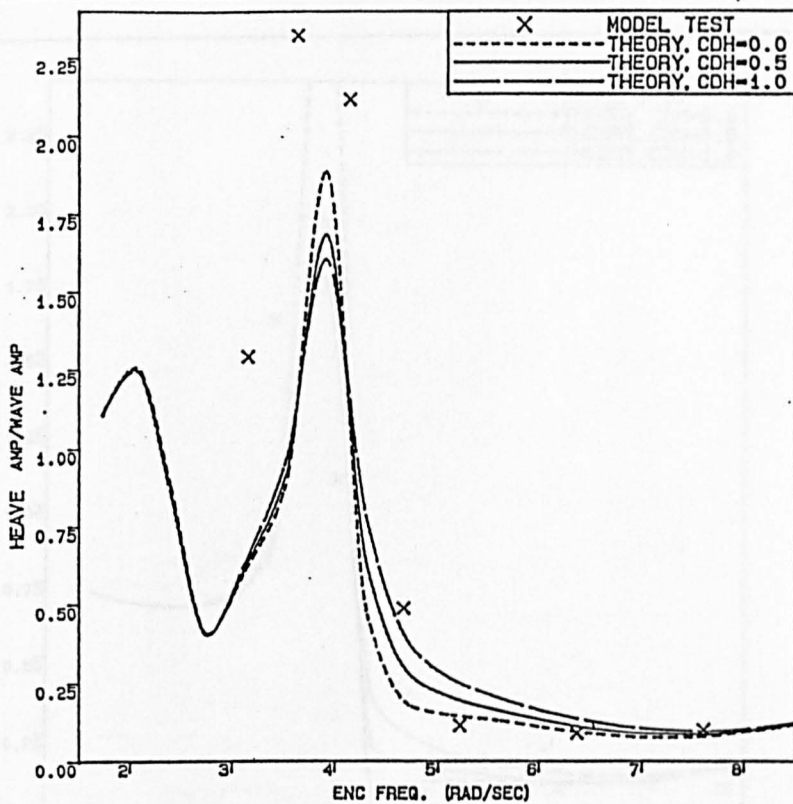
BARE HULL HEAVE A0=0.07
Fn=0.26 (V=1.0 m/s)
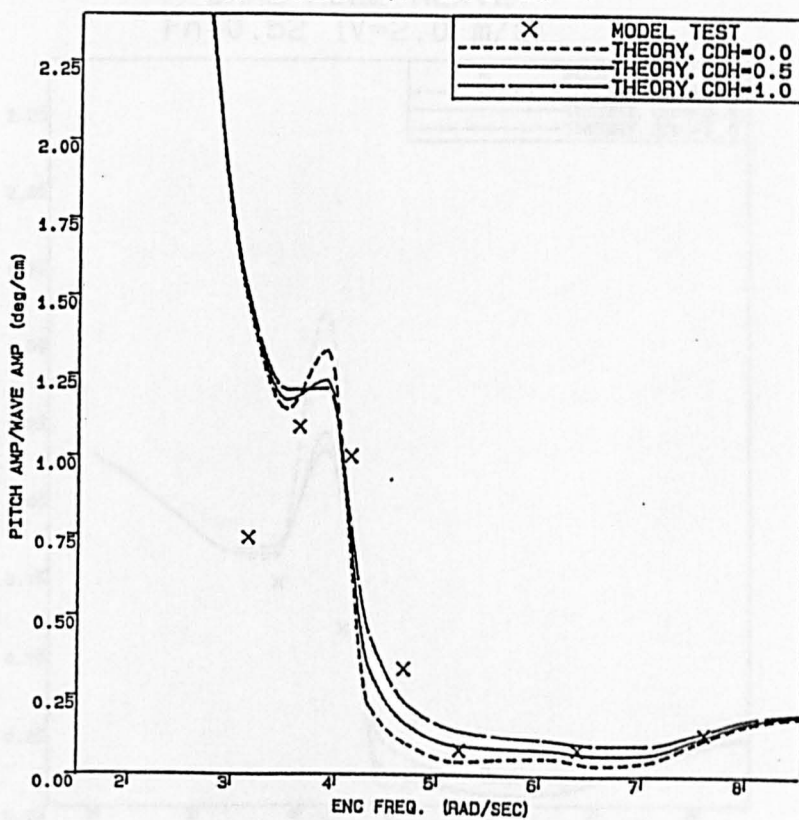
BARE HULL PITCH A0=0.07
Fn=0.26 (V=1.0 m/s)
FIG. 5.16
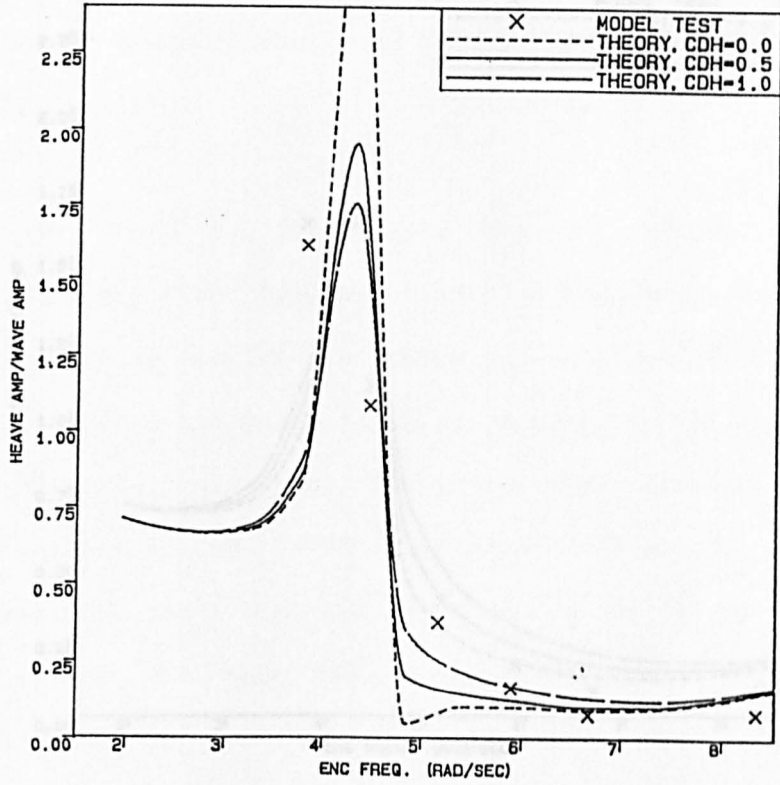
BARE HULL HEAVE
Fn=0.52 (V=2.0 m/s)
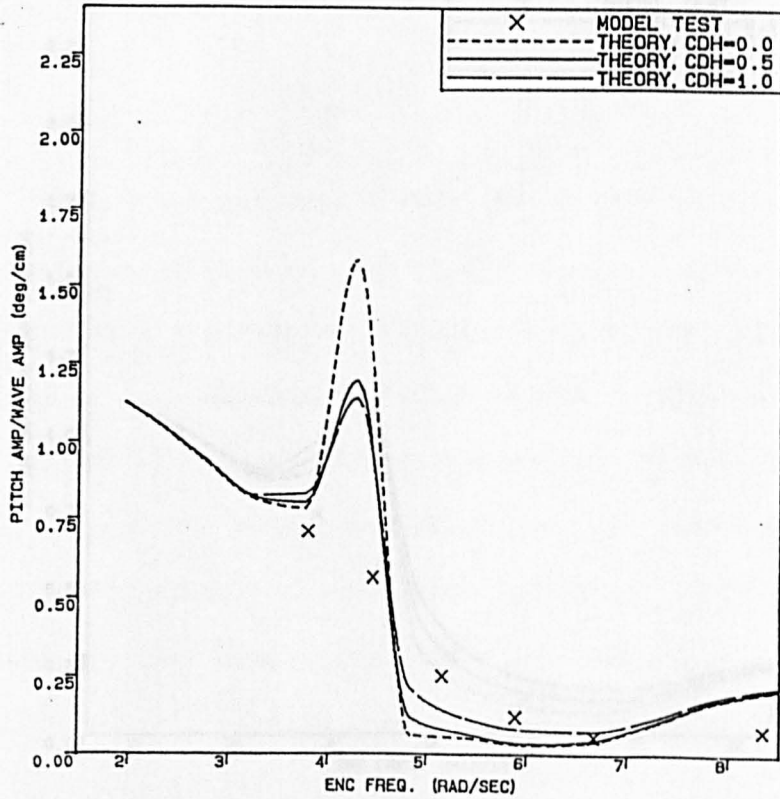
BARE HULL PITCH A0=0.0
Fn=0.52 (V=2.0 m/s)

FIG. 5.17

BARE HULL HEAVE AO=0.07
Fn=0.52 (V=2.0 m/s)
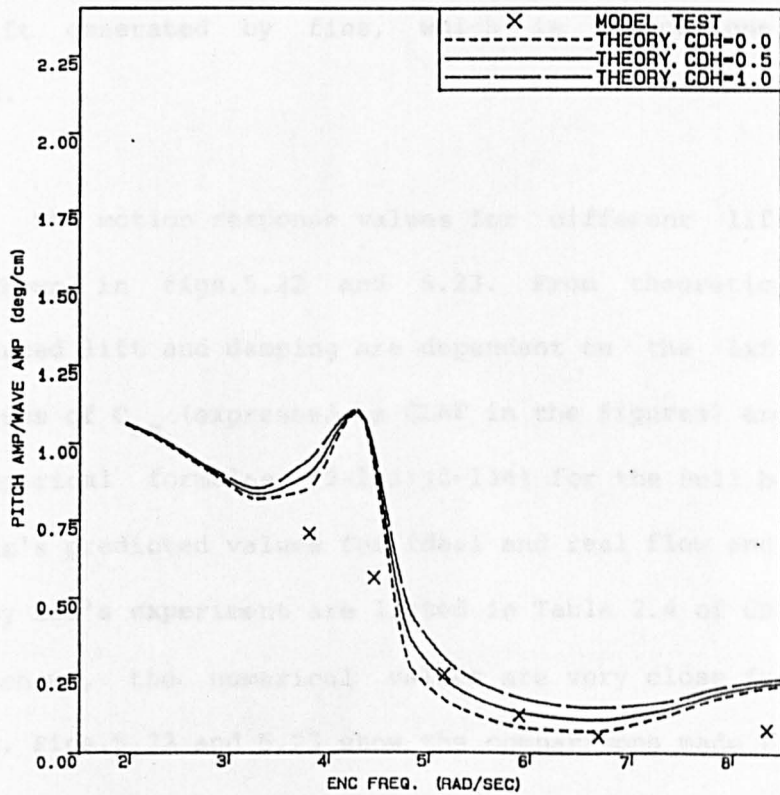
BARE HULL PITCH AO=0.07
Fn=0.52 (V=2.0 m/s)

FIG. 5.18

drag of hull body, C_{DF} is used for the drag coefficient of the fin. The value, as shown in fig. 5.19 from Reference [88], is a function of the angle of attack.

In order to investigate how C_{DF} effects the whole SWATH motion response, figs. 5.20 and 5.21 have been prepared then show the heave and pitch motion for three C_{DF} values (0.0, 0.5, 1.0) at two different speeds. According to these results, the drag force generated by fins was relatively small. Therefore, very little effect on the motion characteristics were experienced when the C_{DF} values changed. The comparisons shown here are based on a value of A_o = 0.07 and C_{DH} = 0.5 for the bare hull. The predictions compared with the experiments are in good agreement in heave and pitch motion for Fn = 0.26 but not for Fn = 0.52 where the corresponding speed is $2.0ms^{-1}$. The discrepancies may arise from the inaccurate estimate of the lift generated by fins, which is proportional to the speed squared.

The motion response values for different lift-curve slopes are shown in figs.5.22 and 5.23. From theoretical prediction, fin-induced lift and damping are dependent on the lift-curve slope. The values of $C_{L\alpha}$ (expressed as CLAF in the figures) are calculated by the empirical formulae (2-133)(2-134) for the hull body-fin effect. Abkowitz's predicted values for ideal and real flow and the numerical value by Lee's experiment are listed in Table 2.4 of Chapter 2. As the table shows, the numerical values are very close for the different methods. Figs.5.22 and 5.23 show the comparisons made for the body-fin effect, Lee's experimental value, and the two-dimension fin theory (where $C_{L\alpha}$ equals 2π). The results show that $C_{L\alpha}$ = 3.3268 obtained by using the body-fin correction gave the best agreement in the motion
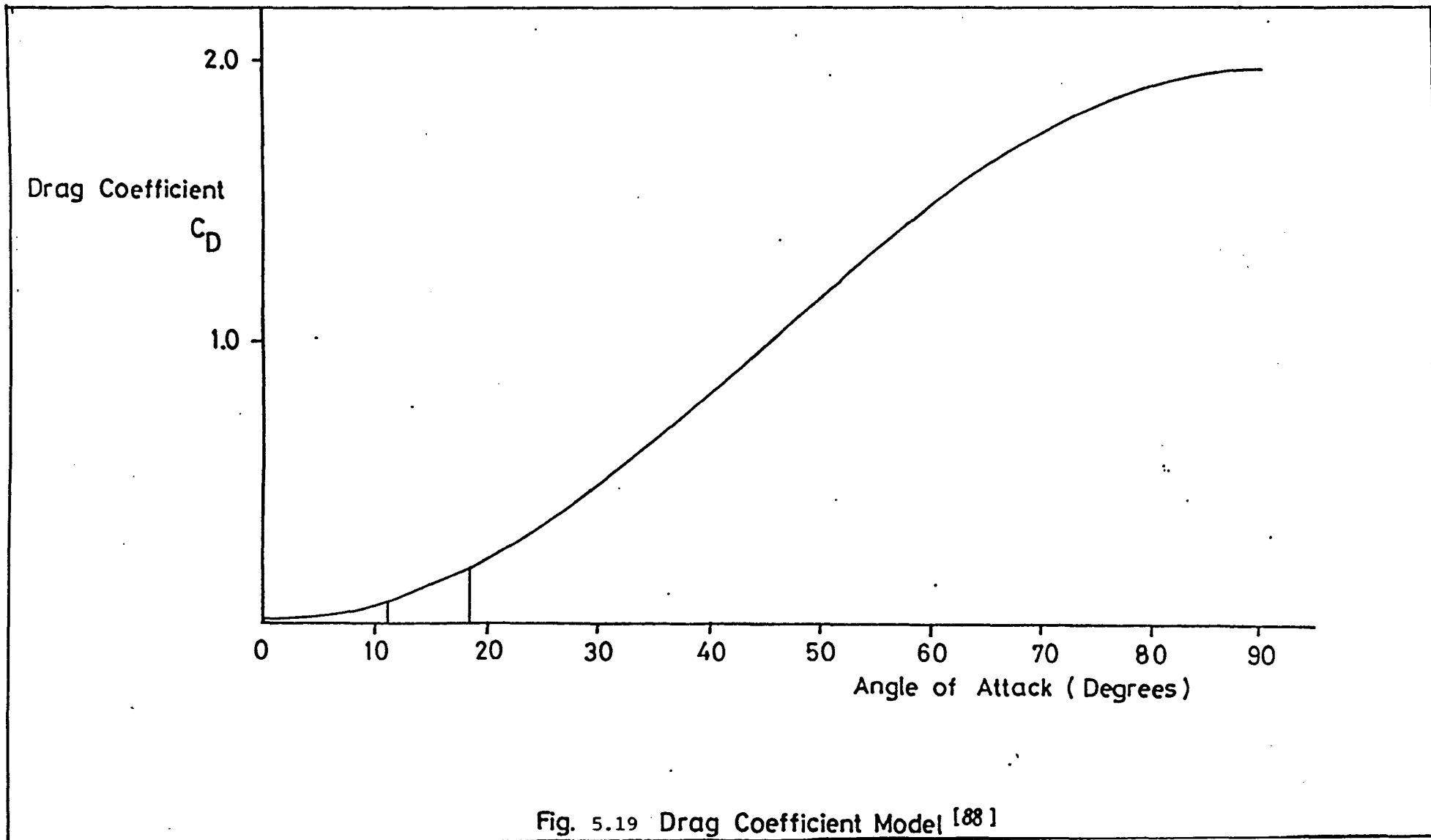
Fig. 5.19 Drag Coefficient Model [88]
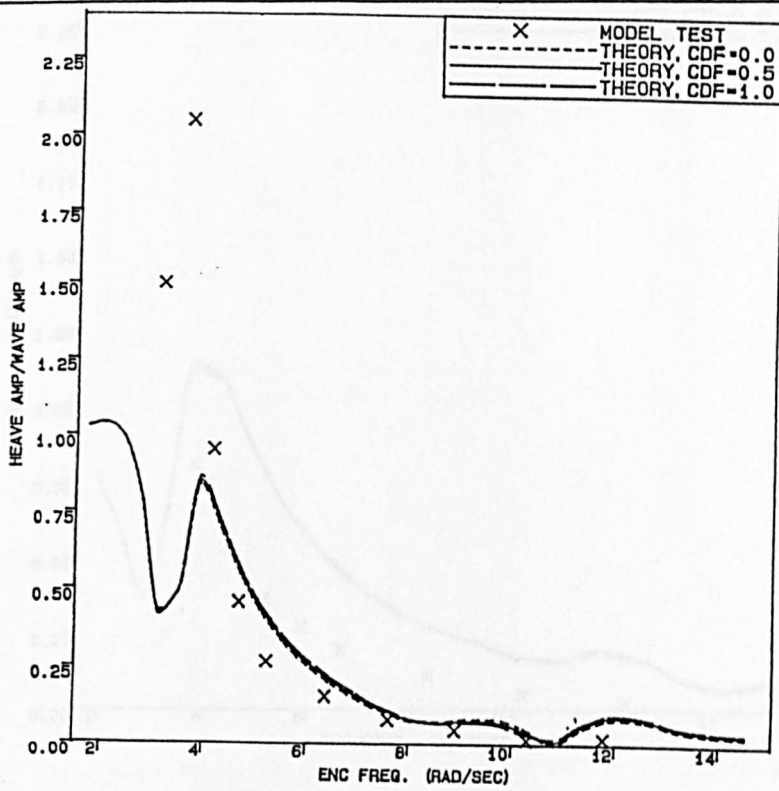
WITH FIXED AFT FINS, HEAVE
Fn=0.26, CDH=0.5, A0=0.07
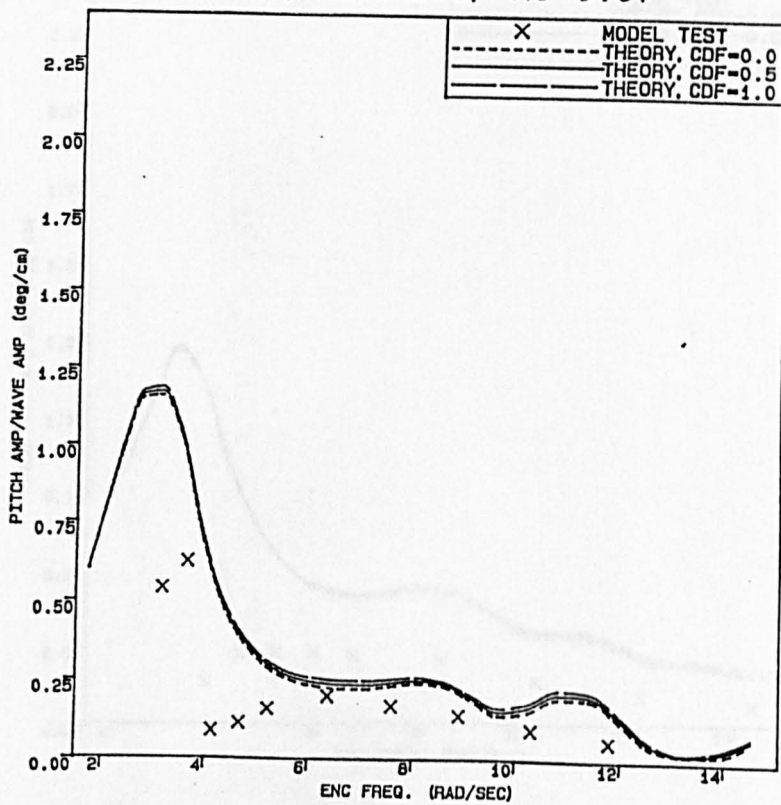
WITH FIXED AFT FINS, PITCH
Fn=0.26, CDH=0.5, A0=0.07

FIG. 5.20
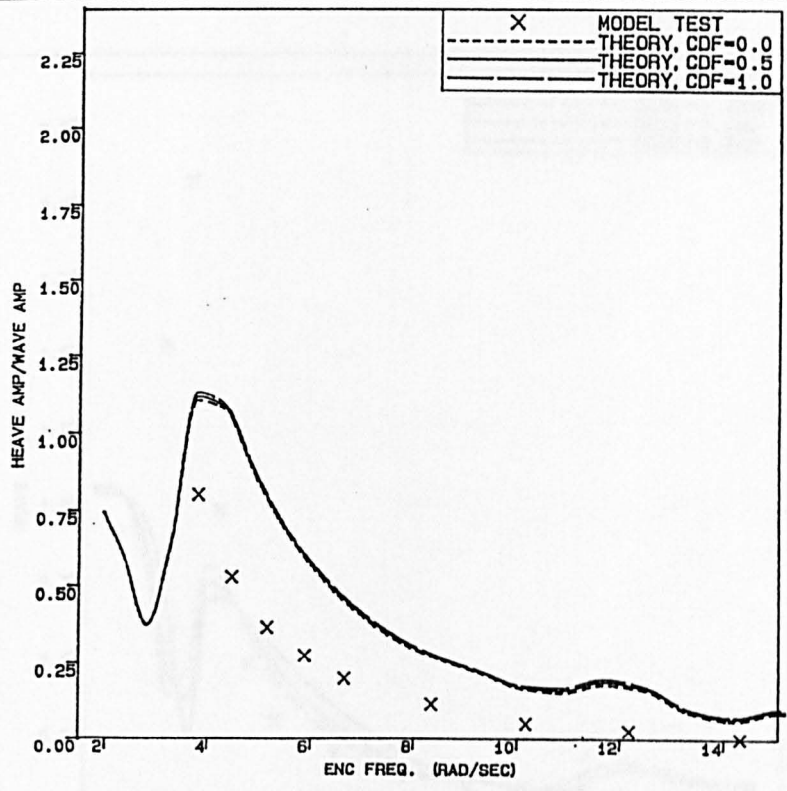
WITH AFT FINS, HEAVE
Fn=0.52, CDH=0.5, A0=0.07
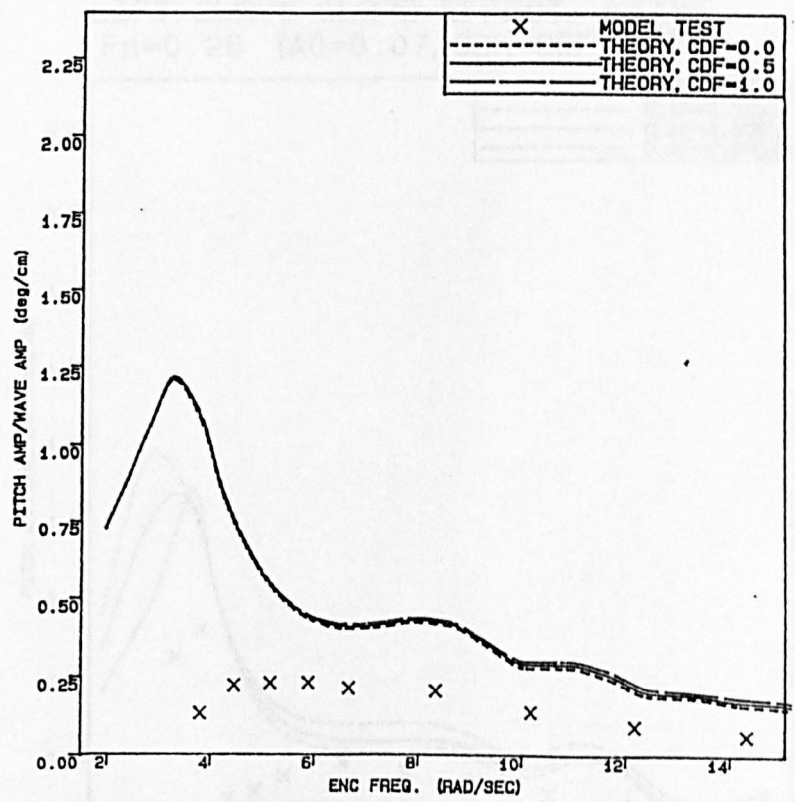
WITH AFT FINS, PITCH
Fn=0.52, CDH=0.5, A0=0.07

FIG. 5.21
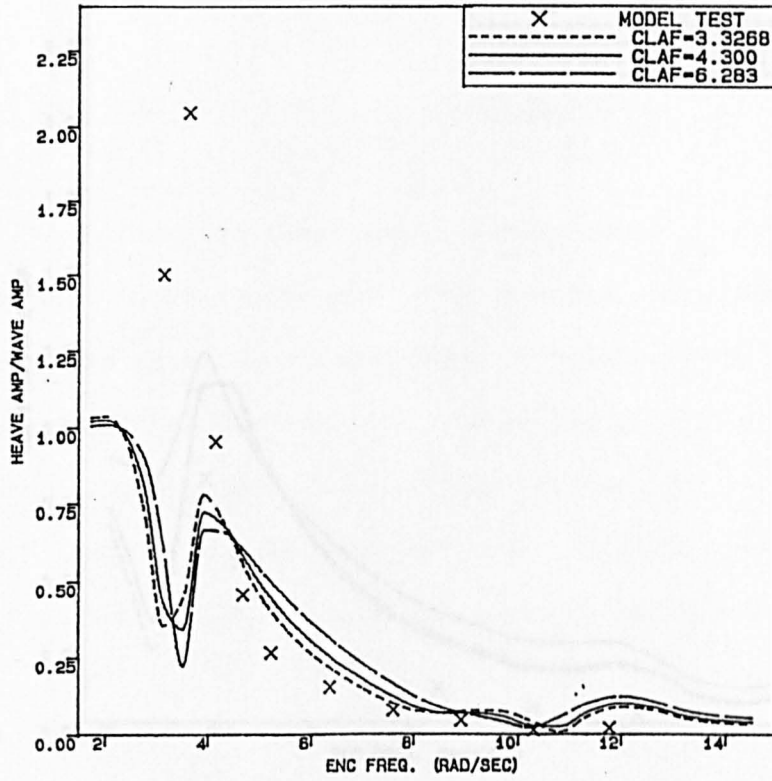
LIFT-CURVE SLOPE EFFECT, HEAVE
Fn=0.26 (A0=0.07, CDH=CDF=0.5)
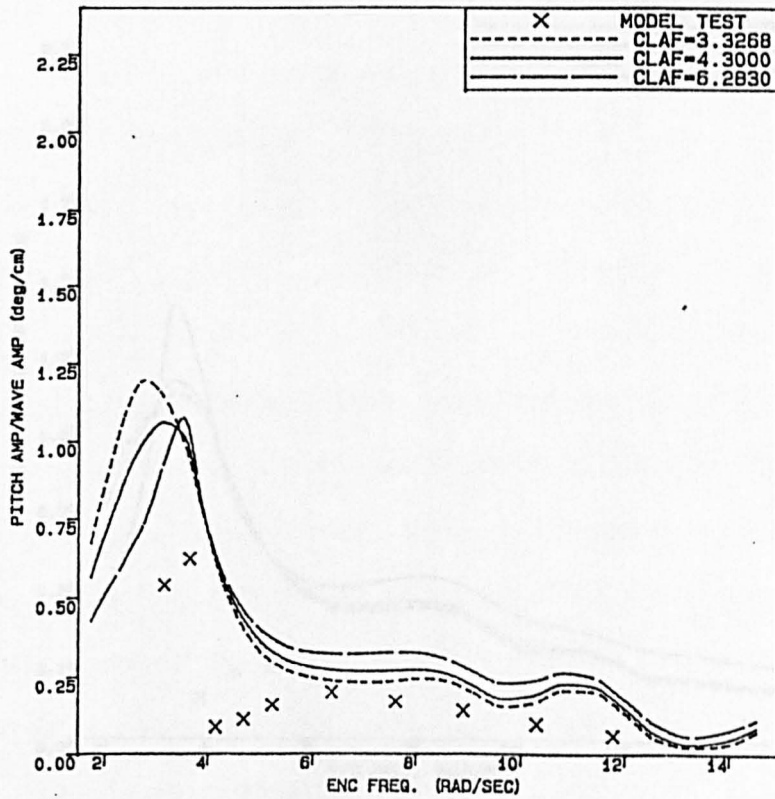
LIFT-CURVE SLOPE EFFECT, PITCH
Fn=0.26 (A0=0.07, CDH=CDF=0.5)

FIG. 5.22
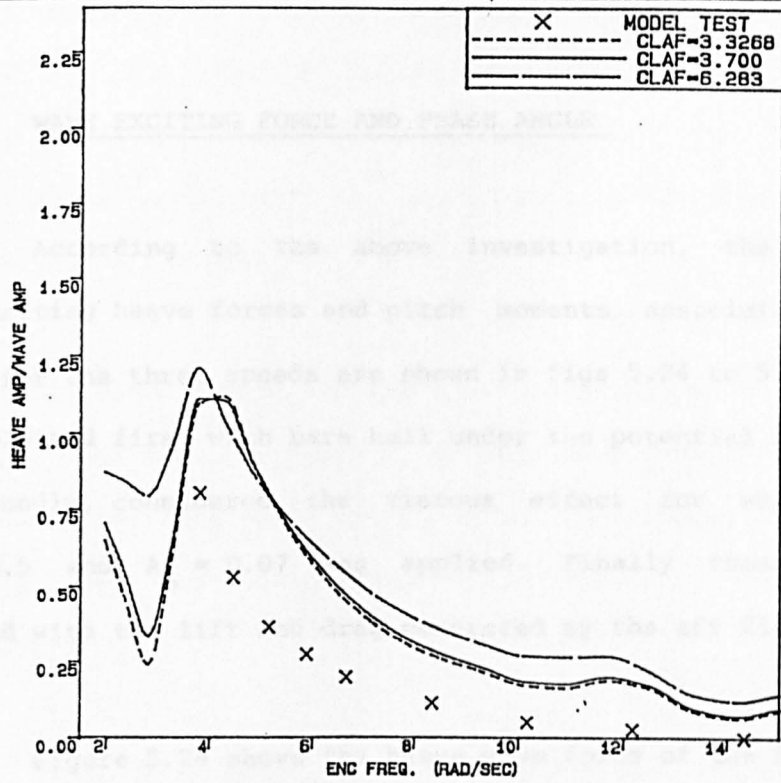
LIFT-CURVE SLOPE EFFECT, HEAVE
Fn=0.52 (AO=0.07, CDH=CDF=0.5)
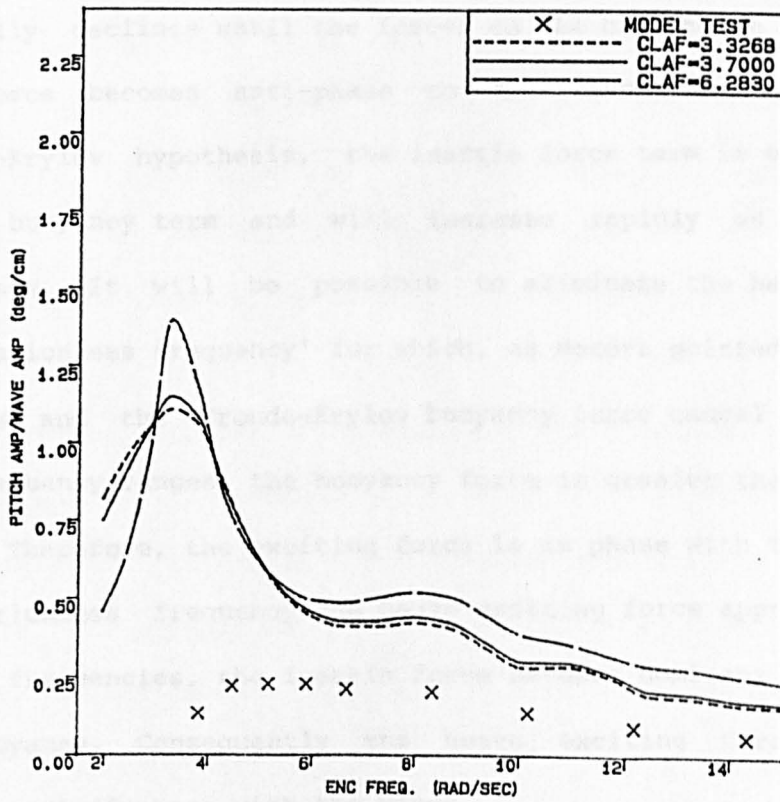
LIFT-CURVE SLOPE EFFECT, PITCH
Fn=0.52 (AO=0.07, CDH=CDF=0.5)

FIG. 5.23

prediction.

3.   WAVE EXCITING FORCE AND PHASE ANGLE

According to the above investigation, the results of the wave-exciting heave forces and pitch moments associated with phase angles for the three speeds are shown in figs 5.24 to 5.29. The curves were plotted first with bare hull under the potential flow assumption and secondly, considered the viscous effect for which the value $C_{DH} = 0.5$ and $A_o = 0.07$ was applied. Finally these results were combined with the lift and drag generated by the aft fins.

Figure 5.24 shows the heave wave force of the SWATH model at zero speed. The characteristics vary with frequency, indicating that in long waves the exciting force is in phase with the wave and gradually declines until the forces on the hull begin to dominate and the force becomes anti-phase to the waves. According to the Froude-Krylov hypothesis, the inertia force term is opposite in sign to the buoyancy term and will increase rapidly as the frequency increases. It will be possible to eliminate the heave force at an 'excitationless frequency' for which, as Motora pointed out [89], the inertia and the Froude-Krylov buoyancy force cancel one another. At low frequency ranges, the buoyancy force is greater than the inertia force. Therefore, the exciting force is in phase with the wave. At the excitationless frequency the heave exciting force approaches zero. At higher frequencies, the inertia force becomes dominant and cancels out the buoyancy. Consequently the heave exciting force becomes 180 degrees out-of-phase with the waves.

According to the equation of motion, at zero wave frequency

the only component of exciting force will be the buoyancy force which is equal to $\rho g \cdot A_{wp}$, where A_{wp} is the waterplane area. The corresponding response curve is shown in fig.5.10, where the ratio (heave amplitude/wave amplitude) is equal to 1 at low frequencies, ie the model contoured the wave.

The pitch moment and its phase angle are plotted in fig.5.25. Since the phase angle of heave is 90 degrees out-of-phase with pitch, therefore in the long waves the pitch has -90 degrees phase difference with the wave and this changes to +90 degrees at the excitationless frequency.

There is no speed effect on the incident and diffraction wave potential for a SWATH model without end sections and thus the excitationless frequency is the same as at zero speed. This is shown in figs. 5.26 and 5.29 where the corresponding Froude numbers are equal to 0.26 and 0.52. However, since the viscous effect is proportional to the square of the forward speed, a significant viscous contribution may be observed in the range of the excitationless frequency with less effect at very low and high frequencies

When the aft fins have been taken into account the inertia term becomes greater because of increase in the added mass of the fins. This also illustrates the importance of viscous damping induced by the control surface in limiting the motion at resonant frequencies. Thus, the excitationless frequency in the forward speed case is shifted to a higher value.

The comparisons of the wave exciting heave force and pitching moment using strip theory and the modified Morison method are plotted

in fig.5.30. The agreement for the heave force at zero speed is very good but this is not true for the pitching moment. Strip theory gives a larger estimate at the lower frequency range but a lower one at higher frequencies.

In the predictions of wave exciting heave force and pitching moment, at forward speeds for the bare hull case, high fluctuation amplitudes occurred at the high frequency range. It indicated that the application of the Frank close-fit method in the very high frequency range still has some limitations. The method tends to break down at higher frequencies and had been improved by Faltinsen in 1969 [34] by applying a numerical fairing technique. Also, the strip theory had been found to be inaccurate at high ship speeds owing to a three-dimensional hydrodynamic problem being replaced by a summation of simplified two-dimensional cross-sectional problems [90].

Particularly in the head sea case, the encounter frequencies become much higher at the high wave frequency range due to the forward speed. Therefore, a further accurate prediction might be checked by a three-dimensional numerical method [91,92] for the oscillatory ship-motion problem, including all the forward speed effects, if necessary. However, in the higher frequency range the SWATH vertical motion is very small. The unsteady fluctuation can normally be ignored and is not important.
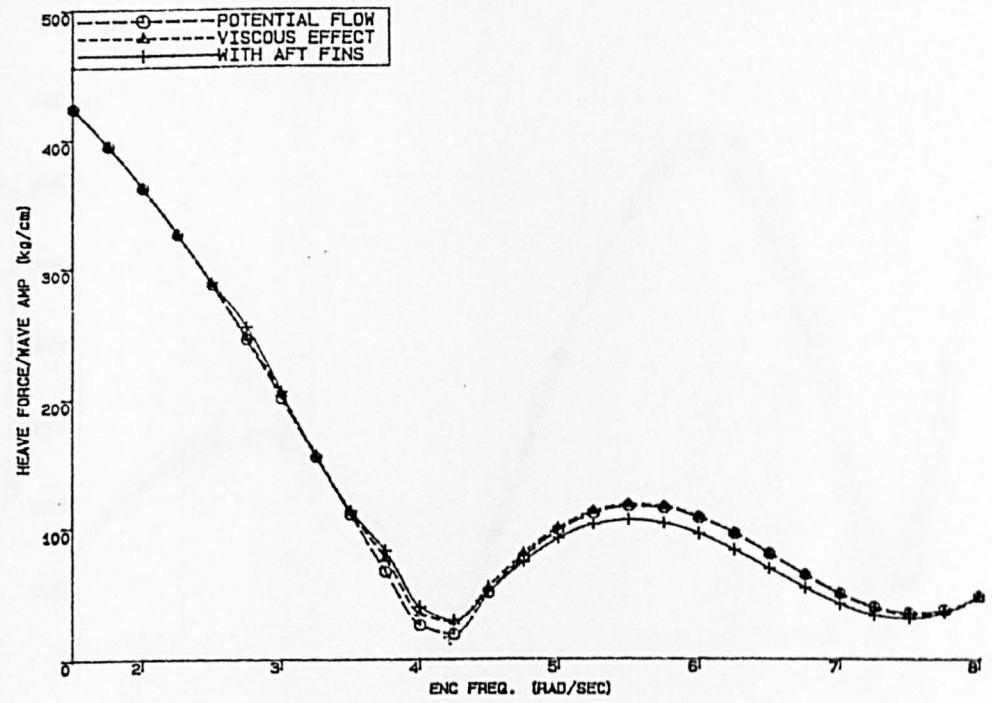
WAVE EXCITING HEAVE FORCE
ZERO SPEED
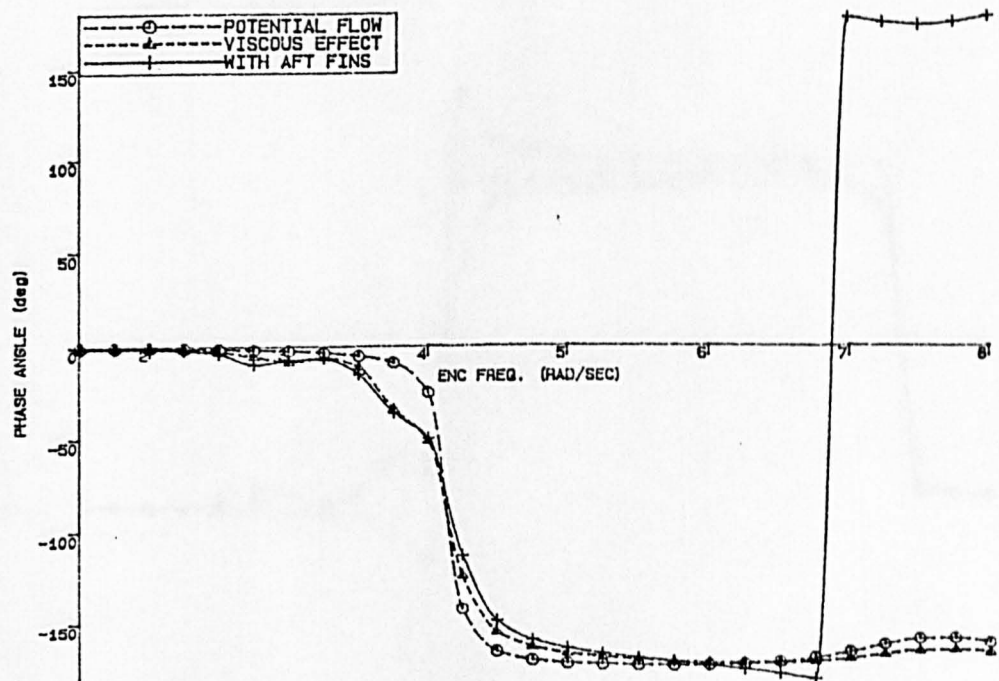
PHASE ANGLE IN HEAVE MODE
ZERO SPEED

FIG. 5.24
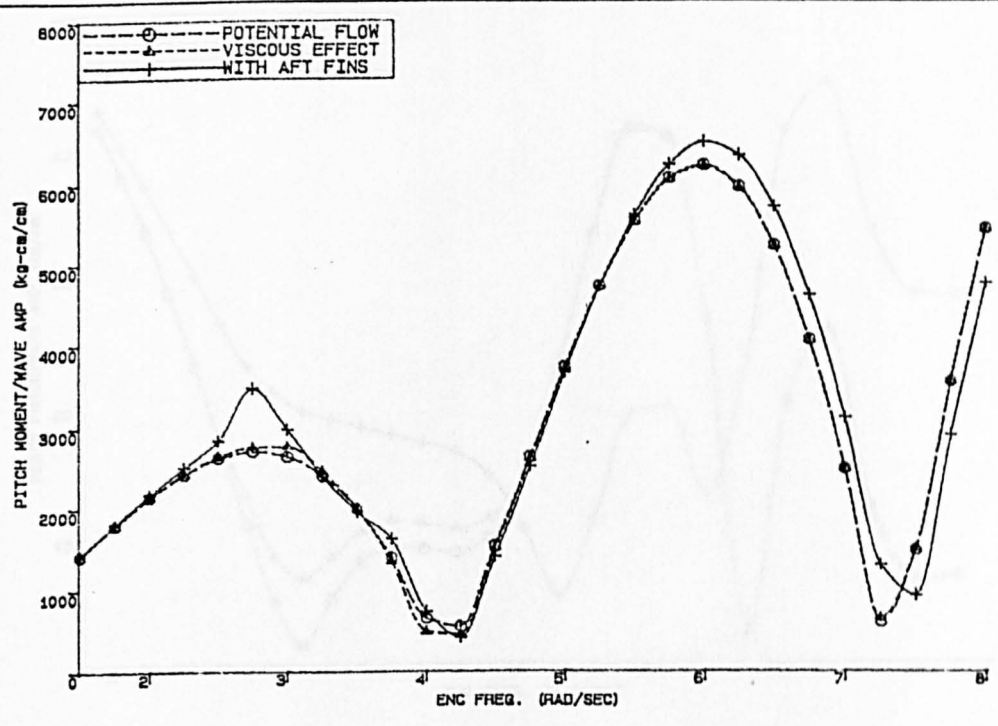
WAVE EXCITING PITCH MOMENT
ZERO SPEED
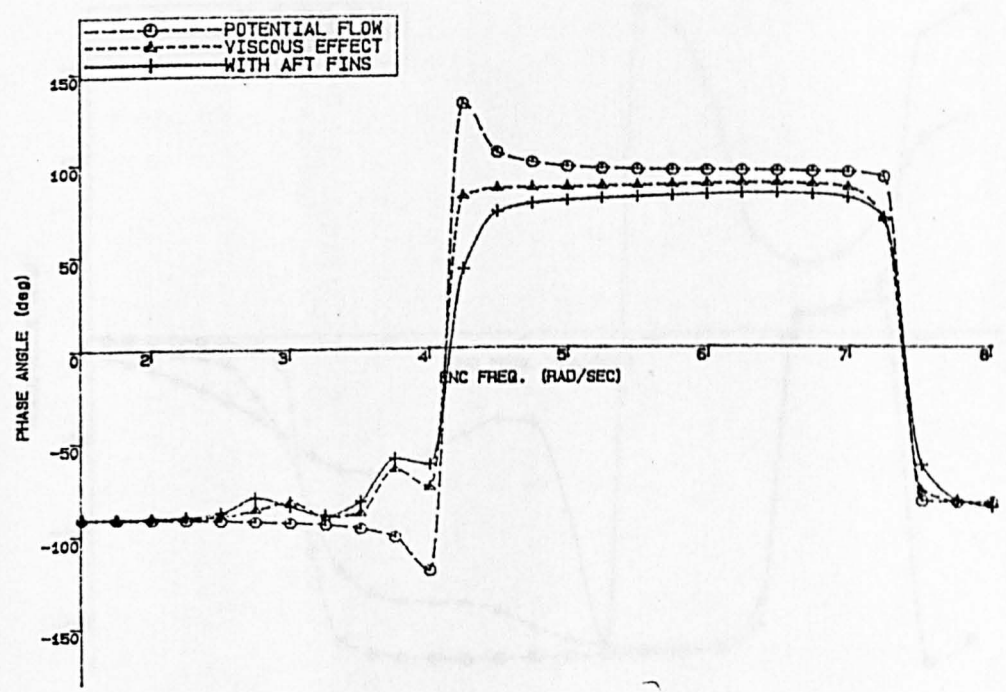
PHASE ANGLE IN PITCH MODE
ZERO SPEED

FIG. 5.25

281:
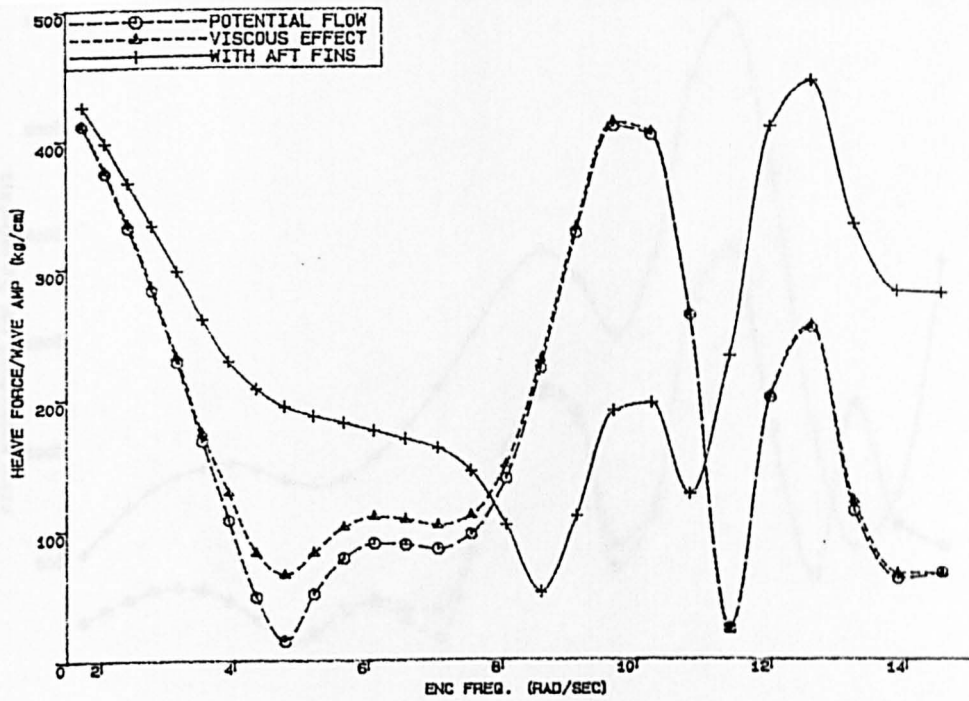
WAVE EXCITING HEAVE FORCE
Fn=0.26
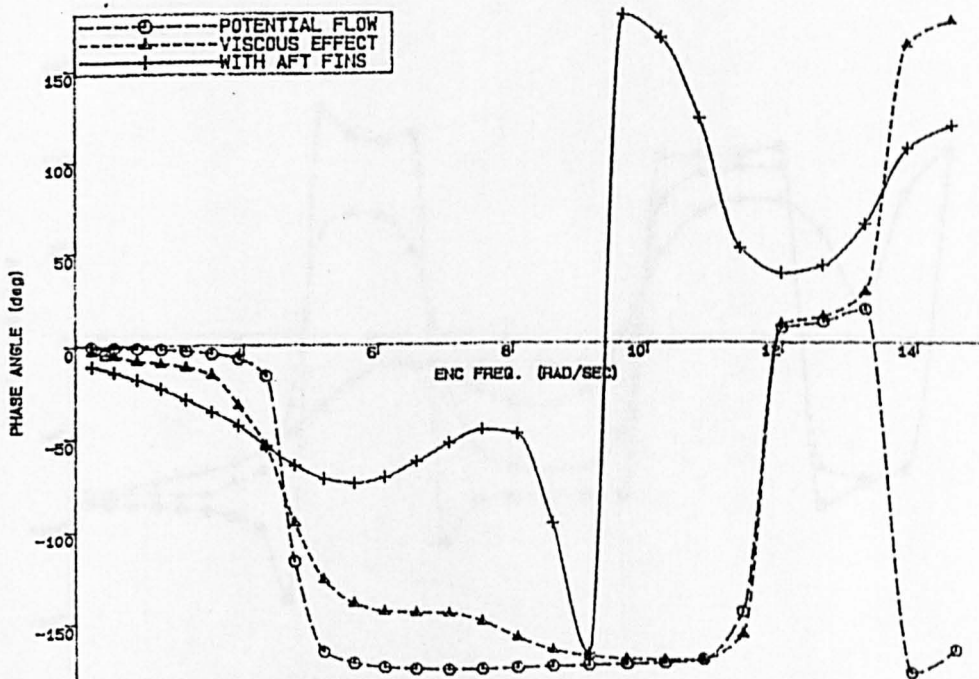
PHASE ANGLE IN HEAVE MODE
Fn=0.26

FIG. 5.26
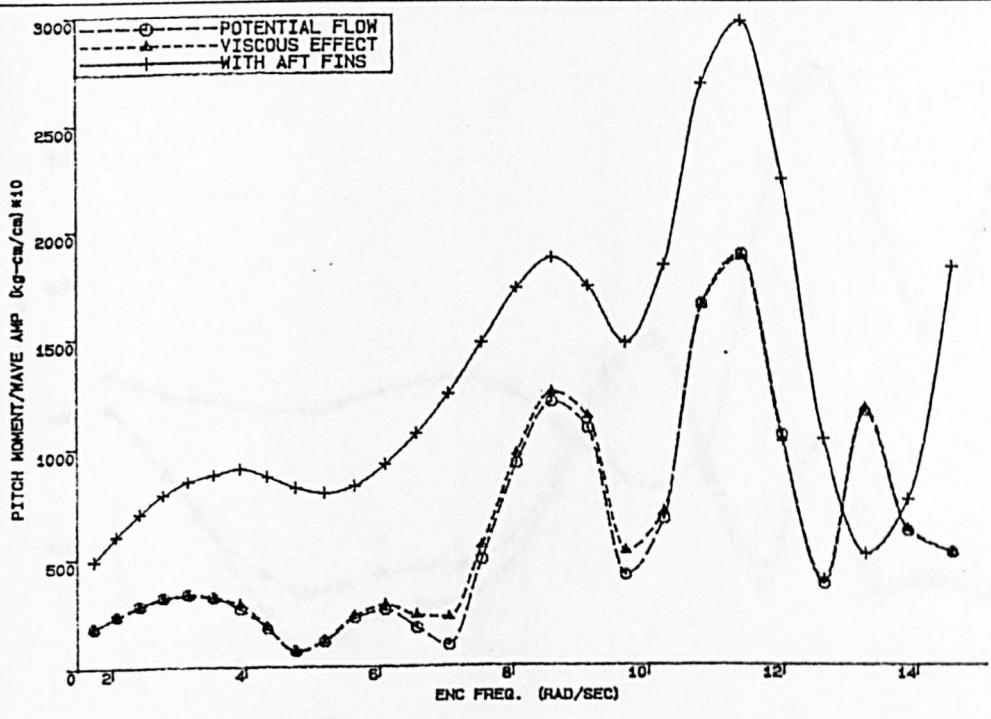
WAVE EXCITING PITCH MOMENT
Fn=0.26
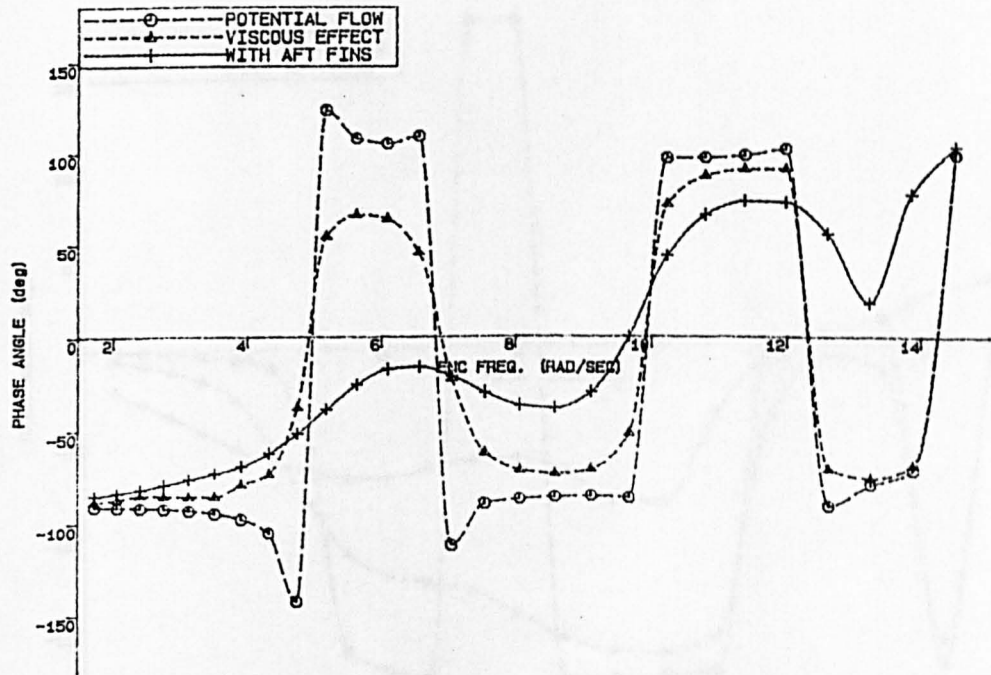
PHASE ANGLE IN PITCH MODE
Fn=0.26

FIG. 5.27
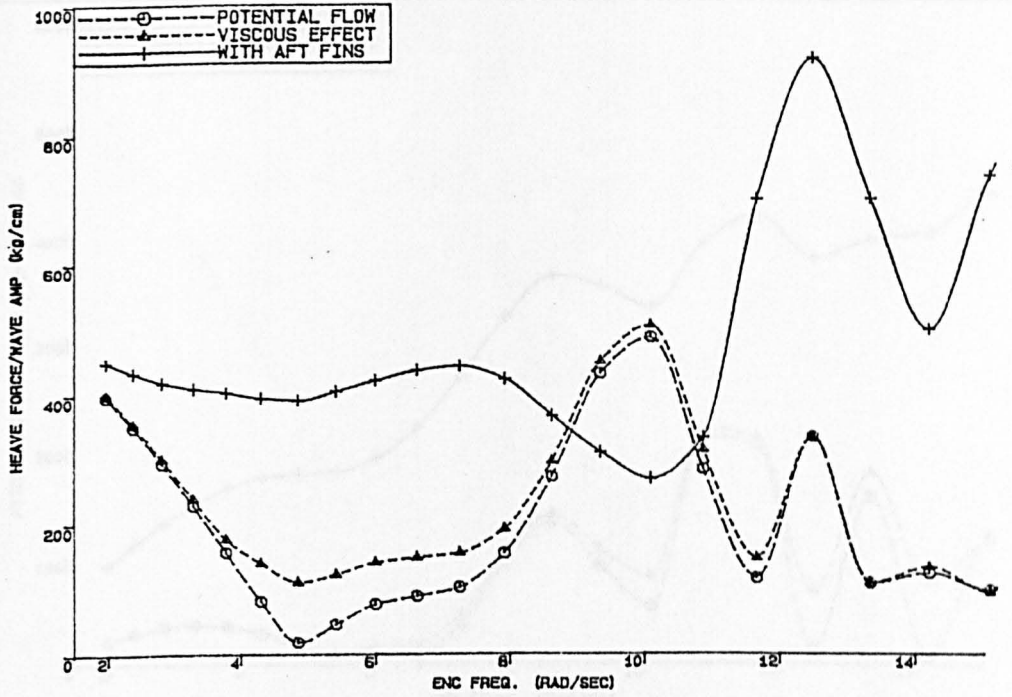
WAVE EXCITING HEAVE FORCE
Fn=0.52
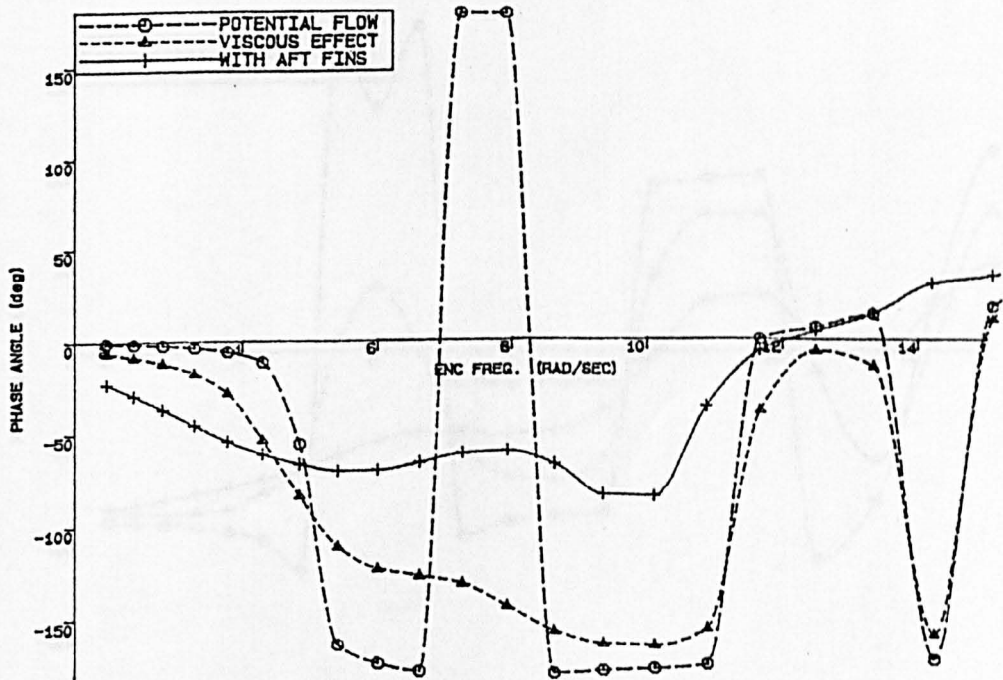
PHASE ANGLE IN HEAVE MODE
Fn=0.52

FIG. 5.28
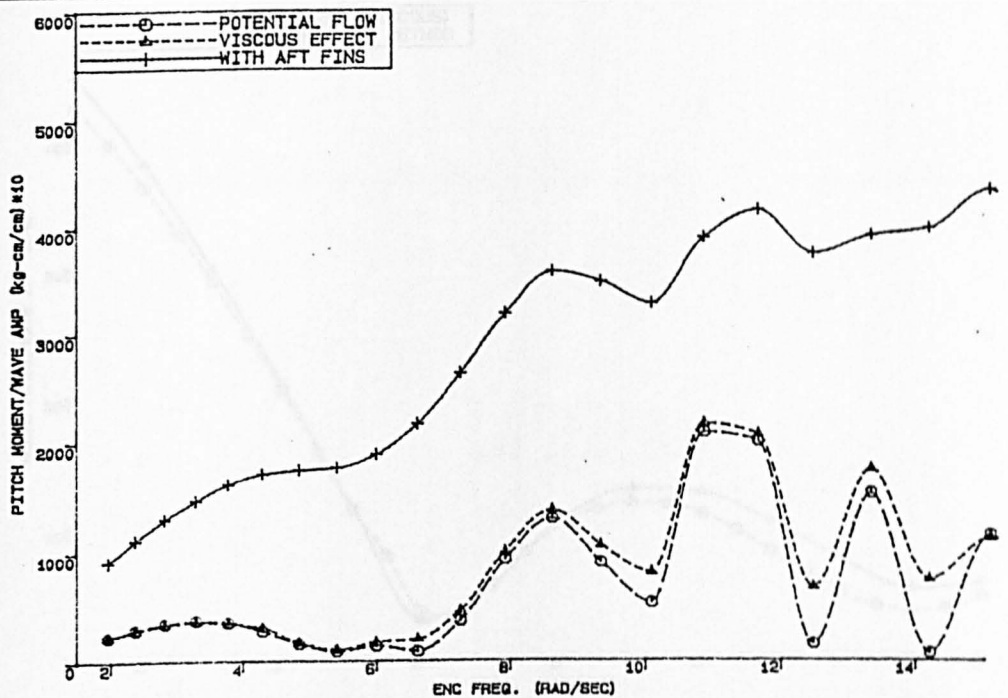
WAVE EXCITING PITCH MOMENT
Fn=0.52
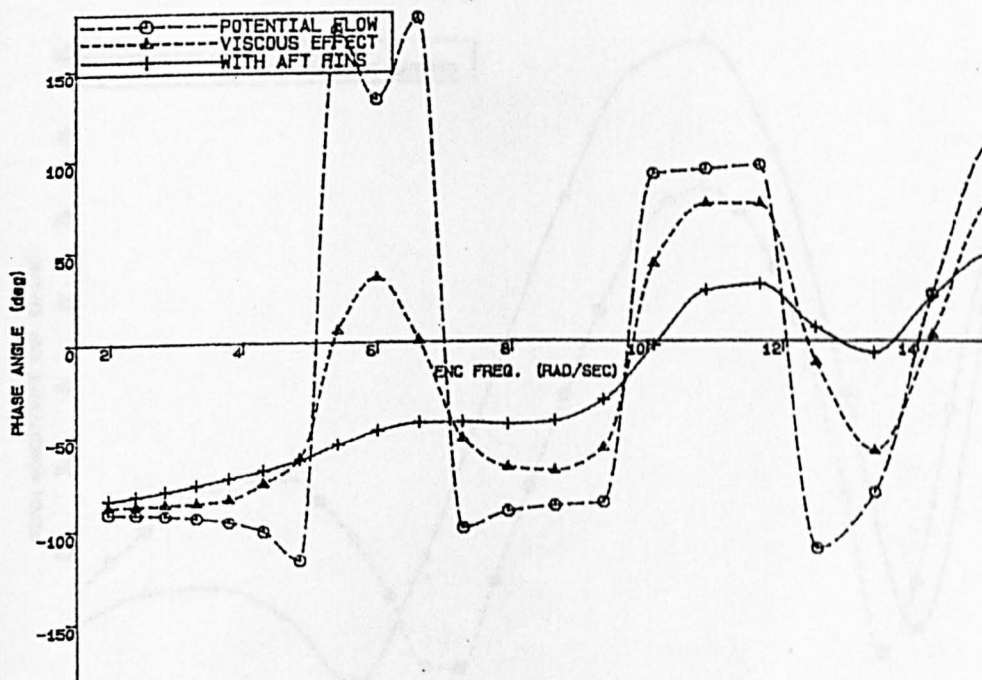
PHASE ANGLE IN PITCH MODE
Fn=0.52

FIG. 5.29
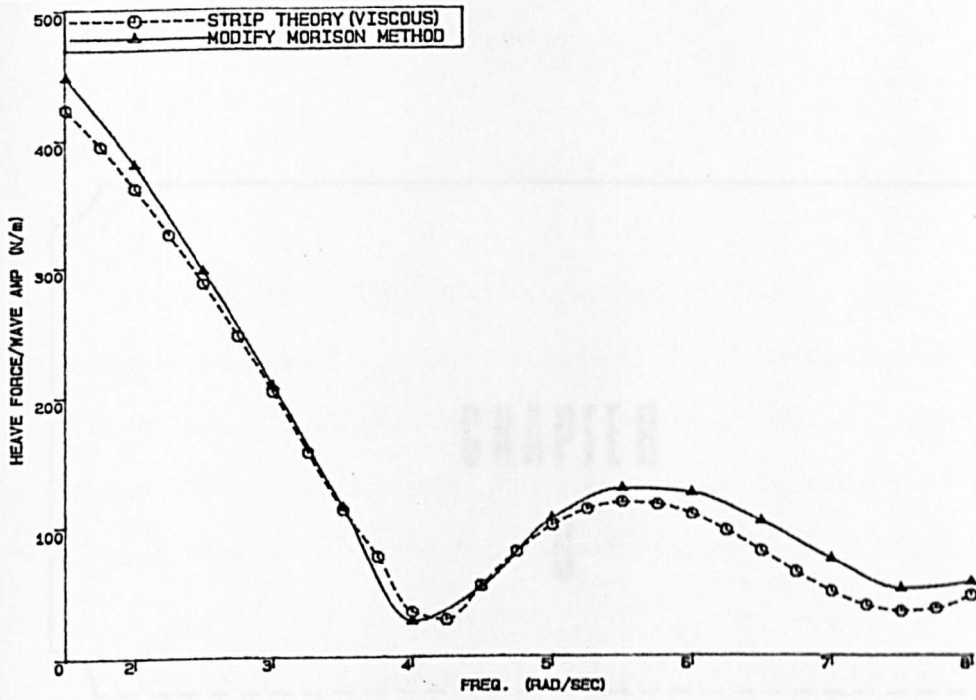
COMPARISON OF HEAVE FORCE
ZERO SPEED
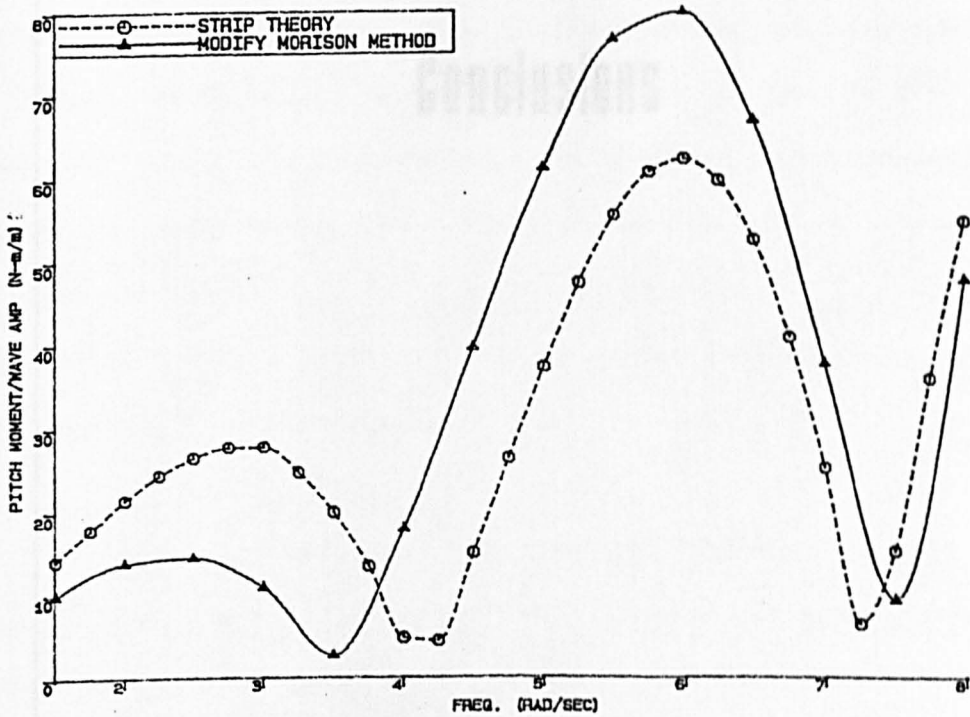
COMPARISON OF PITCH MOMENT
ZERO SPEED
FIG. 5.30

CHAPTER
6

Conclusions

CHAPTER 6

CONCLUSIONS

The theoretical and experimental work carried out has demonstrated that there is, on the whole, good agreement between the theoretically predicted motion and the measured values. However, there are areas when the theory presented needed further development to cover certain aspects of the motion and this will be discussed later.

The chief theoretical conclusions and contributions to design practice are as follows.

1.   Accurate added mass and damping data have been obtained for hull sections alone and for hull strut combination covering the practical range of frequencies, depth of immerses and column width ratio. This work showed that it was necessary to have a minimum of between 15 to 20 points on each half section in order to get accurate results. These results showed that there is a large change in both added mass and damping with frequency when the hull is close to the surface as it is likely to be in most commercial SWATH, from the point of view of minimising draft. Thus any theoretical calculation of SWATH motion must be involved.

2.   The approximate formulae of added mass and dampimg coefficients expressed as functions of frequency, depth of submergence and column width ratio. The results had been confirmed by the comparation of the results directly from the theory. These data can be easily obtained by interpolating the factors demanded .

3.   The viscous effects are found relatively dominant compared to the very low wave damping of a SWATH ship and should be included in the calculation. The engineering approach used in the thesis which take account of the viscous lift generated by an inclined hull with forward speed and the viscous drag associated with the cross-flow drag has been shown to give satisfactory results. Since both the viscous lift and viscous drag effects are proportional to the square of the relative flow velocity, the non-linear effects must be linearised and solved iteratively until a reasonable convergence on the motion amplitude is obtained. The viscous damping increases with increasing amplitude of motion, whereas the wave damping coefficient does not. This explains the importance of the viscous damping in limiting the motion at resonant frequencies for which the amplitude may be large.

4.   The forces contributed by fins are composed of inertia, lift and cross-flow drag and the same iteration procedures are required to account for the viscous effect. The lift-curve slope was corrected for the interaction of the fin and hull-body. Although only aft fins have ben considered, the combination of forward and aft fins could be added linearly. However, some effects such as free surface, downwash on the aft fins from the forward fins, cavitation and the boundary layer effects may be significant in some cases and should be explored further.

5.   The aim of the fin design was to ensure the dynamic stability in the vertical plane at high speed and its effectiveness was confirmed by the experimental investigation.

6.   Fins, being a lifting surface, not only can generate lift when subjected to an angle of attack but also contribute large eddy

damping, which significantly reduces the peak motion at certain low frequencies in head seas. However, at lower speeds or following seas when the encounter frequency is very small, the ship tended to contour the predominant waves and fixed fins were found to be ineffective. This confirms the findings in Reference [45]. Even with active fin control [51,93] it has been found that significant improvements can be achieved only when the speed is over a certain range. This is contrary to what was found on the KAIMALINO trial [58] when large reductions in pitch were evident at the Froude number above 0.24 (7 knots) in following seas. This can be explained by the very big fin area (about 1.46 of the waterplane area) on the KAIMALINO, whereas the ratio is only 0.45 for the 3000 ton SWATH [94] and 0.389 in this study. Thus sufficient lift can be generated by a big fin area even at low speeds, but this involves a great drag and clearly this is one of the critical design decisions.

7. Therefore, for the further fin design, the theory could be expanded by taking account of the wave exciting forces and moments arising from the fins and attempting to obtain an optimum from frequency relationship.

8. In the potential flow assumption stage, the sectional wave exciting forces which were obtained by the Froude-Krylov force from incident velocity potential and the diffraction force. The forward speed was found to have no effect on the Froude-Krylov term except to change the wave frequency into the encounter frequency. Whereas the correction 'end term' due to the speed effect on the diffraction force existed only for a SWATH which has end sections. One more term 'speed dependent' should be corrected in the pitch mode.

9.   The phase difference between the strip sections and the longitudinal centre of gravity (LCG) was found to significantly affect the total wave exciting force and moment, it should be carefully taken into account in the integration procedure.

10.   The restoring force dominates at the lower frequencies, where SWATH vertical motions are important. Therefore, the hydrostatic data (waterplane area, moment of waterplane area, mass moment of inertia and LCG) play an important role in design for good motions.

The main conclusions for the experimental work are:-

1.   In calm water the trim and sinkage of this model was so great at the higher speeds that it would be impossible to operate in a seaway without some form of control device. The aft fins designed for the model was effective in correcting the trim at the higher speeds but had little effect in the sinkage. At low speeds, after the aft fins were fitted, the trim was found to be worse than the bare hull. This is due to the righting moment generated by the lift force on the fins which is proportional to the square of the speed and the fin angle. If the speed is not high enough to generate sufficient lift, the moment generated due to the drag then increase the Munk moment.

2.   The wave frequency has very little effect on trim and sinkage, therefore it is suggested that the number of wave frequencies could be reduced for a further test.

3.   In the motion responses, the fins operated most effectively near the synchronous frequency range and had little influence at higher or lower frequencies.

4.   A significant (nearly 50%) reduction of pitch motion due to the aft fins was found at the low frequency range. As frequencies higher than o.55hz, fins are inefficient. Fortunately, the heave and pitch motions are small at the higher frequencies.

5.   The results also reveal that for particular frequency ranges, reduction of heave and pitch motion can be made by changing the fixed fin angles, the angle of the fixed fin should be changed in order to get the best motion performance on a particular frequency range.

6.   In the following waves, the results showed that the aft fins at fixed angles cannot necessarily reduce the motion responses at lower frequencies. A large surge was found during the tests.

7.   The experimental results emphasised that the SWATH model has a small vertical plane motion in head seas except at the resonant frequencies. No stabilisation fins are necessary for certain wave lengths, therefore it is desirable to design a retractable fin or use active fin control in which the angles are made sensitive or proportional to the motion displacement, velocity or acceleration with or without time lag.

8.   In the forward speed tests, yawing and rolling results from the asymmetry of the model in waves or the wave system, will affect the measurements of the pitch and heave motions. Difficulty was also found in the following seas where surge forces accompanied, the model was pushed forwards and backwards at random. Special attention and improvement needs to be paid to the model guideness (mooring) system.

Objectives of the work have been substantially achieved and a positive contribution has been made to the understanding of SWATH motion and the design procedures necessary for a SWATH control system.

REFERENCES

1. LEE, C M, 'Preliminary Studies Leading to Seakeeping Hull Design'. PRADS 83, 2nd Intl Symp on Practical Design in Shipbuilding, Tokyo & Seoul, 1983.

2. BHATTACHARYYA, A, McCORMICK, M E, 'Dynamics of Marine Vehicles. John Wiley & Son Press p396, 1972.

3. MABUCHI, T, KUMTAKE, Y, NAKAMURA, H, 'A Status Report on Design and Operational Experiences with the Semi-Submerged Catamaran (SSC) Vessels'. Intl Conf on SWATH Ships and Advanced Multi-Hulled Vessels, RINA, 1985.

4. NAKAMURA, H, MABUCHI, T, 'Design and Full Scale Test Results of Semi-Submerged Catamaran (SSC) Vessels'. 1st Intl Marine Systems Design Conf (IMSDC), RINA Paper No 11, pp54, 1982.

5. McGREGOR, R C, 'An Illustration of Some SWATH Vessel Characteristics'. High-Speed Surface Craft Conf, pp248, 1983.

6. LANG, T G, 'S - New Type of High Performance Semi-Submerged Ship'. ASME, Jour Eng for Ind, 1972.

7   PETTY, W, Manuscripts Concerning 'Ye Double Body Shippe'. National Maritime Museum, SPB/16. 1660

8. 'The Double Bottom or Twin-Hull Ship of Sir William Petty'. Oxford University Press

9. LEOPOLD, R, JOHNSON, R S, HADLER, J B, GENALIS, R, 'The Low Water Plane Multi-Hull Ship Principles, Status and Plans for Naval Development. AIAA Paper No 72-603. July 1972.

10. LUNDBORG, C G, 'Construction of Ships'. US Patent No 234794, 1880.

11. BOERICKE, H, Jr, 'Unusual Displacement Hull Forms for High Speed'. Intl Shipbuilding Progress, No 2, 1959.

12. NELSON, US Patent 1905.

13. FRANKEL, E G, 'SEMCAT Report', Arthur D. Little Inc. Report No 63-1, June 1963.

14. LANG, T G, 'The SWATH Ship Concept and its Potential'. AIAA/SNAME. San Diego, California, 1978.

15. LEOPOLD, R, 'A New Hull Form for High-Speed Volume-Limited Displacement-Type Ships'. SNAME Spring Meeting, New York, 1969.

16. LANG, T G, 'Preliminary Design Study of a 3000-ton S^3". NUCTN-574. Sep 71.

17. LANG, T G, et al, 'Naval Feasibility of the NUC Semi-Submerged Ship Concept'. Naval Undersea Research and Development Centre, TP 235, 1971.

18. LANG, T G, HIGDON, D T, 'Hydrodynamics of the 190 Ton SSP'. AIAA 78-328, 1974.

19. LANG, T G, et al, 'Design and Development of the 190 Ton Stable Semi-Submerged Platform (SSP)'. ASME Paper No 73-WA/Oct, 1973.

20. OSHIMA, M, NARITA, H, 'Semi-Submerged Catamaran (SSC) Application in Marine Transport and Ocean Development'. Pacific Congress on Marine Technology (PACON 84), HAWAII, 1984.

21. WOOLAVER, D A, PETERS, J B, 'Comparative Ship Performance Sea Trial for the USCG Cutters Mellon and Cape Corwin and the US Navy SWATH Ship KAIMALINO". DTNSRDC Report 80/037. 1980.

22. McCREIGHT, K K, STAHL, R G, 'Recent Advances in the Seakeeping Assessment of Ships'. Naval Engineers Jour. May 85.

23. ALLEN, R G, HOLCOMB, R S, 'The Application of Small SWATH Ship to Coastal and Offshore Patrol Missions'. Symp on Small Fast Warships and Security Vessels, RINA, 1982.

24. EAMES, M C, 'Prospects for Advanced Types of Surface Warships'. High-speed Surface Craft Conf. pp19. 1983.

25. HIGHTOWER, J D, SEIPLE, R L, 'Operational Experience with the SWATH Ship SSP KAIMALINO. AIAA/SNAME Advanced Marine Vehicles Conf. Paper 78-741. 1978.

26. KUSAKA, Y, et al, 'Hull Form Design of the Semi-Submerged Catamaran Vessel'. 13th Symp on Naval Hydrodynamics, Tokyo, 1980.

27. KOOPS, A, et al, 'SWATH Model Resistance Experiments'. Intl Conf on SWATH Ships and Advanced Multi-Hulled Vessels, RINA, 1985.

28. LANG, T G, SLOGGETT, J E, 'SWATH Developments and Performance Comparisons With Other Craft'. Intl Conf on SWATH Ship and Advanced Multi-Hull Vessels, RINA, 1985.

29. FEIN, J A, 'Vertical and Horizontal Plane Control of SWATH Ships'. Proc 7th Ship Control Systems Symp, Bath, Sep 84.

30. SALVESEN, N, 'Seakeeping Characteristics of Small-Water-Plane Area-Twin-Hull Ships'. Jour of Hydrodynamics, Jan 73.

31. SMITH, S N, 'Design and Hydrodynamic Performance of a Small Semi-Submersible (SWATH) Research Vessel'. RINA Spring Meeting, Paper No 9, 1980.

32. KORVIN-KROUKOVSKY, B V, 'Investigation of Ship Motions in Regular Waves'. Trans SNAME, Vol 63, 1955.

33. KORVIN-KROUKOVSKY, B V, JACOBS, W R, 'Pitching and Heaving Motions of a Ship in Regular Waves'. Trans SNAME, Vol 65, 1957.

34. SALVESEN, N, TUCK, E O, FALTINSEN, O, 'Ship Motions and Sea Loads'. Trans SNAME, Vol 78, pp250-287, 1970.

35. KIM, C H, CHOU, F S, 'Motion and Hydrodynamic Loads of a Ship Advancing in Oblique Waves'. Trans SNAME, Vol 88, pp225-256, 1980.

36. HONG, Y S, 'Prediction of Motions of SWATH Ships in Head and Following Seas'. DTNSRDC/SPD-81-039. Nov 81.

37. HONG, Y S, 'Predicted Motions of High-speed SWATH Ships in Head and Following Seas'. DTNSRDC/SPD-82-036. Jul 82.

38. NEWMAN, J N, SCLAVOUNOS, P, 'The Unified Theory of Ship Motion'. Proc. 13th Symp on Naval Hydrodynamics, Tokyo, Japan. Oct 80.

39. WU, J-Y, 'Experimental Investigation of Vertical-Plane Response of a SWATH Ship With and Without Aft Fins in Head Seas'. University of Glasgow, Department of Naval Architecture and Ocean Engineering Report No NAOE 85-31, 1985

40. ALLAN, J F, 'The Stabilisation of Ships by Activated Fins'. Trans RINA, Vol 87, 1945.

41. CONOLLY, J E, 'Rolling and its Stabilisation by Active Fins'. Trans RINA, Vol 111, 1969.

42. LLOYD, A R J M, 'Roll Stabiliser Fins: A Design Procedure'. Trans RINA, 1974.

43. ABKOWITZ, M A, 'The Effect of Anti-Pitching Fins on Ship Motions'. Trans SNAME, 1959.

44. MATSUI, M, 'On The Controlled Anti-Pitching Fin'. JSNA, Japan, Vol 119, 1966.

45. VUGTS, J H, 'Pitch and Heave With Fixed and Controlled Bow Fins'. Intl Shipbuilding Progress, Vol 14, 1967.

46. JONCKHEERE, H M, 'The Control of Heave and Pitch of a Semi-Submarine in Regular Astern Waves'. MIT Report, 1963.

47. LEE, C M, JONES, H D, CURPHEY, R M, 'Prediction of Motion and Hydrodynamic Loads of Catamarans'. Marine Technology, Vol 10, No 4, 1973.

48. PIEN, P C, LEE, C M, 'Motion and Resistance of a Low Waterplane Area Catamaran'. 9th Symp on Naval Hydrodynamics, Paris, 1972.

49. LEE, C M, 'Theoretical Prediction of Motion of Small-Waterplane-Area,-Twin-Hull (SWATH) Ships in Waves.' DTNSRDC, Report No 76-00467, 1976.

50. LEE, C M, MARTIN, M, 'Determination of Stabilising Fins for SWATH Ships'. 4th Ship Control System Symp, Vol 4, 1975.

51. CLARKE, D, NICHOLSON, K, 'SWATH Vertical Motion Control Using a Frequency Domain Multi-Variable Approach.' Proc 7th Ship Control Systems Symp, Bath, Sep 84.

52. FEIN, J A, FELDMAN, J P, 'Controllability of the Stable Semi-Submerged Platform'. 3rd Ship Control System Symp Paper No IXB-3, 1972.

53. LEE, CM, McCREIGHT, K K, 'Investigation of Effects of Activated Fins on Vertical Motion of a SWATH Ship in Waves'. DTNSRDC Report No SPD-063-01, 197.

54. WARE, J B, BEST, J F, SCOTT, V A, 'Applications of Optimal Control Techniques to SWATH Vertical Plane Control'. ORI, Tech Report No TR-1682, 1980.

55. WARE, J R, SCOTT, V A, 'Comparison of Platforming and Contouring Automatic Control Systems for SWATH Craft - An Optimal Control Approach'. ORI, Tech Report No TR-1790, 1980.

56. CALDEIRA-SARAIVA, F L A, CLARKE, D, 'Application of Multivariable Control Techniques to the Active Motion Control of SWATH Craft'. Intl Conf on SWATH Ship and Advanced Multi-Hull Vessels. RINA, 1985.

57. FEIN, J A, McCREIGHT, K K, OCHI, M D, 'The Seakeeping Characteristics of a Small Waterplane Area, Twin-Hull (SWATH) Ship'. 13th Symp on Naval Hydrodynamics, Vol 3, 1980.

58. FEIN, J A, 'Seakeeping and Motion Control Trails of SSP KAIMALINO in Sea State 4 and 5'. DTNSRDC Report No 81/015, 1981.

59. FRANK, W, 'Oscillation of Cylinders in or Below the Free Surface of Deep Fluids'. NSRDC Report No 2375, 1967.

60. MILLER, N S, 'Semi-Submersible Design: The Effect of Differing Geometries on Heaving Response and Stability'. Tran RINA, 1976.

61. MILLER, N S, 'Semi-Submersible and Tethered Buoyant Platforms, Some Design Considerations'. University of Glasgow, Department of Naval Architecture and Ocean Engineering, Lecture Notes, Sep 1977.

62. WU, J-Y, 'Approximate Formulae for SWATH Heave Added Mass and Damping Coefficients'. University of Glasgow, Department of Naval Architecture and Ocean Engineering, Report No NAOE-83-04, Jan 83.

63. ATLAR, M, 'A Two-Dimensional Method for Estimating Hydrodynamic Loads and Motions of a Twin-Hulled Semi-Submersible Associated with Some Hydrodynamic Aspects in Regular Beam Seas'. Universty of Glasgow, Department of Naval Archtecture and Ocean Engineering, Report No NAOE-85-34, 1985.

64. NEWMAN, J N, 'Marine Hydrodynamics'.MIT Press, 1977.

65. THWAITES, B, 'Incompressible Aerodynamics'. Oxford University Press, pp405-421, 1960.

66. LEE, C M, CURPHEY, R M, 'Prediction of Motion, Stability and Wave Load of Small Waterplane-Area, Twin-Hull Ships'. Trans SNAME, Vol 85, pp94-130, 1977.

67. LEE, C M, HADLER, J B, 'Ocean Catamaran Seakeeping Design, Based on the Experiments of USNS Hayes'. Trans SNAME, Nov 74.

68. WU, J-Y, 'A Study of the Effect of Fin Size on the Pitching and Heaving of a SWATH Ship'. University of Glasgow, Department of Naval Architecture and Ocean Engineering, Report No NAOE-84-55, 1984.

69. WHICKER, L F, FEHLNER, L F, 'Free-Stream Characteristics of a Family of Low-Aspect-Ratio All-Movable Control Surfaces for Aplication to Ship Design'. DTMB Report No 933, 1958.

70. PITTS, W C, NIELSEN, J N, 'Lift and Center of Pressure of Wing-Body-Tail Combinations at Subsonic, Transonic and Supersonic Speeds'. NACA Report No 1307, 1959.

71. NIELSEN, J N, 'Missile Aerodynamics'. McGraw-Hill, pp120, 1960.

72. LEE,   C M,   'Experimental   Investigation   of   Hydrodynamic Coefficients of a Small-Waterplane-Area, Twin-Hull Model'. NSRDC Report No SPD 347-01, 1977.

73. ATLAR, M, 'A Study of the Frank Close-Fit Method - Theory, Application and Comparison with Other Methods'. University of Glasgow, Department of Naval Architecture and Ocean Engineering, Report No NAOE-HL-81-09, 1982.

74. WU, J-Y, 'Approximate Formulae for Sway Added Mass and Damping Coefficients of SWATH Ships'. University of Glasgow, Department of Naval Architecture and Ocean Engineering, Report No NAOE-84-18, Jan 84.

75. CAMERON, R M, 'Computer Aided Curve Fitting'. Shipping World & Shipbuilder, No 1174, Oct 72.

76. VALIDAKIS, J, SEREN, D B, 'Frequency-Dependent Hydrodynamic Coefficient Data for the Heave, Sway and Roll Modes. Part I - Submerged, Symmetrical Single-Hull Sections'. University of Glasgow, Department of Naval Architecture and Ocean Engineering, Report No NAOE-84-02, 1984.

77. VALIDAKIS, J, 'The Results of Curve-Fitting Frequency Dependent Added Mass Coefficients for Two-Dimensional Submerged Sections in the Heave, Sway and Roll Modes'. University of Glasgow, Department of Naval Architecture and Ocean Engineering, Report No NAOE-84-59, 1984.

78. OGILVIE, T F, 'Rational Ship Theory of Ship Motions : Part I'. University of Michigan, College of Engineering, Report No 013, 1969.

79. SEREN, D B, MILLER, N S, 'The SWATH Wave-Lad Program, Progress Report No 5 - A Package to Compute and Control the Weight Distribution, Dynamic Properties and Static Loads of Floating Offshore Configurations'. University of Glasgow, Department of Naval Architecture and Ocean Engineering, Report No NAOE-84-32, 1984.

80. BESSHO, M, KYOZUKA, Y, 'ON the Ship Motion Reduction by Anti-Pitching Fins in Head Seas'. 15th Symp, Naval Hydrodynamics, 1985.

81. WYLIE, D J, 'SWATH Ship Motion Control'. Brown Brothers & Co, Report No 17000046, 1980.

82. ROUTH, E J, 'Dynamics of a System of Rigid Bodies'. 6th Edition, The Macmillan Company, London, 1905.

83. ABKOWITZ, M A, 'Stability and Motion Control of Ocean Vehicles'. Massachusetts Institute Of Technology Press, 1969.

84. FORTRAN Library Manual, NAG (Numerical Algorithms Group), Mark 11, Vols 1-6, 1984.

85. ASHLEY, H, 'Wing-Body Aerodynamic Interaction'. Annual Review of Fluid Mechanics, Vol 4, 1972.

86. WU, J-Y, 'A Prediction Method for SWATH Heave, Pitch and Surge Motion'. University of Glasgow, Department of Naval Architecture and Ocean Engineering, Report No NAOE-83-67, 1983.

87. ALLEN, H J, PERKINS, E E, 'A Study of Effect of Viscosity on Flow Over Slender Inclined Bodies of Revolution'. NACA Report No 1048, 1951.

88. BOSE, N, 'Wind Turbines, Operation in the Windmill Mode'. University of Glasgow, Department of Naval Architecture and Ocean Engineering, Report No NAOE-82-24, 1982.

89. MOTORA, S, KOYAMA, T, 'ON Wave Excitationless Ship Forms'. 6th Naval Hydrodynamics Symp, Washington DC, 1966.

90. SALVESEN, N, 'Five Years of Numerical Naval Ship Hydrodynamics at DTNSRDC'. Jour of Ship Research, Vo 25, No 4, pp219-235, 1981.

91. CHANG, M S, 'Computations of Three-Dimensional Ship Motion with Forward Speed'. 2nd Intl Conf on Numerical Ship Hydrodynamics, California, 1977.

92. SCLAVOUNOS, P D, 'The Diffraction of Free-Surface Waves by a Slender Ship'. Jour of Ship Research, Vol 28, pp29-47, 1984.

93. MATSUSHIMA, M, NAKAMURA, H, KUNITAKE, Y, 'Seakeeping of a Semi-Submerged Catamaran (SSC) Vessel.' Mitsui Zosen Technical Review (in Japanese) Nov 81.

94. HIGDON, D T, 'Active Motion Reduction for a 3000-Ton SWATH Ship Underway in Regular Head and Following Waves'. Seaco Inc, Report No 80-05-01, 1980.